Generation and Characterisation of Catalytic Films of Zeolite Y and ZSM-5 on FeCrAlloy Metal

A thesis submitted to the University of Manchester for the degree of Doctor of Philosophy in the Faculty of Engineering and Physical Science

Rana Th. Abd Alrubaye

2013

School of Chemical Engineering and Analytical Science

List of Contents

CHAPTER 6. N-HEPTANE CRACKING OVER SELECT POWDER AND STRUCTURED ZEOLITE CATALYSTS 184

List of Figures

List of Tables

List of Abbreviation

Abstract

The objective of this work was the development of structured zeolite catalysts by growing of ZSM-5 and Y zeolites layers on the pre-treated FeCrAlloy wires, which could now offer technical advantage in catalytic application. The advantages of implementation of zeolitic coatings in industrial applications are that they have; lower pressure drop, high heat and mass transfer rates compared to standard pelleted or extruded catalysts.

The key focus of this research was the generation of thin films of zeolite ZSM–5 and Y zeolite catalysts on the surface of a FeCrAlloy metal substrate. Using in-situ hydrothermal synthesis, the influence of the synthesis parameters such as substrate oxidation and crystallisation time on the zeolite crystallisation process in both the bulk phase (powder) and on the structured zeolite was studied and optimised. Then powder and structured Na-ZSM-5 and Na-Y were treated by calcination and ion exchange in post-synthesis treatment. Further post-synthesis modification was required in the zeolite Y case to improve the catalytic properties. The post synthetic modification of zeolite Y was carried out using acidified ammonium nitrate which was optimised to produce dealuminated zeolite Y with good crystallinity and a Si/Al = 8. Characterisation was performed after each stage of this work to optimise catalyst development using XRD, SEM, EDAX, BET, MAS-NMR, and TGA.

Once the optimised zeolite Y and ZSM-5 structured catalysts prepared, cracking of n-heptane was carried out to assess the in catalytic performance compared with Y and ZSM-5 pellets in a fixed-bed reactor under the same operation conditions.

The cracking of n–heptane over the pellets and structured catalysts for both ZSM–5 and Y zeolite showed very similar product selectivities for similar amounts of catalyst with apparent activation energy of around 60 kJ mol^{-1}. This research demonstrates that structured catalysts can be manufactured with excellent zeolite adherence and when suitably activated/modified give comparable cracking results to the pelleted powder forms. These structured catalysts will improve temperature distribution in highly exothermic and endothermic catalysed processes.

Declaration

I declare that this research is the result of my own work except as cited in the references and it has not been submitted in support of an application of any other degree or qualification for any institute or other university.

Copyright Statements

I would like to dedicate my thesis to the memory of my late beloved father, and my affectionate mother

Acknowledgements

I am adduced to **Dr. Arthur Garforth,** my gratitude and appreciation for supervision, continuous guidance, utmost efforts, interest throughout the work that contributed to its completion, and for the trust he showed in me.

I would like also to express my grateful admiration to **Dr. Patrick Hill** for providing the help to implement the SEM and EDAX analyses, **Dr. Aaron Akah** and **Dr. Richard Holmes** for all the help and effort.

My regardful respect and thanks to the staff of Dr Arthur Garforth's group, especially **Mr. Bashir Yousif Al-Zaidi** and **Mr. Faisal Al-Qtaibi** for the ultimate interest they showed, their useful notices and providing all the necessary the help.

I would like to pay my regards to all relatives, colleagues and friends for all the help they showed.

I wish to explicit my sincere thanks to my sponsor, Republic of Iraq – Ministry of Higher Education & Scientific research for the sponsor me to study PhD in chemical engineering.

I would like to express my very deep respect, and sincere appreciation to my family, in particular my **mother** whose patience and moral encouragement gave me so much hope and support.

Above all, my great thanks to **ALLAH** for his mercy and blessing.

Rana

Chapter 1

Structured Catalyst Overview

1.1 Introduction

Zeolites are known for their versatility in pore structure, separation properties, shape, polarity, acidity and chemical composition in many chemical and petrochemical processes. Usually, zeolites are used in powder composite form (pellets) and they form a fixed bed in a reactor then the flow passes through this fixed bed. The principal disadvantages with this configuration are non-uniform access of reactants to the fixed bed catalytic surface, a higher pressure drop, diffusion problems, and hot spots. Moreover, the design of the reactor is limited to the reactor's diameter and the catalyst particle size which should be small in order to avoid channelling and to raise catalytic activity but not too small to create a pressure drop [1, 2].

Therefore, considerable research has been conducted in a bid to eliminate some of these setbacks; one approach being the use structured catalysts. Structured catalysts are made by attaching the catalytically active ingredients uniformly onto the surface of a substrate.

The structured catalysts with large channels ensure the low pressure drop, improving mass and heat transfer [3, 4]. In addition, small zeolite crystals provide higher effectiveness, lower coke formation, faster diffusion and higher external surface area with easier cation exchange and template extraction due to the large contact surface area [5, 6]. Therefore, depositing a thin layer of zeolite crystals on the metallic surface to form structured catalysts can offer same properties as small crystals by providing a high surface area-to-volume ratio in the range of 10,000–50,000 m^2 m^{-3}. Furthermore, because the catalysts are in a thin layer rather than pellets, the diffusion path is reduced, thereby improving catalyst activity and selectivity [3, 7, 8].

Thin layers of zeolite have been coated on various metal substrates [7, 9-11]. The substrates can influence catalyst performance [12]. Metallic substrates have higher mechanical resistance, higher thermal conductivity and lower pressure drop [13, 14]. However, the growth of zeolite films on metallic surface is difficult [14]. One interesting metallic substrate is FeCrAlloy. FeCrAlloy is an alloy containing Fe, Cr, Al, Y and Zr and when heated in air to high temperatures, the Al preferentially migrates to the alloy surface and forms a thin film layer of Al_2O_3 on the metal surface [15]. This oxide layer could then be useful for anchoring the catalytically active phase such as zeolite [16].

Attachment of zeolite crystals onto the metal surface can be achieved using various methods. The difference between these methods is whether or not a binder has been used to form the structured catalysts. A binder will work as a glue to ensure that the zeolite crystals, which are already synthesised, adhere to the metal surface. The binder is predominantly used in the dip-coating method whereas in in–situ growth synthesis method the zeolite crystals are grown onto the substrate surface and no bounder is used [17].

The dip-coating technique is applied by inserting the substrate into a stabilised suspension of zeolite crystals containing the binder and other additives followed by the drying process to evaporate the solvent then calcinations of the structured catalyst [18, 19]. The in-situ technique is conducted without the binder present by immersing the substrate in an aged zeolite gel under hydrothermal conditions to ensure that crystallisation occurs [11, 20].

During the crystallisation process two mechanisms occur; the first mechanism is homogeneous nucleation in the mother liquid and the second is heterogeneous nucleation on the surface of the metallic substrate, followed by the growing of all formed nuclei [2].

Pre-treatment and cleaning of the metallic substrate is favourable in all cases to ensure that roughness and a thin oxide layer are formed on the metal surface [12, 18, 21]. These surface defects can prove useful for obtaining an improved interaction between the zeolite gel and the substrate by anchoring the nuclei of zeolite on the metal surface to obtain homogenous seeding along the metallic substrate [7, 22-24].

Cleaning the metallic substrate is the first step in the pre-treatment procedure. The pre-treatment can consist of mechanical, chemical and thermal pre-treatments [25-29].

Several studies review the application of zeolitic coatings [24, 30] with zeolite membranes and monoliths being the principal applications [30-32]. Structured catalysts and their use is a relatively new field. Recently, research has demonstrated the potential of using zeolitic coatings for oxidation of phenol to benzene [33], dehydrogenation of methane [34], and ammoxidation of ethane to produce acetonitrile [35, 36]. The zeolitic coatings could be implemented in many industrial applications due to the combination of the large surface area of zeolite ($400 - 700$ m^2 g^{-1}) with a large geometric surface area of micro structured catalyst ($5000 - 10,000$ m^2 m^{-3}) [8].

1.2 Objectives of the research

The purpose of this research is to investigate the coating of a metal support with zeolite and their application as catalytic packings. This was achieved by establishing the factors that were crucial in optimising zeolite synthesis. Within this work the focus was on zeolite Y and zeolite ZSM-5, both containing a 3-dimensional channel: zeolite Y with pore size (0.74×0.74) nm and ZSM-5 with pore size (0.53×0.56) nm and (0.51×0.55) nm [1].

Then the focus falls on to the metallic substrate in practical FeCrAlloy preparation before it was coated with zeolite film to optimise the synthesis of structured catalysts. The preparation of FeCrAlloy is achieved by applying mechanical, chemical and thermal pre-treatments respectively to ensure the formation of a thin oxide layer on the FeCrAlloy surface.

Finally, FeCrAlloy wires were coated with zeolite using in-situ techniques. Initially, the structured catalyst films have characterised using a range of techniques, including X-ray diffraction (XRD), Scanning electron microscopy (SEM), Energy Dispersive X–ray analysis (EDAX) and Thermogravimetric Analysis (TGA). The transition from oxide-on-alloy wires to hydrothermally synthesised uniformly zeolite coated surfaces were followed using SEM and XRD. In addition, the robustness of the prepared coating was confirmed by subjecting these to thermal cycling (ambient to 550°C).

A dealumination method using acidified ammonium nitrate was optimised for zeolite Y and structured catalyst coated with zeolite Y prior to catalytic testing. The cracking of n–heptane over the pellets and structured catalysts for both ZSM–5 and Y zeolite revealed similar product selectivities for the same zeolite type and for similar amounts of catalysts with apparent activation energy of around 60 kJ mol^{-1}.

References

1.   Chau, J.L.H., A.Y.L. Leung, and K.L. Yeung, *Zeolite micromembranes,* Lab on a Chip, 2003. **3**(2): p. 53-55.

2.   Eleta, A., P. Navarro, L. Costa, and M. Montes, *Deposition of zeolitic coatings onto Fecralloy microchannels: Washcoating vs. in situ growing,* Microporous and Mesoporous Materials, 2009. **123**(1): p. 113-122.

3.   Kiwi-Minsker, L. and A. Renken, *Microstructured reactors for catalytic reactions,* Catalysis Today, 2005. **110**(1-2): p. 2-14.

4.   Clet, G., J.C. Jansen, and H. van Bekkum, *Synthesis of a Zeolite Y Coating on Stainless Steel Support,* Chemistry of Materials, 1999. **11**(7): p. 1696-1702.

5.   Koroglu, H.J., *Effects of low-temperature gel aging on the synthesis of zeolite Y at different alkalinities,* Journal of Crystal Growth, 2002. **241**(4): p. 481-488.

6.   Di Renzo, F., *Zeolites as tailor-made catalysts: Control of the crystal size,* Catalysis Today, 1998. **41**(1-3): p. 37-40.

7.   Wang, Z., J. Hedlund, and J. Sterte, *Synthesis of thin silicalite-1 films on steel supports using a seeding method,* Microporous and Mesoporous Materials, 2002. **52**(3): p. 191-197.

8.   Mies, M.J.M., J.L.P. Van Den Bosch, E.V. Rebrov, J.C. Jansen, M. De Croon, J.C. Schouten, *Hydrothermal synthesis and characterization of ZSM-5 coatings on a molybdenum support and scale-up for application in micro reactors,* Catalysis Today, 2005. **110**(1-2): p. 38-46.

9.   Yamazaki, S. and K. Tsutsumi, *Synthesis of a mordenite membrane on a stainless-steel filter and polytetrafluoroethylene plate substrates,* Microporous Materials, 1995. **5**(4): p. 245-253.

10.   Erdem-Senatalar, A., M. Tatlier, and M. Ürgen, *Preparation of zeolite coatings by direct heating of the substrates,* Microporous and Mesoporous Materials, 1999. **32**(3): p. 331-343.

11.   Shan, Z., W. E. J. van Kooten, O. L. Oudshoorn, J. C. Jansen, H. van Bekkum, C. M. van den Bleek, H. P. A. Calis, *Optimization of the preparation of binderless ZSM-5 coatings on stainless steel monoliths by in situ hydrothermal synthesis*, Microporous and Mesoporous Materials, 2000. 34(1): p. 81-91.

12.   Zamaro, J.M., M.A. Ulla, and E.E. Miró, *Growth of mordenite on monoliths by secondary synthesis: Effects of the substrate on the coating structure and catalytic activity,* Applied Catalysis A: General, 2006. **314**(1): p. 101-113.

13.   Nerea Burgos, M.P.a.M.M., *Preparation of Al_2O_3/Al monoliths by anodisation of aluminium as structured catalytic supports,* J. Mater. Chem., 2003. **13**: p. 1458 - 1467.

14.   Zamaro, J.M., M.A. Ulla, and E.E. Miró, *ZSM5 growth on a FeCrAl steel support. Coating characteristics upon the catalytic behavior in the NO_x SCR,* Microporous and Mesoporous Materials, 2008. **115**(1-2): p. 113-122.

15.   Badini, C. and F. Laurella, *Oxidation of FeCrAl alloy: influence of temperature and atmosphere on scale growth rate and mechanism,* Surface and Coatings Technology, 2001. **135**: p. 291-298.

16.   Yuranov, I., A. Renken, and L. Kiwi-Minsker, *Zeolite/sintered metal fibers composites as effective structured catalysts,* Applied Catalysis A: General, 2005. **281**(1-2): p. 55-60.

17.   Meille, V., *Review on methods to deposit catalysts on structured surfaces,* Applied Catalysis A: General, 2006. **315**: p. 1-17.

18.   Zamaro, J.M., M.A. Ulla, and E.E. Miró, *Zeolite washcoating onto cordierite honeycomb reactors for environmental applications,* Chemical Engineering Journal, 2005. **106**(1): p. 25-33.

19.   Avila, P., M. Montes, and E.E. Miró, *Monolithic reactors for environmental applications: A review on preparation technologies,* Chemical Engineering Journal, 2005. **109**(1-3): p. 11-36.

20.   Ulla, M.A., R. Mallada, J. Coronas, L. Gutierrez, E. Miró, J. Santamaría, *Synthesis and characterization of ZSM-5 coatings onto cordierite honeycomb supports,* Applied Catalysis A: General, 2003. **253**(1): p. 257-269.

21.   Avila, P., M. Montes, and E.E. Miro, *Monolithic reactors for environmental applications: A review on preparation technologies,* Chemical Engineering Journal, 2005. **109**(1): p. 11-36.

22.   Mintova, S., V. Valtchev, and L. Konstantinov, *Adhesivity of molecular sieve films on metal substrates,* Zeolites, 1996. **17**(5–6): p. 462-465.

23. Camra, J., E. Bielańska, A. Bernasik, K. Kowalski, M. Zimowska, A. Białas, M. Najbar, *Role of Al segregation and high affinity to oxygen in formation of adhesive alumina layers on FeCr alloy support,* Catalysis Today, 2005. **105**(3-4): p. 629-633.

24. Bonaccorsi, L. and E. Proverbio, *Synthesis of thick zeolite 4A coatings on stainless steel,* Microporous and Mesoporous Materials, 2004. **74**(1-3): p. 221-229.

25. Wu, X., Weng, D.Zhao, S.Chen, W., *Influence of an aluminized intermediate layer on the adhesion of a [gamma]-Al$_2$O$_3$ washcoat on FeCrAl,* Surface and Coatings Technology, 2005. **190**(2-3): p. 434-439.

26. Wu, X., D. Weng, L. Xu, H. Li, *Structure and performance of [gamma]-alumina washcoat deposited by plasma spraying,* Surface and Coatings Technology, 2001. **145**(1-3): p. 226-232.

27. Zhao, S., J. Zhang, D. Weng, X. Wu *A method to form well-adhered [gamma]-Al$_2$O$_3$ layers on FeCrAl metallic supports,* Surface and Coatings Technology, 2003. **167**(1): p. 97-105.

28. Valentini, M., G. Groppi, C. Cristiani, M. Levi, E. Tronconi, P. Forzatti, *The deposition of [gamma]-Al$_2$O$_3$ layers on ceramic and metallic supports for the preparation of structured catalysts,* Catalysis Today, 2001. **69**(1-4): p. 307-314.

29. Reymond, J.P., *Structured supports for noble catalytic metals: stainless steel fabrics and foils, and carbon fabrics,* Catalysis Today, 2001. **69**(1-4): p. 343-349.

30. Jansen, J.C., J.H. Koegler, H. van Bekkum, H.P.A. Calis, C.M. van den Bleek, F. Kapteijn, J.A. Moulijn, E.R. Geus, N. van der Puil, *Zeolitic coatings and their potential use in catalysis,* Microporous and Mesoporous Materials, 1998. **21**(4-6): p. 213-226.

31. Wan, Y.S.S., J. L. H. Chau, A. Gavriilidis, K. L. Yeung, *Design and fabrication of zeolite-based microreactors and membrane microseparators,* Microporous and Mesoporous Materials, 2001. **42**(2-3): p. 157-175.

32. Wloch, E., A. Łukaszczyk, Z. Żurek, B. Sulikowski , *Synthesis of ferrierite coatings on the FeCrAl substrate,* Catalysis Today, 2006. **114**(2-3): p. 231-236.

33. Waclaw, A., K. Nowinska, and W. Schwieger, *Benzene to phenol oxidation over iron exchanged zeolite ZSM-5,* Applied Catalysis A: General, 2004. **270**(1-2): p. 151-156.

34.   Osawa, T., I. Nakano, and O. Takayasu, *Dehydrogenation of Methane over Mo/ZSM-5. Effects of Additives in the Methane Stream,* Catalysis Letters, 2003. **86**(1): p. 57-62.

35.   Li, Y. and J.N. Armor, *A Reaction Pathway for the Ammoxidation of Ethane and Ethylene over Co-ZSM-5 Catalyst,* Journal of catalysis, 1998. **176**(2): p. 495-502.

36.   Baerlocher, C., W.M. Meier, and D. Olson, *Atlas Of Zeolite Framework Types.* 2001: p. 79-150.

Chapter 2

Literature Review

2.1 Zeolite

2.1.1 Introduction

A zeolite is a hydrated crystalline aluminosilicate that has a three–dimensional framework structure occupied by exchangeable cations and which shows reversible water adsorption. Historically, the word zeolite was derived from the Greek words "zeo" and "lithos" meaning "boiling stone". It was referred to as a "zeolite" because it evolves water vapour when gently heated [1, 2]. In 1759, A.F. Cronstedt, a mineralogist from Sweden, discovered the first zeolite mineral [3].

Damour stated in 1840 that the majority of zeolites that were known could be reversibly dehydrated without structural changes (transparency or morphology),

and in 1845 Schafhaulte synthesised quartz by heating silica gel with water using an autoclave. There were many attempts to identify the general characteristics and properties of the zeolite between 1850 and the 1930s, and a search of the literature identifed properties of zeolites such as; ion exchange (by Way and Thompson in 1850 and Eichhorn in 1858), adsorption (by Grandjean in 1909), molecular sieving (by Weigel and Steinhoff in 1925) and structure (by Taylor and Pauling in 1930 and Mc Bain in 1932) [2, 4, 5]

However, it is difficult to provide evidence to prove that the early researchers were capable of synthesising new zeolite since there was no approved method to determine the complete characteristics of the products. Barrer was the first scientist to discover a synthesis route to a zeolite (Mordenite) and introduce the pioneering classification of zeolite depending on molecular size [6].

Subsequently, there was a need to discover a new material to fulfil the industrial requirements as a result of the large number of synthetic zeolites have been synthesised as zeolite A and X [6], zeolite beta [7], ZSM-5 and zeolite P [8].

In addition, zeolites find many applications in areas such as catalysis, absorption and ion exchange, with the unique properties of enabling them to play a crucial role in the environmental technologies. For instance, catalysis for selective catalytic reduction (SCR) of NO_x with NH_3 like Cu-ZSM-5 [9], H-ZSM-5 and H-mordenite[10], and Fe-ZSM-5 [11].

2.1.2 Zeolite description

Zeolites are three dimensional framework structured crystalline alumina-silicates which enclose cavities filled with water molecules and large ions [12]. The smallest structural unit of a zeolite is represented by:

$$Mx/n[(AlO_2^-) \, x \, (SiO_2)y] \, zH_2O$$
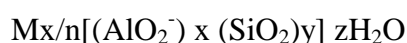
Where M is an extra-framework cation that satisfies the anionic charge of the framework, n is the cation valence for M, x and y are the total number of aluminates and silicates per unit cell and z is the number of water molecules per unit

cell [13]. As such, the cation plays a crucial role in specifying the zeolite properties depending on cationic positions within the cavities [4, 6, 12, 14].

Zeolites are structured from primary and secondary building units (**Figure 2-1**), with the primary building units consisting of TO_4 tetrahedra molecules, (where T is any tetrahedrally coordinated cation Si or Al). In general, gathering the same secondary building unit (SBU) gives distinctive structural polyhedra formed from smaller ring units. Zeolites structures consist of silicon cations (Si^{4+}) and aluminium cations (Al^{3+}) that are surrounded by four oxygen anions (O^{2-}). Each oxygen anion shares two cations and this introduces a macromolecular three-dimensional framework, with net neutral SiO_2 and negatively charged AlO_2^- tetrahedral building blocks. The negative charge is the result of exchanging silicon for aluminium cations, which is then compensated by extra-framework cations such as (Na^+) [13, 14].

Moreover, the basic building unit or BBU (TO_4 corner–sharing) are 3-dimensional, 4-connected framework structure, with the size of the pore openings and the dimensionality of the channel system characterising the framework structure of the zeolite.

Zeolites are classified according to the size of the rings, which define the pore openings and have diameter ranges from 3 Å to 12 Å related to the number of T atoms in the ring. Generally, an 8 ring is a small pore opening with a diameter (effective pore width-calculated using an oxygen radius of 1.35 Å) of 4.1 Å, a 10-ring is a medium one with a diameter of 5.5 Å, and a 12- ring is a large one with a free diameter of 7.4 Å [13, 14].
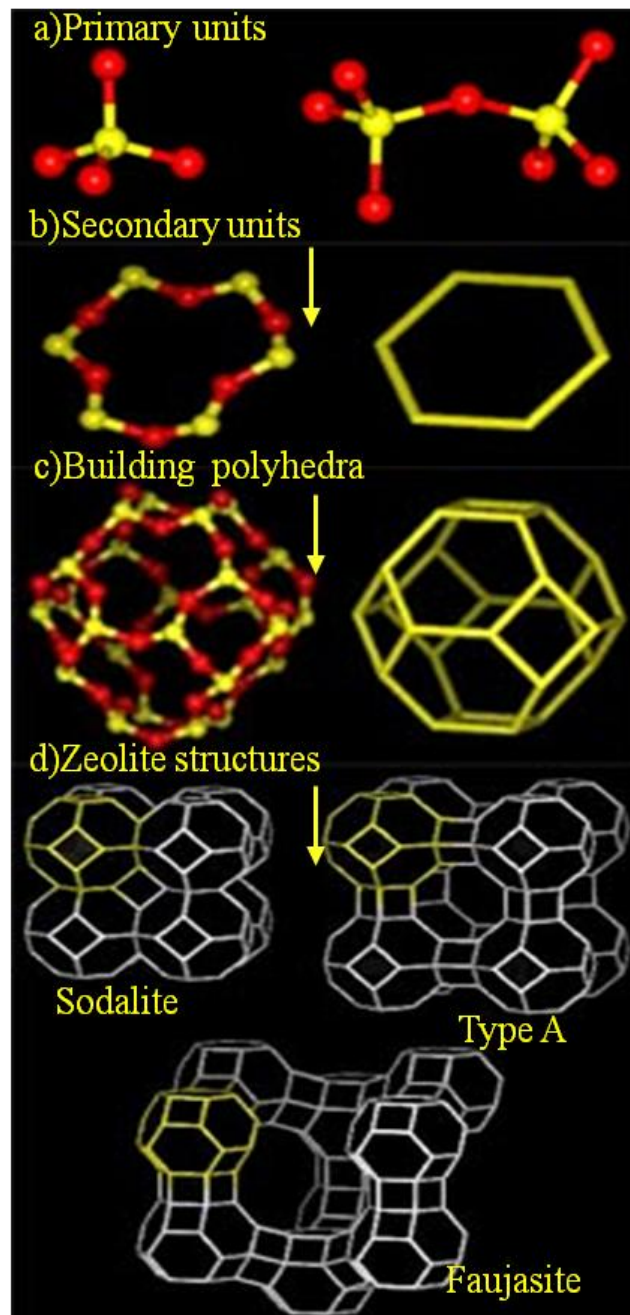
Figure 2-1: Formation of three common zeolite from primary SiO_4 and AlO_4^- tetrahedral units through a combination of secondary ring units, and ultimately different mixes of tertiary polyhedra modified from [1].

According to the International Zeolite Association (IZA) the framework symmetries with an identification code of three letters can be used as a classification method to classify zeolites [5]. For example the FAU framework type has a 12-ring pore openings and a 3-dimensional channel system e.g., zeolite X and Y, while the MFI framework has a 3-dimensional 10-ring channel system e.g., ZSM-5, and LTA framework has a 3-dimensional, 8-ring channel system e.g., zeolite A [6]. **Figure 2-2** shows the various types of structures produces depending on pores oriented in one, two or three directions leading to the different dimensionalities of the channel system.
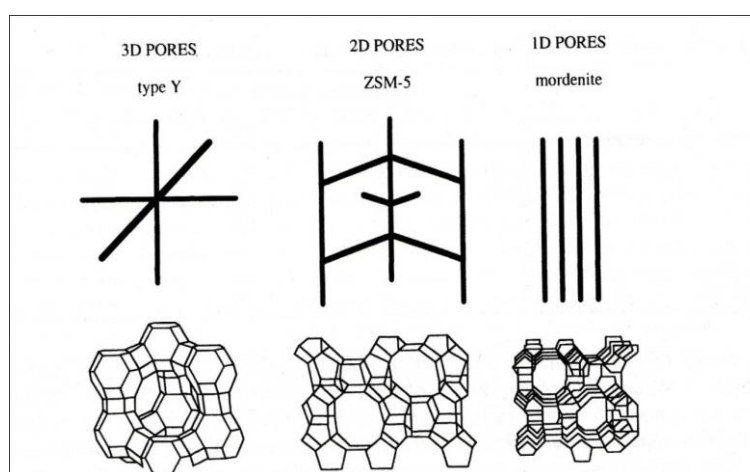
Figure 2-2: Different dimensionalities of zeolites [13].

2.1.3   Zeolite crystallization

Zeolite synthesis is attributed to the conversation of amorphous reactants containing silicon and aluminium which are mixed together with a cation source and water to form a microporous crystalline aluminosilicate via a series of complex chemical reactions. The literature on the crystallization mechanism by hydrothermal synthesis is vast [15, 16] and so far the mechanism for the formation of zeolites has not been fully understood.

It is commonly accepted that an aluminosilicate hydrogel amorphous or precipitate is formed directly after the addition of a solution of sodium aluminate (aluminium source) to a silica source. The mineralizing agent provides the solution

with monomers and oligomers (silicate and aluminate) by dissolution of the solid phase (gel phase). Monomers and oligomers are more likely to organise into extended precursor structures and finally into a crystalline phase, with the ageing of the hydrogel being essential to accelerate the crystallisation and achieve the preferred crystalline phase, this takes place at ambient temperature or slightly increased temperature, lower than that of the crystallisation process, which is achieved at a temperature range of between 60 and 200°C [15-17].

Thus, it is necessary to comprehend the three steps involved in the crystallisation of zeolite. These steps are super-saturation, nucleation and crystal growth.

The achievement of super-saturation occurs during the ageing time when the amorphous solid phase dissolves, causing a rise in the concentration of the aluminosilicate precursor species. Ageing time leads to a mechanically stronger cross–linked network by the depolymerisation of silica particles which is catalyzed by hydroxyl ions [16].

Studies focused on the evolution of gel ageing in super–saturation solution [15, 18, 19] have shown that the silicate ratio in the solution increases by increasing ageing time and this is due to the release of monomeric silicate anions which form silicate oligomers. The condensation and hydrolysis of silicate oligomers with monomeric tetrahedral aluminate anions, $Al(OH)^{-}_{4}$, occurs through a nucleophilic mechanism catalysed by hydroxyl ions, OH^{-}. A high concentration of OH^{-} anions increases the solubility of Si units by weakening the siloxane bonds and forming silanol groups. The ageing time in hydrothermal synthesis leads to an increase in the concentration of precursor species and concentration of nuclei and this enhances the nucleation step in the crystallization process.

Nucleation occurs by chemical aggregation of aluminosilicate precursor species which create germ nuclei. These germs tend to concentrate in the boundary layer surrounding the amorphous solid particles. Spontaneously, germs will grow in time and form nuclei. The nucleation process can be either a homogenous or heterogeneous reaction. Heterogeneous nucleation involves the introduction of

crystals by the seeding technique. These crystals extend in size as crystalline material is deposited onto them. The seeding technique results in crystal growth with high surface area compared to the fresh nuclei which have a significant impact on the decreasing of the crystallisation time [20].

The third step in the crystallisation process, crystal growth, is attributed to the condensation of the gel phase via hydroxyl anions–mediated dissolution onto the crystal surface. As previously mentioned, OH^- anions have an impact on the nucleation and crystallization process. The OH^- anions play a crucial role in reaching a super–saturated state in these processes. During the crystallization process under high OH^- anion concentration, the pH of the solution changes. The hydrolysis of the amorphous aluminosilicate consumes the hydroxyl anions, leading to a drop in the pH of the solution. Subsequently, the pH of the solution increases when the condensation reaction takes place [15].

2.1.4 Synthesis of Zeolite

Naturally occurring zeolites are found in volcanic and metamorphic rocks. Their formation mechanisms and geological conditions differ and depend on temperature, pressure, pH (8 - 9) and time (years) [21].

In 1948, Barrer was the first to confirm synthesis of an analogue of mordenite zeolite [22]. Subsequently, Milton and Beck [23] successfully achieved the synthesis of zeolite A using low temperatures (100^oC) and at higher alkalinity. During the 1960s, Barrer and Denny [24] opened the door for zeolite synthesis by substituting inorganic bases (NH_4OH) with organic molecules.

The use of organic templates led to the discovery of ZSM-5 which has a significant unique property as a result of its high Si/Al ratio. In the 1980s, new zeolite categories such as microporous and aluminophosphates were introduced in industrial fields [25].

Zeolite are synthesised under hydrothermal conditions using chemical raw materials typically a silicon source, aluminium source, metal ions, mineralizer and water Table 2-1. When the source materials are mixed, the heterogeneous synthesis mixture gel phase consists of either a homogenous dispersed phase or a more separated solid phase with different reactant ratios. [4].

Table 2-1: Chemical sources which are needed for zeolite syntheses [4].

Sources	Function (s)
SiO_2	Primary building units of the framework
AlO_2	Origin of framework charge
Alkali cation, template	Counter ion of AlO_2^-, TPAOH
Water	Solvent

The reaction temperature governs the choice of the reaction vessel type and is typically between 60^oC and 300^oC. Various kinds of reaction vessels are listed in **Table 2-2 and Figure 2-3** illustrates an autoclave PTFE-lined for high temperature synthesis of zeolites.
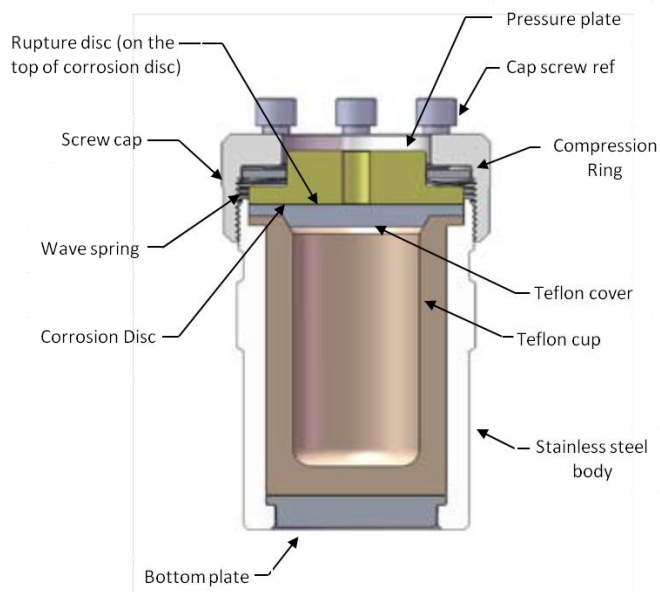
Figure 2-3: Autoclave PTFE-lined for high temperature synthesis of zeolites.

Table 2-2: Lab –scale reaction vessels and temperature range [3].

Reaction vessel	Volume (ml)	Temperature (^{o}C)
Plastic bottles	<11	<100
Stainless steel (S.S.) Autoclave	<51	<200
Teflon lined (S.S) Autoclave	<21	<200
Quartz – lined autoclave	<5	<200

2.1.5 Factors controlling zeolite synthesis

There are many factors that affect zeolite synthesis. This section provides an overview of the factors controlling zeolite synthesis.

2.1.5.1 Composition for zeolite synthesis

The reactant's composition in parent gel is crucial for determining the final zeolite produced during the hydrothermal process. For instance, varying the composition of Na_2O, SiO_2 or Al_2O_3 can produce different types of zeolite. Despite this, synthesis takes place under the same crystallization conditions; **Figure 2-4**. However, the results presented in **Figure 2-5** indicate that differences in the molar ratio of SiO_2/Al_2O_3 can lead to the formation of high silica molecule sieves such as ZSM-5 and ZSM-35. In addition, the crystallization of zeolite also imposes constraints on the amount of H_2O in the parent mixture [26].
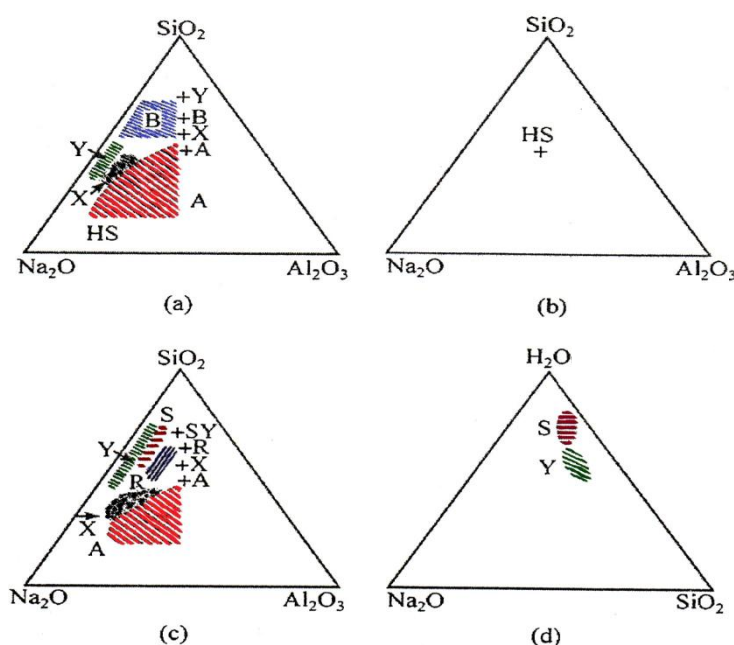
Figure 2-4: Crystallisation field. (a) Na_2O –Al_2O_3 – SiO_2 - H_2O, 100°C, H_2O content of gels is 80 – 90 mole%; silicon source: sodium silicate; (b) Same as (a) with 60 – 85 mole% H_2O in the gel; (c) same as (a), silicon source: colloidal silica; (d) Effect of water.
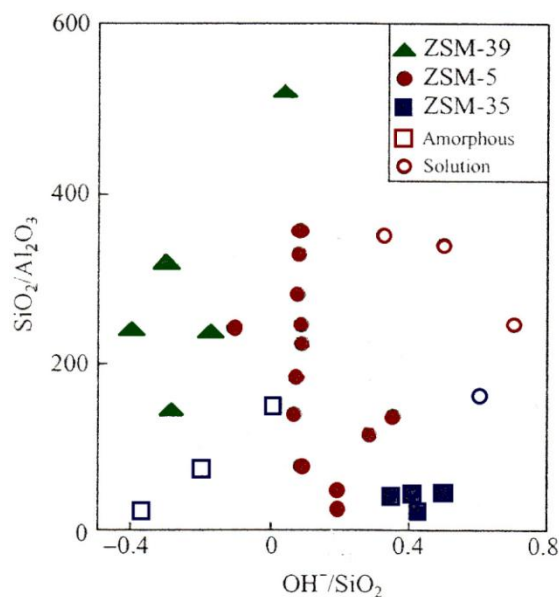
Figure 2-5: Effect of the amount of base and aluminium on the crystallisation of zeolites (H_2O/SiO_2=40, template/SiO_2 =0.68, 150°C, 40 h [27].

2.1.5.2 OH⁻ /Mineraliser

A mineraliser is used as a mineralising agent and it allows the dissolution and crystallisation of the less stable solid phase to a more stable solid in parent solution. Hydroxyl ions promote the solubility of silica by dissolution of amorphous silica particles. The basic environment (pH < 10) enhances crystal growth rates and shortens the nucleation period. Another anion F⁻, which is of a completely different nature, may work as a mineraliser. Fluoride anions act as hydroxyl ions, however, fluoride anions do not have an influence on the pH of the system [3, 15].

2.1.5.3 Cations sources

Generally, an alkali cation is used as a structure directing agent during the nucleation and/or crystal growth processes and at the same time balance the charge of the zeolite framework. The structure directing agent called the template can be divided into organic and inorganic types. Template cation creates a particular structure (initial building units) by organizing TO_4 in a tetrahedral formation around itself [4]. Alkali metal and alkaline earth hydroxides are the main sources for inorganic cations. Templates are mostly applied in the synthesis of high silica zeolites such as ZSM-5 because of the limitation of variables that affect their

synthesis most commonly used are TPAOH and TPABR. This limitation arises because of the high Si/Al ratio and low alkali metal ion concentration which is particularly required of defect sites to balance the charge of the template [27].

2.1.5.4 Solvent sources

Water has a crucial role to play in zeolite synthesis. The main role for water molecules is the dissolution of all reactants in the presence of a mineraliser. Moreover, water is used to fill the void to stabilise the porous oxide framework. Therefore, water molecules interacting with the template are part of template effect in crystal growth [28].

2.1.5.5 Silica and alumina sources

Si–source has a significant effect on crystal form and the chemical properties of zeolite. In comparison, Al–source is not as critical as the Si- source. Mostly, Al–source is pure and consists of small particles, while impurities in the Si-source may have an effect on the crystallization of particular zeolites [4]. Some of more common Si-sources and Al sources are listed in **Table 2-3**.

Table 2-3: Frequently used silicon source and aluminium source reactants.

Silicon sources	Aluminium sources
Water glass($Na_2O.xSiO_2$)	Sodium aluminate (Na_2AlO_2)
Sodium silicate ($Na_2SiO_3.H_2O$)	Boehmite (AlOOH)
Silica gel (Ludox-AS- 40)	Aluminium hydroxide ($Al(OH)_3$)
Colloidal sol (Ludox-HS-40)	Aluminium isopropoxide ($Al(O-C_3H_7)$)
Fume silica (Aerosil-200)	Aluminium nitrate ($Al(NO_3)_3.9H_2O$)
Ethyl orthosilicate (TEOS), Methyl orthosilicate (TMOS)	Metallic aluminium

2.1.5.6 Temperature

Generally, temperature has a significant influence on the crystallisation process. However, temperature has less of an effect on the nucleation rate than the crystal growth rate. As a result, rises in the synthesis temperature of hydrothermal synthesis produce large crystal sizes instead of small crystals [8].

2.1.6 Zeolite and Catalysis

Zeolite properties make them suitable to play an essential role in catalysis. The unique properties of zeolites are based on the fact that the basic unit of zeolites consist of four oxygen ions which are filled with Al^{3+} and Si^{4+} ions in different ratios of Si/Al; connecting these tetrahedrons through apical oxygen atoms [6].

Zeolite properties can be represented by: firstly, zeolites which are highly crystalline with well–defined structures. The zeolite framework consists of cavities which are occupied by water molecules and alkaline ions, for instance Na^+. Alkaline ions are used to balance the aluminosilicate charge in the zeolite framework. Pore openings (range from 0.3 nm to 0.1 nm in diameter) and high void dimensions (internal surface area is large (>500 m^2 g^{-1})) are responsible for catalytic shape selectivity. Essentially, the cavities and pore openings govern which molecules are diffused and which are excluded. Therefore, zeolites are referred to as molecular sieves [29].

Secondly, zeolite has the ability to easily exchange ions within the cavities with numerous alternative ions. Ion exchange can be applied to disperse metal such as Pt on a zeolite. It is worthy of note that ion exchange reaction is involved in both bulk phase reaction and surface reaction. In addition, ion exchange is a stoichiometric reaction [12].

Thirdly, zeolite is a super acid catalyst, about 100 times more acidic than amorphous silica-alumina [12]. Al content in the zeolite framework has a significant effect on zeolite acidity. Zeolite acidity can be modified by ammonium-ion exchange followed by calcination and dealumination [30].

2.1.6.1 Shape selectivity

In 1960, Weisz and Frilette were the first to observe the shape selectivity of zeolites [31]. The reactions within internal channels or cavities in zeolite pores are restricted by the size of the reactants, products or transition states (intermediate). The significance of the shape selectivity phenomenon in zeolite results from the dimensional pore systems for the zeolite framework; thus, there are three mechanisms of molecules shape selectivity technology:

Reactant selectivity

This is illustrated in **Figure 2-6** where a straight hydrocarbon chain can enter the zeolite pore, whereas the branched chain is large with respect to the dimensions of the pore openings. When the reactant diffuses towards the active sites the reactions occur. The two following mechanisms (product or transition state selectivity) can occur inside the cavities.

Product selectivity

This happens when undesired products are too large and cannot diffuse out of the cavities, whereas the desired ones can. These large molecules are either converted into smaller molecules or block the pores deactivating the catalyst. This is illustrated in **Figure 2-6**:

Transition state selectivity

This occurs when transition state molecules cannot form in the cavities because they are restricted by the size of the cavities **Figure 2-6.**

a) REACTANT SELECTIVITY

CH₃OH +

b) PRODUCT SELECTIVITY

c) TRANSITION STATE SELECTIVITY
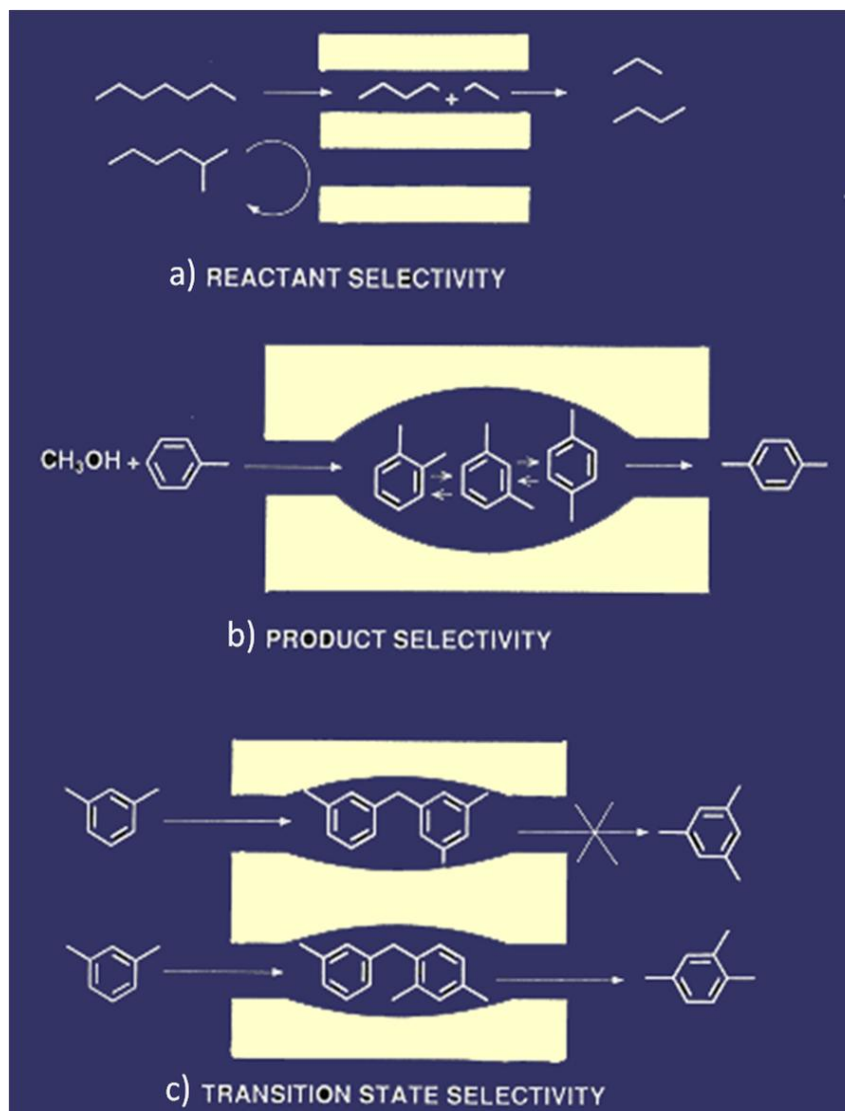
Figure 2-6: Shape selectivity in zeolites modified from [32].

2.1.6.2 Ion exchange

Zeolite is composed of a tetrahedral Si and Al framework and because of the shared O atoms there is a negative charge associated with aluminium (i.e. AlO_2^-) bearing negative charges and these charges are neutralized by ions of the opposite sign such as alkali e.g. Na^+, K^+ cations, alkaline earth cations (Mg^+, Ca^+), and others including NH_4^+, H_3O^+ (H^+), and rare–earth noble metal cations. These cations can easily replace in the ion exchange process. Ion exchange is used to introduce different cations into zeolite either to change the acidity of the catalyst or to distribute homogeneously small amounts of transition and/or platinum group metal ions on the zeolite surface to form dual functional catalysts. Since 1858, when it

was first established that the natural zeolite could reverse cation exchange, there have been numerous studies exploring this phenomenon [15, 33].

2.1.6.3 Acidity

Acidity is an intrinsic property of zeolites. The acidic properties arise from zeolite's ability to accept a pair of electrons, which occurs after high temperature treatments (Lewis acid sites) and donate a proton (Brönsted acid sites) as shown in **Figure 2-7** [27].
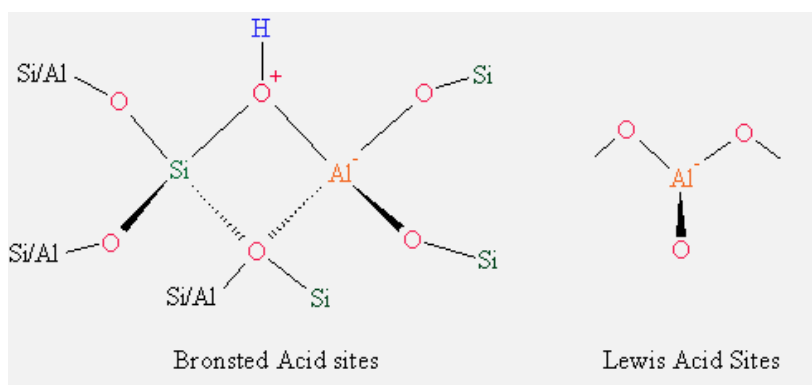
Figure 2-7: Brönsted and Lewis acid sites in zeolites.

This can be explained by the fact that the tetravalent framework cation Si^{4+} replaces a lower charge cation Al^{3+} and this give a negative net charge for the zeolite framework which is neutralized by a positive ion. The Brönsted acid sites are attributed to hydroxyl (Si-O-H), whereas Lewis acid sites are produced when the structure of the zeolite is heated and the water in the zeolite framework is driven off, followed by the condensation process (**Figure 2-8**). Furthermore, it is necessary to determine the nature of acid sites, their concentration and their strength. The density of Brönsted acid sites is attributed to the Si/Al ratio. The strength of the acid sites is dependent on the acid strength distribution and the location within the crystalline framework [34].
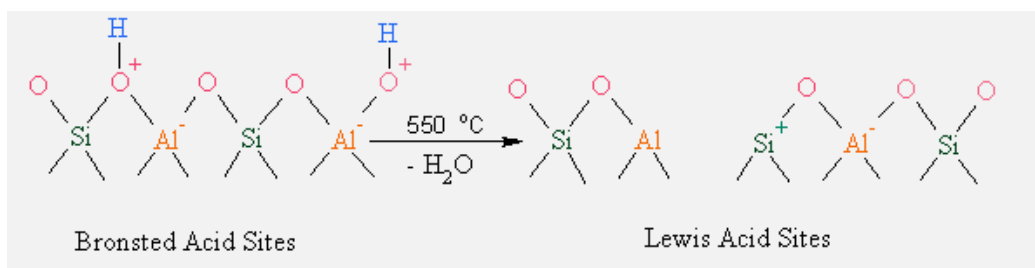
Figure 2-8: Mechanism to form Lewis acid sites adapted from [35].

2.1.7 Zeolite Y

In 1842, the French geologist, Damoure, discovered zeolite Y (Faujasite). Zeolite Y has since become the most important cracking catalyst because it has a high acid strength, large pore size, high activity and stability at higher temperatures due to the higher Si/Al ratio. Also, zeolite Y has the ability to increase the yield of gasoline and diesel fuel from crude oil feedstock by cracking heavy paraffins into gasoline grade naphtha. Furthermore, by using platinum/palladium support, zeolite Y is used in hydrocracking units to increase the aromatic content of reformulated refinery products used in acidic forms [29, 35].

The framework topology of FAU–type belongs to the sodalite family (**Figure 2-9**) where sodalite cages create a supercage with tetrahedrally-oriented 12-ring pore openings and a 3-dimensional channel system along <110> in the FAU framework type [36].

FAU zeolite can be synthesised in a narrow range of Si/Al ratio typically between 1.5 and in excess of 3 [30]. Zeolite Y is synthesised from alumina sources and silica sources; all reactants are dissolved in a basic solution to give a gel. The gel is crystallised under hydrothermal conditions (>100°C). The synthesis of the zeolite is in Na^{+} form and it has to be converted in the acid form by ion exchange with ammonium and calcination to remove the ammonium ion.
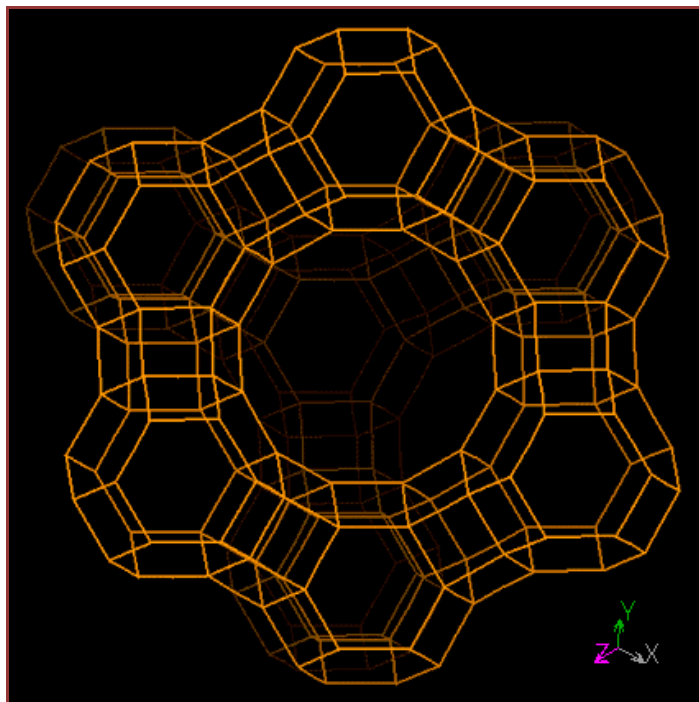
Figure 2-9: The FAU framework type and its supercage [37].

2.1.8 Zeolite ZSM-5

In 1972, the Mobil Oil Company discovered the MFI-type zeolite, known as zeolite ZSM-5 and has a wide range of industrial applications thanks to the zeolite shape selectivity. These applications vary depending on the use of the ZSM-5 in adsorption processes to heterogeneous catalysis. In catalysis ZSM-5 is used in different processes such as Fluid Catalytic Cracking (FCC), alkylation of aromatics, xylene isomerisation and the disproportionation of toluene [28, 31].

The MFI framework consists of pentasil units (see **Figure 2-10**). These units consist of 12 T atoms. Each 12 T atom unit contains two 5-1 units that are joined to one another to form pentasil chains which are connected to mirror image pentasil chains via oxygen bridges to form corrugated sheets with 10-rings [36].

MFI-type zeolite offers great flexibility by allowing a change in the degree of freedom from hydrophilic to hydrophobic, due to the possibility of varying the Si/Al ratio within 10-∞. Generally, ZSM-5 is synthesised at high temperature (up to 170°C) in autoclaves. The reaction mixture contains silicon source, aluminium source and the template is dissolved in a basic solution to give a gel. The reaction

takes place under hydrothermal conditions to produce zeolite. The synthesised zeolite is then treated by ion exchange and calcination to obtain the desired acid catalyst [37].
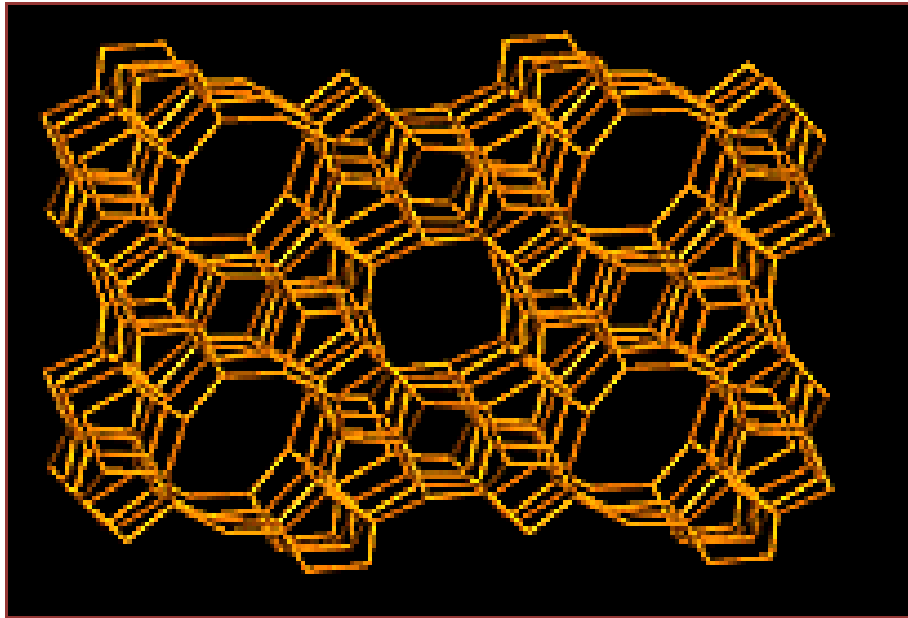
Figure 2-10: MFI Framework type with pentasil chains [38].

2.2 Synthesis of coated zeolites and potential use

2.2.1 Introduction

In recent decades, there has been considerable progress in the improvement of zeolite coating synthesis methods and in controlling synthesis conditions [38]. The zeolite coatings have unique properties compared to pelleted zeolites, providing mechanical strength, high thermal resistance, low pressure drop with high flow rate, a narrow residence time distribution and high heat and mass transfer rates [39-43].

Zeolite coatings have unusual properties which make them suitable for wider industrial applications. There are many potential uses for zeolite coatings such as exhaust gas treatment, catalytic distillation, separation and catalytic membranes [44-46].

Generally, zeolites are synthesised by hydrothermal treatment of synthesis gel which contains an aluminium source, an alkali source and a silica source. The main parameters that determine the type of zeolite are the mixture composition and preparation condition. These include the synthesis temperature and duration of synthesis. Usually, there are two basic synthesis methods by which zeolite film coatings can be introduced on support surfaces. These methods are in-situ and dip-coating techniques, while zeolite coating catalysts can be produced using different types of supports and zeolite types.

Hydrophilic and hydrophobic supports are the most common supports used in the synthesis of zeolites. **Table 2-4** shows the supports currently used in the preparation of zeolite coatings with their chemical and physical properties. Hydrophilic supports are the preferred type of support because the properties ensure a good wetting is reached for the zeolite synthesis mixture and they possess a good chemical and/or physical interaction potential with zeolites. In contrast, hydrophobic supports, such as carbon disks, have a poor interaction with zeolite and because of this, it is necessary to add a binder phase to improve compatibility in the system [47, 48].

Metallic supports offer the following advantages: higher mechanical resistance and thermal conductivity, the flexibility to design thinner walls which makes it easier to achieve higher cell densities and lower pressure drop which is useful in micro-reactors. The metallic support has a significant impact on the progress of applications in industrial fields [49]. Thus, the objective of this work is to focus on the coating of the metallic surface with a thin film of zeolite and characterisation and then testing of the final catalyst.

Table 2-4: Various types of support with their physical and chemical properties [39].

Support material	Nature	Surface area[a]	relative stability at high pH	Amount of surface OH-groups[b]
Spheres / extrudates:				
α- Al_2O_3	hydrophobic	high	+-	low
γ - Al_2O_3	hydrophilic	high	-	high
Single crystal wafers:	hydrophilic	low	-	high
Si, TiO	hydrophilic	low	+	medium
Sapphire (α- Al_2O_3)	hydrophobic	low	+	low
Plates/disks:				
Stainless steel	hydrophilic	low	+	high
Quartz	hydrophilic	low	-	high
Vitreous glass	hydrophilic	low	-	high
Pressed carbon	hydrophobic	high	+	low
Foams:				
α- Al_2O_3	hydrophilic	high	+	low
Fibers:				
Carbon	hydrophobic	medium	+	low
Vegetable	hydrophilic	medium	+	medium
Inorganic	hydrophilic	medium	+	high
Inert:				
Gold	hydrophobic	low	+	low
Teflon	hydrophobic	low	+	low

[a] Low: < 1 m^2 g^{-1} ; medium: l-10 m^2 g^{-1}; high: > 10 m^2 g^{-1}.
[b] Low**:** $< l$ OH.nm^{-2} ; medium:l-2.5 OH nm^{-2}: ; high: >2.5 OH nm^{-2}.

Moreover, all kinds of supports should be cleaned (pre-treated) before they can be coated with zeolite. For instance, the pre-treatment of the metal supports before synthesis or dip-coating processes was significantly improved the wetting of metal supports by enhancing physical and chemical interactions between the metal surface and seeding layer [39]. The different ways of pre-treating samples include: high temperature surface oxidation [50], acid etching and the deposition of precursor layers [51].

2.2.2 Synthesis of Zeolite Coatings on Metallic Supports

Currently there is a growing interest in metallic supports due to their ability to cope with higher operating temperatures and their efficiency in reducing emissions from industrialised power plants and motor vehicles which are major contributors to environmental pollution.

The first step before the synthesis of a thin film of zeolite on the metal surface is pre-treating the metal support. Then, the pre-treated support will be coated by zeolite and this can be achieved using an in-situ synthesis method or dip coating method. The latter is carried out by dipping the support in zeolite slurry which is followed by evaporation of the liquid. This ensures that crystals are formed in solution and then the crystals are deposited onto the support surface. In contrast, the in-situ synthesis is achieved by crystallization of zeolite film on the support. The support should be fixed in the zeolite synthesis mixture and the crystal should be grown from the support surface, not from solution. The following sections emphasise the pre-treatment technology of the support and synthesis and **Table 2-5** presents a selection of the empirical research conducted in this area.

This study will focus on the in-situ synthesis of zeolites Y and ZSM-5 on aluminium alloy (FeCrAlloy).

Table 2-5: Summary of the synthesis of zeolite coating on metal supports.

References	Support type	Synthesis methods	Zeolite type	Support structure
Juan M. Zamaro [52]	FeCrAlloy	Secondary synthesis	Mordenite	Monolithic
Juan M. Zamaro [53]	FeCrAlloy	Direct Synthesis, Secondary synthesis	In-mordenite	monolithic monoliths
Juan M. Zamaro [48]	FeCrAlloy	Direct Synthesis, Secondary synthesis	ZSM-5	foils
Mario Montes [54]	FeCrAlloy	Wash coating with additives (PVOH, colloidal silica Synthesis, Secondary synthesis)	ZSM-5	monolithic
Lucio Bonaccorsi [51]	AISI 304 stainless steel	washcoating Synthesis (Direct Synthesis, Secondary synthesis	zeolite 4A	foil
E. Włoch [55]	FeCrAlloy	Coating	ferrierite	FeCrAlloy foil
Ronnie Munoz& Yushan Yan [56]	Al 2024-T3	Coatings by a three-step synthesis method	zeolite Y ZSM-5	large sheet foil

2.2.2.1 Support pre-treatments

The crucial point in the production of structural catalysts on metallic supports is the creation of a thin porous layer on the support surface. FeCrAlloy has the ability to withstand arduous oxidative and corrosive environmental conditions up to temperatures such as 1300°C by forming a thin film of alumina whisker crystallites on its surface [48, 57]. This film is then beneficial in the coating process.

The pre-treatment of FeCrAlloy is important for the removal of contamination and improving interaction between the support and the synthesis surrounding [58]. The first step in pre-treatment is cleaning the metallic support either by immersing the support into a vessel with acetone in an ultrasonic bath before washing it with water [52] or by merely putting the metal support in an ultrasonic water bath [48].

The pre-treatment of the metallic support can be used to create roughness on the surface of the metal and their defects might help the zeolite nucleation process on the surface during synthesis or could trap seeds on the surface of the metal. Pre-treatment can be classified into physical treatments, chemical treatments, thermal treatments and anodic oxidation and a good review is given by Meille [59].

Physical treatment can be achieved by polishing the metal surface or by applying acid leaching. Acid leaching may be conducted by coating the metal surface with a binder (cationic polymer) to reverse the charge of the surface of the support [48, 56]. The anodic oxidation is applied to obtain a porous alumina layer at the surface of the support containing aluminium by applying a direct current to electrolyte in contact with the aluminium surface [59].

Finally, thermal oxidation is carried out to increase the catalyst adhesion by forming a scale of aluminium oxide on the FeCrAlloy surface. Numerous studies have reported on the oxidation of the FeCrAlloy support before applying the coating layer of zeolite in the pre-treatment stage by exposure to the FeCrAlloy at high temperature ranges within 900°C for 22 h [48, 52-54, 60, 61].

2.2.2.2 Slurry/dip coating method

The slurry/dip coating method is based on the deposition of a thin layer of synthesised zeolite onto the surface of the support. However, the main difference between these two processes is that the dip coating method consists of adding a binder which acts as a glue to adhere the zeolite crystal onto the surface of the support, whereas the slurry-coating method does not require a binder to be added [62].

There are crucial factors that affect the coating process. These factors are the concentration of the ingredients, the size of the suspended particles, the nature of the surface being coated, and desired thickness of the coating layer [59]. In the coating technique, the support is immersed in a solution containing synthesised zeolite crystals, the binder in the dip coating case, a solvent, and other additives. This is followed by drying the surface of the support and then calcination. **Figure 2-11** illustrates the schematic diagram for the synthesis. The dip/slurry coating is used for coating ZSM-5 and Beta on the ceramic and metallic for environmental applications [59].
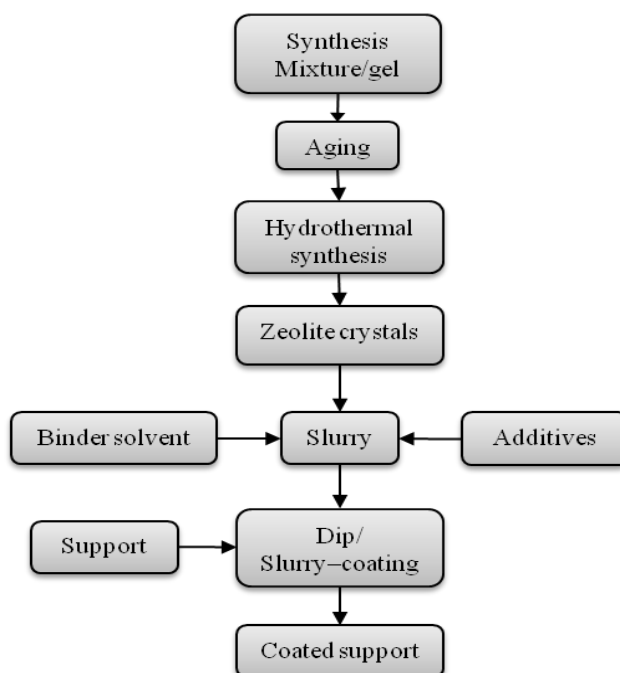
Figure 2-11: Dip/Slurry Coating Process Schematic.

2.2.2.3 Direct In-situ Synthesis

In the in-situ method (growth method), the pre-treatment support is introduced directly into the precursor synthesis mixture under hydrothermal operation conditions to merge the deposition/adhesion of zeolite crystals on the support with the zeolite crystallisation in one step [63]. In spite of the complexity involved, this method forms a thin layer with a strong adhesion to the support because the hydrothermal synthesis of the zeolite crystal and the growth progressing of the film occur in one step [52].

The mechanism of the in-situ synthesis onto the support has not been fully understood until now. In 1997, Nakazawa [64] suggested that small nano-sized particles grow either on the surface of the gel (which is the first layer formed on the support surface) or within the gel. Then the ZSM-5 crystals are formed on the support surface by aggregation or growth of the particle size over time. The gel layer which is formed on the support surface is considered the initial step where the nucleation and growth of the crystals occurring with the presence of Si-sources and template [65]. Generally, there are two in-situ techniques to grow zeolite film on the support surface: direct and secondary zeolite growth [66].
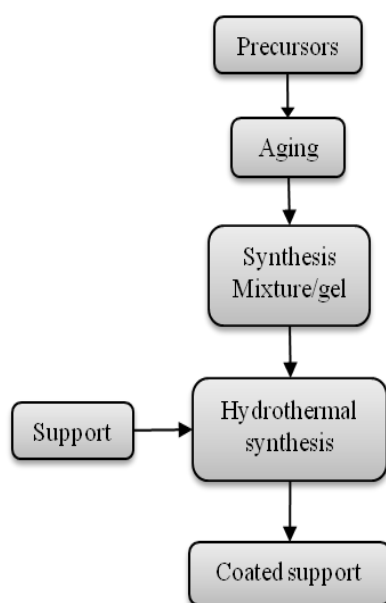
Figure 2-12: Direct hydrothermal method.

The difference between the direct and secondary growth is that in the latter the first step for synthesis is depositing small zeolite crystals on the support surface and this leads to the binding and growth of zeolite seeds on the support in the secondary growth solution, where the secondary crystallisation occurs without forming a gel [67]. **Figure 2-12** and **Figure 2-13** illustrate the scheme for the two techniques:
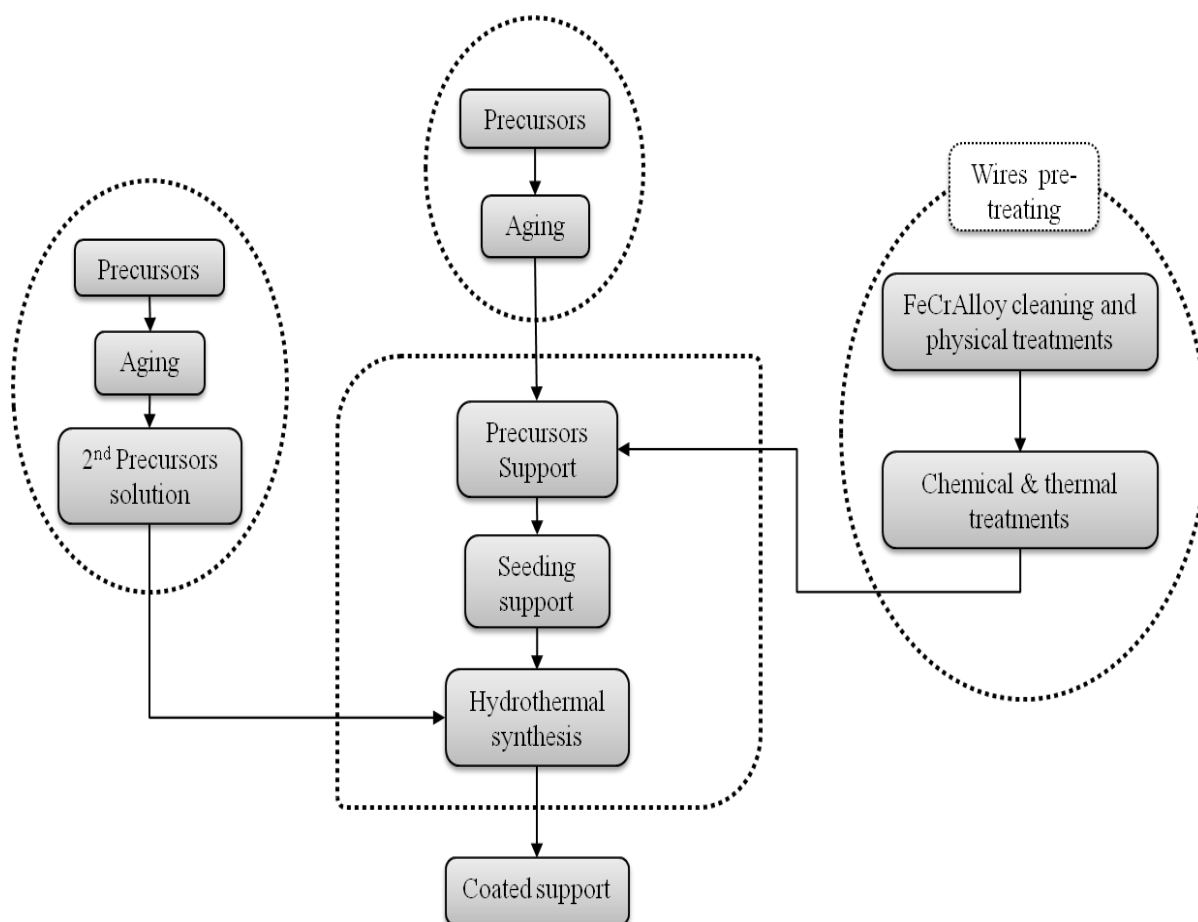
Figure 2-13: Secondary in-situ method.

2.2.3 Application of the Coating Zeolite on the Support

Coating a zeolite on the support significantly extends the range of the zeolite application in industrial fields. The most common application fields are monolithic reactors [68], sensors [69], chromatography [70], membrane reactors [71], adsorption and separation [66]. This thesis will develop ZSM-5 and Y zeolite catalysts on FeCrAlloy wires by in–situ synthesis. A list of catalyst applications of structured zeolite-coated supports is presented in **Table 2-7**:

Table 2-7: Applications for coated zeolite on different support [68].

Application	Support	Zeolite type
$DeNO_X$ SCR with ammonia	Cordierite	Fe-ZSM-5
Automotive emission control	Cordierite, α- Al_2O_3 SiC foams	ZSM-5, Beta
TWC	Cordierite	Pt-Beta
N_2O decomposition and SCR	Extruded Fe-ZSM-5, Cordierite	Fe-ZSM-5 Fe-ZSM-5
Benzene hydroxylation to phenol	Stainless-steel plates Catalyst packing	ZSM-5 ZSM-5
HC cracking	Cordierite	ZSM-5
Acylation of aromatics	Cordierite	Beta, Y
Fiedel-Crafts	SiC foam	Beta
MTO conversion	SiC foam	ZSM-5

References

1. *University of Portsmoth, Centre for Molecular Design (CMD),Molecular Modelling of Zeolites*, [Accessed 2012] Available from: http://www.port.ac.uk/ esearch/cmd/research/zeolitemodelling/.

2. Breck, D.W., *Zeolite molecular sieves: structure, chemistry, and us,* Vol. 245. 1974: p. 25, Wiley-Interscience New York.

3. Bekkum, H.van., *Introduction to zeolite science and practice*, Vol. 137. 2001, Elsevier Science.

4. van Bekkum, H., E.M. Flanigen, and J. Jansen, *Introduction to zeolite science and practice*, Vol. 58. 1991.

5. Milton, R.M., *Molecular Sieve Science and Technology,* Zeolite synthesis, 1989, US Patent 3,308,069. **398**.

6. Čejka, J. and H. van Bekkum, *Zeolites and ordered mesoporous materials: progress and prospects: the 1st FEZA School on Zeolites, Prague, Czech Republic, August 20-21, 2005*. Vol. 157. 2005: Elsevier Science.

7. Oaspnta, R.L.W., *Catalytic composition of a crystalline zeolite*, 1967, US Patent 3,308,069.

8. Barrer, R.M., *Hydrothermal chemistry of zeolites*, Vol. 109. 1982: Academic Press London.

9. Shelef, M., *Selective catalytic reduction of NO_x with N-free reductants,* Chemical Reviews, 1995. **95**(1): p. 209-225.

10. Eng, J. and C.H. Bartholomew, *Kinetic and Mechanistic Study of NO_x Reduction by NH_3 over H-Form Zeolites,* Journal of catalysis, 1997. **171**(1): p. 27-44.

11. Akah A, Nkeng G, and Garforth.A.T., *The role of Al and strong acidity in the selective catalytic oxidation of NH_3 over Fe-ZSM-5,* Applied Catalysis B-Environmental, 2007. **74**(1-2): p. 34-39.

12. Richardson, J.T., *Principles of catalyst development*. 1989: p. 87.

13. Bartholomew, C. and R.J. Farrauto, *Fundamentals of industrial catalytic processes,* Recherche, 2005. **67**.

14. Richardson, J.T., *The effect of faujasite cations on acid sites,* Journal of catalysis, 1967. **9**(2): p. 182-194.

15. Ertl, G., H. Knözinger, and J. Weitkamp, *Preparation of solid catalysts.* 1999:p. 4-20.

16. Cundy, C.S. and P.A. Cox, *The hydrothermal synthesis of zeolites: Precursors, intermediates and reaction mechanism,* Microporous and Mesoporous Materials, 2005. **82**(1): p. 1-78.

17. Occelli, M.L. and H. Kessler, *Synthesis of porous materials: zeolites, clays, and nanostructures*, Vol. 69. 1997.

18. Cook, J.D. and R.W. Thompson, *Modeling the effect of gel aging,* Zeolites, 1988. **8**(4): p. 322-326.

19. Hamidi, F., A. Bengueddach, F. Di Renzo, and F. Fajula, *Control of crystal size and morphology of mordenite,* Catalysis Letters, 2003. **87**(3): p. 149-152.

20. Kacirek, H. and H. Lechert, *Growth of the zeolite type NaY,* The Journal of Physical Chemistry, 1975. **79**(15): p. 1589-1593.

21. Tsitsishvili, G., T.G. Andronikashvili, G. N. Kirov, and L.D.Filizova, *Natural zeolites*, 1992.

22. Barrer, R., *Syntheses and reactions of mordenite,* Journal of the Chemical Society, 1948(0): p. 2158-2163.

23. Milton, B.R.M., *Crystalline zeolite B*. 1961, US Patent 3,008,803.

24. Barrer, R. and P. Denny, *201. Hydrothermal chemistry of the silicates. Part IX. Nitrogenous aluminosilicates,* J. Chem. Soc., 1961(0): p. 971-982.

25. Lin, C.H., S.L. Wang, and K.H. Lii, *A Novel Porous Gallium Phosphate Containing 24-Ring Channels,* Journal of the American Chemical Society, 2001. **123**(19): p. 4649-4650.

26. Xu, R., *Chemistry of zeolites and related porous materials: synthesis and structure*, 2007.

27. Lobo, R.F., I. Stacey, and R.C. Medrud, *Synthesis and Rietveld refinement of the small-pore zeolite SSZ-16,* Chemistry of materials, 1996. **8**(10): p. 2409-2411.

28. Thomas, J.M. and W.J. Thomas, *Principles and practice of heterogeneous catalysis*, 1997.

29. Flanigen, E.M., *Molecular Sieve Materials: Their Synthesis, Properties, and Characterizations,* Catalysis Reviews Science and Engineering, 1984. **26**(3-4): p. 483-483.

30.   Heinemann, H., *Technological applications of zeolites in catalysis,* Catalysis Reviews—Science and Engineering, 1981. **23**(1-2): p. 315-328.

31.   Weisz, P. and V. Frilette, *Intracrystalline and molecular-shape-selective catalysis by zeolite salts,* The Journal of Physical Chemistry, 1960. **64**(3): p. 382-382.

32.   Mark E. Davis Research Group. Catalysis August 15, 2012 [Accessed 2012] Available from: http://www.che.caltech.edu/groups/med/catalysis.html.

33.   Yamazaki, S. and K. Tsutsumi, *Synthesis of a mordenite membrane on a stainless-steel filter and polytetrafluoroethylene plate substrates,* Microporous Materials, 1995. **5**(4): p. 245-253.

34.   Stöcker, M., *Gas phase catalysis by zeolites,* Microporous and Mesoporous Materials, 2005. **82**(3): p. 257-292.

35.   Thomas, J.M. and W.J. Thomas, *Principles and practice of heterogeneous catalysis*, 1997.

36.   Shan, Z., W.E.J. Van Kooten, O.L. Oudshoorn, J.C. Jansen, H.Van Bekkum, C.M. Van Den Bleek, and H.P.A. Calis,*Optimization of the preparation of binderless ZSM-5 coatings on stainless steel monoliths by in situ hydrothermal synthesis,* Microporous and Mesoporous Materials, 2000. **34**(1): p. 81-91.

37.   Mies, M., J.L.P. Van Den Bosch, E.V. Rebrov, J.C. Jansen, M. De Croon, and J.C. Schouten, *Hydrothermal synthesis and characterization of ZSM-5 coatings on a molybdenum support and scale-up for application in micro reactors,* Catalysis Today, 2005. **110**(1): p. 38-46.

38.   Mintova, S., B.J. Schoeman, V. Valtchev, and J. Sterte, *ZSM-5 films prepared from template free precursors,* Advanced Material, 1997. **9**: p. 585.

39.   Jansen, J.C., J.H. Koegler, H.Van Bekkum, H.P.A. Calis, C.M. Van Den Bleek, F. Kapteijn, J.A. Moulijn, E.R. Geus, and N. Van der Puil, *Zeolitic coatings and their potential use in catalysis,* Microporous and Mesoporous Materials, 1998. **21**(4-6): p. 213-226.

40.   Mies, M.J.M., J.L.P. Van Den Bosch, E.V. Rebrov, J.C. Jansen, M.De Croon, and J.C. Schouten, *Hydrothermal synthesis and characterization of ZSM-5 coatings on a molybdenum support and scale-up for application in micro reactors,* Catalysis Today, 2005. **110**(1-2): p. 38-46.

41. Vaughan, D.E.W., *Zeolites as selective adsorbents,* Chemcail Engineering Progress, 1988. **84**: p. 25-31.

42. Noack, M., P. Kölsch, R. Schäfer, P. Toussaint, and J. Caro, *Molecular Sieve Membranes for Industrial Application: Problems, Progress, Solutions,* Chemical Engineering & Technology, 2002. **25**(3): p. 221-230.

43. Xu, X., Y. Bao, C. Song, W. Yang, J. Liu, and L. Li, *Microwave-assisted hydrothermal synthesis of hydroxy-sodalite zeolite membrane,* Microporous and Mesoporous Materials, 2004. **75**(3): p. 173-181.

44. Kiwi-Minsker, L. and A. Renken, *Microstructured reactors for catalytic reactions,* Catalysis Today, 2005. **110**(1-2): p. 2-14.

45. Louis, B., L. Kiwi-Minsker, P. Reuse, and A. Renken, *ZSM-5 coatings on stainless steel grids in one-step benzene hydroxylation to phenol by N_2O: Reaction kinetics study,* Industrial & engineering chemistry research, 2001. **40**(6): p. 1454-1459.

46. Wan, Y.S.S., J. L. H. Chau, A. Gavriilidis, and K. L. Yeung, *Design and fabrication of zeolite-based microreactors and membrane microseparators,* Microporous and Mesoporous Materials, 2001. **42**(2-3): p. 157-175.

47. Van der Vaart, R., H. Bosch, K. Keizer, and T. Reith, *Preparation of an MFI zeolite coating on activated carbon,* Microporous Materials, 1997. **9**(3-4): p. 203-207.

48. Zamaro, J.M., M.A. Ulla, and E.E. Miró, *ZSM5 growth on a FeCrAl steel support. Coating characteristics upon the catalytic behavior in the NO_x SCR,* Microporous and Mesoporous Materials, 2008. **115**(1-2): p. 113-122.

49. Nerea Burgos, M.P.a.M.M., *Preparation of Al_2O_3/Al monoliths by anodisation of aluminium as structured catalytic supports,* Journal of Materails Chemistry, 2003. **13**: p. 1458 - 1467.

50. Kadiri, H.E., R. Molins, Y. Bienvenu, and M. F. Horstemeyer, *Abnormal High Growth Rates of Metastable Aluminas on FeCrAl Alloys,* Oxidation of Metals, 2005. **64**(1): p. 63-97.

51. Bonaccorsi, L. and E. Proverbio, *Synthesis of thick zeolite 4A coatings on stainless steel,* Microporous and Mesoporous Materials, 2004. **74**(1-3): p. 221-229.

52. Zamaro, J.M., M.A. Ulla, and E.E. Miró, *Growth of mordenite on monoliths by secondary synthesis: Effects of the substrate on the coating structure and catalytic activity,* Applied Catalysis A: General, 2006. **314**(1): p. 101-113.

53. Zamaro, J.M., M.A. Ulla, and E.E. Miró, *Improvement in the catalytic performance of In-mordenite through preferential growth on metallic monoliths,* Applied Catalysis A: General, 2006. **308**: p. 161-171.

54. Eleta, A., P. Navarro, L. Costa, and M. Montes, *Deposition of zeolitic coatings onto Fecralloy microchannels: Washcoating vs. in situ growing,* Microporous and Mesoporous Materials, 2009. **123**(1): p. 113-122.

55. Wloch, E., A. Łukaszczyk, Z. Żurek, and B. Sulikowski, *Synthesis of ferrierite coatings on the FeCrAl substrate,* Catalysis Today, 2006. **114**(2-3): p. 231-236.

56. Munoz, R., D. Beving, Y. Mao, and Y. Yan, *Zeolite Y coatings on Al-2024-T3 substrate by a three-step synthesis method,* Microporous and Mesoporous Materials, 2005. **86**(1-3): p. 243-248.

57. Ltd, G. *Material Information-FeCrAlloy*, [Accessed 2010] Available from: http://www.goodfellow.com/E/Fecralloy-Iron-Chromium.html.

58. Yuranov, I., A. Renken, and L. Kiwi-Minsker, *Zeolite/sintered metal fibers composites as effective structured catalysts,* Applied Catalysis A: General, 2005. **281**(1): p. 55-60.

59. Meille, V., *Review on methods to deposit catalysts on structured surfaces,* Applied Catalysis A: General, 2006. **315**: p. 1-17.

60. Camra, J., E. Bielańska, A. Bernasik, K. Kowalski, M. Zimowska, A. Białas, and M. Najbar, *Role of Al segregation and high affinity to oxygen in formation of adhesive alumina layers on FeCr alloy support,* Catalysis Today, 2005. **105**(3-4): p. 629-633.

61. Seo, Y.-S., S.-P. Yu, S.-J. Cho, and K.-S. Song, *The catalytic heat exchanger using catalytic fin tubes,* Chemical Engineering Science, 2003. **58**(1): p. 43-53.

62. Stöcker, M., H.G. Karge, J.C. Jansen, and J. Weitkamp, *Advanced zeolite science and applications*, Vol. 85. 1994: p. 653: Access Online via Elsevier.

63. Okada, K., Y. Kameshima, and C.D. Madhusoodana, *Preparation of zeolite-coated cordierite honeycombs prepared by an in situ crystallization method,* Science and Technology of Advanced Materials, 2004. **5**(4): p. 479-484.

64. Nakazawa, T., M. Sadakata, and T. Okubo, *Early stages of MFI film formation,* Microporous and Mesoporous Materials, 1998. **21**: p. 325-332.

65.   Clet, G., J.A. Peters, and H. van Bekkum, *Key Role of the Interface Gel−Support in the Synthesis of Zeolitic Coatings,* Langmuir, 2000. **16**(8): p. 3993-4000.

66.   Caro, J., M. Noack, P. Kölsch, and R. Schäfer, *Zeolite membranes-state of their development and perspective,* Microporous and Mesoporous Materials, 2000. **38**(1): p. 3-24.

67.   Gouzinis, A. and M. Tsapatsis, *On the Preferred Orientation and Microstructural Manipulation of Molecular Sieve Films Prepared by Secondary Growth,* Chemistry of Materials, 1998. **10**(9): p. 2497-2504.

68.   Avila, P., M. Montes, and E.E. Miró, *Monolithic reactors for environmental applications: A review on preparation technologies,* Chemical Engineering Journal, 2005. **109**(1-3): p. 11-36.

69.   Vilaseca, M., J. Coronas, A. Cirera, A. Cornet, and J.R. Morante, *Use of zeolite films to improve the selectivity of reactive gas sensors,* Catalysis Today, 2003. **82**(1-4): p. 179-185.

70.   Delmas, M.P.F. and D.M. Ruthven, *Monolayer coating of capillary Chromatographic columns with small zeolite crystals,* Zeolites, 1996. **16**(4): p. 313-315.

71.   Xomeritakis, G., A. Abibi, and M. Dickson, *Growth, microstructure, and permeation properties of supported zeolite (MFI) films and membranes prepared by secondary growth,* Chemical Engineering Science, 1999. **54**(15-16): p. 3521-3531.

Chapter 3

Characterisation Techniques and Experimental Work

3.1 Introduction

This chapter divided into two main sections; first section is presenting the various characterisation techniques which have been performed on synthesised/modified structured and pelleted ZSM-5 and Y zeolites, the FeCrAlloy surface and the structured synthesised/modified zeolite catalyst to investigate the surface morphology and chemical composition.

Second section presenting an overview of the synthesis of zeolites Na–Y and Na–ZSM-5, the pre-treatment of FeCrAlloy wires intended to support the catalyst and the preparation of the structured zeolite grown onto the FeCrAlloy support wire.

3.2 Characterisation techniques

3.2.1 X-Ray Diffraction (XRD)

X-ray diffraction is used to determine the phase purity and material crystallinity for the synthesised of zeolite. When an X-ray beam hits an atom with a crystalline substance, the electrons surrounding the atoms start to oscillate with the same frequency as the incoming beam. The X-ray beam will leave the sample in different directions; the specific diffraction pattern can be obtained. Each crystalline material has a unique characteristic X-ray diffraction pattern which is used as a fingerprint to distinguish the zeolite type. The Structure Commission of International Zeolite Association (IZA) has gathered the ideal known zeolite structural diffraction patterns with other crystal data in the *Collection of Simulated XRD Powder Patterns for Zeolites* [1] as well as in the online database of the IZA [2, 3] .

In 1895, Roentgen discovered that invisible rays have the ability to penetrate opaque objects. In 1912, X-ray diffraction by crystals was established which led to a new method being developed for investigating the fine structure of matter [4]. Subsequently, Bragg developed a law which is the principle equation applied in X-ray powder diffraction:

$$n\lambda = 2d_{hkl} \sin\theta_{hkl}$$

Equation 3-1

Where n is an order of diffraction (n = 1, 2...), λ is the wavelength of the X-rays (λ = 1.54178 Å for CuKα where Kα is the required radiation to pass throughout the specimen), d_{hkl} is the spacing between the planes in the atomic lattice, θ_{hkl} is the angle between the incident ray and the scattering planes. The indices (hkl) of plane in crystal system are also called the Miller–Bravais indices [5] as shown in **Figure 3-1.**

The unit cell can also be determined for faujasite using **Equation 3-2**, because the faujasite crystal has cubic shape symmetry.
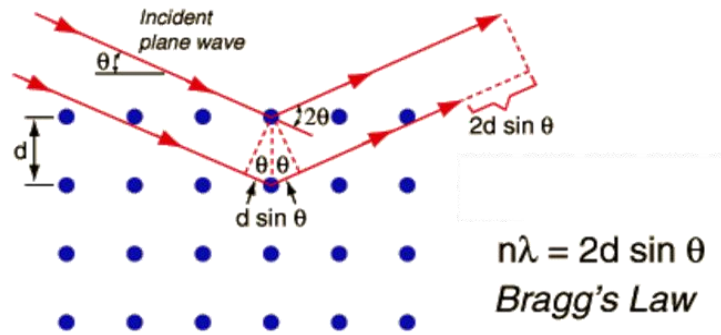
Figure 3-1: Diffraction of X-ray beam from crystal lattice [6, 7].

$$a_o = \lambda\sqrt{h^2 + k^2 + l^2} \Big/ 2\sin\theta$$

Equation 3-2

Breck and Flanigen [8], Fichtner-Schmittler [9] and Sohan [10] reported a relationship between the Si /Al ratio and the unit cell for zeolite X and Y [11]:

$$N_{Al} = 101.202\left(a_o\Big/\phi - 24.2115\right)$$

Equation 3-3

$$Si\Big/Al = \left(192\Big/N_{Al}\right) - 1$$

Equation 3-4

Where N_{Al} is the concentration of aluminium atoms in the lattice, a_o is the unit cell size. ϕ is the correction factor by Jorik [12] is approximately 1 for a synthesised faujasite and 0.9957 and 0.9966 for sodium X and Y zeolite. This

method is applicable for cubic zeolite and becomes more complex for non–cubic zeolites. The total number of SiO_4 and AlO_4 tetrahedra is equal to 192 in the unit cell.

The tested samples were compared with an X–ray diffractogram pattern of standard faujasite sample to evaluate the purities of the zeolite phase. **Table 3-1** and **Table 3-2** show the XRD–data for typical faujasite and MFI with CuKα radiation, and λ = 1.5418 Ȧ [3], where the distinguished angles are chosen carefully as a reference to compare with tested diffraction pattern samples.

The XRD instrument consists of the X–ray tube (**Figure 3-2**), a wavelength filter, a sample holder and an X–ray detector. The X–ray is produced by heating a filament in the cathode ray tube. Applied voltage will accelerate the electrons to the target sample. The characteristic X–ray spectra are produced when the ray penetrate the inner electron shell of the target sample.
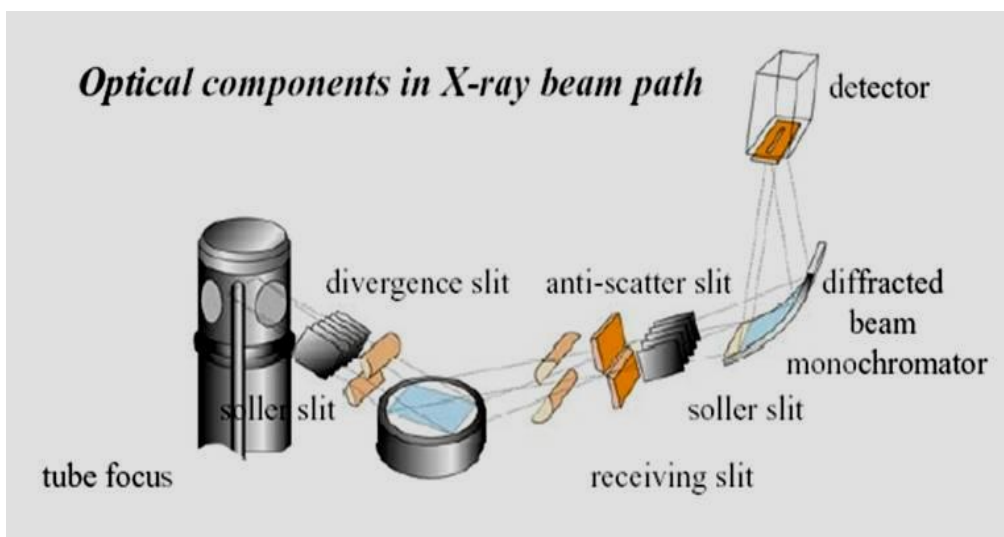
Figure 3-2: Schematic diagram of an X–ray diffractometer [13].

Table 3-1: XRD – data for standard Na-Y sample.

h	k	l	2θ (°)	d (Å)	I_{rel}
2	2	0	10.11	8.747	1.4
3	1	1	11.86	7.459	2.0
4	0	0	15.61	5.676	4.5
5	1	1	18.64	4.761	2.7
4	4	0	20.30	4.373	2.5
5	3	3	23.58	3.773	5.6
6	4	2	26.97	3.306	2.4
7	3	3	29.55	3.022	0.5
8	2	2	30.66	2.916	1.1
5	5	5	31.31	2.857	2.0
8	4	0	32.37	2.766	1.1
6	6	4	33.99	2.637	1.3
6	6	6	37.79	2.381	0.6

Table 3-2: XRD – data for standard ZSM-5, Si/Al = 11 sample.

h	k	l	2θ (°)	d (Å)	I_{rel}
1	0	1	7.95	11.126	68.4
0	2	0	8.89	9.950	36.8
2	1	0	9.89	8.943	4.70
1	2	1	11.93	7.417	10.4
0	0	2	13.23	6.692	6.80
3	0	1	14.83	5.973	10.9
2	0	2	15.93	5.563	6.20
2	1	2	16.55	5.358	1.80
0	4	0	17.83	4.975	5.60
0	1	3	20.40	4.353	7.10
4	2	1	20.95	4.241	8.90
4	3	0	22.25	3.995	5.60
3	3	2	23.11	3.849	4.00
1	3	3	24.45	3.640	39.7
4	3	2	25.97	3.430	13.6
3	5	2	29.34	3.044	11.9
0	5	3	30.09	2.970	9.10
10	0	0	45.29	2.002	5.80
4	3	6	46.64	1.948	2.90

Preparation of the powder samples to test is crucial for the diffraction results. The preparation of powder samples is performed by grinding the sample into fine particles (0.002 - 0.005 mm), packing the fine powder into a sample holder and assuring a flat smooth surface for the sample by pressing the sample into a sample holder using a glass slide [11].

A zeolite diffraction pattern (**Figure 3-3**) has factors that could be essential in the characterisation of zeolite. These factors are: the peak position which is represented by 2θ and related to the d-spacing of the diffraction planes; the width of a diffraction peak which is associated with the size of the crystallite; the peak which becomes broader as the size of the crystal decreases, background which represents highly crystalline zeolite with no amorphous material and the relative intensities of the peaks which is related to the level of zeolite crystallisation. The average degree of the crystallinity for the samples can be calculated using the following equation:

$$\text{Average degree of crystallinity\%} = \frac{\sum \text{Intensities of the peaks of zeolite sample}}{\sum \text{Intensities of the peaks of reference zeolite sample}} \times 100$$
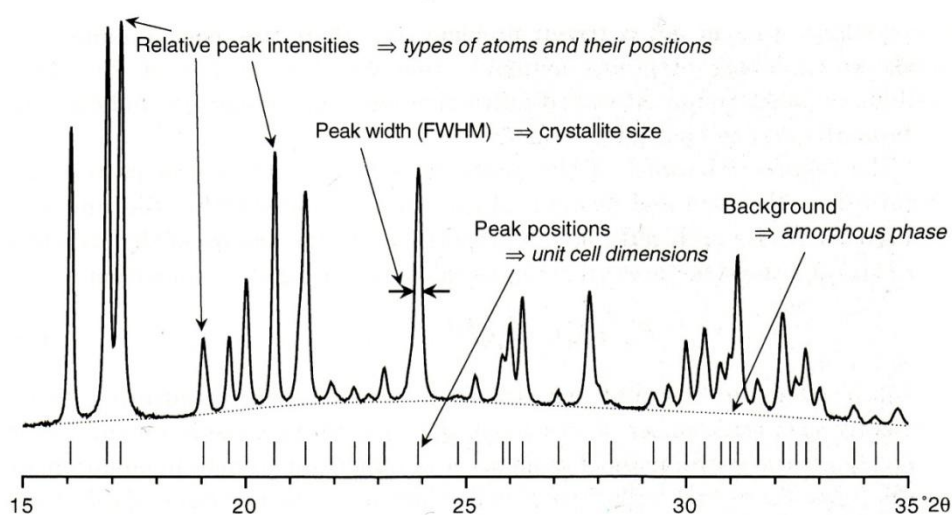
Figure 3-3: The main features of powder diffraction [11].

The characterisation for zeolite samples were performed on Philips X'pert Pro PW3719 with $CuK\alpha_2$ radiation source (λ = 1.5418 Å, tension = 40 kV, current = 30 mA, scan speed = 0.0289 ^{o} sec^{-1}, slit width = 1/8 and 1/4, numbers of the steps = 4368, and total time = 30:45 min). FeCrAlloy pre–treated/non–pre–treated wires samples and the zeolite Y/ZSM–5 structured catalyst were studied using the same instrument (*Philips X'Pert PRO)* and the same settings except the X–ray diffraction meter scanning rate was 0.000832^{o} sec^{-1}. The XRD patterns for the crystal growth of zeolite on the wire surface were compared with the crystal growth in the bulk phase.

X'Pert Highscore software was used to analyse the peak position and intensity. The scan range was between 2 and 50°. A commercial and standard zeolite for both zeolite Y and ZSM–5 were analysed under the same conditions used for the analysis of zeolite powder.

3.2.2 Scanning Electron Microscopy (SEM)

Scanning electron microscopy (SEM) was used to study the surface topography and the composition of the samples by scanning with a focused beam of electrons which interact with electrons in the sample, producing various signals that can be detected as images with a resolution of 1 nm.

SEM consists of a vacuum system, electronics and an electron optical column controlled by software. The SEM produces high magnification images (>100,000 x) of a sample surface by scanning it with a high-energy beam of electrons (**Figure 3-4**). The beam of electrons is generated in the column located at the top of the SEM (**Figure 3-5**). The electrons are provided by heating a tungsten filament located in the electron gun. Then the monochromatic electron stream is condensed to focus on a small beam using a series of electromagnetic lenses in the electron beam section. Following this, the electron beam is directed and focused onto the sample surface using coils at the end of the column. This electron beam can be directed either onto a single point (10 Å) or scanned along a line for X-ray analysis [14].
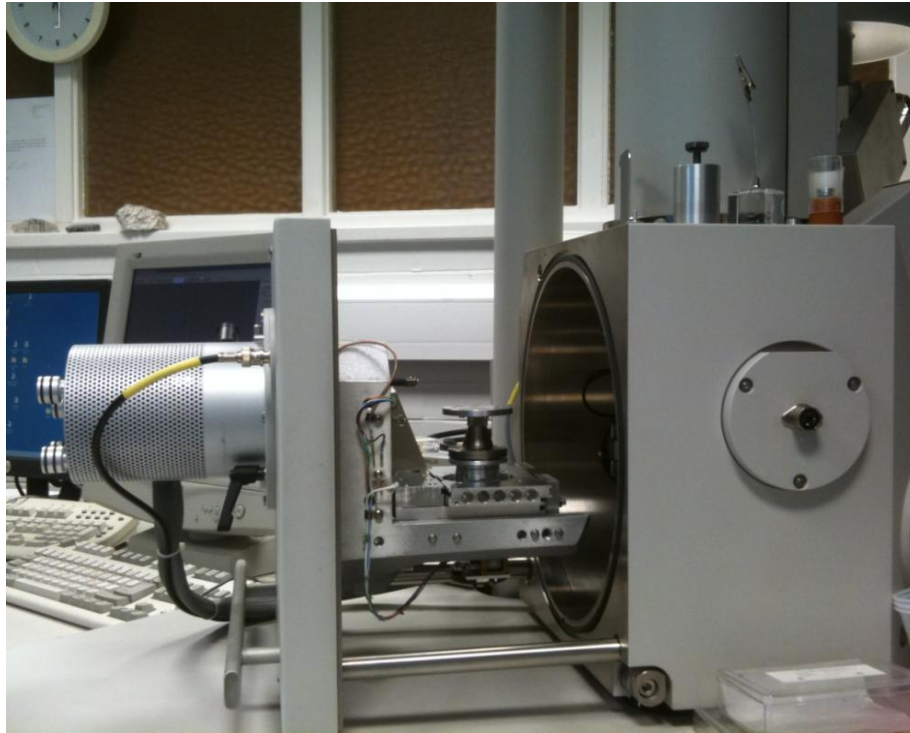
Figure 3-4: SEM opened sample chamber.

There are different types of signals that can be generated from a SEM. These types are secondary electrons, back-scattered electrons (BSE), characteristic X-rays, light (cathodoluminescence), specimen current and transmitted electrons. The most common signals are the secondary electron analysis which produces high–resolution images of less than 1 to 5 nm in size.

SEM is able to reveal details about the surface structure of the samples. The FEI Quanta 200 which has been used in this study can be operated in three separate vacuum modes; high vacuum (10^{-6} to 10^{-7} torr), and low vacuum (0.1 to 20 torr).
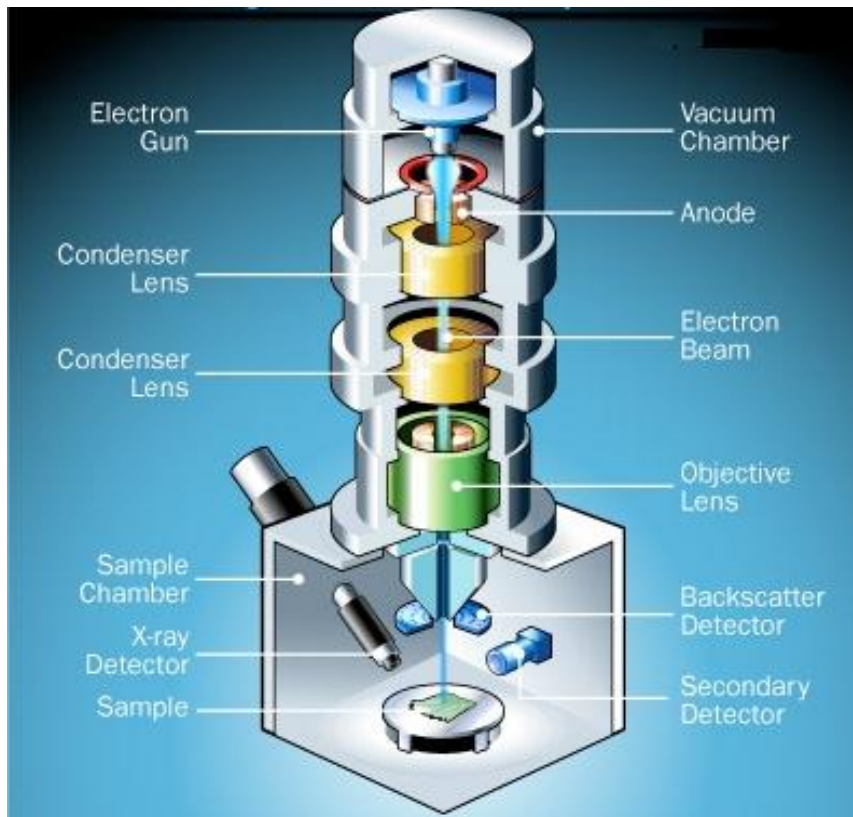
Figure 3-5: Schematic of a scanning electron microscope [15].

3.2.3 Energy Dispersive Spectroscopy (EDAX)

Energy Dispersive Spectroscopy (EDAX) is a chemical analysis technique used to determine the concentration of elemental species in a tested sample. The fundamental principle behind this method is the emission and detection of X-rays from a given sampling volume that are characteristic to specific elements. When the electron beam hits the electrons in the inner k-shell in the surface of the sample they will become excited, producing a hole in the k-shell which is filled by an atom from the outer shells and emitting an X-ray with various levels of energy will be ejected from the atoms of the different elements equal to that between two electrons as shown in **Figure 3-6.** Each element has a specific energy level which is determined by the element types. The EDAX is able to analyse the samples to a depth of a few microns. Therefore it is used to determine the bulk analysis [16].
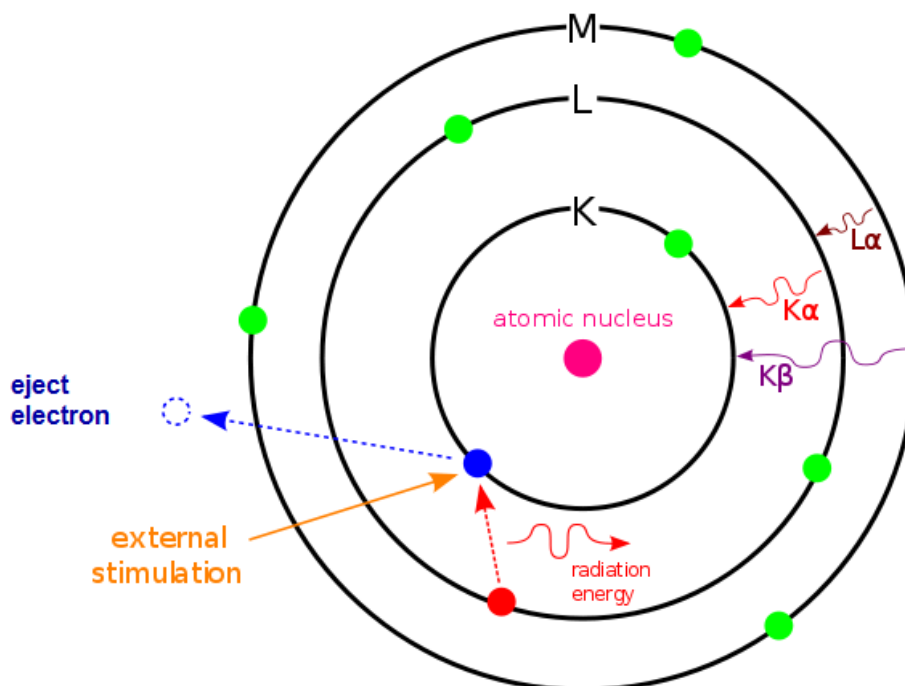
Figure 3-6: Schematics of EDAX operation [17].

Figure 3-7 demonstrates the EDAX spectrum of the zeolite Y sample synthesised. The EDAX spectrum represents the energy levels for each element within the sample. The EDAX is able to identify the elements and their concentrations on selected spots posited on the surface of the sample.

A specimen should be electrically conductive on the surface and electrically grounded in order to hinder electrostatic charge accumulation at the surface during electron irradiation. Zeolite is a non-conductive material and it tends to charge when scanned. Therefore, it is essential that it is coated with an ultrathin coating of electronically–conducting material such as gold or carbon. This can be achieved either by sputter coating or by high vacuum evaporation.
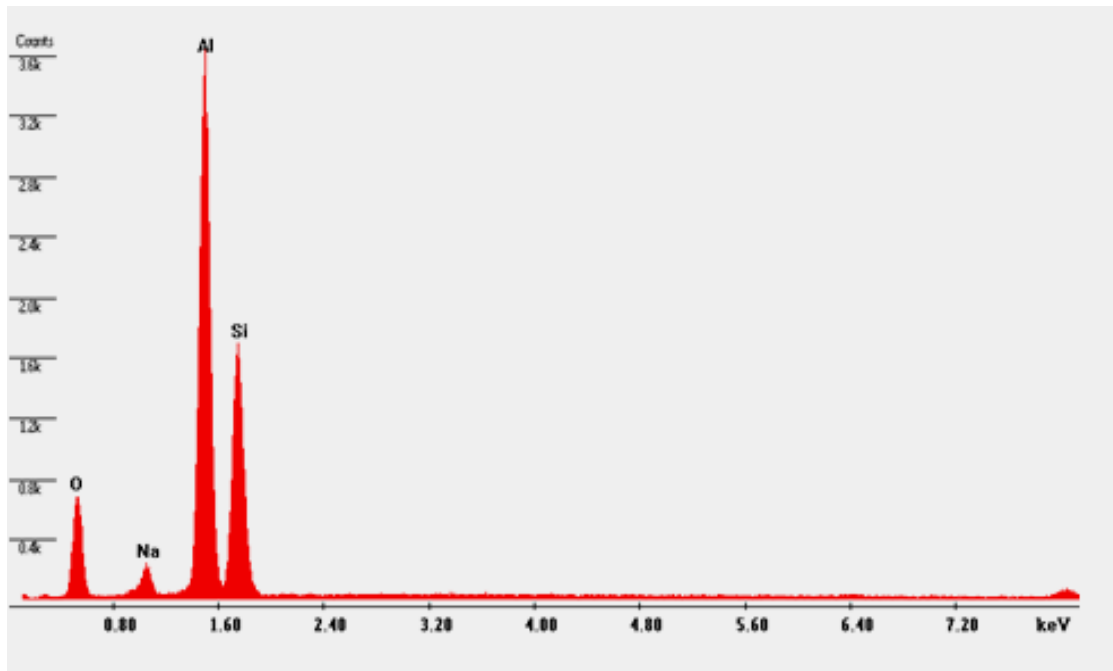
Figure 3-7: EDAX Spectrum for zeolite sample.

3.2.4 Sample preparation for the SEM and EDAX analysis

Analysis is performed in Quanta 200 Environmental SEM-with EDAX Genesis EDS X-Ray analysis with high resolution (1 nm). Because the SEM operation depends on electric fields, the samples must be prepared specifically for this purpose by making them an electronically conductive material.

The FeCrAlloy wires and structured zeolites are mounted directly onto aluminium stubs using double–sided conductive tapes. The powdered zeolite is difficult to mount and might be lost, flying off the stubs in the vacuum and under the beam. Hence, a small amount of powder is dispersed in acetone (a volatile solvent) and then drops of the dispersed mixture are dripped onto stubs before being dried. For a large amount of zeolite powder, this is compressed into small discs and mounted onto stubs. Subsequently, the stub samples are placed into a sputtering coater for gold coating to reduce image distortion caused by the charging effect.

Because a well polished surface is required for EDAX analysis and concentration mapping, the structured zeolite and FeCrAlloy wire samples were prepared by immersing the wires vertically into a resin. They were then sectioned using a diamond saw to obtain a clean surface, grinded with SiC sandpaper and polished with Al_2O_3 to achieve a smooth, flat surface. The samples are then rinsed with alcohol to remove contamination and finally sputter coated with a carbon layer.

SEM and EDAX analyses are performed in order to determine the quality and homogeneity of ZSM-5 and Y powder, FeCrAlloy wires and structured zeolite (vertical cross-section along the channels direction), and the zeolite layer thickness (horizontal cross-section).

3.2.5 Solid–state magic angle nuclear magnetic resonance spectroscopy (MAS–NMR)

In recent decades, NMR spectroscopy has been increasing used for characterising the structure of various types of porous materials such as zeolite [18, 19]. Between 1979 and 1981, it was used to provide information about the zeolite framework structure by employing ^{29}Si NMR and ^{27}Al NMR [11, 20].

The fundamental principle of the MAS-NMR spectroscopy operation is that the nuclei in the magnetic field absorb energy from the electromagnetic (RF) pulses and emit the absorbed energy in radio–frequency (RF) range [21].

In order to overcome the excessive line broadening in solid state NMR spectra due to the rigid lattice of the solid which led to distinct nuclear spin interactions such as: chemical shift anisotropy (CSA), dipolar, quadrupolar interactions, long spin-lattice relaxation times, due to the lack of translation- and rotation–motions; magic angle spinning (MAS) was used for averaging interactions of chemical shift anisotropy (CSA) and dipolar, quadrupolar interactions to zero, or reduce them to the isotropic values, allowing the registration of high-resolution NMR spectra of solids as well [21, 22].

The powder sample is packed into rotors (a special zirconia tube with an outer diameter of 7.0 – 2.5 mm) and placed in a large homogeneous magnetic field (B_o, typically 1 - 14 Tesla) with rapid spinning of samples using small turbines with gas bearing systems (the spinning rate is 5 – 40 kHz). Furthermore, a RF field (a board–band pulsed, 0 – 400 MHz) at magic angle (54.73^o) with respect to the direction of B_o is applied (**Figure 3-8**). Subsequently, the re–radiated RF signals produced by exciting and de–exciting the nuclei simultaneously are detected by electromagnetic induction and result in a Fourier transformed graph of intensity versus normalised frequency [20, 21, 23].
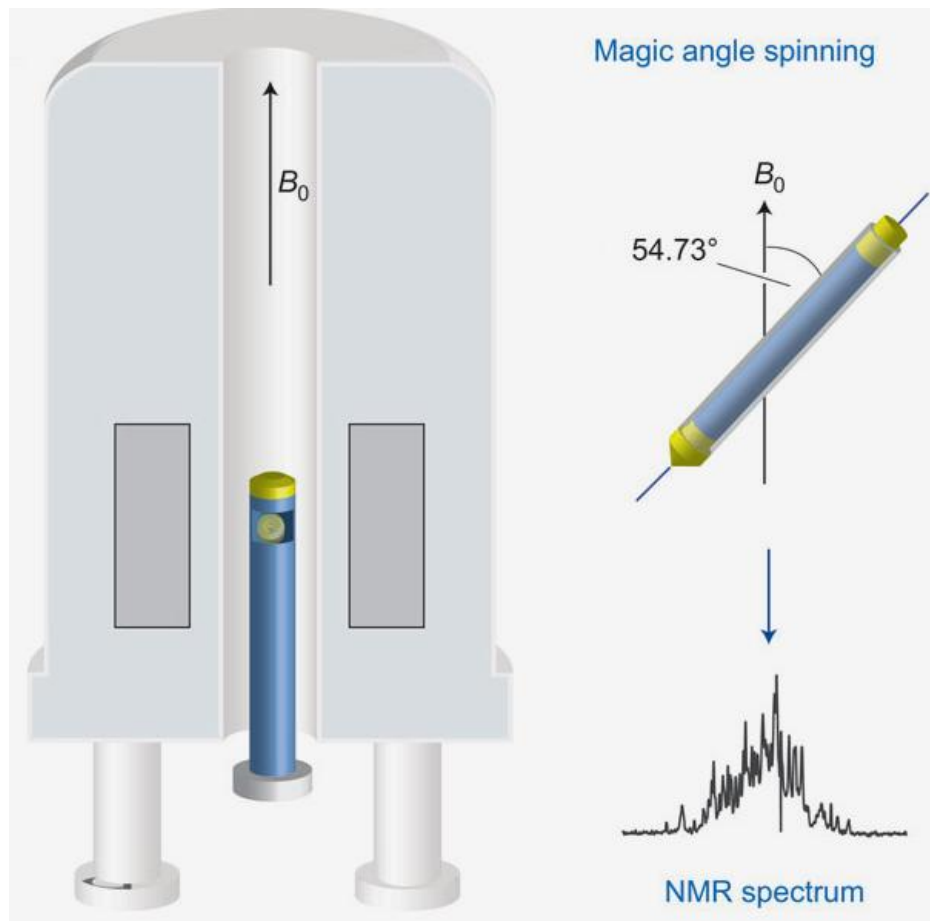
Figure 3-8: A schematic representation of a transient sedimentation NMR experiment [20].

The most important structural information revealed from a high–resolution MAS-NMR spectrum of solids is the number of signals, the relative signal intensities (I), the isotropic chemical shift (δ_{iso}), and quadrupole coupling constant (QCC). The signals appear in the MAS-NMR spectrum relative to the difference in the structural environments of the nucleus present in the samples while the relative signal intensities reveal occupancies of different environments. δ_{iso} is the position of the line in the MAS-NMR spectrum corresponded to the standard sample and that measured from the location of the signal maximum on calibrated δ-scale (in ppm) [11]. In order to correct the magnitude of δ, the RF of the tested samples is measured relative to an external reference such as adamantine ($C_{10}H_{16}$).

Because the zeolite framework is constructed with silicon atoms at the central position and some of these may occupied by aluminium, gallium, iron etc, the ^{29}Si MAS-NMR characteristic of the SiO_4^{-4} units are characterised by up to five different environments present as Si(nAl) in the case of aluminium, where n = 0, 1, 2, 3, 4 (**Figure 3-9**). Meanwhile, for the aluminium ^{27}Al MAS-NMR in the as synthesis zeolite framework shows only a single tetrahedral Al environment (Al(OSi$_4$)) which made the ^{27}Al MAS-NMR spectrum less complex than the ^{29}Si MAS-NMR as the AlOAl linkage is forbidden [11].
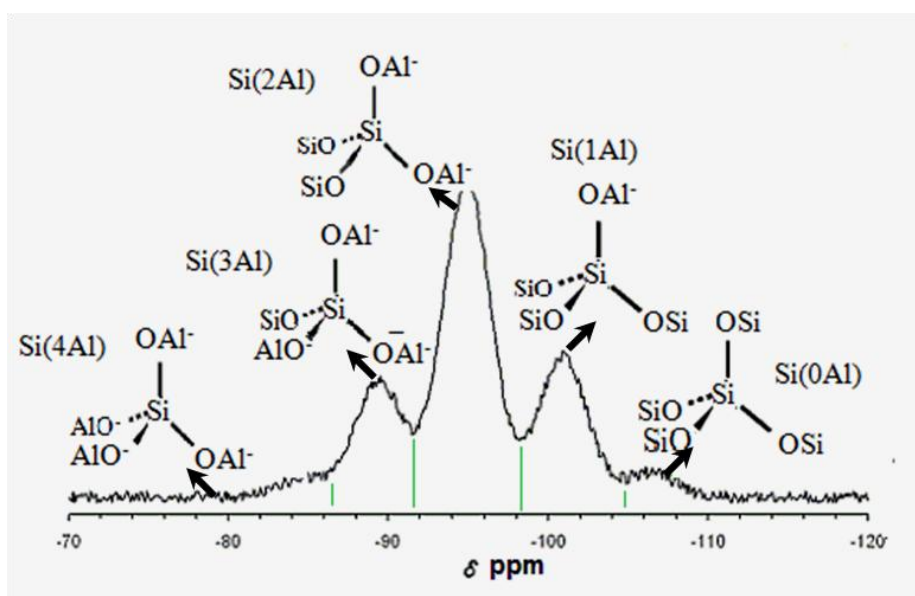
Figure 3-9: ^{29} Si MAS-NMR spectrum for zeolite NaY modified from [24].

3.2.5.1 ^{29}Si and ^{27}Al MAS-NMR and zeolite framework

The ^{29}Si MAS-NMR spectra of a zeolite shows distinct signals for different environments forming the tetrahedral zeolite framework (Si(nAl)). The peak intensity corresponds to the concentration of the different Si(nAl) units. Increasing the Al-atoms in the zeolite structure leads to a reduction in the peak intensities of the aluminium-rich at the right side of the spectra (**Figure 3-9**). However, if the aluminium atoms are replaced by silicon atoms or removed by acid leaching, this shifts the spectra to the low field (**Figure 3-10**). The ^{29}Si MAS-NMR spectra can be used to calculate the Si/Al framework ratio of the zeolite (**Equation 3-5).**
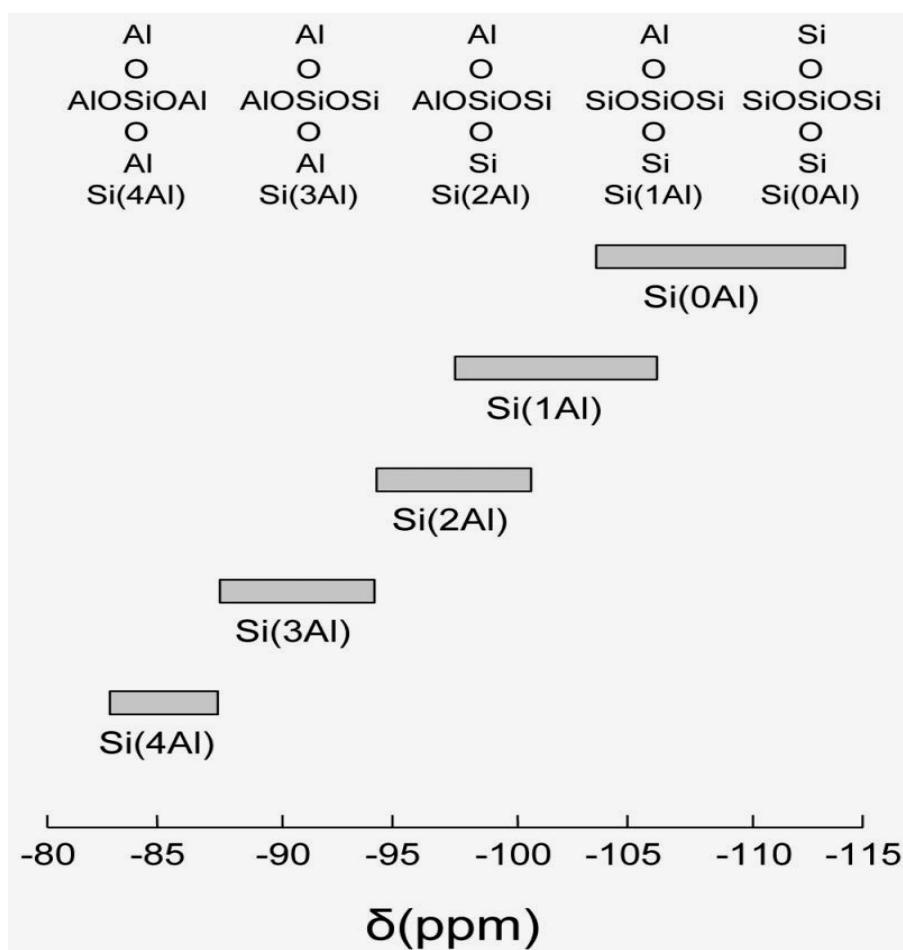
Figure 3-10: ^{29}Si chemical shift values of Si(nAl) units in zeolites [11].

$$Si/Al = \sum_{n=0}^{n=4} ISi(nAl) \bigg/ \sum_{n=0}^{n=4} 0.25nISi(nAl)$$

Equation 3-5

Where, I = the intensities of the Si(nAl) peaks

n= 0, 1, 2, 3, and 4, the number of coordinated Al-atoms for the given peaks (excluding non-framework aluminium present in thermally or chemically treated zeolite) [11].

^{27}Al MAS-NMR spectra of zeolite material can detect and characterise non-framework aluminium atoms formed after hydrothermal or chemical treatments. The ^{27}Al MAS-NMR spectra for Na-zeolite form show a sharp signal at about 60ppm corresponding to the four-coordinated tetrahedral framework aluminium atoms (Al(OSi)$_4$). Meanwhile, the ^{27}Al MAS-NMR spectra of the zeolite are de-aluminated zeolite using hydrothermal or chemical treatment methods show an extra peak at 0 ppm for six-coordinated octahedral non-framework aluminium atoms in addition to the tetrahedral framework aluminium at 60 ppm.
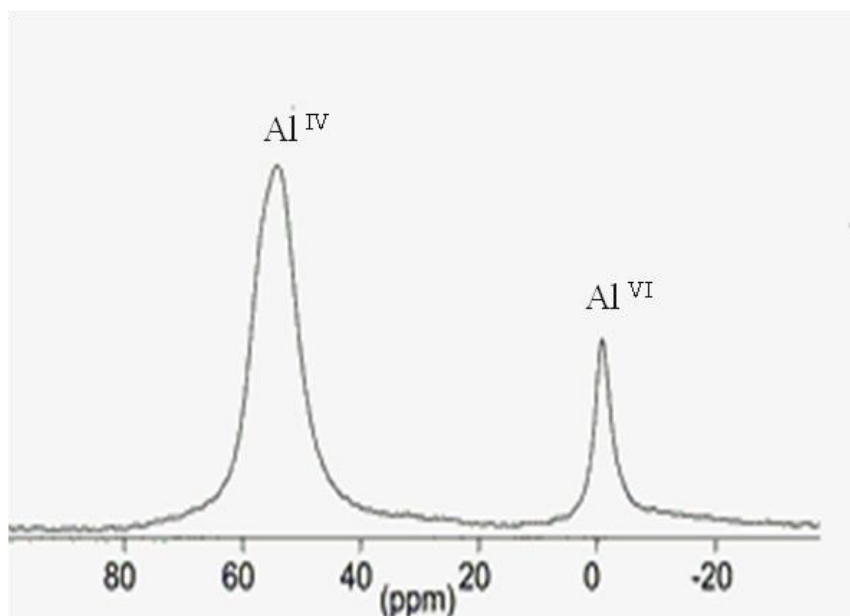
Figure 3-11: Typical ^{27}Al MAS-NMR of dealuminated zeolites modified from [11].

In this thesis a Bruker Avance III-400 spectroscopy instrument is used on 0.1 g of zeolite powder milled and carefully packed into a 4mm zirconia rotor. The rotor is inserted into a magnetic field (B_o) inside the coil. The ^{27}Al MAS-NMR operation conditions were 100 scans, relaxation time 5, acquisition times 0.00824, resonance frequencies condition 104.26 and total time for the test 8.33 min. For the ^{29}Si MAS-NMR operation conditions were: numbers of scans 1000, relaxation time 40, acquisition times 0.02135, resonance frequencies condition 79.49 and total time for the test 11.11 hours.

3.2.6   Gas adsorption measurement with N₂ (BET isothermal)

The surface area measurement of the catalyst is used to monitor the activity and stability of the catalyst. The most common procedure for estimating the internal surface of zeolite depends on the isothermal adsorption-desorption of nitrogen at liquid nitrogen temperature ($-196.15^{o}C$). The adsorption is defined as adhesion of atoms or molecules of gas to the surface of the solid and it differs from the absorption, in which a fluid permeates a liquid or solid. The gas adsorbed amount depends on the exposed surface, temperature, gas pressure and the strength of the interaction between gas and the zeolite surface.

In 1916, Irving Langmuir developed his theory which is related to the monolayer adsorption of gas molecules and based on the assumption that all of the surface sites have the same adsorption energy for adsorbate, the area on the sample where one molecule can adsorb onto known as surface site, the adsorption of solvent on one site is independent of the gas adsorption at neighbouring sites and there is only one particle in each active site [25]. Later in 1938, Stephen Brunauer, Paul Emmett and Edward Teller developed the BET theory to extend the Langmuir theory to multilayer adsorption with an additional assumption: infinite layers of gas molecules will adsorb on a solid surface with no interaction between these layers and the theory can be applied to each layer [27] (see **Figure 3-12**).
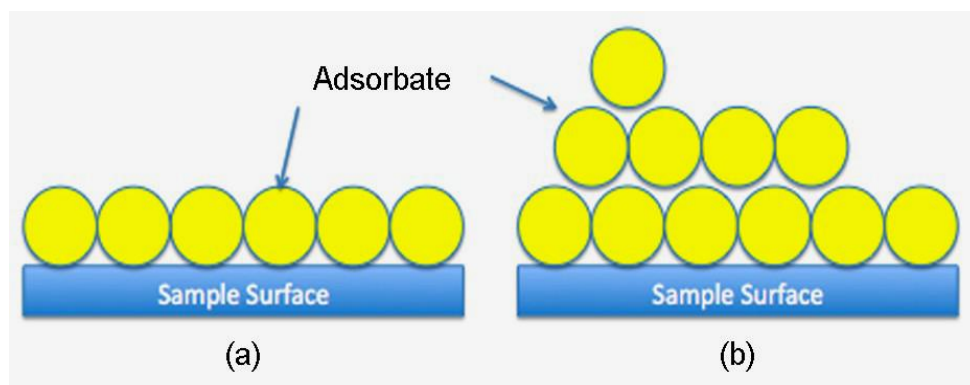
Figure 3-12: Schematic of the adsorption of gas molecules onto the surface of a sample based on (a) Langmuir theory and (b) BET theory [25].

According to Brunauer, Deming, Deming and Teller (BDDT) [27], there are five types of isothermal adsorption (**Figure 3-13**). Type I is the typical Langmuir isothermal adsorption type and this is more common for crystalline microporous material (zeolite). Type II is typical for BET isothermal adsorption with unlimited adsorption volume; type III and type V are typical of vapour adsorption on hydrophobic materials; and type IV is similar to type II except with infinite adsorption volume [26].
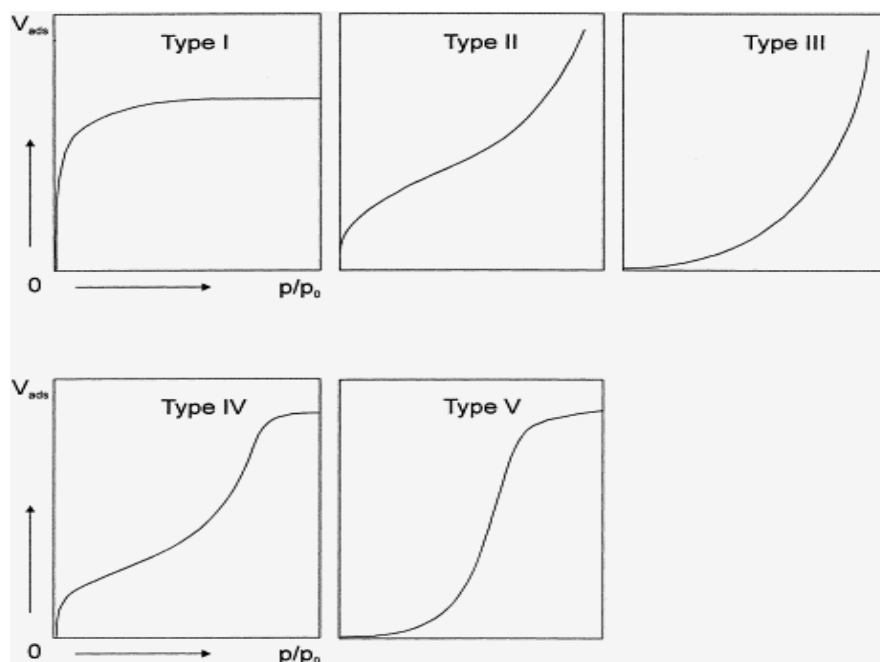
Figure 3-13: Type of isotherm adsorption according to BDDT [26, 27].

The adsorption and desorption curve correspond to the pore structure of the solid and reveals in the hysteresis loop in the curve (**Figure 3-14**), in which the increase in mesopores and decrease in microspores into the structure raise the hysteresis loops [28]. The information driven from the adsorption desorption isothermal is used to determine the surface area of the zeolite sample by applying the following equation:

$$\frac{p/p^o}{V_a(1-p/p^o)} = \frac{p}{V_a(p^o-p)} = \frac{1}{V_m.C} + \left[\frac{C-1}{V_m.C}\right] \times \frac{P}{P^o} \qquad \textbf{Equation 3-6}$$

Where, slope $= \dfrac{C-1}{V_m.C}$ and   intercept $= \dfrac{1}{V_m.C}$

V_m= Volume of the adsorbed gas in the monolayer (cm^3 g^{-1})

V_a= Volume of gas adsorbed at the equilibrium adsorbate pressure, and at the temperature of adsorption (-196.15^{o}C for nitrogen)

C = BET-constant, representing the interaction between the adsorbent and adsorbate

The total surface area S_{total} and the specific surface area S_{BET} are given by

$$S_{total} = \frac{v_m N_s}{V} \qquad \textbf{Equation 3-7}$$

$$S_{BET} = \frac{S_{total}}{a} \qquad \textbf{Equation 3-7}$$

Where, N = Avogadro's number

V= molar volume of the adsorbate

a= mass of the adsorbent.
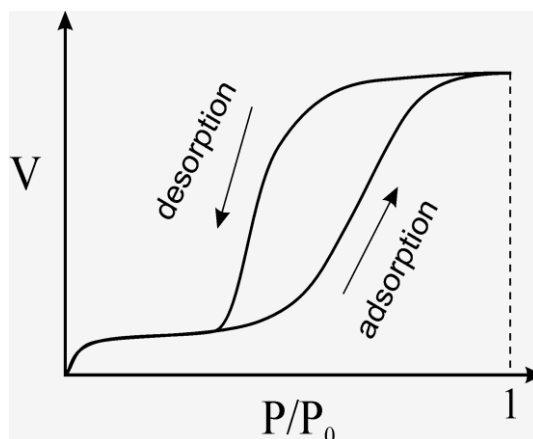
Figure 3-14: The hysteresis loop in isotherm adsorption according [11].

3.2.6.1 Sample preparation and experimental setup

For measuring the BET isothermal surface area, a Micromeritics ASAP 2010 (**Figure 3-15**) was used with N_2 as the adsorbate because of its availability in high purity and its strong interaction with most solids. A 0.5 g zeolite powder was loaded into the bulb ended quartz tube of 6mm diameter. Prior to any analysis being conducted, the samples were degassed by heating the sample tube cell with heating mantles to a high temperature without causing any damage to the zeolite structure ($350^{o}C$) under vacuum for 16 h to remove contaminants and moisture. The weight of the dry zeolite powder sample was recorded after the degassing process.

Figure 3-15: Micromeritics ASAP 2010.
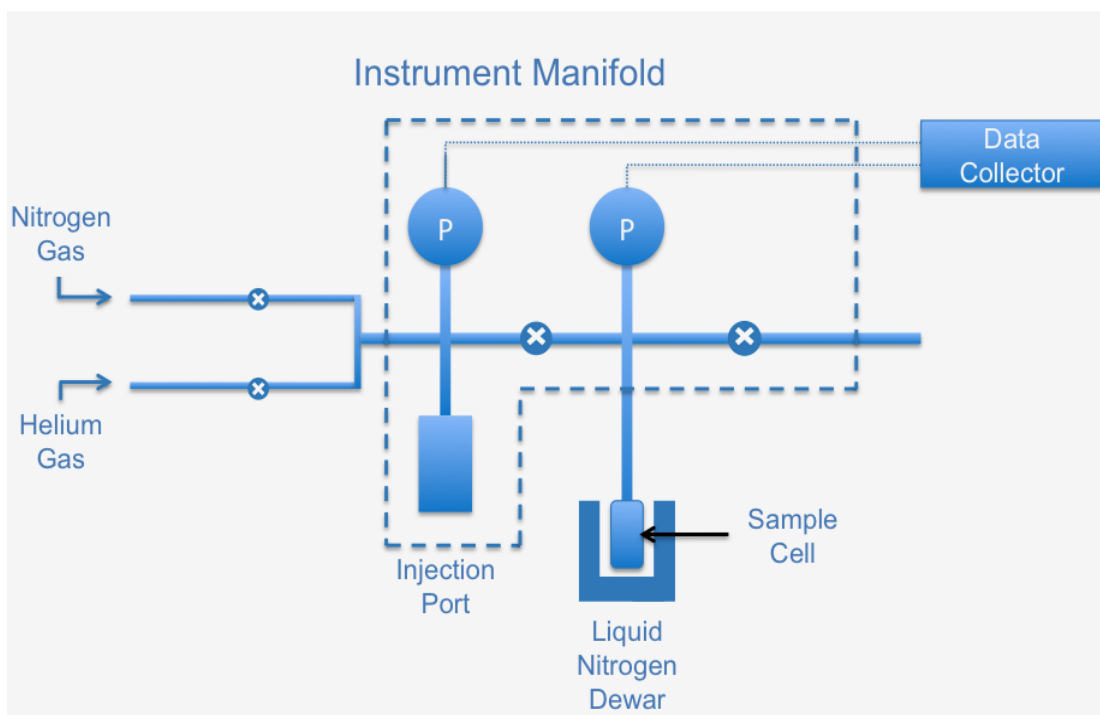
Figure 3-16: Schematic of the BET instrument [25].

Subsequently, (**Figure 3-16**) the sample tube cell was moved from the degassing port to the analysis port and a glass rod was placed within the cell to minimise the dead space in the tube sample cell and the system was placed under vacuum. Liquid N_2 was used to cool the tube cell by bringing the temperature to -196.15^{o}C to gain a detectable amount of adsorption to fill the pipeline (V_1) and the sample tube (V_2), At -196.15^{o}C the sample cell, N_2 molecules were adsorbed and no more adsorption occurs regardless of any further increase in pressure. Then the adsorbed N_2 was released from the material and quantified. The adsorption isotherm was obtained by repeating the procedure several times. The data collected were displayed in the form of a BET isotherm, which plots the amount of gas adsorbed as a function of the relative pressure.

3.2.7 Thermo-gravimetric analysis (TGA)

Thermo-gravimetric analysis (TGA) is a technique in which the changes of the physical and chemical properties of materials are associated as a function of temperature or as a function of time in a controlled environment. Measurements are used to determine the weight loss or gain due to decomposition, oxidation or dehydration [29].

The powder and structured zeolite for all samples were studied using a thermo-gravimetric analyser *(Q5000IR TA Instruments)* controlled by TA universal software for data analysis and acquisition (**Figure 3-17**). The weight loss curve from the TGA was used to characterise the temperature at which weight loss occurs, the thermal stability of materials, the oxidative stability of materials, and the amount of moisture, coke and volatiles on the samples.

Figure 3-17: Thermo-gravimetric analyser [30].

Platinum or ceramic pans located inside a programmable furnace can be used to hold the samples (10 mg). This pan was connected to a sensitive microbalance to detect any weight loss with an accuracy of 0.1 μg. A thermocouple is located inside the small furnace to monitor temperature. A reference pan was placed in a separate chamber. The weight change was recorded over the period of time in N_2 and He at a rate of 25 ml min^{-1} following the purge gas line could also be used to feed other reactive gases such as O_2 and H_2. **Figure 3-18** shows a schematic diagram of a typical TGA analyser.
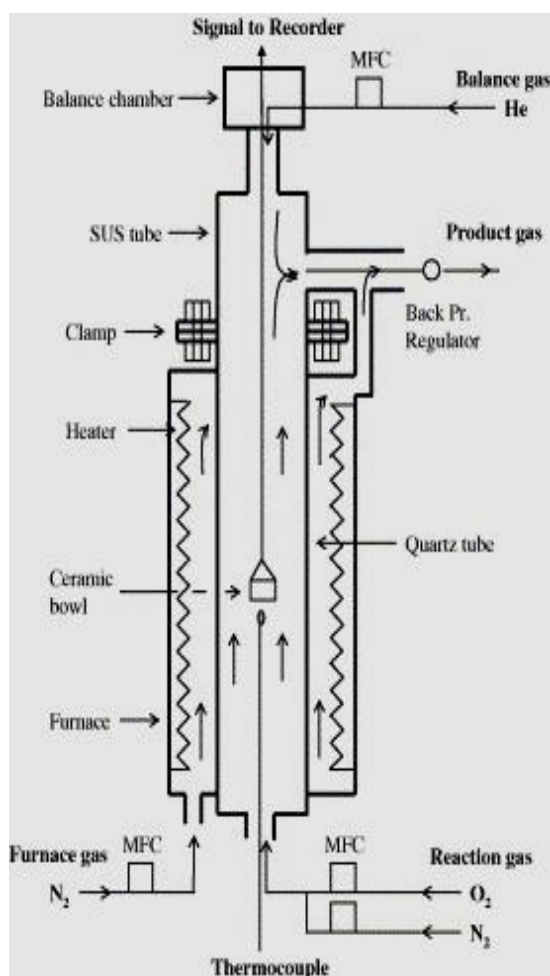
Figure 3-18: Schematic of the thermo-gravimetric analyser [30].

3.3 Synthesis of the Structured Zeolite

This section covering the preparation of the structured zeolites prepared by growing the zeolite layers directly on the substrate surface (FeCrAlloy) under hydrothermal operation conditions is described here. FeCrAlloy wires (0.5 mm diameter) were used as substrate and were pre-treated prior to immersion in a synthesis homogenous gel. Zeolite crystals and zeolite-coated wires were then purified by repeated washing with a deionise water followed by drying overnight. The following sections will show the synthesis for zeolite Y and ZSM-5 structured catalysts.

3.3.1 FeCrAlloy Pre-treatment

FeCrAlloy annealed wires (0.5 mm diameter) were supplied by GoodFellows with a pre-determined chemical composition by weight of Fe 72.8%, Cr 22%, Al 5%, Y 0.1% and Zr 0.1% (**Table 3-3**).

Table 3-3: physical properties of FeCrAlloy[31].

FeCrAlloy properties	
Wire diameter (mm)	0. 50
Specific surface area ($m^2 \ g^{-1}$)	0.005
Thermal conductivity ($W \ m^{-1} \ K^{-1}$)	16.70
Thermal capacity ($J \ g^{-1} \ K^{-1}$)	1050
Density ($g \ cm^{-3}$)	7.400
Maximum temperature (^oC)	1300

One of the major advantages of using FeCrAlloy is that the aluminium in the substrate can be oxidised at high temperatures to form a thin film of aluminium oxide (Al_2O_3) on the surface. This oxide layer can then be used to anchor and subsequently grow the active zeolite phase. For this, the pre-treatment step is crucial as it requires the formation of uniform thin aluminium oxide layer on the metal surface. This film then increases the wetting of the support by the synthesis gel mixture and/or promotes the nucleation of zeolite crystals [32].

In this work, the oxidation of the FeCrAlloy wire process was conducted using a muffle furnace (Progen Scientific) at $1000^{o}C$. The pre–treatment process occur over four distinct stages: surface roughness, solvent wash, alkali wash and finally acid wash.

1. The surface was roughened and cleaned to remove possible contaminants using No. 100 glass paper. Then, FeCrAlloy wires were immersed in acetone ultrasonic bath for 5 minutes then rinsed with de-ionised water to remove any containment.

2. The wires were immersed in a 0.1 M KOH solution for 10 minutes to increase the roughness on the surface, rinsed with de–ionized water. They were heated for 10 minutes at $80^{o}C$ in a 0.1 M HNO_3 solution to create a superficial aluminium oxide [33, 34]. The wires were rinsed with de-ionised water, washed with acetone in an ultrasonic bath (Cam sonix C080T) for 5 minutes, and then cleaned with de-ionised water.

Oxidation of the wires was carried out at $1000^{o}C$ for 3, 6, 9, and 24 hours in a muffle furnace (Progen Scientific) in order to study the oxide layer growth on the FeCrAlloy surface, with the furnace temperature ramped at a rate of $10^{o}C$ min^{-1}. Furnace calibration has been reported in **Appendix A**. Wire samples were inserted into the furnace and hung on each side of a stainless steel tripod to ensure even oxidation of the surfaces. The wires were held at $1000^{o}C$ for a 3, 4, 5, 6, 9, and 24 hours, they were subsequently removed from the furnace at $1000^{o}C$ and exposed

instantly to room temperature. The mass of oxide coating was determined by assessing the mass of the wires before and after oxidation.

The thermal treatment procedure developed aluminium oxide layer with nodules and whiskers, with the wires studied by scanning electron microscopy (SEM) and energy dispersive X-Ray analysis (EDAX) using Quanta 200 instrument (FEI, UK), located in the School of Chemical Engineering and Analytical Science at the University of Manchester.

3.3.2 Preparation of Synthesis gel of zeolite

The second phase in the generation of the structured catalyst was the preparation of the zeolite gels. Zeolite Na–Y and Na–ZSM-5 synthesis mixtures were prepared using sodium aluminate (Sigma–Aldrich, 50.9 wt% Al_2O_3, 32.1 wt% Na_2O, and 17.9 wt% H_2O), sodium hydroxide (Merck, 99 wt% NaOH) and de-ionised water were used.

3.3.2.1 Zeolite Na–ZSM-5

Synthesis mixtures of zeolite Na–ZSM-5 gel were made with colloidal silica (Ludox AS-40 from Sigma–Aldrich with 40 wt% SiO_2, and 60 wt% H_2O) as the silica source, and sodium aluminate (Sigma–Aldrich with 50.9 wt% Al_2O_3, 32.1 wt% Na_2O, and 17.9 wt% H_2O) as the aluminium source. The sodium concentration was increased by adding sodium hydroxide (Merck, 99wt% NaOH), and a minimal amount of tetrapropylammonium hydroxide (TPAOH/SiO_2 = 0.0033) was added to the Na–ZSM-5 synthesis (TPAOH solution, 1 M, Sigma–Aldrich) as a template.

The gel synthesis was conducted using a seeding gel of Na–ZSM-5 with a composition of $4.5Na_2O:3TPAOH:60SiO_2:1200H_2O$. This was achieved by adding 2.54 g TPAOH solution to the sodium hydroxide solution followed by the introduction of 7.5 g Ludox slowly into caustic solution with continuous stirring. The gel was sealed in a polypropylene bottle and mixed for 30 minutes at room

temperature using magnetic stirrer. Then gel was aged at $100^{o}C$ overnight without agitation.

The second stage in the synthesis of zeolite Na–ZSM-5 was the preparation of the feed stock gel ($6.5Na_2O:2Al_2O_3:60SiO_2:1916H_2O$) by dissolving $NaAlO_2$ in NaOH solution and a weighed amount of Ludox AS-40 was added to the mixture and stirred for 1 hour at room temperature.

Subsequently 3.2 g of seeding mixture was added to the feedstock gel leading to an overall gel with a final composition ($6.36Na_2O:1.86Al_2O_3:0.2TPAOH:60SiO_2:1864H_2O$) then stirred for 30 minutes. The overall gel was then collected in a PTFE–lined container ready for the next step to in the synthesis the structured catalyst process. **Figure 3-19** shows the scheme flow chart for synthesis gel of Na–ZSM-5.
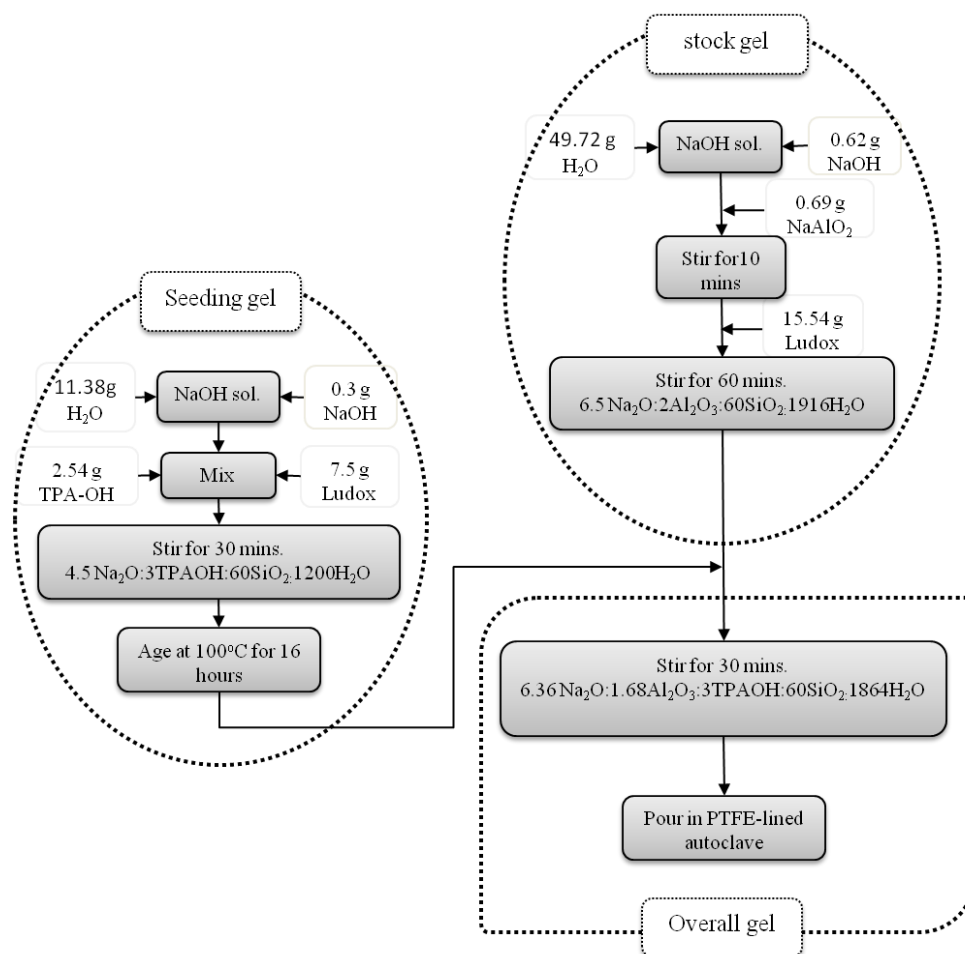
Figure 3-19: Schematic synthesis of Na–ZSM-5 gel.

3.3.2.2 Zeolite Na–Y

A Zeolite Na–Y precursor solution was prepared with a gel composition $3.3Na_2O:Al_2O_3:10SiO_2:120H_2O$, and the synthesis was started by the preparation of two solutions; The first solution was prepared by adding sodium hydroxide (1.35 g NaOH Sigma–Aldrich) to 1/3 H_2O de-ionised water (3.92 g), stirred thoroughly and then allowed to cool to less than 25°C. Sodium aluminate (1 g NaAlO$_2$ Fisher Scientific) was then dissolved in (1/3) de-ionised water and mixed with the sodium hydroxide solution. The second solution was obtained by diluting Ludox (10.04 g Ludox AS-40, Sigma–Aldrich) in de-ionised water (3.92 g) (**Figure 3-20**), the synthesis gel was then poured into polypropylene bottles and placed in the oven at 100°C between 8-72 h.
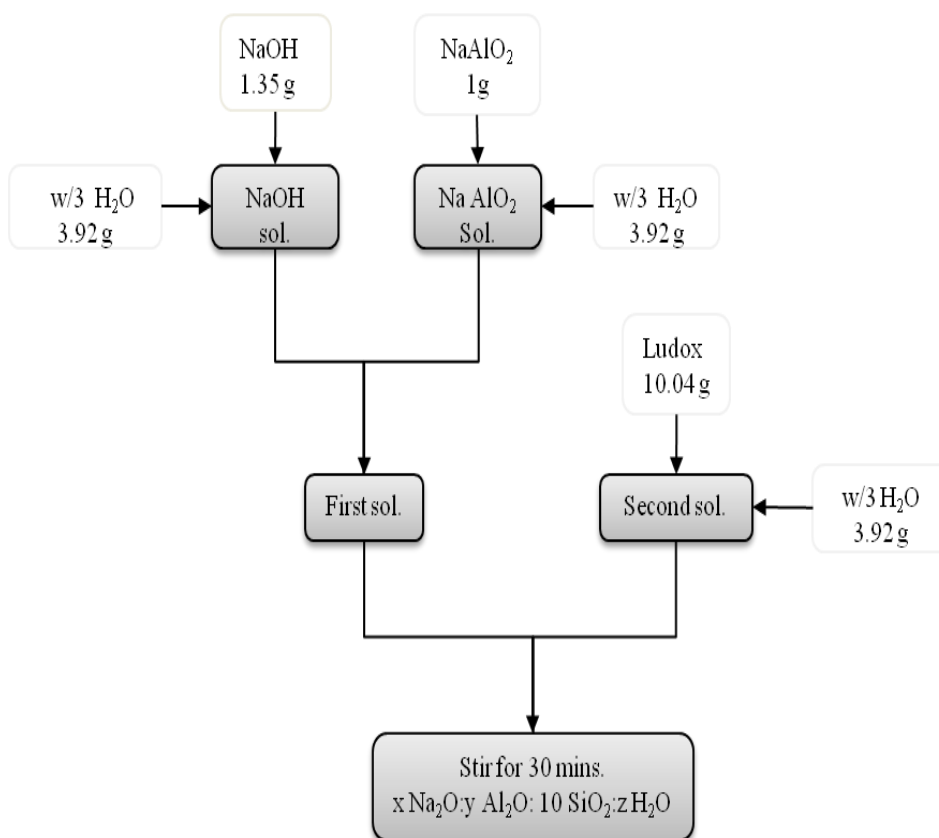
Figure 3-20: Schematic of the Synthesis of Na–Y gel.

3.4 Synthesis of zeolite structured catalysts

The FeCrAlloy wires (0.5 mm diameter 25 mm length, Goodfellows) pre-treated at $1000^{o}C$ for 3-24 h was inserted vertically into a PTFE-lined autoclave (ZSM-5) or 25 ml polypropylene bottles (Na-Y). The hydrothermal synthesis of the zeolite coating on FeCrAlloy wires was performed as detailed below:

The wires were placed in vertical position using designed Teflon-disk as holder (25 mm diameter and 6 holes where located on the desk 0.5 mm diameters (**Figure 3-21**) and inserted into a Teflon-lined autoclave. Next the Na–ZSM-5 gel was poured into the Teflon-lined autoclave, the autoclave was sealed and inserted in the oven at $180^{o}C$ for 4, 8, 12, 16, 20 , 48 and 72 hours.

The autoclave was cooled to ambient temperature and the wires were removed rinsed with de-ionised water and then washed in de-ionised water using an ultrasonic bath for 10 minutes, and then dried at room temperature. All wires were weighed before and after each step of the synthesis. The Na–ZSM-5 powder, which was precipitated inside the Teflon-lined autoclave and remained unattached to the wire surfaces, was collected, washed and dried. **Figure 3-22** shows the schematic diagram for the preparation of the zeolite Na–ZSM-5 structured catalysts.
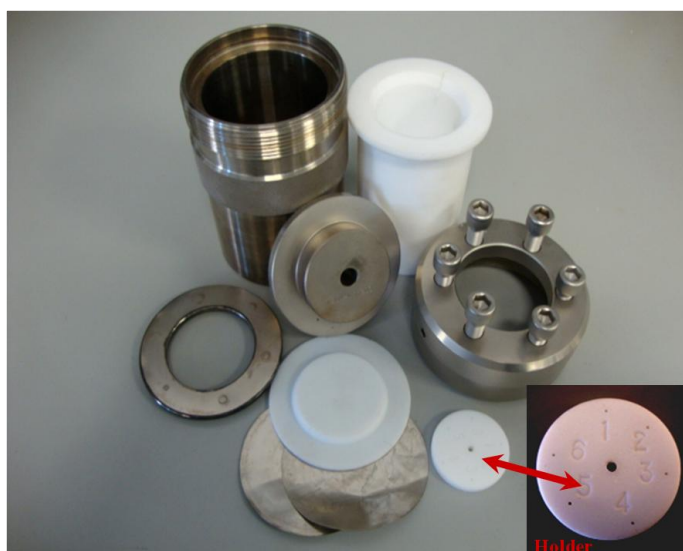
Figure 3-21: Teflon-lined autoclave with custom modified Teflon–disk.
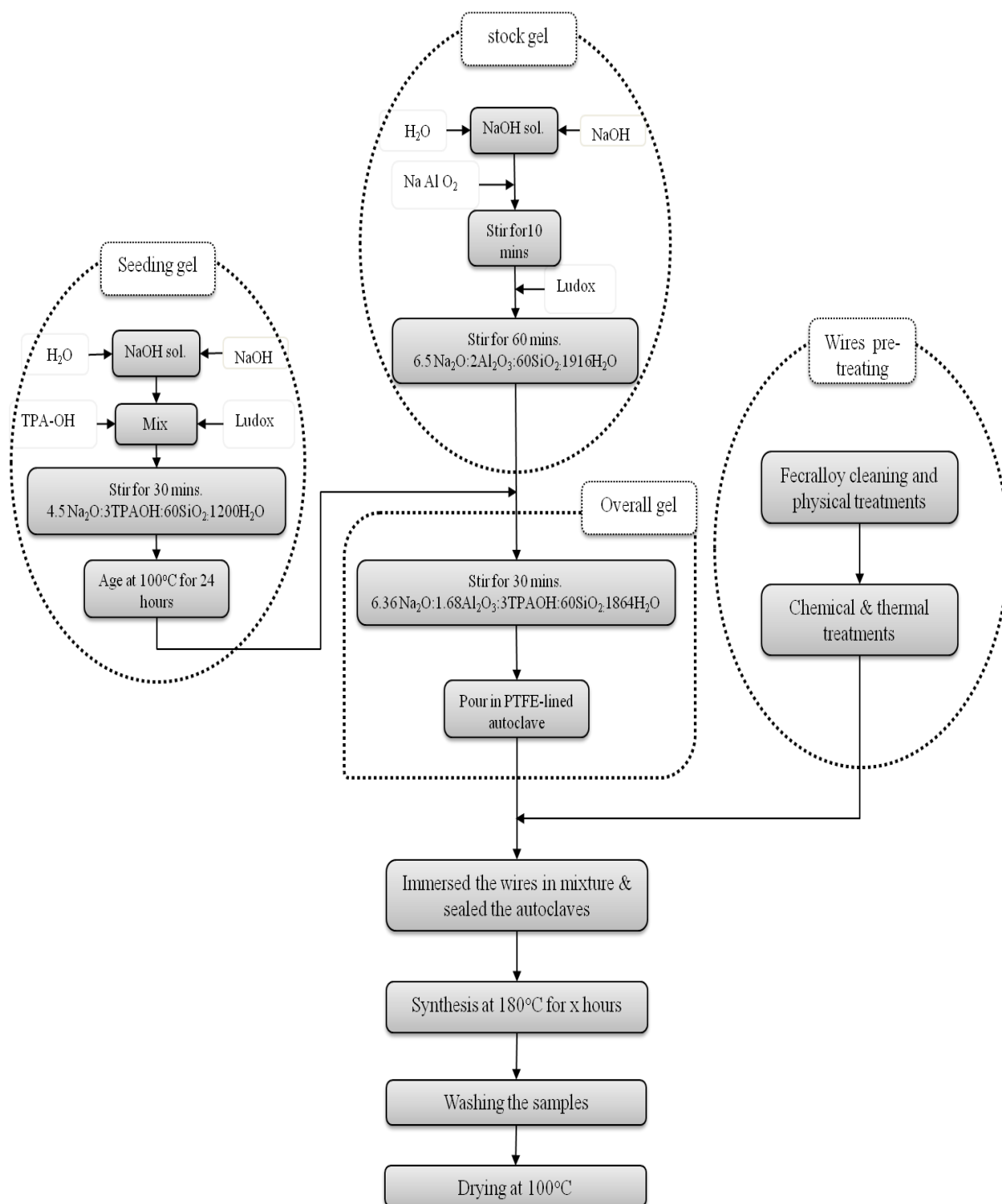
Figure 3-22: Schematic diagram for the Na–ZSM-5 structured catalyst synthesis.

The synthesis of the Na–Y zeolite followed the same procedure as that for the synthesis of the Na–ZSM-5 structured catalysts, except that 25 ml polypropylene bottles were used in place of the PTFE-lined autoclave, and a Teflon-disk. The wires were placed in horizontal position using designed Teflon-disk as holder (10 mm diameter and 6 holes where located on the desk 0.5 mm diameters. These were heated to 100°C in a custom designed heating system for 8, 16, 24, 32, 40, 48, 56, 64, and 72 hours. The heating system (**Figure 3-23**), was designed using two heating elements placed at the ends of aluminium block containing 15 holes with diameter (35 mm) in order to accommodate 15×25 ml bottles.

Ten thermocouples were located throughout the system and were connected to the heating control system in order to monitor the temperature changes. After hydrothermal synthesis, both the zeolite precipitated in the bottles and the coated wires were removed, rinsed with de-ionised water and then washed in de-ionised water in an ultrasonic bath for 10 min. The wires and the synthesised zeolites were dried overnight at 100°C. **Figure 3-24** shows a scheme diagram of synthesis.
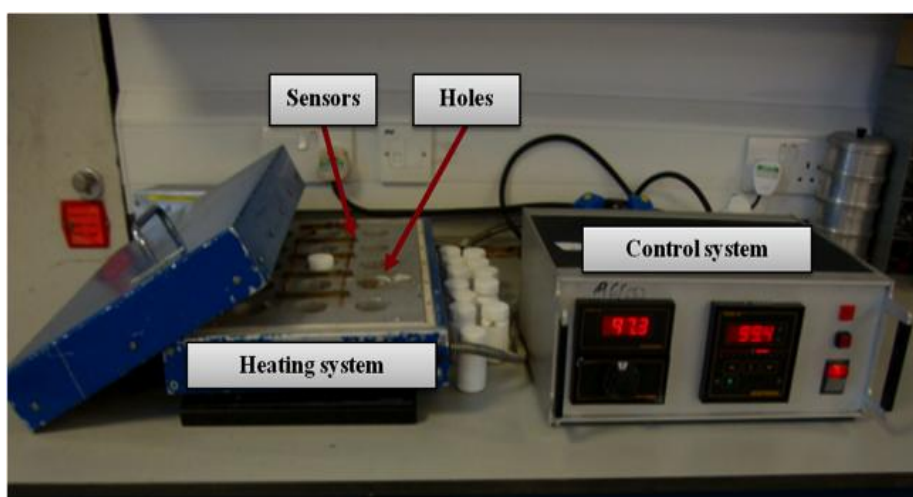
Figure 3-23: Heating and control system.
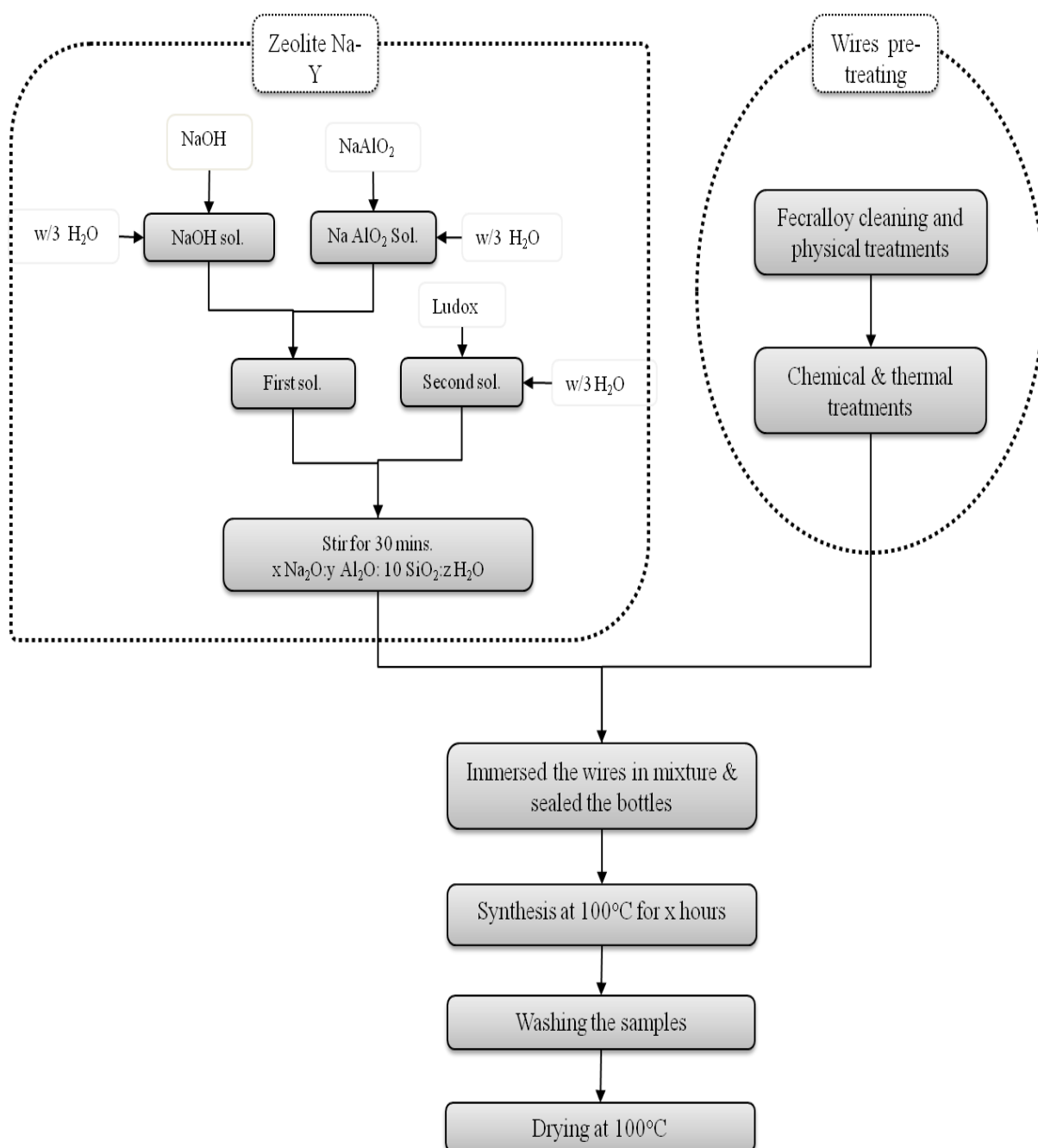
Figure 3-24: Schematic diagram for the Na–Y structured catalyst synthesis.

References

1. Treacy, M.M.J. and J.B. Higgins, *Collection of Simulated XRD Powder Patterns for Zeolites Fifth (5th) Revised Edition*, 2007.

2. Baerlocher, C. and L. McCusker. *Database of zeolite structures*, Structure Commission, Int. Zeolite Assoc. 2011[Accessed 2012] Available from: www. iza-structure. org/databases.

3. C Baerlocher, L.M.I.Z.A., *International Zeolite Association, Database of zeolite structures be found under,* 2012 [Accessed 2013] Avilable from : *http:/ /www. iza-structure. org/databases.*

4. Cullity, B.D. and S.R. Stock, *Elements of X-ray Diffraction*, Vol. 3. 2001.

5. Froome, K., *Determination of the velocity of short electromagnetic waves by interferometry,* Proceedings of the Royal Society of London. Series A. Mathematical and Physical Sciences, 1952. **213**(1112): p. 123-141.

6. Nave, C.R.R. *Bragg's Law, HyperPhysics, Quantum Physics* 2012 [Accessed 2013] Available from: http://hyperphysics.phy-astr.gsu.edu/hbase/quantum/ bragg .html.

7. Thornton, S.T. and A.F. Rex, *Modern physics for scientists and engineers*, 2012.

8. Breck, D.W. Flanigen, *Molecular Sieves,* Society of Chemical Industry, 1968.

9. Fichtner-Schmittler, H., U. Lohse, G. Engelhardt, and V. Patzelova, *Unit cell constants of zeolites stabilized by dealumination determination of Al content from lattice parameters,* Crystal Research and Technology, 1984. **19**(1): p. K1-K3.

10. Sohn, J.R., S.J. DeCanio, J.H. Lunsford, and D.J. O'Donnell, *Determination of framework aluminium content in dealuminated Y-type zeolites: a comparison based on unit cell size and wavenumber of ir bands,* Zeolites, 1986. **6**(3): p. 225-227.

11. Van Bekkum, H., *Introduction to zeolite science and practice*, Vol. 137. 2001.

12. Jorik, V., *Semiempirical approach to determinationof framework aluminum content in faujasite-type zeolites by X-ray powder diffraction,* Zeolites, 1993. **13**(3): p. 187-191.

13. *XRD in the Workplace-Practical XRD Techniques In The Workplace*, Cleveland Analytical [Accessed 2012] Available from: http://www. clevelandanalytical.co.nz/X-Ray%20Diffractometers/XRD%20in%20the%20 Workplace%20-%20Practical%20XRD%20Techniques%20In%20The%20 Workplace.

14. Van Bekkum, H., E.M. Jansen, and J.C. Jacobs, *Introduction to ZeoliteScience and Practice*, ed. 2nd. 2001, Amsterdam: Elsevier.

15. *Radiological and Environmental Management, Scanning Electron Microscope*, 2013 [Accessed 2013] Available from: http://www.purdue.edu/rem /rs/sem.htm.

16. Peterson, B.P., *Energy Dispersive Spectroscopy Characterization of Solute Segregation in Ti-6Al-4V*, in *School of Materials Science and Engineering*. 2011, The Ohio State University.

17. *Principle of EDAX*, 2007 17 December 2007 [Accessed 2012; Available from: http://commons.wikimedia.org/wiki/File:EDX-scheme.svg.

18. Odin, C., *Critical behavior of KDCO$_3$ from 2H and 39K single crystal NMR,* Magnetic Resonance in Chemistry, 2008. **46**(1): p. 9-16.

19. Che, M. and J.C. Védrine, *Characterization of solid materials and heterogeneous catalysts*, 2012.

20. Alia, A., S. Ganapathy, and H.J. de Groot, *Magic angle spinning (MAS) NMR: a new tool to study the spatial and electronic structure of photosynthetic complexes,* Photosynthesis research, 2009. **102**(2-3): p. 415-425.

21. Bartholomew, C.H. and R.J. Farrauto, *Fundamentals of Industrial Catalytic Processes,* John Wiley & Sons, Inc.: New York, ISBN, 2006. **13**.

22. de Groot, H.J., *Solid-state NMR spectroscopy applied to membrane proteins,* Current opinion in structural biology, 2000. **10**(5): p. 593-600.

23. Chester, A.W. and E.G. Derouane, *Zeolite characterization and catalysis*, 2009:p.72-80.

24. Agger., J., *NMR-Analysis, CHEM 20710 Materials & Computational Chemistry, Undergraduate Course – The University of Manchester* 2009.

25. *BET Surface Area Analysis of Nanoparticles*, Science and Technology 2011 [Accessed 2013] Available from: http://cnx.org/content /m38278/1.1/.

26. Jendrasiak, G.L. and R.L. Smith, *The effect of the choline head group on phospholipid hydration,* Chemistry and Physics of Lipids, 2001. **113**(1–2): p. 55-66.

27. Brunaue S., P. Emmett., and E. Teller, *Theory of the Van Waals Adsporption of gases,* Journal of the American Chemical Society, 1940. **62**(7): p. 1723.

28. Do, D. and K. Wang, *A new model for the description of adsorption kinetics in heterogeneous activated carbon,* Carbon, 1998. **36**(10): p. 1539-1554.

29. Coats, A.W. and J.P. Redfern, *Thermogravimetric analysis. A review,* Analyst, 1963. **88**(1053): p. 906-924.

30. TA Instruments. *Thermogravimetric analyzer (TGA),* 2012 [Accessed 2013] Available from: http://www.directindustry.com/prod/ta-instruments/ thermogravimetric -analyzers -tga -38477-273568.html.

31. FeCrAlloy® *Goodfellow Cambridge Ltd*, 2012 [Accessed 2011] Available from: http://www.goodfellow.com/E/Fecralloy-Iron-Chromium. html.

32. Nikolakis, V., G. Xomeritakis, A. Abibi, M. Dickson, M. Tsapatsis, and D.G. Vlachos, *Growth of a faujasite-type zeolite membrane and its application in the separation of saturated/unsaturated hydrocarbon mixtures,* Journal of Membrane Science, 2001. **184**(2): p. 209-219.

33. Yasaki, S., Y. Yoshino, K. Ihara, and K. Ohkubo, *Method of manufacturing an exhaust gas purifying catalyst*, 1993, US Patent 5,208,206.

34. Valentini, M., G. Groppi, C. Cristiani, M. Levi, E. Tronconi, and P. Forzatti, *The deposition of [gamma]-Al_2O_3 layers on ceramic and metallic supports for the preparation of structured catalysts,* Catalysis Today, 2001. **69**(1-4): p. 307-314.

Chapter 4

Results and Discussion of the Synthesis and Characterisation

4.1 Introduction

This chapter presents characterisation of the pre-treated FeCrAlloy wires intended to support the catalyst and the the structured zeolite grown onto the FeCrAlloy support wire.

The samples have been characterised using a range of techniques, including X-ray diffraction (XRD), Electron microscopy (SEM), Energy Dispersive X–ray analysis (EDAX) and Thermogravimetric Analysis (TGA). The transition from oxide-on-alloy wires to hydrothermally synthesised uniformly zeolite coated surfaces was followed using SEM and XRD. In addition, the robustness of the

prepared coating was confirmed by subjecting these to thermal cycling (ambient to 550°C).

The target of this work was to use synthesised structured catalysts in catalytic an application where the combined properties of both the substrate and the zeolite might enhance the overall catalytic application.

4.2 Influence of oxidation time on the Aluminium oxide growth on FeCrAlloy wires

Different pre-treatments methods were applied to the FeCrAlloy wires before the final pre-treatment method was chosen, with Scanning electron microscopy (SEM) analysis carried out before and after each treatment step. **Figure 4-1** shows the surface of the wire magnified 240,000 times for the as-supplied wire, the cleaned wire, the acid and caustic washed wire, and finally the wire after all these treatments and oxidised at 1000°C for 4 h. The roughness of the surface can be seen to increase after each pre-treatment step with an oxide layer (Al$_2$O$_3$) observed on the FeCrAlloy surface after heating to 1000°C for 4 h. The aluminium oxide scales helping in the seeding the zeolite onto the support surface, therefore the thermal pre-treatments on the FeCrAlloy substrate has been applied in order to grow thin films of aluminium oxide scales on the FeCrAlloy surface [1].

Characterisation was carried out on two sets of thermal pre-treated samples, the first set of experiments was performed on two FeCrAlloy wires samples which had not been washed with acid or caustic, but which had been oxidised at 1000°C for different period (3 and 6 hours). The second set of experiments was conducted on the wires that had undergone physical pre-treatment and subsequent oxidation 3-24 hours at 1000°C. SEM was used to image the microstructure of FeCrAlloy wires surface, and in addition weight gain with the FeCrAlloy wires recorded followed by adhesion testing of the aluminium oxide layer formed on the metal surface.
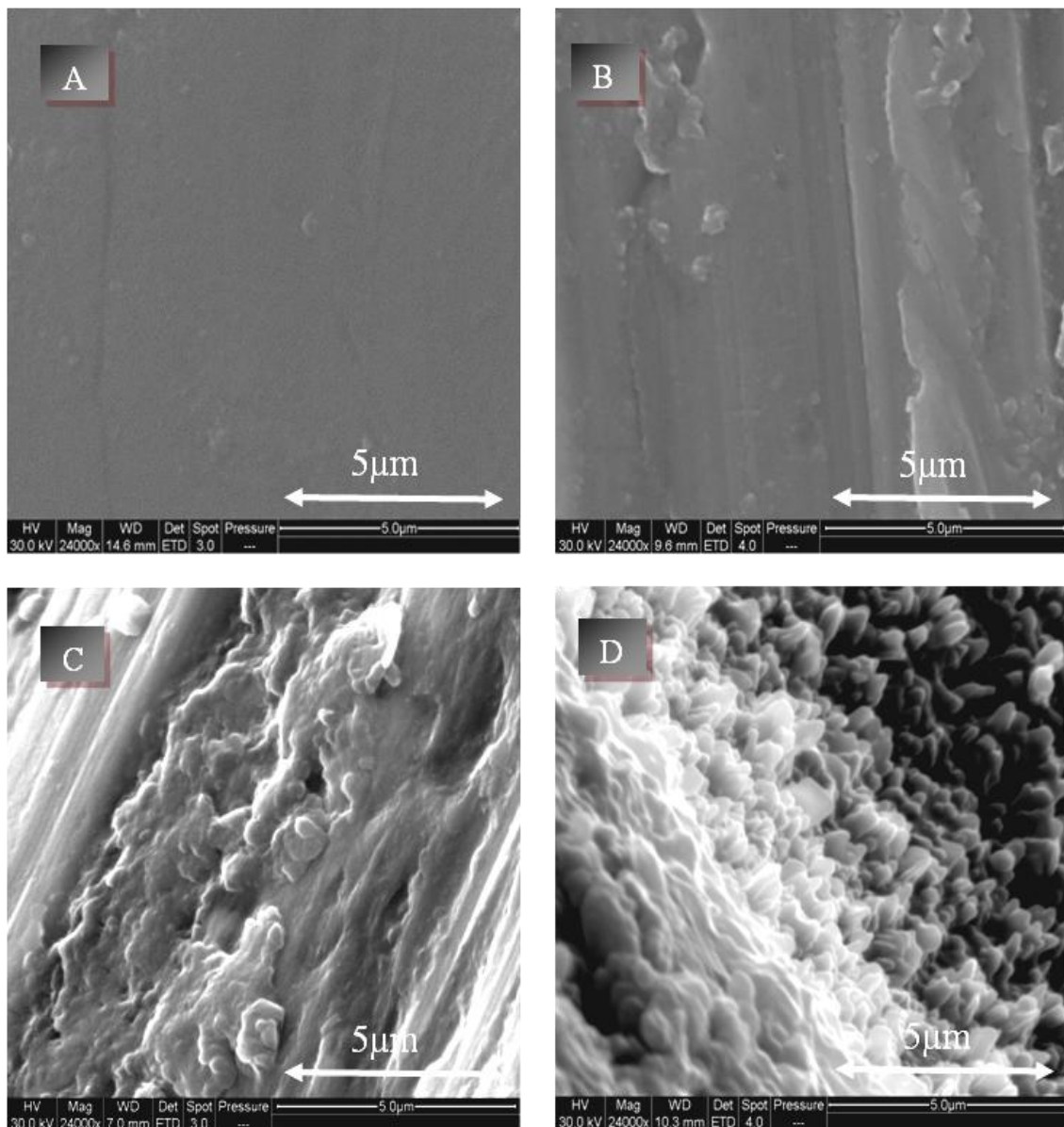
Figure 4-1: FeCrAlloy wires before and after the physical pre-treated A) as-supplied B) sand-papered, C) acid and base washed and D) oxidised for 4 h at 1000°C.

Figure 4-2 shows the formation of the aluminium oxide scale on surface of the FeCrAlloy samples without any acid and caustic pre-treatment. The oxidation was performed for 3 and 6 hours in order to study the effect when varying the oxidation time on the morphology of the samples. After 3 hours of oxidation, a non-uniform oxide layer started to form on the surface and the whisker-like morphology began to growth on the surface due to the diffusion of aluminium ions from the

material to the exterior [2]. Moreover, the growth of the oxide layer was increasingly developed as the oxidation period was extended up to 6 hours [3]. This is seen by the increase in the Al/Fe weight ratio from 0.82 to 1.11 for 3 and 6 hours respectively in EDAX analysis (**Figure 4-3**) no further work was carried out on untreated wires. However, it was found this growth was not uniform over the entire surface of the sample.

Second set of the physical pre-treated FeCrAlloy wires oxidised 3-24 hours at 1000°C results were detailed as followed.
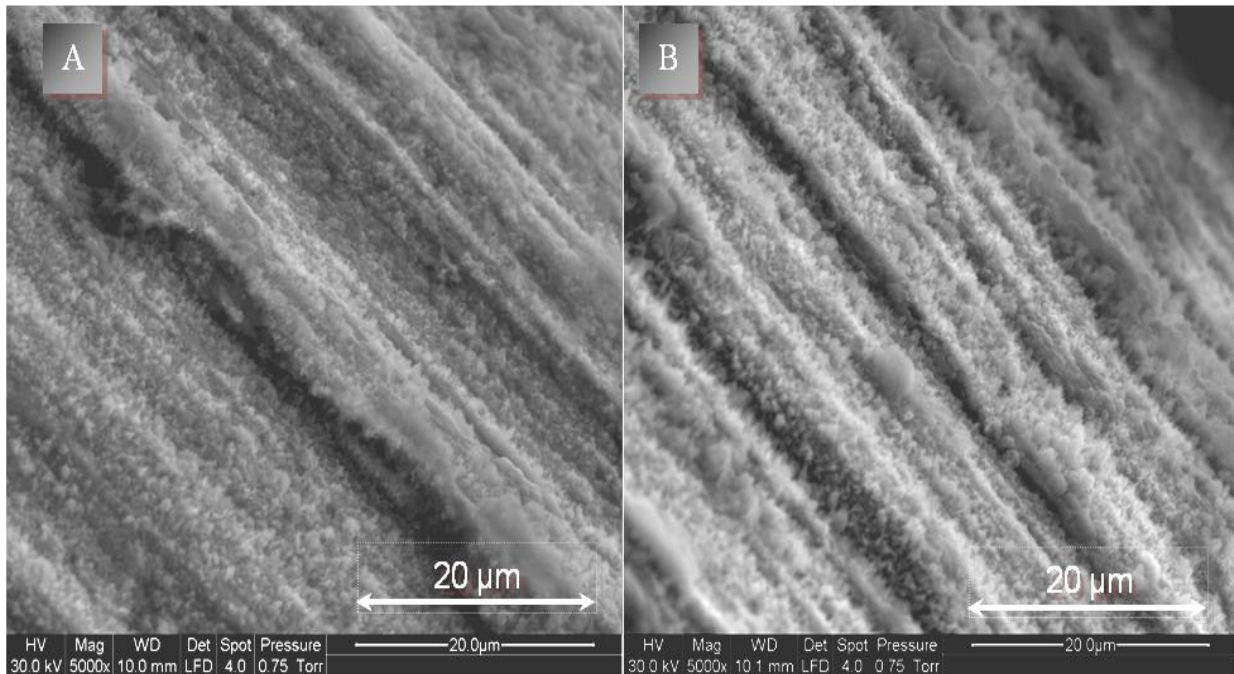
Figure 4-2: SEM analysis of FeCrAlloy wires without acid and caustic pre-treatments oxidise at 1000°C for A) 3 h, B) 6 h.
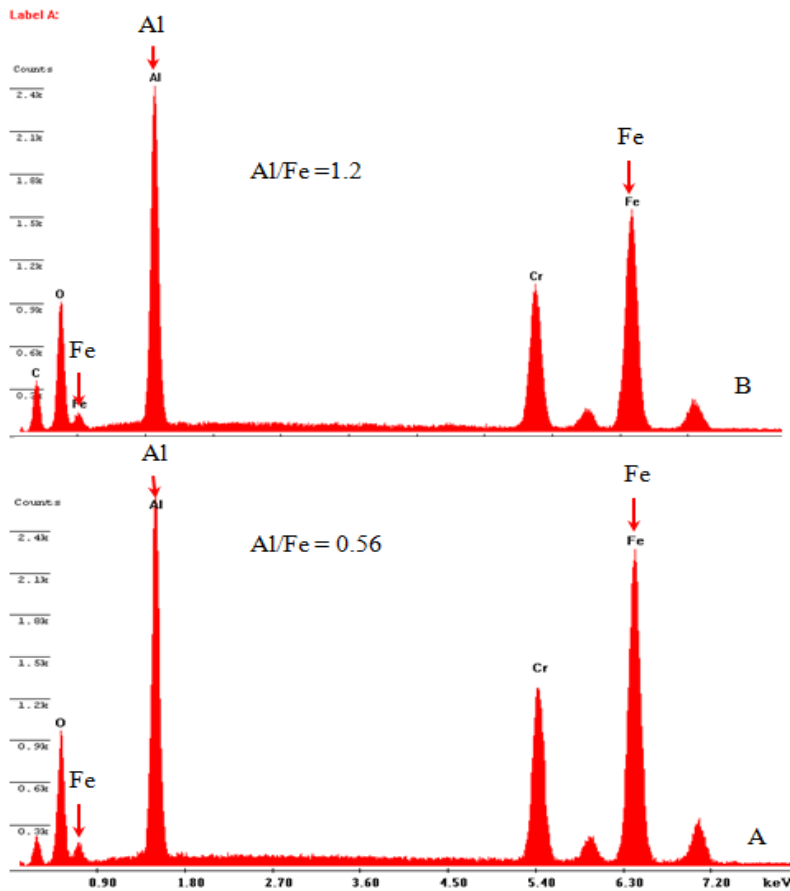
Figure 4-3: EDAX analysis of FeCrAlloy wires without acid and caustic pre-treatments oxidise at 1000°C for A) 3 h, B) 6 h.

Figure 4-4 shows the weight-gain measurements obtained by taking the weight measurement for the acid and caustic pre-treatment wires before and after oxidation at 1000°C in order to determine the weight-gain corresponding to heat treatment. Generally, the weight-gained percentage tended to increase when the oxidation period was extended, conclusions which are in good agreement with the literature [4-6]. This behaviour indicates that there is phase transformation from platelet-like formations of γ-Al$_2$O$_3$ to smoothened surface α-Al$_2$O$_3$ at 1000°C after four hours, with the metastable alumina (γ-, δ-, or θ- alumina) oxides formed at 800°C [7] and transformed to stable α-Al$_2$O$_3$ in range of 925-1200°C [8, 9]. The fact that there was increase in the weight-gain throughout the oxidation period confirms the formation of an oxide layer on the FeCrAlloy surface.
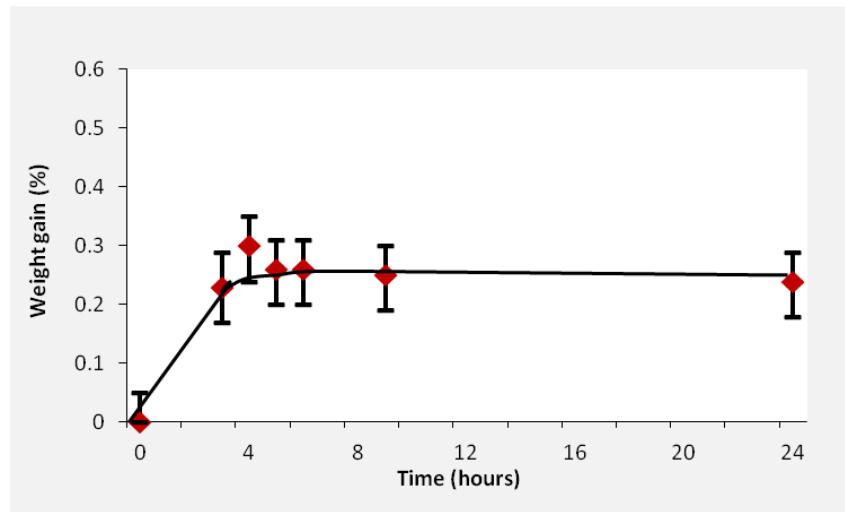
Figure 4-4: Weight gain on FeCrAlloy wires with time at 1000°C.

Table 4-1: Elemental analysis, weight gain and layer thickness of oxide layer on wire surface at different oxidation times.

Elements	0h	3h	4h	5h	6h	9h	24h
O (wt %)	0.0	14.9	15.6	12.6	12.4	12.4	8.1
Al (wt %)	8.8	53.0	57.9	54.0	50.0	42.8	36.4
Cr (wt %)	22.7	5.6	3.3	3.4	8.2	9.1	9.9
Fe (wt %)	68.5	26.5	23.3	30.0	29.4	35.7	45.6
Al/Fe	0.1	2.0	2.5	1.8	1.7	1.2	0.8
Oxide layer (μm)	0.0	2.0	4.1	3.4	2.8	2.1	2.5
Weight gain (%)	*0.00*	*0.23*	*0.26*	*0.30*	*0.26*	*0.25*	*0.24*

In addition, SEM images (**Figure 4-5**) showed the formation of the oxide layer with time, oxide whiskers became evident at 4 h, and then become a smoother layer after 6 h of oxidation. The results indicate that the whiskers-like formation developed on the surfaces between 3 and 6 hours at 1000°C. However, prolonging the oxidation time to more than 9 hours resulted in smoothing the surface due to the formation of α-Al_2O_3 with less surface area.

Elemental EDAX analysis were carried out on typically more than four spot points of the FeCrAlloy wire surface for each sample (**Figure 4-6** and **Table 4-1**). Taking a close detailed look at the result obtained below 3-5 h revealed that FeCrAlloy wires for 3 hours in muffle furnace at 1000°C was insufficient time to grow a uniform oxide layer on the surface and the platelet like growth was formed in small clusters along the surface (typically 2 Al/Fe ratios).
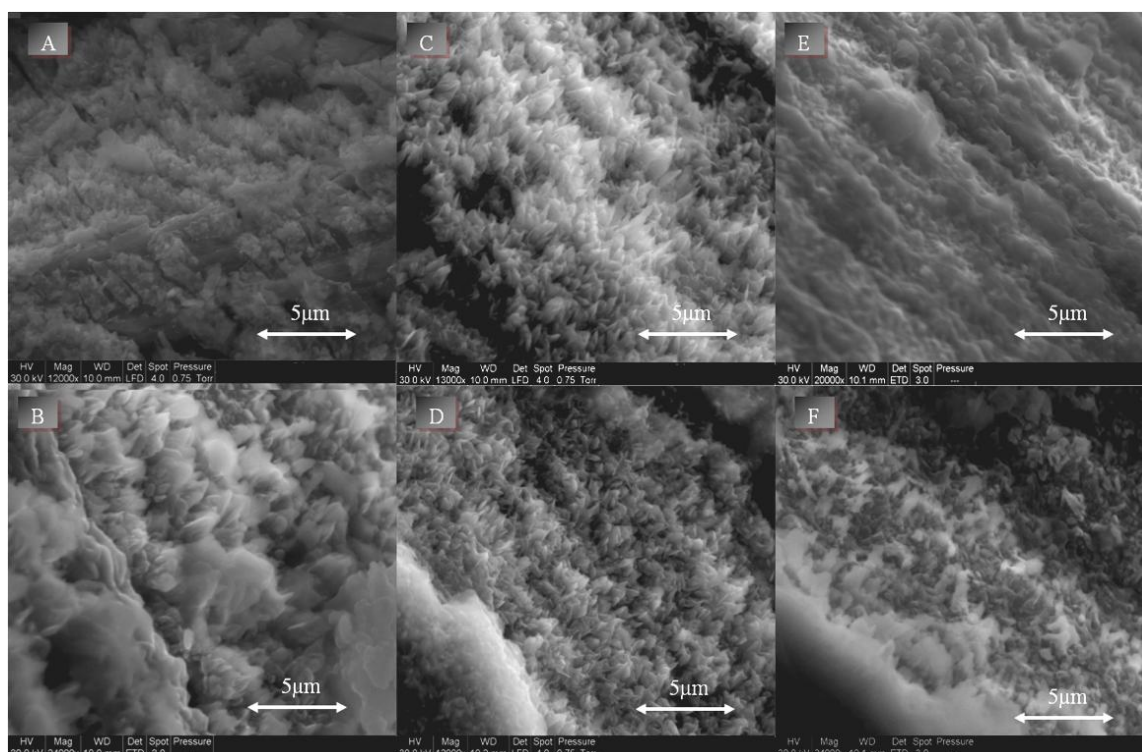
Figure 4-5: Surface morphology after different oxidation times

A) 3 h, B) 4 h, C) 5 h, D) 6 h, E) 9h, F) 24 h.
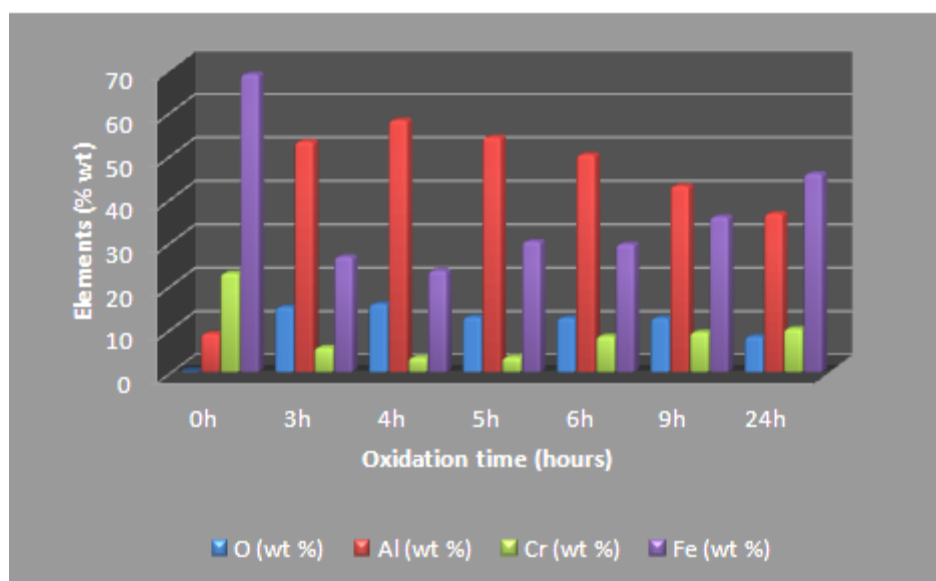
Figure 4-6: Elemental analysis of the wire surface at different oxidation times.

After 4 hours of oxidation the platelets were the main alumina morphology growing on the FeCrAlloy surface with higher Al/Fe ratio up to 2.5 and EDAX mapping spectra for the cross-sections of the 4 hours oxidised wire confirmed the depth of oxide layer was 4.1 µm (**Figure 4-7**).

Extending the oxidation time to 5 hours resulted in the formation of uniform whiskery structures much like those seen after 4 hours, however the Al/Fe weight ratio was seen to decrease to 1.8 and the layer depth decreased. By extending the oxidation time the flat oxide scales gradually predominated on the surface until this was evenly formed across the entire surface of the wire sample after 24 hours. As such, the Al/Fe weight ratio dropped to a minimum value of 0.8.

The EDAX analysis results shown in **Table 4-1** reveal the presence of Fe and Cr in addition to aluminium oxide, with the average concentration for these oxides decreasing within 3-9 hours. These results are similar to the results obtained by Badini [2], who found that the Cr and Fe oxide concentrations were seen to decrease with prolonged oxidation time as long as 12-30 days at 900 and 1200°C.
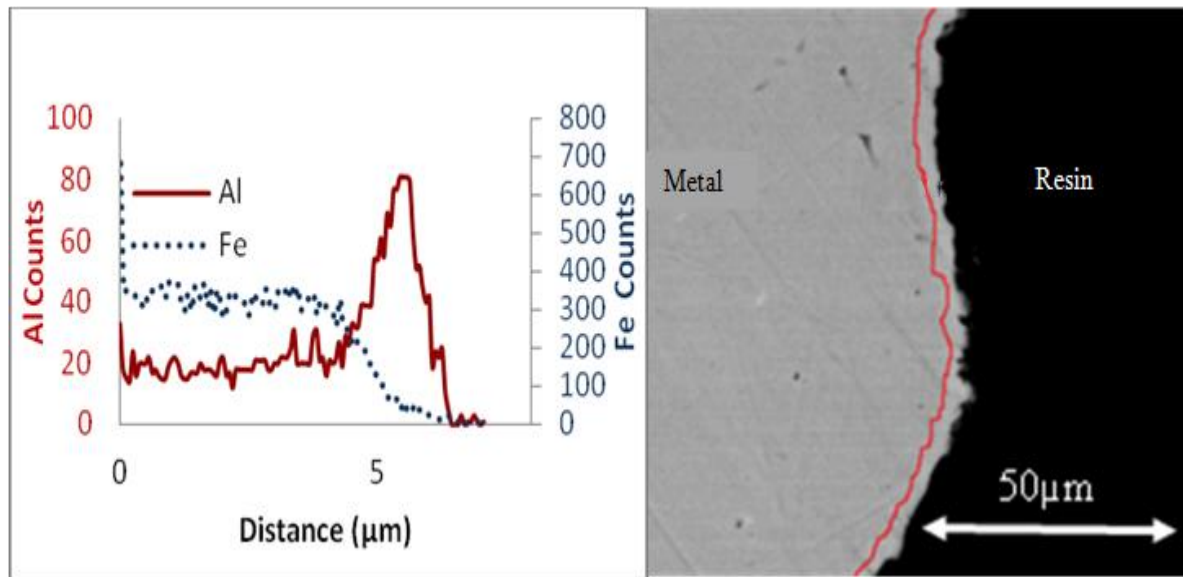
Figure 4-7: Elemental line scans cross the wires oxidised for 4 h at 1000 $^{\circ}$C (for clarity, the red line approximates the position of oxide layer).

According to Herbelin [10], a metastable aluminium oxide is formed at 900°C in the oxidation process and led to a rapid consumption of the Al-reservoir within the first ten hours of oxidation, and the oxide growth rates slow down after a short time. Correspondingly, in this research, for 24 hours oxidation the Al/Fe weight ratio dropped to 0.8 and the oxide layer start to peel from the surface to reveal the fresh iron/iron oxide beneath, suggesting that the Al-depletion is enhanced over an extended oxidation time up to 24 hours. A comparison of selected FeCrAlloy wires using XRD (**Figure 4-8**) showed the XRD reflection for the aluminium oxide layer was reduced suggesting a decrease in the Al content in oxide layer after 24 h.
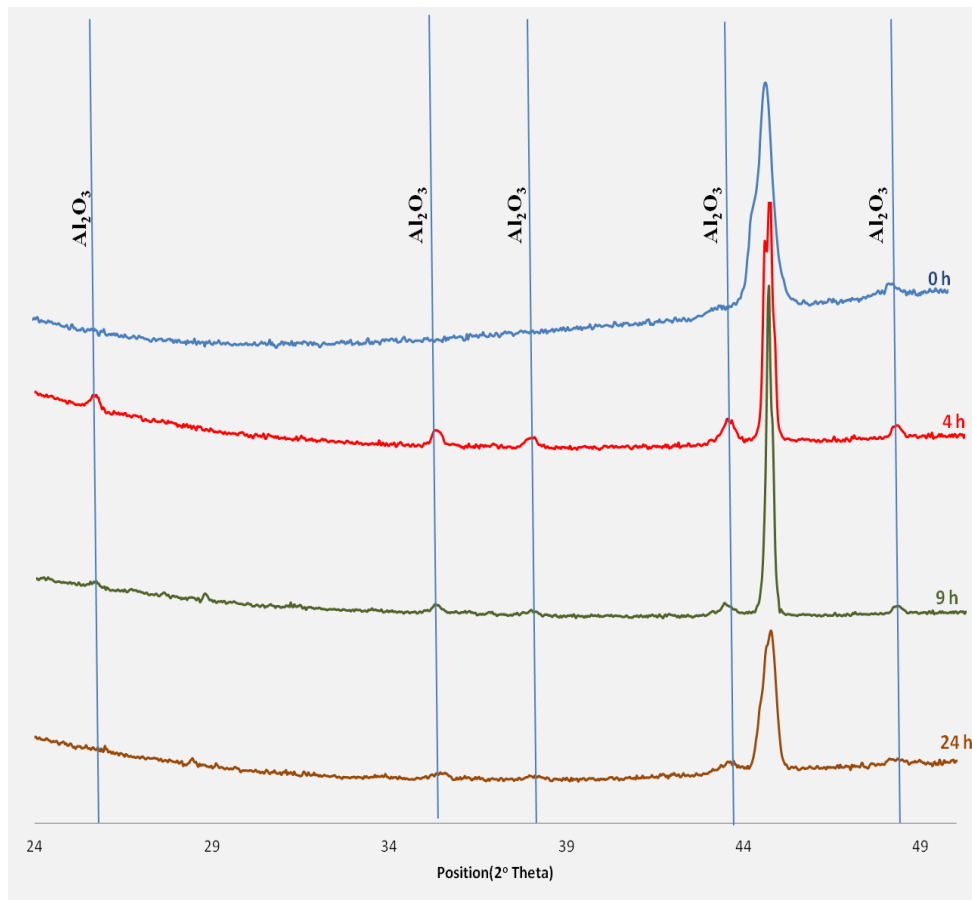
Figure 4-8: XRD patterns for pre-treated wires at different oxidation time.

4.3 Influence of oxidation time on the zeolite growth on the aluminium oxide FeCrAlloy Surface

In order to investigate the possibility of the growing the zeolite layer onto a non-oxidised FeCrAlloy wire surface, an experiment was conducted where non-oxidised FeCrAlloy wires were immersed in a synthesis gel for 48 hours. From examination of the wires surface, it was concluded that there was no zeolite growth, however growth was observed when the wires were oxidized for between 3-24 h prior to immersion in the zeolite gel under hydrothermal conditions. This procedure was applied to both zeolite Na–ZSM-5 and zeolite Na–Y in order to ascertain the effect of the oxide layer grown on the FeCrAlloy surface for different zeolites.

One set of oxidised wires was immersed in $6.36Na_2O:1.86Al_2O_3:0.2TPAOH:60SiO_2:1864H_2O$ in autoclave and heated to 180^oC for 48 hours, and another set of oxidised wires were immersed in zeolite Y gel with composition $(3.Na_2O:Al_2O:SiO_2:12H_2O)$ at 100^oC for 48 hours. The remaining powder from both zeolite Na–ZSM-5 and zeolite Na–Y processes was subsequently collected and characterized using the XRD and SEM to confirm the formation of a pure zeolite phase.

The influence of oxidation time on the FeCrAlloy wires of the zeolite layer growth was investigated in terms of coverage (namely the increase in the mass of zeolite film verses the surface area of the wires (g m^{-2})), morphology, the adhesivity of the zeolite layer, and finally the mass-gained during the coating procedure.

Calcination and thermal cycling of the zeolite layers was studied using thermogravimetric analyzer *(Q5000-IR TA Instruments)*. All structured zeolite wires were calcined to remove the template from the zeolite by heating from ambient at a rate of 1^oC min^{-1} to 550^oC where it was held for 480 min. The adhesion of the zeolite layers was tested by thermal cycling, where selected wires were heated and cooled at 10^oC min^{-1} between ambient to 550^oC. The wires were held at both the high and low temperatures for 30 min and this process repeated five.

4.3.1 Zeolite Na-ZSM-5

For the Na–ZSM-5 layer grown on the wires oxidised for 3, 4, 5, 6, 9 and 24 hours calcination was applied before the thermal cycling process was started, with **Figure 4-9** showing a uniform layer of Na–ZSM-5 covering the oxidised wires with a range of coverage ratios. The coated-wires were then calcined and thermally cycled using a TGA to determine adhesivity of the zeolite films on the substrate surface (**Table 4-2**).

All the TGA pans were weighed before and after each step to determine any mass loss during calcination and thermal cycling, with this mass-loss resulting from the loss of volatile components, chemisorbed water and physisorbed water, in addition to the breakdown of TPAOH.

During the thermal cycling process, wires had been oxidised for 3-5 h showed very little weight loss (0.1%), however, wires oxidised for between 9-24 h showed significant peeling of the zeolite layer (typically 8–11%), with the weight losses recorded in **Table 4-2.** SEM and TGA analyses indicated that for the 4 hour oxidised wires had the highest Na-ZSM-5 zeolite loading and also possessed excellent resistance to thermal cycling.
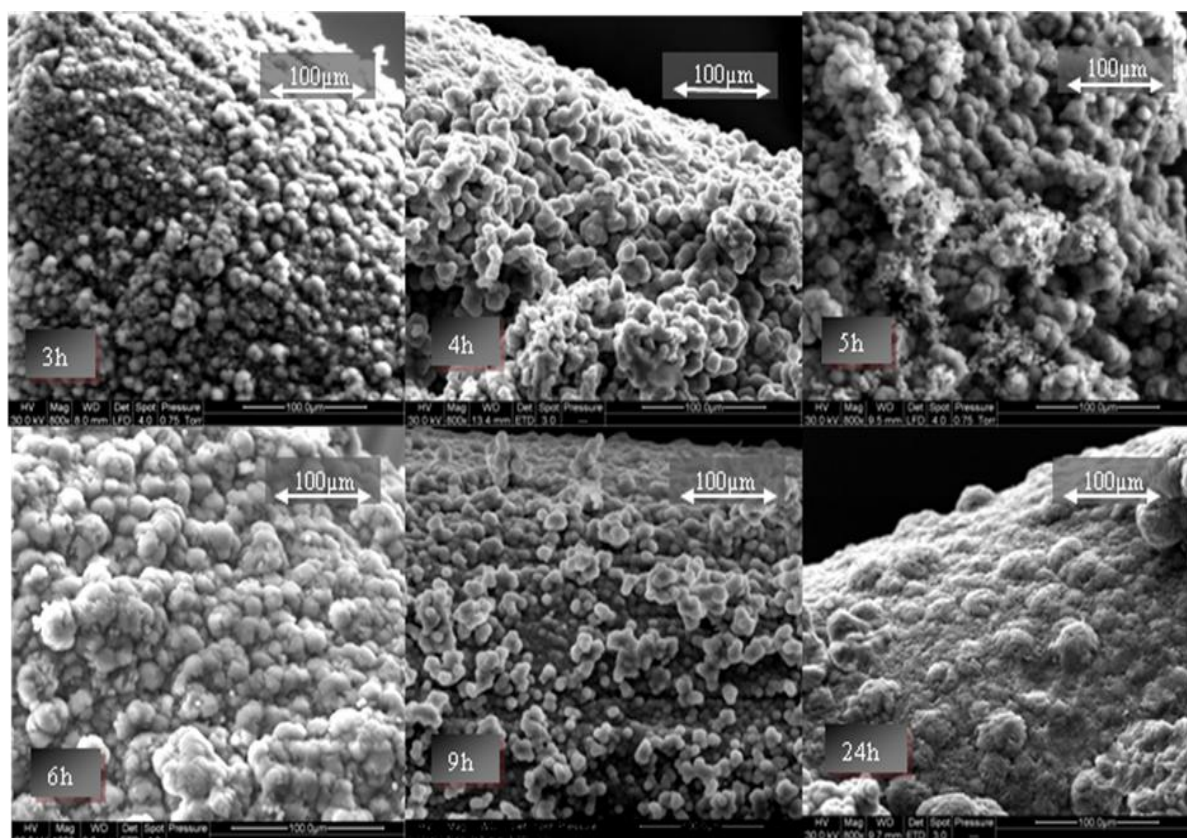
Figure 4-9: SEM morphology after calcination of Na–ZSM-5 coated wires following oxidisation for 3-24 h.

Table 4-2: The change in zeolite Na–ZSM-5 coverage of oxidised wires (3-24 h) and the weight change after calcination and thermal cycling.

Wires	3 h	4 h	5 h	6 h	9 h	24 h
Zeolite coverage (g m^{-2})	192	317	161	151	142	102
Weight loss on calcination (%)	3.4	3.2	2.5	2.0	1.9	1.8
Weight loss after thermal cycling ×5, (%)	0.1	0.1	0.1	1.0	7.8	10.9
Thickness Layer (µm)	130	150	125	120	80	51

The morphology of Na–ZSM-5 on the oxidised wires was investigated after calcination (**Figure 4-9**), with no significant difference in the zeolite layer on the surface being observed after TPAOH removal (calcination).

Figure 4-10 shows the initial calcination for each structured Na-ZSM-5 zeolite prepared at different oxidation times. This is followed by thermal cycling (at least ×5). As oxidation time increases there is a fall in the amount of the weight lost. All the structured Na-ZSM-5 zeolite typically loses 0.5% weight between ambient temperature and 125°C. The oxidation of TPAOH take place as expected above 300°C and is complete around 475°C. The overall weight loss is detailed in **Table 4-2**, however varies from 1.8% weight loss (24 h) to 3.4% wt loss at 3 h and not too surprisingly, as the zeolite layer thickness decreases so does the weight loss due to TPAOH.

On thermal cycling, SEM analysis revealed that there was also no change in the morphology of the zeolite layers between 3-5 hours; however, the zeolite layer had begun to peel off the wires when they were oxidised for more than 6 h, with this peeling increasing in significance for wires oxidised at 9 hours or longer. The surface damage that results from extended periods of oxidation of the structured zeolite and subsequent thermal cycling is shown in **Figure 4-11**.
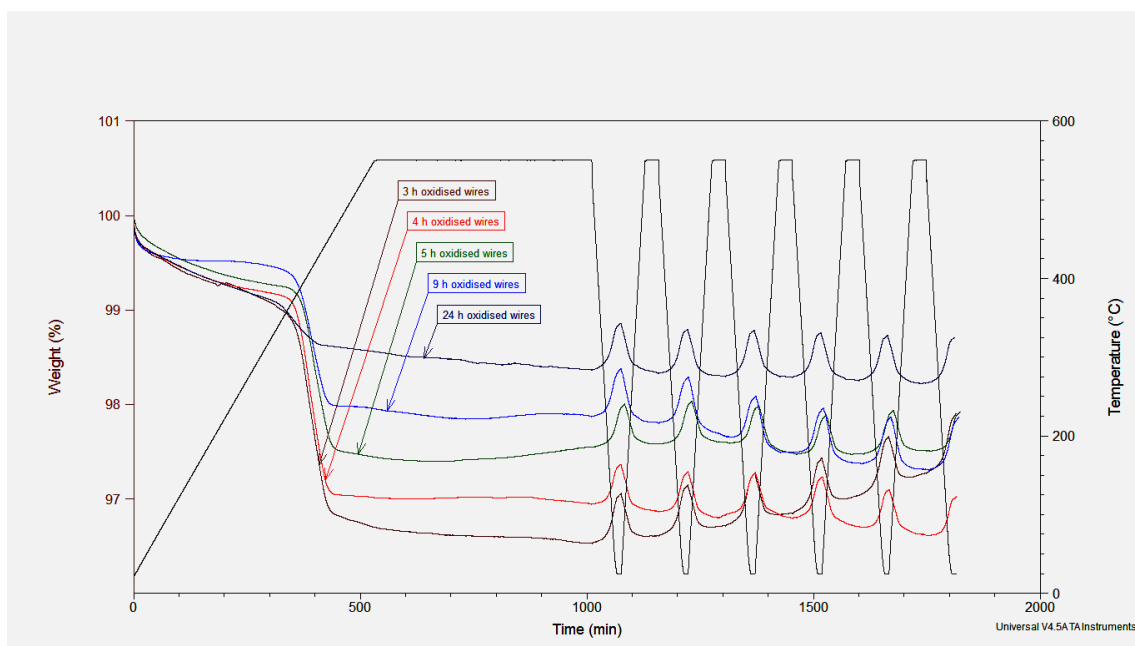
Figure 4-10: TGA comparison of the ZSM-5 zeolite on the different oxidised wires.
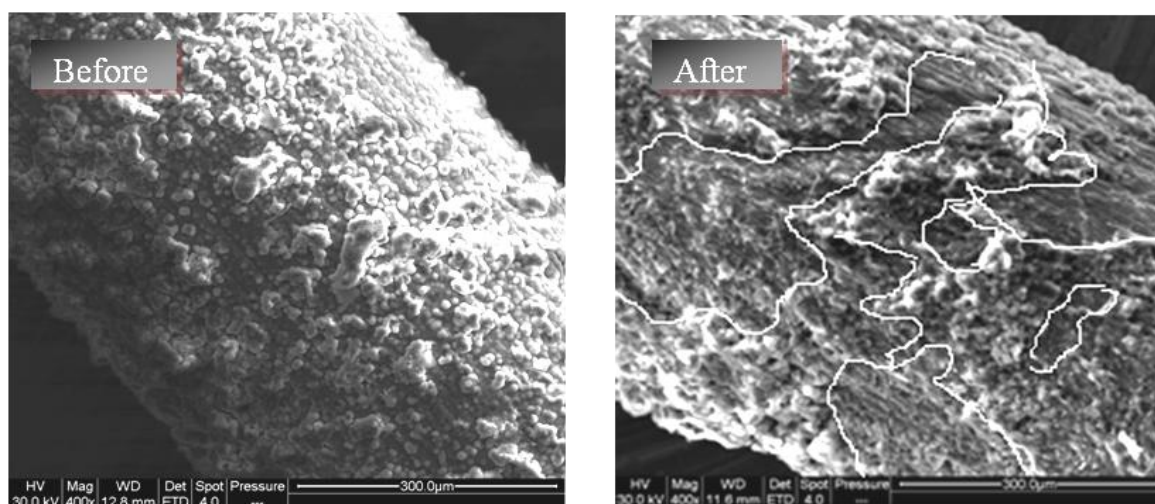
Figure 4-11: SEM morphology before and after calcination and thermal cycling for Na–ZSM-5 coated wires oxidised for 24 h. Note the highlighted area where peeling has occurred.

4.3.2 Zeolite Na-Y

The hydrothermal synthesis of zeolite Na–Y on oxidised wires was carried out in order to study the effect of oxidation time on the zeolite loading and the thermal stability of the structured zeolite. The processes used were identical to the tests used for the Na–ZSM-5 growth on the oxidised wires (**Figure 4-12**).

The calcination process showed that the weight loss that occurred between 25–300°C was due to the removal of the volatiles in the zeolite structure. For all wires, the weight loss on calcination was related to the H_2O loss from the zeolite (**Table 4-3**), and SEM micrographs showed that the calcined zeolite Y layers on the oxidised wires between 3-24 h were continuous (**Figure 4-13**). As with the Na–ZSM-5, the SEM analysis showed no change in the morphology post-calcination, and unlike with Na–ZSM-5, zeolite Na–Y coverage of the surface was uneven, with thinner layers achieved (**Table 4-3**).
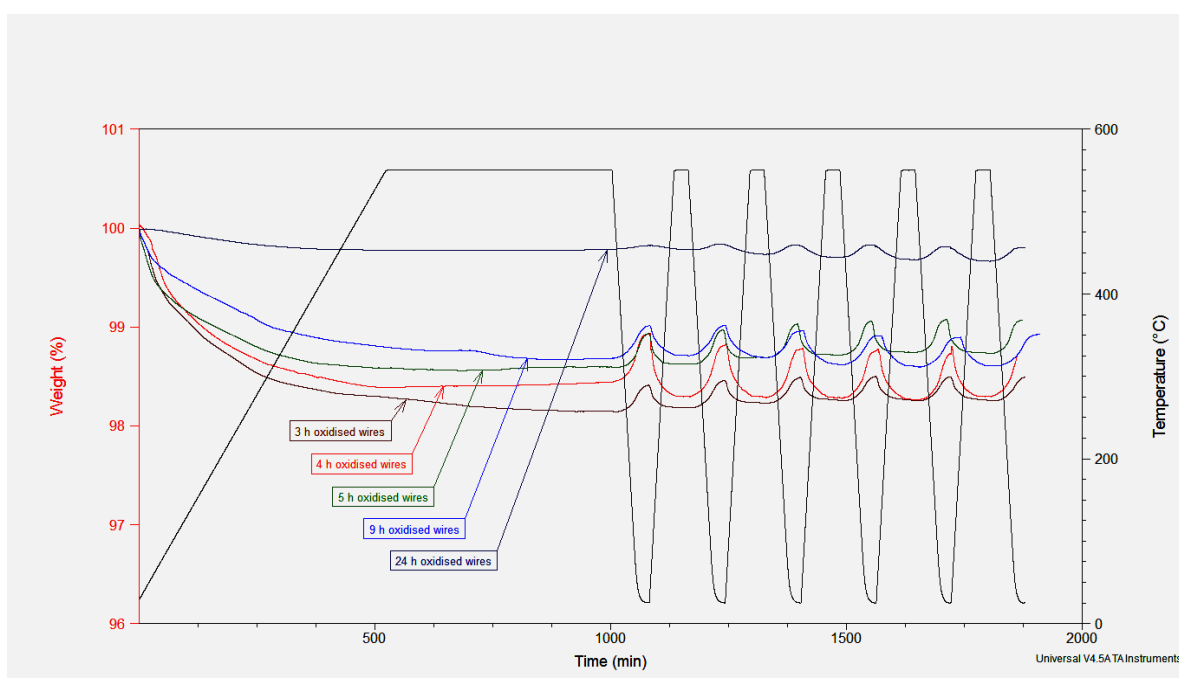
Figure 4-12: TGA comparison of the Na–Y zeolite on the different oxidised wires.

Table 4-3: The change in zeolite Na–Y coverage of wires oxidised between 3-24 h and the weight change after calcination and thermal cycling.

Wires	3 h	4 h	5 h	6 h	9 h	24 h
Zeolite coverage (g m^{-2})	52	57	51	24	20	9.89
Weight loss after calcination (%)	1.5	1.5	1.1	0.9	0.2	0.20
Weight loss after thermal cycling ×5 (%)	0.0	0.0	0.0	0.2	1.4	2.20
Thickness Layer (μm)	20.3	23	20.1	8.43	4.5	2.10

Adhesivity of zeolite Na–Y layers on the substrate surface was studied by thermal cycling using TGA. Overall, the weight loss on calculation was between 1-2% with almost all weight loss complete by 450°C. As expected the overall weight loss was related to the zeolite layer thickness Similar to the Na-ZSM-5 zeolite on thermal cycling, zeolite Na–Y showed evidence of peeling for wires oxidised at 6 h and above. Zeolite coatings were first observed falling away from wires that had been oxidised for 6 h **Table 4-3.**

The residue weight percentages confirmed that the wires subjected to oxidation for over 4 h showed no weight loss, and possessed the highest surface coverage. As with previous experiments, increasing the oxidation time to 24 h resulted in additional damage to the quality of the zeolite surface coating, as shown in **Figure 4-14**. The weight losses for the zeolite Na–Y layer were significantly lower than for the ZSM-5 layer for wires oxidised for similar times, with this attributed to the coverage of zeolite Y being less than coverage of the ZSM-5.

In addition, there was a difference in the interaction between the zeolite precursors gel and the aluminium oxide layer growth on FeCrAlloy surface, which was seen to depend on the synthesis conditions (for zeolite Y = 100°C while for ZSM-5 = 180°C), the gel composition (Si/Al ratio difference in the synthesis gel), and substrate surface morphology (roughness and hydrophilicity) [11, 12]. It was also found that low Si/Al ratio in the zeolite gel composition led to decrease in the nucleation and growth rates [13], and also that the roughness of the surface affected the number of the nucleation sites, resulting in the generation of superficial defects

[14]. Finally, it was shown that it was feasible to grow a zeolite Na–Y surface without the use of a template, however this did affect the coverage and most likely resulted in the low surface coverage observed when using this method.
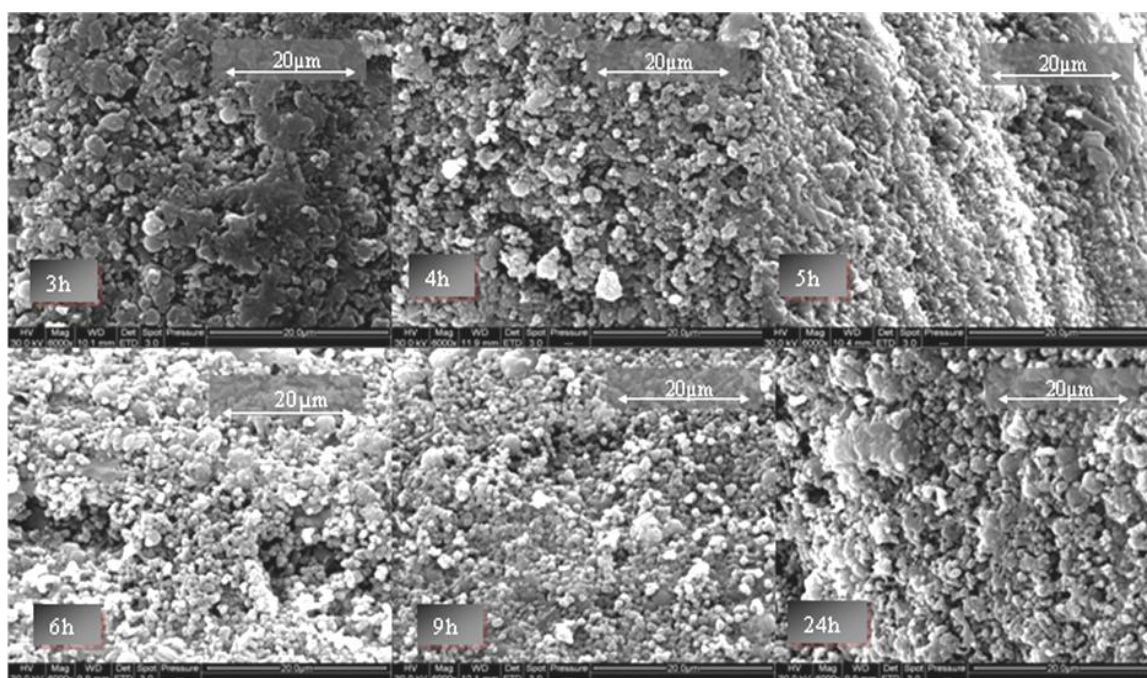
Figure 4-13: SEM of zeolite Na–Y on the surface of wires oxidised for different times.
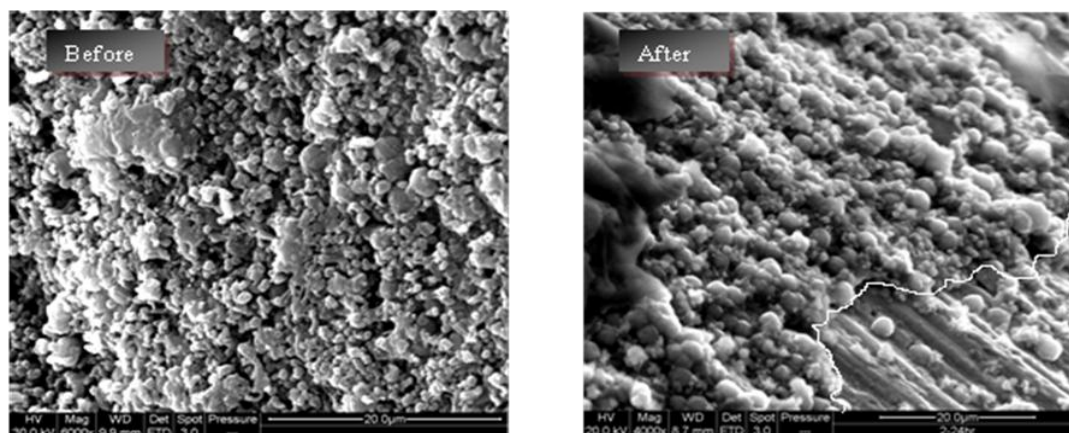
Figure 4-14: SEM morphology before and after the calcination and thermal cycling for 24 h oxidised coated zeolite Na–Y wire. Note the highlighted area showing peeling.

4.4 Influence of zeolite crystallisation time

The hydrothermal synthesis of target Na-ZSM-5 and Y zeolites was carried out using a range of different crystallisation times, preceded by an initial seeding of FeCrAlloy wires which had been oxidised for 4 h. In order to study the growth of the zeolite on the metal surface, analyses were performed on the zeolite produced in the bulk phase as well as the zeolite grown on the metal surface.

The analyses performed were XRD, to determine the phase and degree of crystallinity, scanning electron microscopy (SEM) to define the topology and the crystals size, and EDAX to ascertain the elementary analysis.

4.4.1 Powder Na-ZSM-5 zeolite

The Na–ZSM-5 structured zeolite and powder Na–ZSM-5 zeolite were prepared using synthesis times (4-72 h) and were examined using XRD. This data was compared with both standard zeolite data (**Figure 4-15**) [15] and commercial zeolite data (**Figure 4-16**) in order to evaluate the influence of crystallisation time on the degree of crystallinity and the zeolite structure. It was observed from the X-ray diffraction patterns that the crystallisation of the Na–ZSM-5 zeolite started after 20 hours of hydrothermal synthesis with the crystalline phase being hardly distinguishable for periods under sixteen hours. The appearance of the Na–ZSM-5 phase after 24 hours (**Figure 4-17**) revealed a slow growth rate as there was incomplete crystallisation before 24 hours. By increasing the crystallisation period, the crystalline phase materials increased and the baseline remained relatively flat and no other phases were obtained for the various crystallisation times.
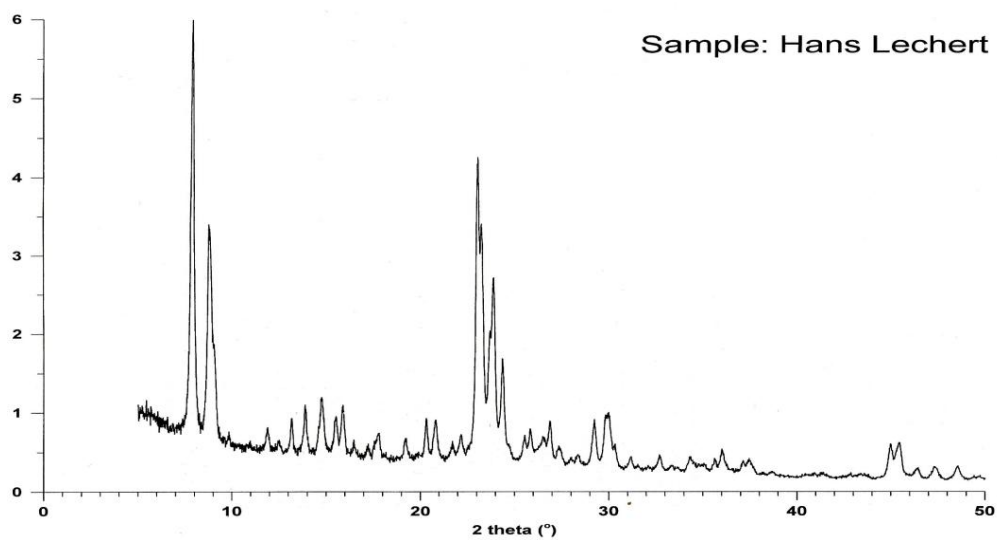
Figure 4-15: XRD patterns of the standard Na–ZSM-5 in the bulk phase.
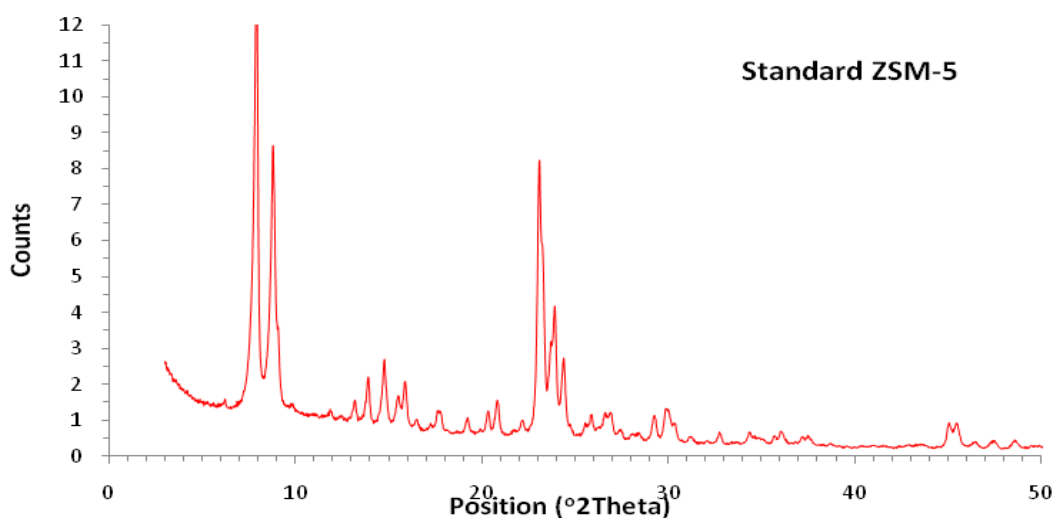
Figure 4-16: XRD patterns of the commercial Na–ZSM-5 in the bulk phase.
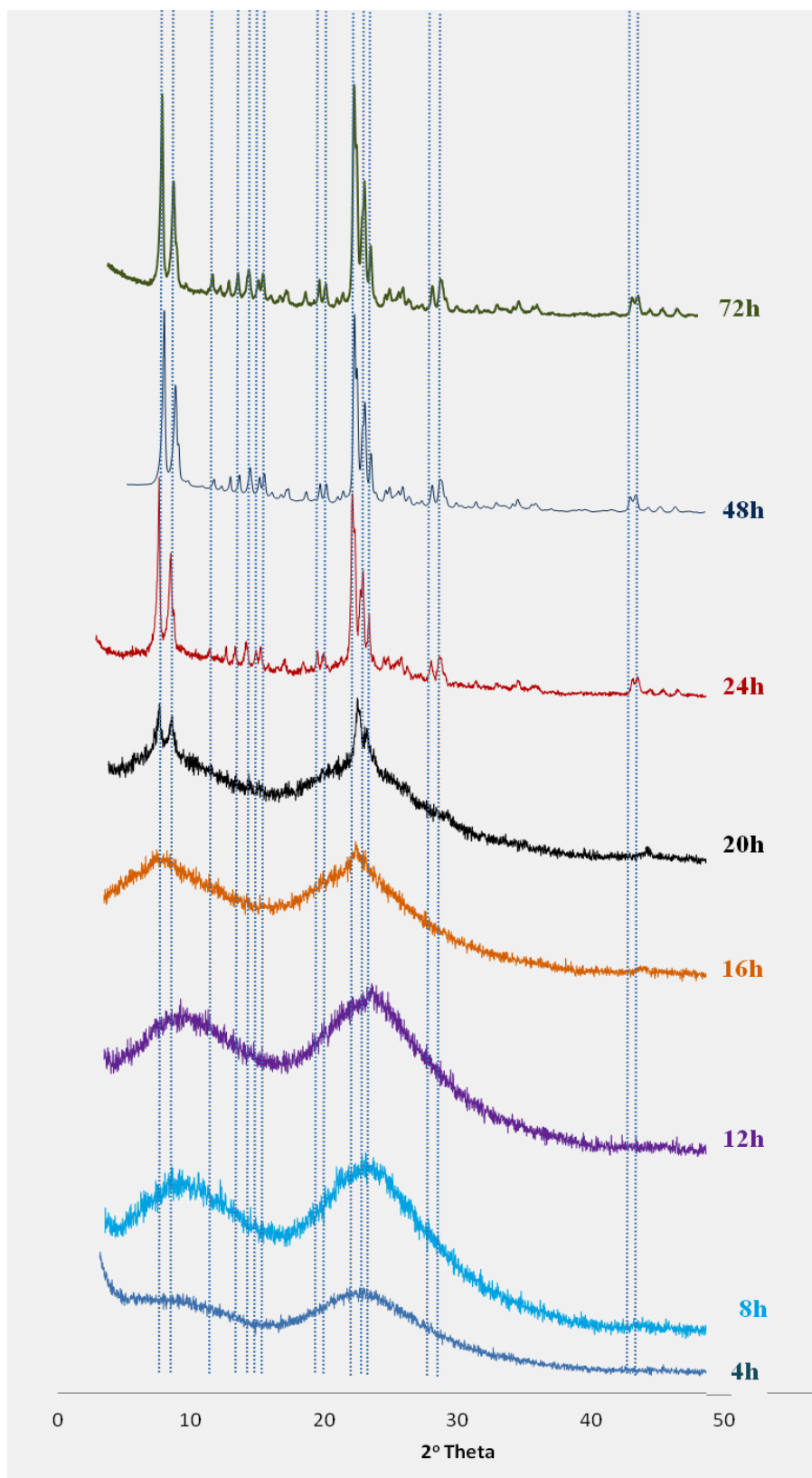
Figure 4-17: XRD patterns of the Na–ZSM-5 in the bulk phase at varying corresponded to the crystallisation times.

The XRD data tabulated in **Table 4-4** and summarised in **Figure 4-17** for the different crystallisation times offers a comparison with commercial zeolite samples. The intensity of the peaks for the 48 hours Na–ZSM-5 zeolite were the highest and, therefore, the degree of crystallinity of the samples was compared with a commercial zeolite which analysed under the same XRD settings. The degree of the crystallinity was been calculated using following equation.

$$\text{Average degree of crystallinity\%} = \frac{\sum \text{Intensities of the characteristic peaks of zeolite sample}}{\sum \text{Intensities of the peaks of reference zeolite sample}} \times 100$$

The typical reflection at the low angle (2θ = 7.9-8.9^{o}) for the Na–ZSM-5 zeolite was observed after 20 hours and the triplet in the range 2θ = 23–24°, at after 16 hours of synthesis time. The intensity of reflections increased when the synthesis time was extended up to 48 hours, and also only pure crystalline phase of Na–ZSM-5 was observed. For extended periods of synthesis time above 48 hours the intensity of the peaks tended to decrease suggesting a re-crystallisation effect [16] or to the collapse of the zeolite structure [17]. Finally, XRD analysis indicated that the optimum time for the crystallisation reaction was 48 h, with higher degrees of crystallinity obtained for the Na–ZSM-5 zeolite, when compared to the commercial Na–ZSM-5.

The topology of the synthesised Na–ZSM-5 at different synthesis times was studied using scanning electron microscopy (**Figure 4-18** and **Figure 4-19**). Overall the particles were spherical in shape and there was no significant change in the crystal size (2.71-2.79 µm diameter) when the crystallisation time was increased from 24 hours to 72 hours. No amorphous materials or other impurities were observed for synthesis times between 24-72 h. There was slightly change in Si/Al weight ratio between 11.4-11.53 (**Table 4-5**).

Table 4-4: Comparison of X-ray diffraction data for the different crystallisation time of the synthesised Na–ZSM-5 zeolites with a commercial zeolite.

Commercial MFI	Synthesis samples					
2θ	I_{rel} commercial	I_{rel} 16 hours	I_{rel} 20 hours	I_{rel} 24 hours	I_{rel} 48 hours	I_{rel} 72 hours
7.96	14.65		0.001	10.59	10.53	7.57
8.85	8.81		0.001	5.97	6.97	5.04
9.85				1.86	1.96	1.72
11.94	1.24			1.72	1.86	1.69
13.22	1.57			1.41	1.97	1.43
14.77	2.68			2.24	2.52	2.14
15.95	2.09			2.50	2.12	2.54
17.82	1.34			1.20	1.32	1.63
20.34	1.57			1.27	1.52	1.02
23.05	8.24	0.001	0.001	7.90	10.53	7.63
23.91	4.20			4.57	6.25	4.57
24.39	2.80			2.74	3.94	2.34
25.53	0.96			0.90	1.78	0.74
29.19	1.17			1.08	1.71	0.99
29.83	1.42			1.24	1.90	0.90
45.48	1.02	0.001	0.003	0.55	1.01	0.52
46.41	0.44		0.005	0.61	0.63	0.41
$\sum$	54.20	0.002	0.01	48.35	58.52	42.88
Crystallinity % $=\sum I_{rel\ sample}/\sum I_{rel\ commercial}$	*100*	*0.00*	*0.01*	*89.21*	*107.97*	*79.11*
Crystallinity % $= \sum I_{rel\ Sample}/\sum I_{rel\ 48\ hours}$	*92.62*	*0.00*	*0.01*	*82.62*	*100*	*73.27*
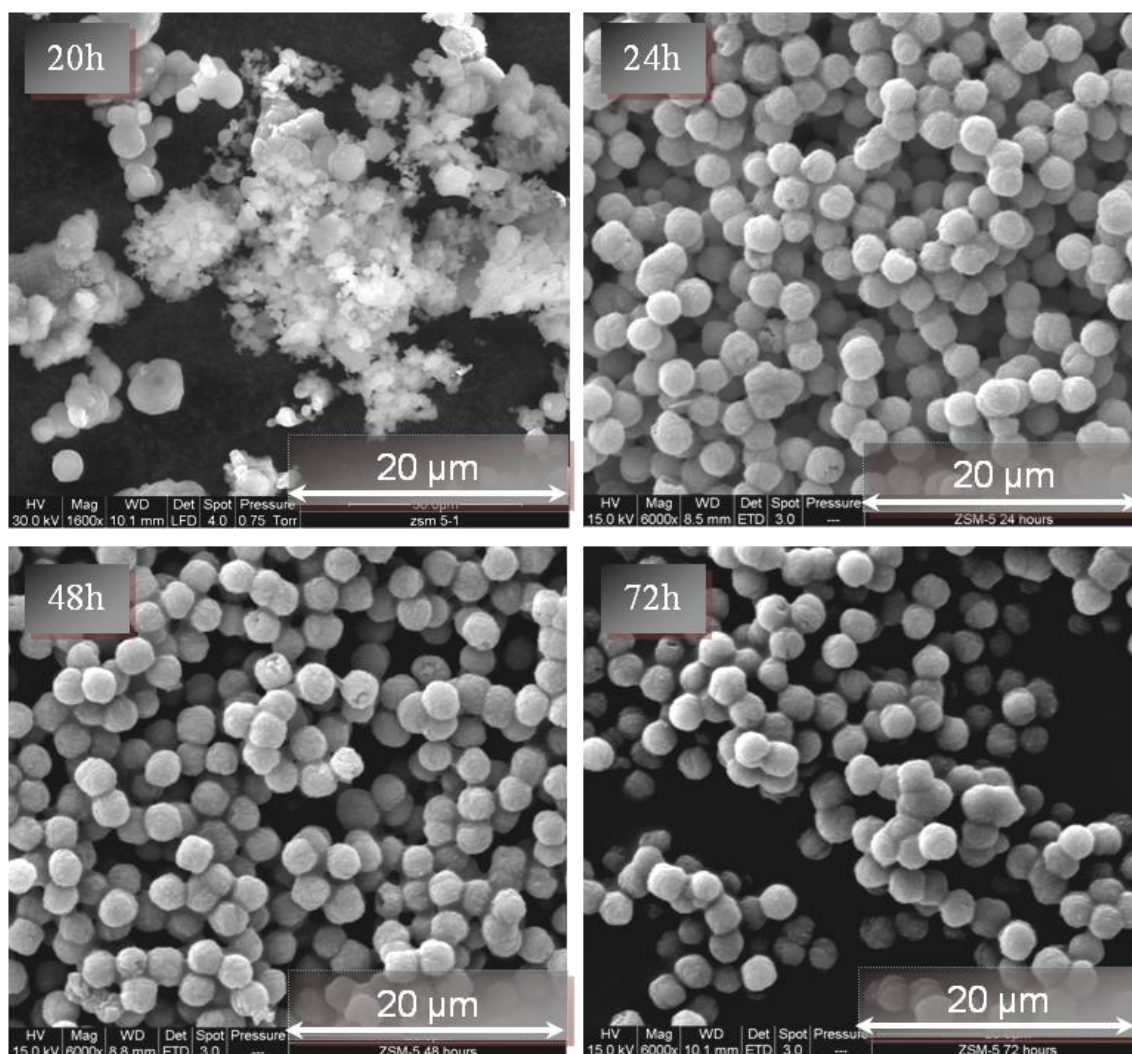
Figure 4-18: SEM images for the Na–ZSM-5; 20 hour crystallisation time, 24 hour crystallisation time, 48 hour crystallisation time, 72 hour crystallisation time.
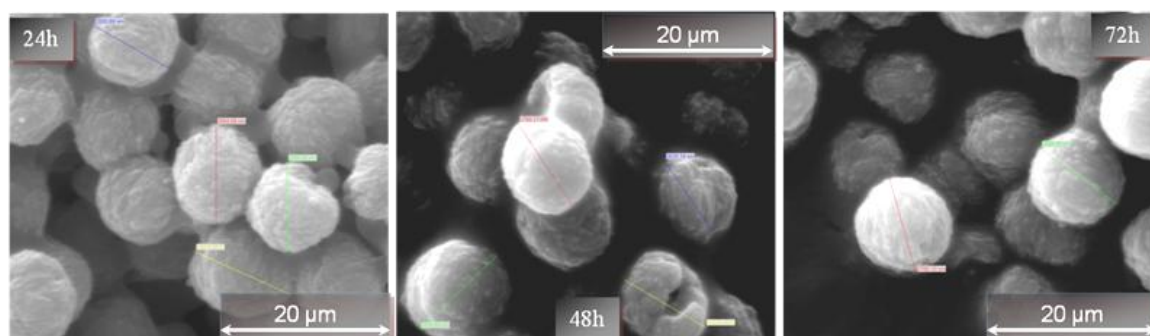
Figure 4-19: Average Na–ZSM-5 crystal diameters for; 24 hours crystallisation (2.79 μm), 48 hours crystallisation (2.74 μm), 72 hours crystallisation (2.71 μm).

Table 4-5: EDAX analysis for Na–ZSM-5 synthesised different crystallisation time.

Elements	8h	16h	20h	24h	48h	72h
O, wt%	43.54	45.69	43.12	42.00	34.81	42.38
Na, wt%	3.04	3.11	4.24	3.15	3.43	3.12
Al, wt%	4.29	4.17	4.21	4.50	3.96	4.10
Si ,wt%	49.13	47.04	48.44	51.30	45.18	47.27
Si/Al ratio	11.46	11.28	11.52	11.40	11.41	11.53

In summary, the characterisation and analysis of the all the samples of synthesised Na–ZSM-5 established that 48 h presents the optimum crystallisation conditions, with crystals having higher degrees of the crystallinity (100%), 11.5 Si/Al bulk ratio and average crystal diameters of around 2.74 µm.

4.4.2   Structured Na-ZSM-5 zeolite

X-ray diffraction patterns in **Figure 4-20** showed that crystallisation of the Na-ZSM-5 phase grown on the aluminium oxide layer of the FeCrAlloy wires was observed after 12 hours. The appearance of the characteristic Na–ZSM-5 phase after 20 hours was more obvious with little change in the peak intensity after 24 hours. It was clear that by increasing the crystallisation period, the quantity and quality of the crystalline phase materials increased with no additional crystal phases observed.
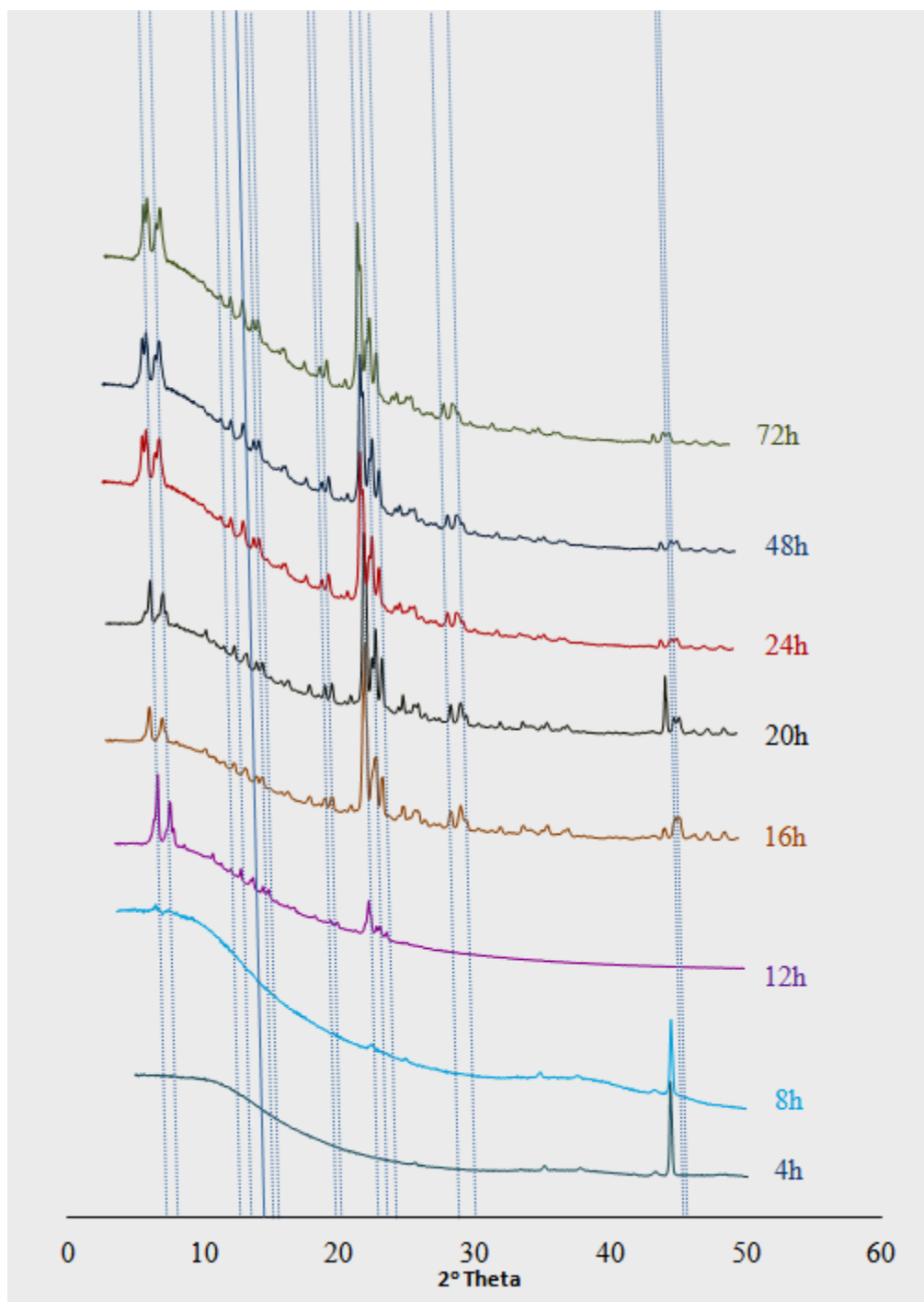
Figure 4-20: XRD patterns of the Na–ZSM-5 grown on the FeCrAlloy surface at different crystallisation times.

Overall, the Na–ZSM-5 crystallisation occurred faster on the alumina-rich metal surfaces (12 h) whilst forming slower in the bulk phase (typically taking 20 h **Figure 4-17**). This suggests that the crystallisation process is assisted by the additional aluminium oxide layers in the formed on the FeCrAlloy surface. Finally, the XRD patterns indicated that the crystallisation was completed after 48 h under hydrothermal conditions for both the bulk powder and the FeCrAlloy wires.

SEM images taken at different crystallisation times and at different magnifications of the wires surface are shown in **Figure 4-21,** with these images revealing differences in the zeolite coverage. Good coverage was observed at crystallisation times of between 20 and 48 h, with these showing spherical crystals with crystal twinning. Initially growth occurred on the FeCrAlloy wire surface, with the crystals subsequently growing on top of other crystals already present, creating a multilayer system.

Element mapping of the wires (**Figure 4-22**) showed predominately homogenous layer of Si and Al with the core wire containing iron and chromium elements. A defect was highlighted in the Si scan and back scattering SEM images, however sample preparation was difficult.
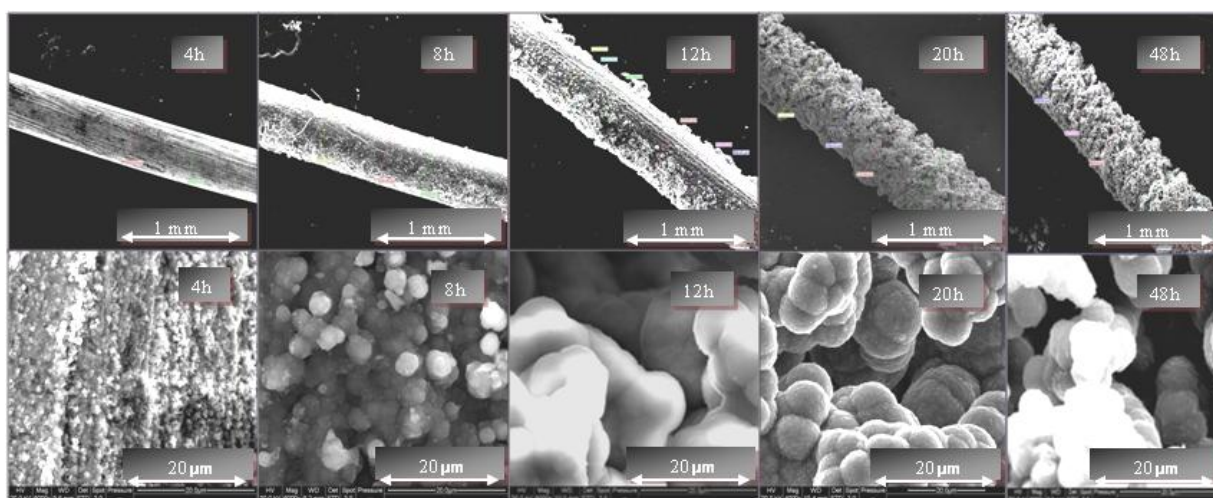
Figure 4-21: SEM pictures of the Na–ZSM-5 coverage at different crystallisation time.

Figure 4-22: SEM-EDAX micrograph of the Na–ZSM-5 structured zeolite 48 h crystallisation time: A) BSE image, (B, C, D and E) element mapping for Fe, Cr, Si and Al respectively.

EDAX surface analysis revealed that, as the crystallisation time increased so did the surface coverage and a typical Si/Al ratio of 11 was achieved (**Table 4-6**). **Figure 4-23** showed the EDAX elemental line scans across Na–ZSM-5, aluminium oxide layer and the substrate. The Kα signals were plotted for silicon, aluminium, iron and chromium started where the EDAX elemental line-scan was made on a chosen range to demonstrate the structural catalyst (substrate, aluminium oxide layer, zeolite layer).

Interestingly there was a sharp peak in the aluminium Kα signals plotted indicating the aluminium oxide layer on the metal surface which decreased after 4 µm. The EDAX analysis showed that after 48 h crystallisation the zeolite layer had reached 146 µm in thickness with a Si/Al ratio equal to 11; a similar Si/Al ratio was found for the bulk Na–ZSM-5 powder.

Table 4-6: Na–ZSM-5 weight gain, layer thickness and Si/Al ratio at different crystallization times.

Time (h)	Zeolite (wt %)	Thickness Layer (μm)	Coverage (g m^{-2})	Si/Al
4	0.03	4.7	0.25	0.03
8	1.8	10	15.67	8.00
12	11.3	50	100.37	11.21
16	15.0	100	150.92	11.15
20	18.0	120	152.00	11.04
24	23.0	134	212.00	11.02
48	35.0	146	317.00	11.00
72	35.6	147	318.00	11.00
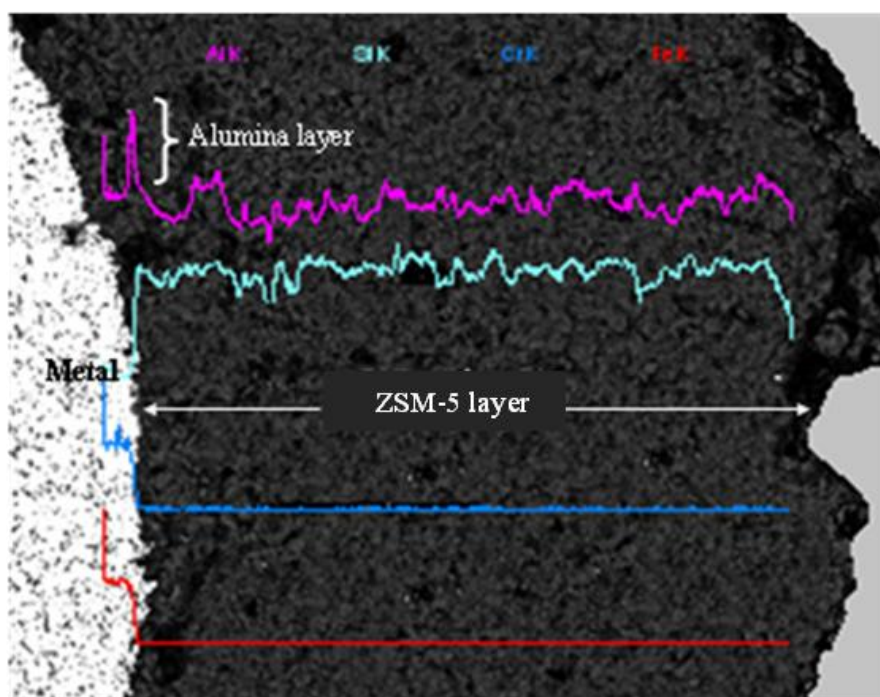
Figure 4-23: Cross-sectional line scan of through the wire, alumina and Na-ZSM-5 zeolite phase (after 48 h crystallisation time).

4.4.3 Powder Na–Y zeolite

In order to optimise the reaction time for the zeolite Na–Y synthesis, crystallisation times were varied between 8 to 72 hours, with the samples analysed using X-ray diffraction and compared with the standard XRD diffraction patterns found in the "Collection of Simulated XRD powder Patterns for Zeolites of Na–Y phase" [18] (**Figure 4-24**) and with commercial zeolite samples (**Figure 4-25**). Using zeolite Na–Y, structured zeolite synthesis samples were prepared at different synthesis times (8-72 h), with both the bulk zeolite and coated wires collected and thoroughly washed to remove sodium silicate from the zeolite structure; these samples were then dehydrated overnight at $100^{\circ}C$.

The degree of crystallisation was calculated, using the XRD-data (**Figure 4-26**) for Na–Y (FAU) with the CuKα radiations where $\lambda = 1.5418$ Å and it was found that the degree of crystallinity was higher than the references zeolites, in some cases showing values of 105% relative, with **Table 4-7** illustrating the difference in the heights of the relative intensities of the peaks (I_{rel}) for synthesis of Na–Y compared to the reference standards.

The major intensities of the peaks (I_{rel}) occurred at a 2θ range of 10 to 40 degrees [19], with **Table 4-7** listing the X-ray diffraction data of the synthesised samples as a function of change in crystallisation time.

Generally, the synthesised samples (8-72 h) tended to have higher crystallinity with no amorphous material compared to the commercial Na–Y zeolite when using the same settings for the XRD instrument. This is not surprising when considering the different scales of the industrial and laboratory syntheses.
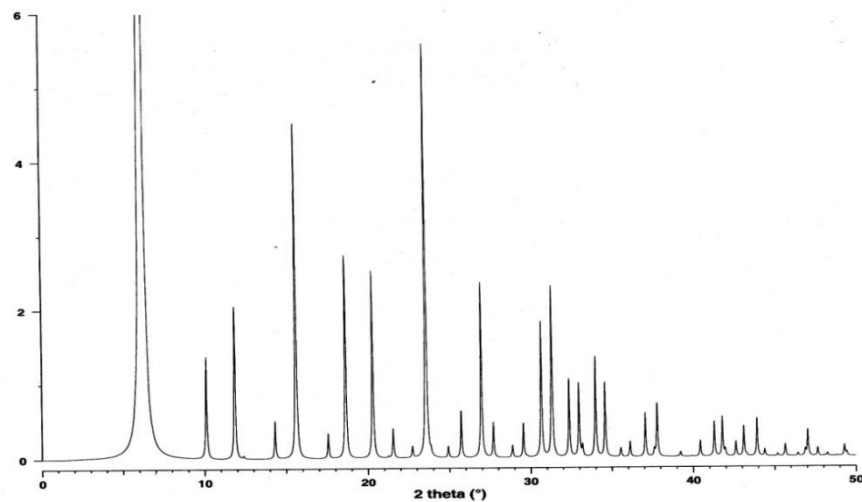
Figure 4-24: XRD patterns for standard zeolite Na–Y synthesis.
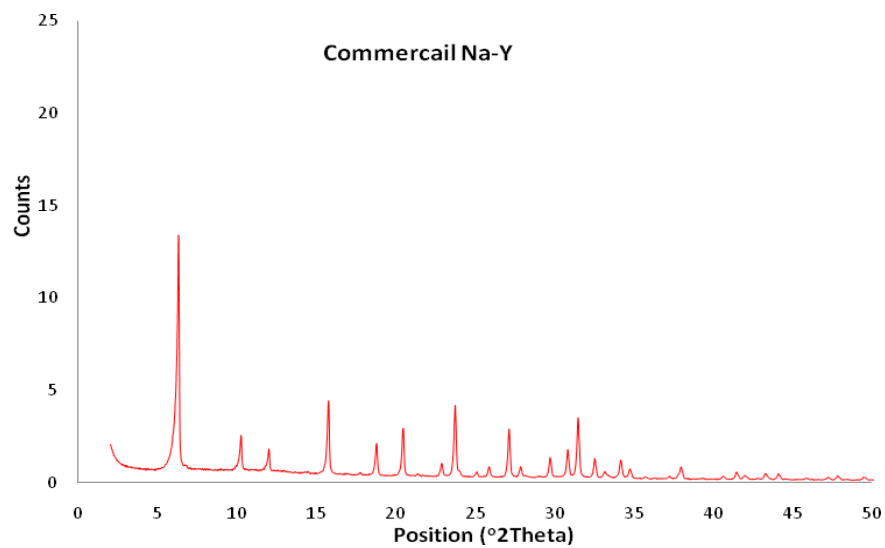
Figure 4-25: XRD patterns for commercial Zeolite Na–Y.
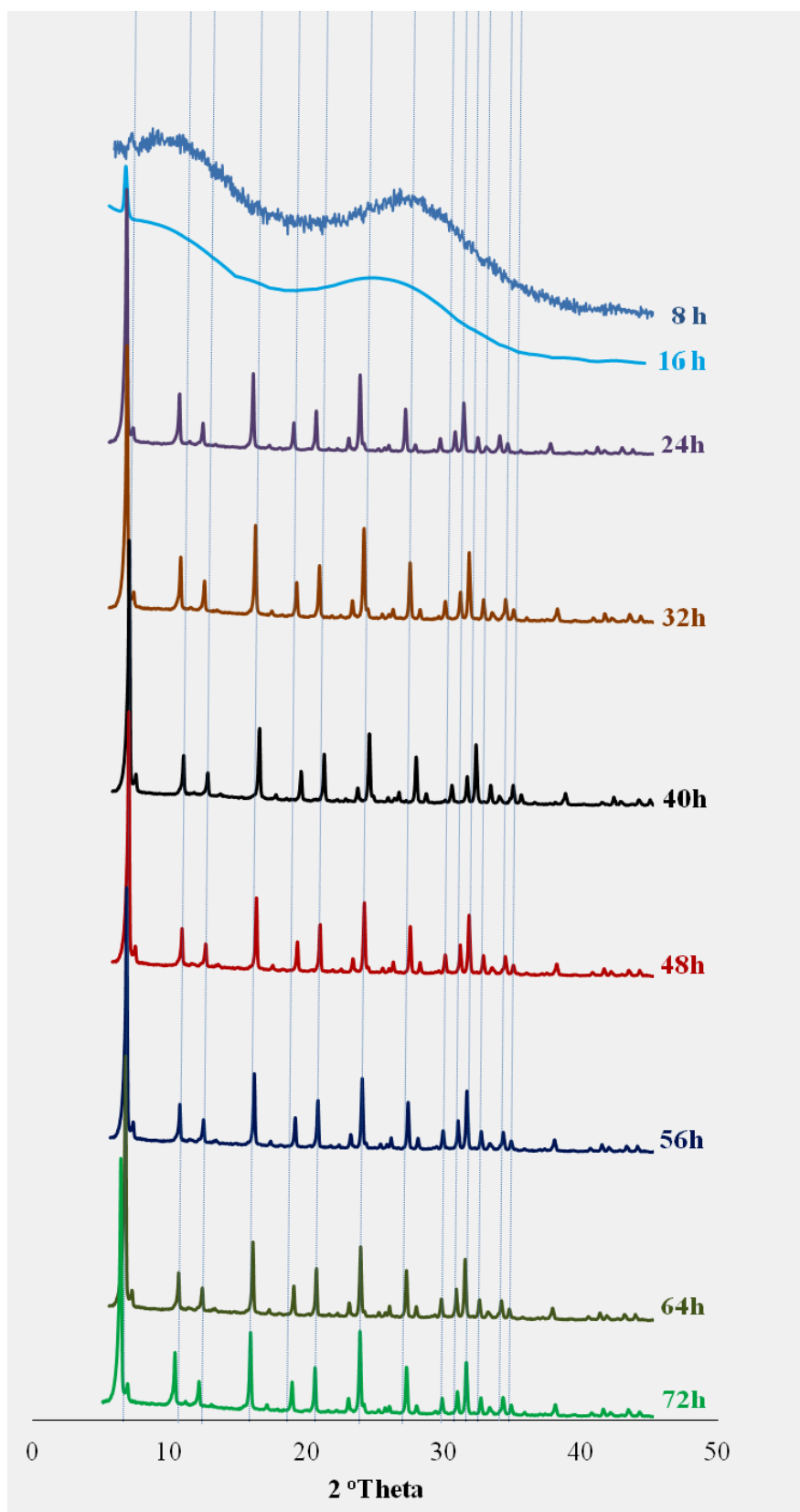
Figure 4-26: XRD patterns of zeolite Na-Y growth in the bulk phase.

Table 4-7: Comparison of XRD data for Na-Y synthesised in the bulk at different times with reference sample.

Faujasite								
2θ	I_{rel} commercial	I_{rel} 24 hours	I_{rel} 32 hours	I_{rel} 40 hours	I_{rel} 48 hours	I_{rel} 56 hours	I_{rel} 64hours	I_{rel} 72 hours
10.11	15.0	19.9	14.4	15.4	21.3	19.5	15.9	17.5
11.86	9.4	8.6	8.9	9.4	9.8	11.5	9.6	11.5
15.61	30.7	29.5	28.2	28.4	31.4	34.1	31.5	30.7
18.64	13.7	10.7	11.5	11.5	11.9	13.1	13.5	12.5
20.30	20.3	15.7	18.9	18.4	18.1	20.1	21.5	20.0
23.58	30.2	29.8	27.2	27.5	33.1	34.0	30.3	32.5
26.97	20.5	16.6	18.2	18.0	18.9	21.4	20.9	22.9
29.55	8.5	5.1	7.2	6.9	6.9	6.8	8.0	9.2
30.66	12.0	7.4	10.5	10.7	8.9	10.4	11.4	12.5
31.31	25.7	19.4	22.7	23.7	21.6	25.2	25.9	26.3
32.37	8.0	5.9	6.8	7.3	6.7	2.6	7.6	8.4
33.99	7.6	6.5	6.8	7.4	6.8	2.6	7.6	8.4
37.79	5.1	0.6	4.3	4.4	4.4	4.6	4.8	4.6
Σ	207	178	186	189	200	206	208	217
Crystallinity % $= \sum I_{rel\ sample}/\sum I_{rel\ commercial}$	*100*	*85*	*90*	*91*	*97*	*100*	*101*	*105*
Crystallinity % $= \sum I_{rel\ Sample}/\sum I_{rel\ 72\ hours}$	*95*	*81*	*86*	*87*	*92*	*95*	*96*	*100*

The growth of the zeolite Na–Y followed the typical S-shaped growth curve (**Figure 4-27**), which correlates with the results reported in the references [20]. The optimum crystallisation time is ~72 hours with the highest degree of crystallinity. However, excellent crystallinity was observed from 48–72 h.

The Na–Y zeolite samples obtained were coated with gold to prevent the accumulation of charge and analysed by SEM, (**Figure 4-28)** the images demonstrate the topography of the Na–Y zeolite samples and also the configurations of crystals within the zeolite powder.

In addition, EDAX analysis was used to determine the Si/Al ratio in the synthesised sample; with more than three different points on the surface of the each sample chosen randomly for the analysis (**Table 4-8**).
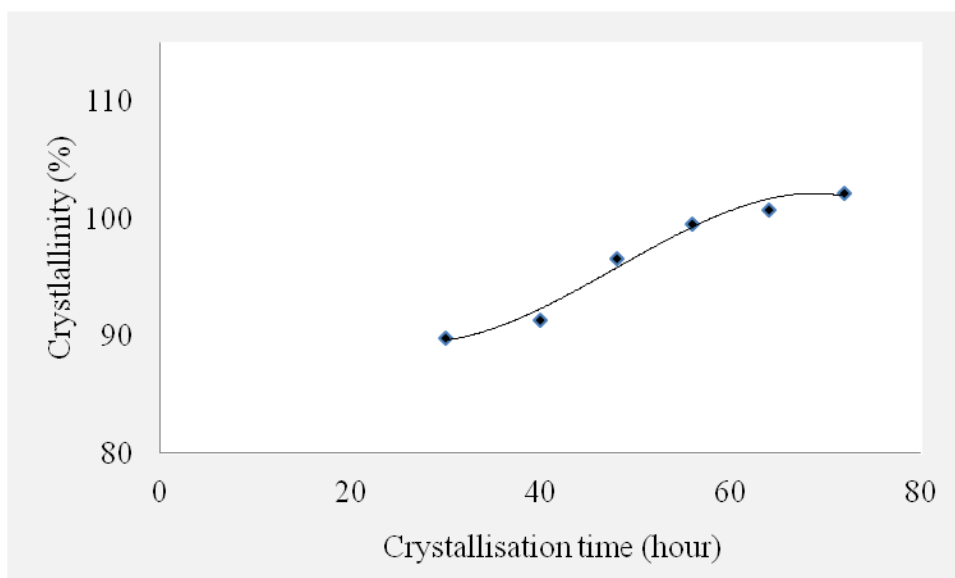
Figure 4-27: Effect of the crystallisation time on the degree of the crystallinity of Na–Y.
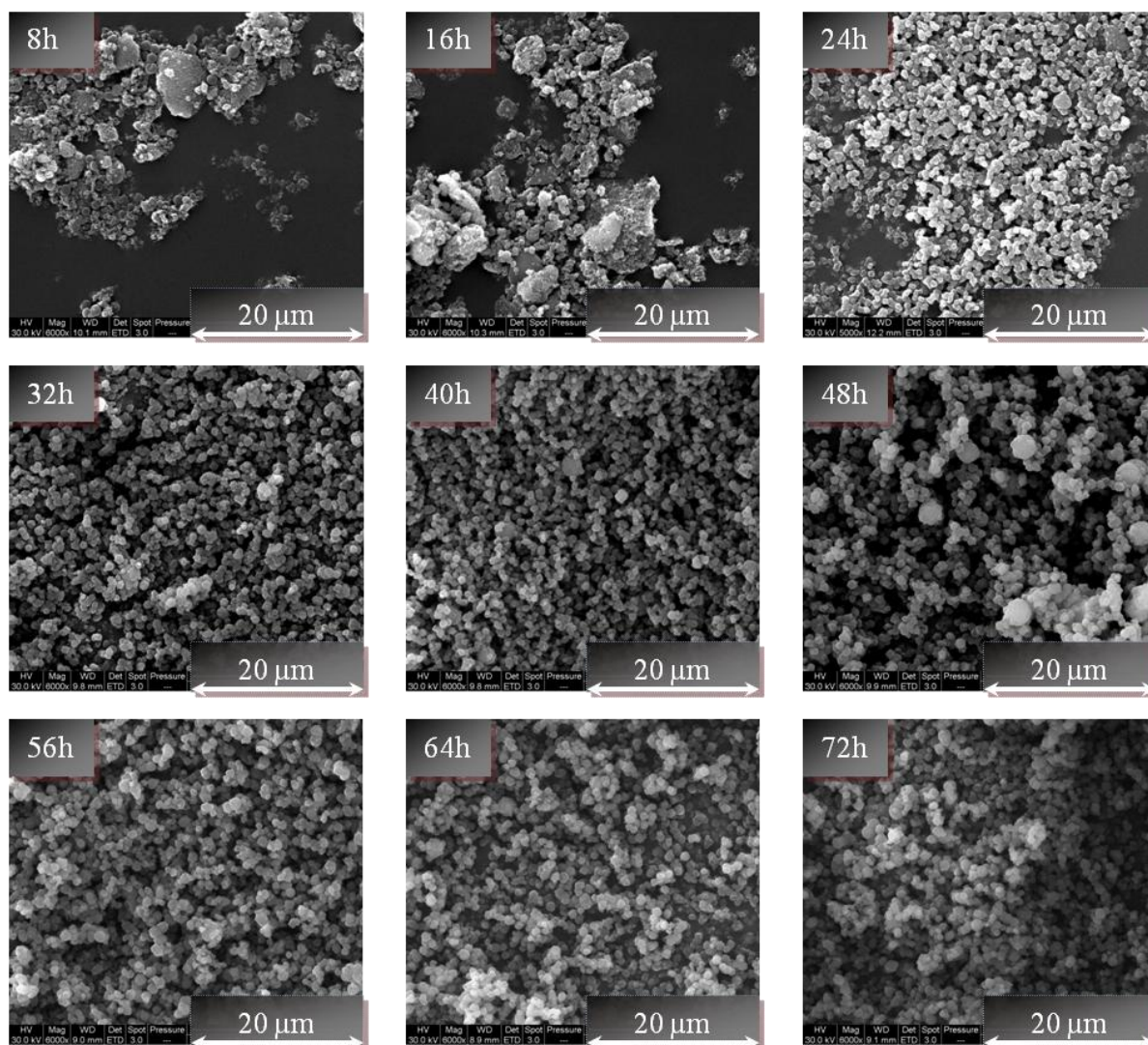
Figure 4-28: SEM images for the Na-Y at different crystallisation time.

Table 4-8: EDAX analysis data for the different crystallisation time of the Na-Y zeolites.

Elements	16h	24h	32h	40h	48h	56h	64h	72h
O, wt%	42.63	38.62	44.90	38.19	39.8	41.64	41.77	41.61
Na, wt%	9.28	8.30	8.37	8.30	8.3	8.28	8.27	8.28
Al, wt%	12.88	14.18	12.18	13.98	13.8	13.44	13.44	13.48
Si, wt%	35.23	38.90	33.54	38.49	38.1	36.64	36.62	36.63
Si/Al ratio	2.74	2.74	2.75	2.75	2.76	2.73	2.72	2.72

It is clear from the SEM images 8 and 16 hours that only amorphous materials were present, however by increasing the crystallisation time from 24 to 72 hours, the crystals were formed with sharp edges and the presence amorphous materials were much diminished.

Furthermore, the XRD, revealed the formation of a pure crystalline phase of Na–Y after prolonged crystallisation periods of up to 72 hours. The Si/Al molar ratio also rose 2.76 and then decreased after 48 hours to a value of 2.72 at 72 hours. These results agree with Hatay's results [21] who observed similar behaviour for Na–Y zeolite when the crystallization time was prolonged.

Moreover, these results correlate with the XRD analysis, which indicates a rise in the degree of crystallinity when increasing the crystallisation time, with the change in crystals size at different times of crystallisation determined by measuring the apparent dimensions obtained from the scanning electron micrographs (**Figure 4-29**). As such, it is clear that the crystal sizes change with crystallisation time, with crystals diameters for synthesised Na–Y being measured at 0.6 µm, 07 µm and 0.8 µm for 42, 48 and 72 hours respectively.
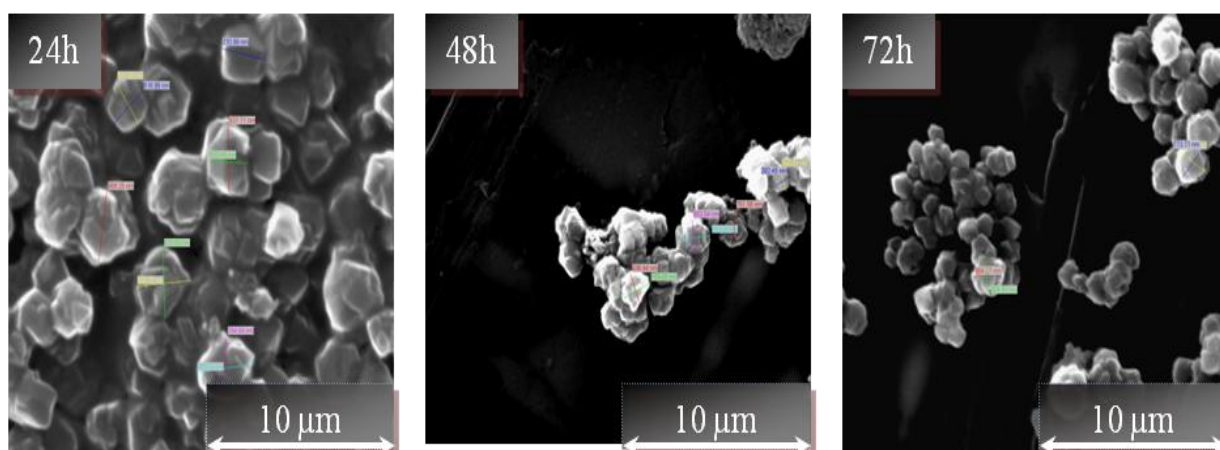
Figure 4-29: SEM of the average crystal size of the Na-Y for different crystallisation time.

4.4.4 Structured Na–Y zeolite

The Zeolite Na–Y characterisation analyses obtained confirmed that the optimum crystallisation time was 72 h, and the next step was to compare the powder analysis with the structured catalyst analysis in order to study the zeolite Na–Y layer growth on the aluminium oxide surface on FeCrAlloy wires over a range of different crystallisation time.

There were significant problems observed when following the growth of the zeolite Na–Y on the metal surface using the XRD because the deposited crystals of zeolite Na–Y were in a relatively low concentrations on the FeCrAlloy surface and only started to be noticeable at low angle of reflection ($2\theta = 6.1–10.4^{o}$) for zeolite Na–Y after 16 hours. In addition, the XRD pattern of zeolite Na–Y on the wire showed the presence of other phases (e.g. potentially GIS, GME, CHA), which increased when the synthesis time was extended towards 72 hours (**Figure 4-30**).

SEM analysis (**Figure 4-31**) indicated that by direct synthesis, the nucleation and growth paths for the zeolite Y phase onto the FeCrAlloy wires was preferred, even though the degree of development is very low. At 8 h the oxidised alumina whiskers are clearly visible, by 16 h, layer is present which was confirmed to be zeolite Y by XRD analyses (with a typical reflection of the low angle $2\theta = 6.1–10.4^{o}$). This suggests that the crystallisation process was initiated by the formation of an inter-phase layer on the surface of the FeCrAlloy wire (**Figure 4-31**–16 h). After 24 h, zeolite Na–Y crystals appeared along with cracks in many position on the surface, most these cracks were likely due to the tensions created on the thin layer during the calcination process. The crystallisation was completed after 72 h with crystals having the same size and shape as the zeolites found in the bulk phase, this suggested a combination of coating of the aluminium oxide and subsequently dissolution taking place. SEM (**Figure 4-31**) suggested a scarce development of crystals which became uniformly coated on the FeCrAlloy wire surface with changes in the coverage and layer thickness with time. The deposition of new small crystals on the top of the existing ones after 48 h is also apparent.
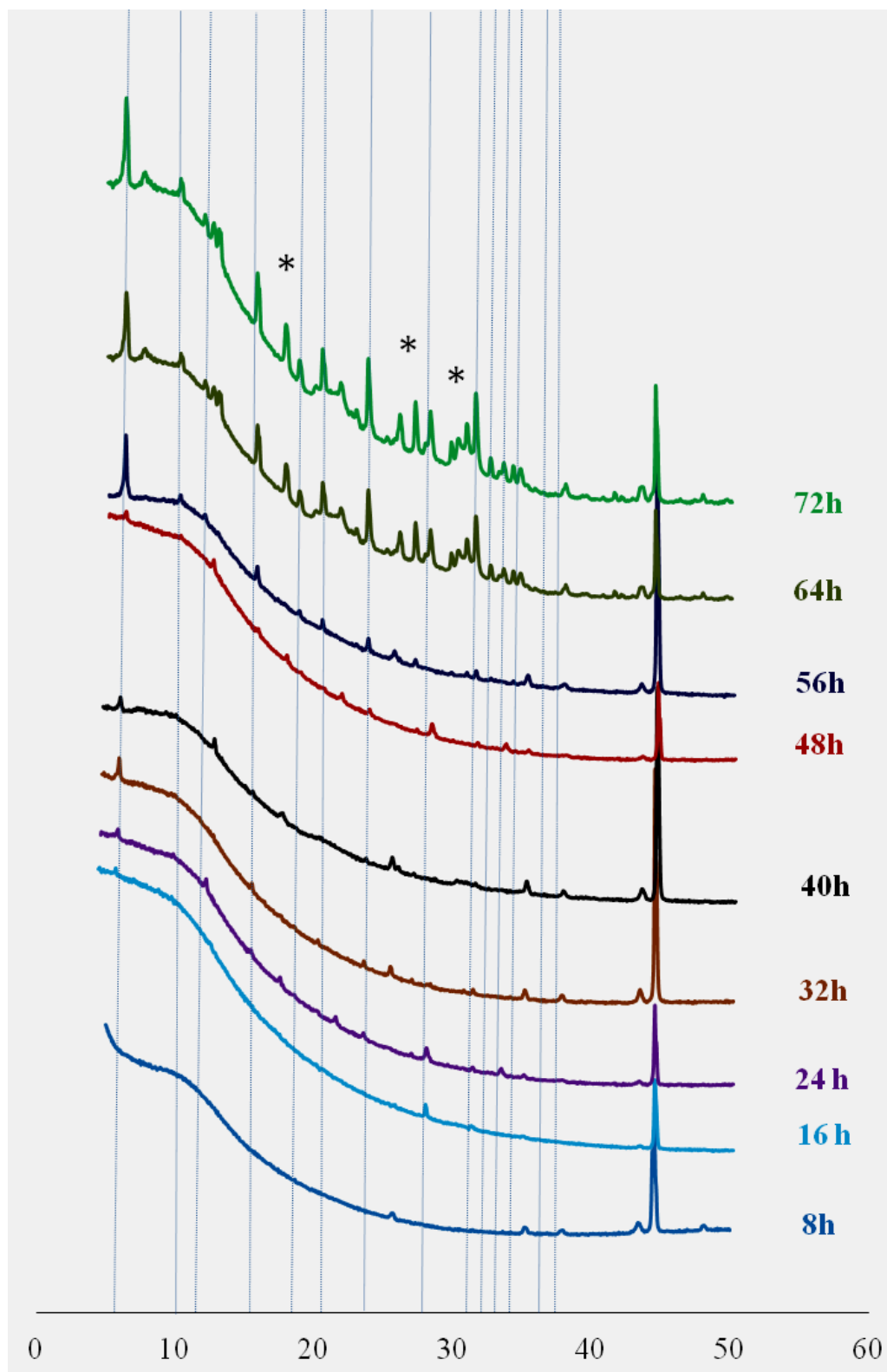
Figure 4-30: XRD patterns of wire surface oxidised for 4 h where zeolite Na–Y is growing on the wire at different times. Impurities in the zeolite Y phase are highlighted (*).
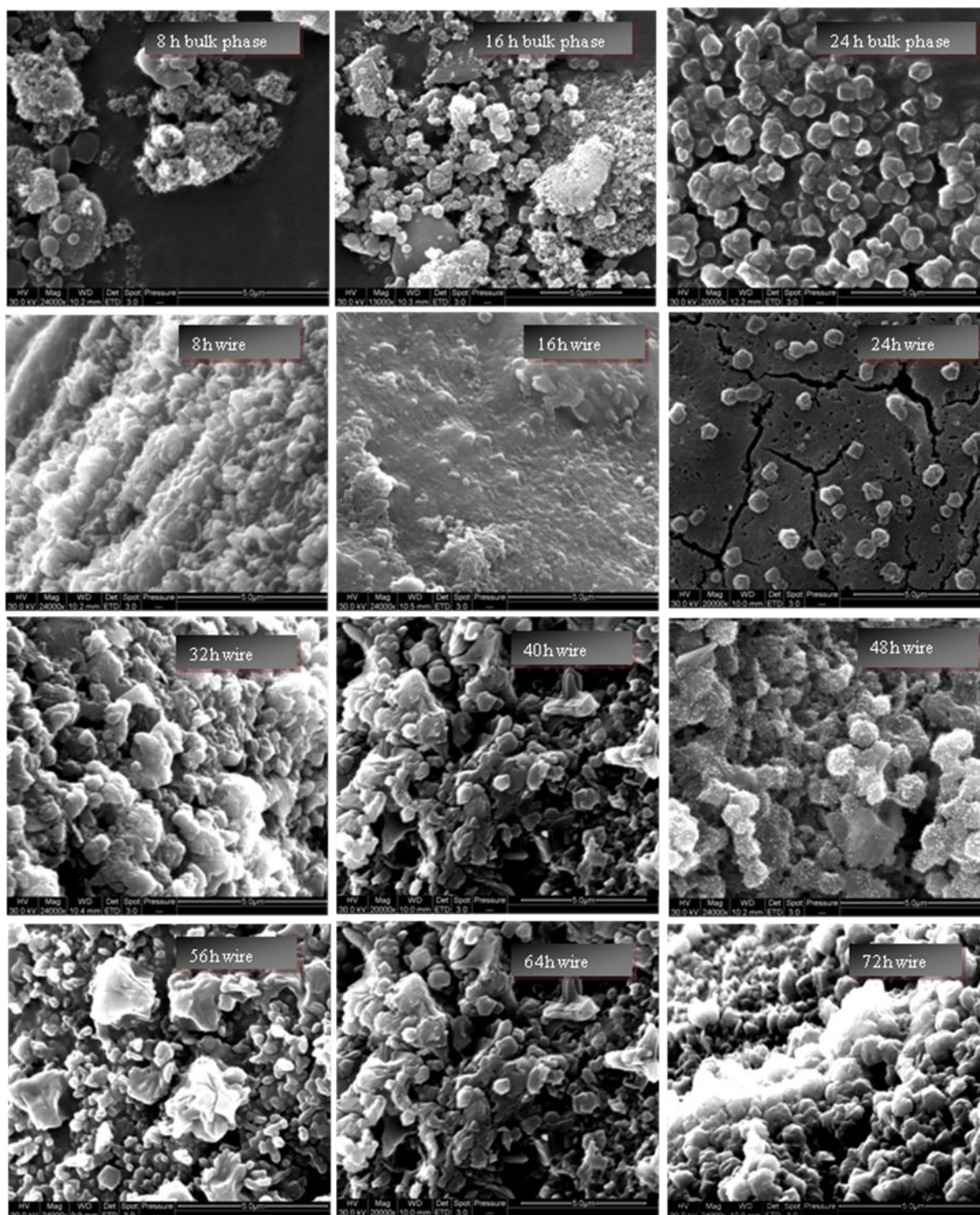
Figure 4-31: SEM images of zeolite Na-Y crystallised in the bulk phase at 8–24 h (top) and on the wire at different times (8-72h).

EDAX analysis (**Table 4-9**) of the Na–Y structured catalysts confirmed an increase in the zeolite weight gain, layer thickness and coverage surface achieved when extending the crystallisation time and the bulk Si/Al ratio was between 2.72 and 2.77.

EDAX elemental line scans across the wire and zeolite layers at 72 h shown in **Figure 4-32** illustrate that unlike the Na–ZSM-5, the zeolite Na–Y layer was thinner, at around 23 µm thickness. Again, Kα Si, Al, Fe and Cr signals plotted across the substrate, aluminium oxide layer and zeolite layer indicated that the aluminium peak appeared to confirm the presence of an aluminium oxide layer on the FeCrAlloy surface which is also shown in **Figure 4-33**. After 72 hours, the zeolite Na–Y layer thickness on the FeCrAlloy surface reached a maximum of 23 µm with a Si/Al ratio equal to 2.72. The elemental maps show much more heterogeneity in the zeolitic layer with clumps of Si obvious and many structural imperfections

Table 4-9: Zeolite Na–Y weight gain, layer thickness and Si/Al ratio at different crystallization times.

Zeolite Y Film Properties	Time (h)								
	8	16	24	32	40	48	56	64	72
Zeolite (wt %)	1.17	1.22	2.14	2.81	5.43	5.77	5.84	5.92	6.38
Thickness Layer (µm)	1.46	3.73	4.43	8.73	19.84	20.45	20.50	20.50	23.00
Coverage (g.m^{-2})	10.42	10.85	19.07	24.97	48.31	51.33	51.96	52.72	56.76
Si /Al ratio	2.77	2.75	2.75	2.74	2.76	2.76	2.72	2.72	2.72

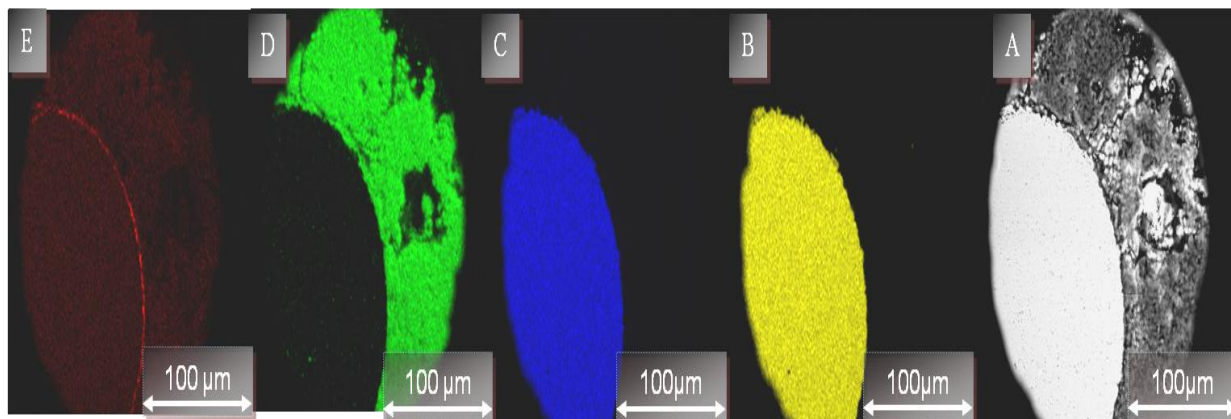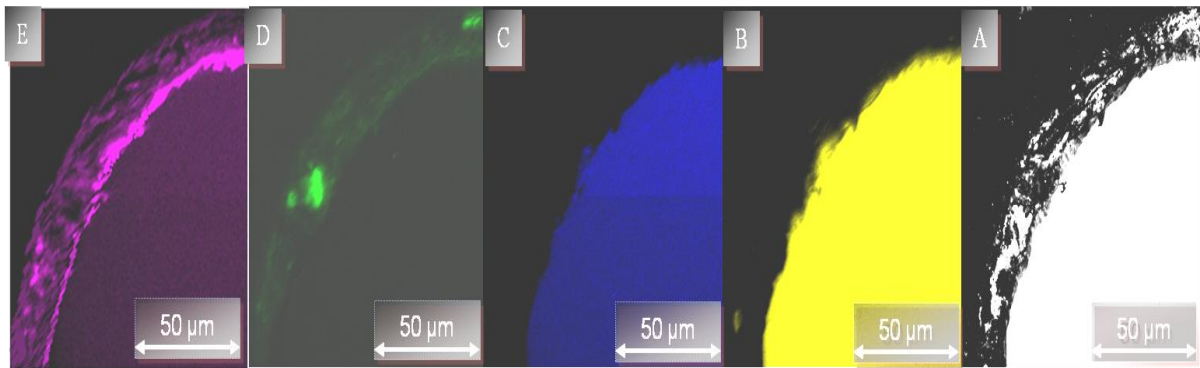**Figure 4-32: SEM-EDX micrograph of the Na-Y structured zeolite 72 h crystallisation time: A) BSE image, (B, C, D and E) element mapping for Fe, Cr, Si and Al respectively.**
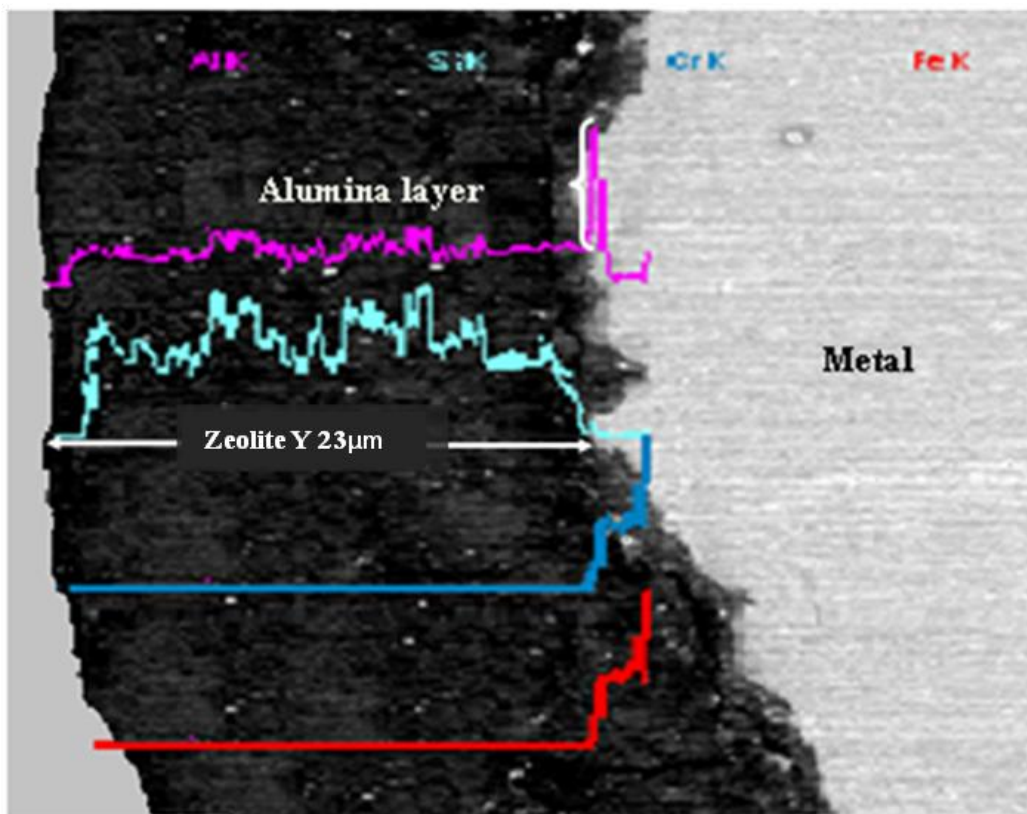
Figure 4-33: SEM images of zeolite Na–Y coverage at 72 h on structured zeolite.

Summary

The optimum technique developed was to pre-treat the FeCrAlloy wires was by applying a physical pre-treatment method before oxidising at 1000°C. The optimum oxidation time was chosen to be 4 hours as the analysis results demonstrated the following:

- The chemical pre-treatment enhanced the alumina oxide layer growth on the FeCrAlloy surface (see **Section 4.4.1**).

- Metastable alumina scales on the FeCrAlloy surface were transformed into stable alumina forms after a short oxidation time at 1000°C.

- For prolonged oxidation times, the morphology of the samples showed flat surfaces with decreasing Al/Fe ratio suggested the depletion or even exhaustion of the aluminium reservoir in the alloy.

The analysis shows that the optimum conditions for synthesis of the Na–ZSM-5 structured zeolite were synthesis under hydrothermal condition using an in-situ method for 48 hours at 180°C. The major observations were:

- The average degree of the crystallinity gradually increased when extending the crystallisation time, then until 48 hours and diminished due to the collapse of the zeolite structure, or gradual transformation of Na–ZSM-5 into the crystal.

- The formation of a compact layer about 146 μm thickness attached to the FeCrAlloy surface. The thin alumina oxide scales formed by chemical oxidised pre- treated wires resulted in a surface that, when exposed to hydrothermal synthesis conditions turned reactive, with the reactive support enhanced the crystals growth rate at the metal surface rather than in the bulk solution.

The Na–Y structured catalyst was synthesised and compare to the powder Na–Y collected from the bottom of the reactor. Further, from the study it could be concluded that:

- By increasing the reaction time the crystals size increased.

- The degree of the crystallinity increase until this reached a maximum value of 100%.

- The Si/Al molar ratio rose to a maximum value and then diminished with increases in the crystallisation time; this could be explained due to nutrient depletion of the active silicate species in the reaction mixture.

- The crystals dimensions increased with a decrease in the Si/Al molar ratio, because the Si-O bond distance are shorter than the length of Al-O bond and the Si atomic radius is smaller than that of Al.

- Furthermore, the X-ray diffractogram patterns, which revealed the formation of a pure crystalline materials phase of Na–Y after prolonged crystallization periods of up to 72 hours, despite seeing the Si/Al molar ratio rise to an optimal point of 2.77 and then decrease after 48 hours to reach 2.72 at 72 hours.

- EDAX analyses of the Na–Y structured catalyst confirmed an increase in the zeolite weight gain, layer thickness and coverage surface was achieved when extending the crystallisation time, with the Si/Al ratio being between 2.72 and 2.76.

- Unlike the Na–ZSM-5, the zeolite Na–Y layer was thinner and only provided a layer of 23 μm thickness, however, after 72 hours, the zeolite Na–Y layer thickness on the FeCrAlloy surface reached 23 μm with Si/Al ratio equal to 2.72.

Generally, the Na–ZSM-5 and Na–Y structured zeolite analyses which were synthesis under hydrothermal conditions using an in-situ method. The major observations were:

- Thermal cycling of the wires that had been oxidised for 3-5 h showed very little weight loss with no zeolite loss. However, wires oxidised for 9-24 h showed significant peeling in the zeolite layer for both Zeolite Na–Y and Na–ZSM-5. SEM and TGA analyses indicated that the 4 hr oxidised and coated wire had the highest catalyst loading and thus excellent resistance to thermal cycling.

- The weight losses for zeolite Na–Y layer was much lower than for Na–ZSM-5 layer for the same oxidised wires and this could be attributed to the fact that the coverage of zeolite Na–Y was less.

- The formation of the zeolite layers was deepened on the synthesis conditions for zeolite Na–Y and Na–ZSM-5 such as; the use of template (in the case of ZSM-5 zeolite), the $[OH]^-$, and Si/Al ratio and other factors would need further studying.

References

1.   Zamaro, J.M., M.A. Ulla, and E.E. Miró, *ZSM-5 growth on a FeCrAl steel support. Coating characteristics upon the catalytic behavior in the NO$_x$ SCR,* Microporous and Mesoporous Materials, 2008. **115**(1): p. 113-122.

2.   Badini, C. and F. Laurella, *Oxidation of FeCrAl alloy: influence of temperature and atmosphere on scale growth rate and mechanism,* Surface and Coatings Technology, 2001. **135**(2): p. 291-298.

3.   Blachère, J., E. Schumann, G.H. Meier, F.S. Pettit, *Textures of alumina scales on FeCrAl alloys,* Scripta Materialia, 2003. **49**(9): p. 909-912.

4.   Kadiri, H.E., R. Molins, Y. Bienvenu, M.F. Horstemeyer, *Abnormal high growth rates of metastable aluminas on FeCrAl alloys,* Oxidation of Metals, 2005. **64**(1): p. 63-97.

5.   Camra, J., E. Bielańska, A. Bernasik, K. Kowalski, M. Zimowska, A. Białas, M. Najbar, *Role of Al segregation and high affinity to oxygen in formation of adhesive alumina layers on FeCr alloy support,* Catalysis Today, 2005. **105**(3-4): p. 629-633.

6.   Levin, I. and D. Brandon, *Metastable alumina polymorphs: crystal structures and transition sequences,* Journal of the American Ceramic Society, 1998. **81**(8): p. 1995-2012.

7.   Richardson, J.T., *Principles of catalyst development*, 1989.

8.   Kochubey, V., *Effect of Ti, Hf and Zr additions and impurity elements on the oxidation limited lifetime of thick-and thin-walled FeCrAl-components*, 2005, Ruhr-Universität Bochum, Universitätsbibliothek.p.113.

9.   Huntz, A., L. Maréchal, B. Lesage, and R. Molins, *Thermal expansion coefficient of alumina films developed by oxidation of a FeCrAl alloy determined by a deflection technique,* Applied Surface Science, 2006. **252**(22): p. 7781-7787.

10.   Herbelin, J.M. and M. Mantel, *Effects of Al addition and minor elements on oxidation behaviour of FeCralloys,* Le Journal de Physique IV, 1995. **5**(C7): p. 365-374.

11.   Bhatia, S., *Zeolite catalysis: Principles and applications*, 1990.

11. Rebrov, E.V., G.B.F. Seijger, H.P.A. Calis, M. de Croon, C.M. van den Bleek, J.C. Schouten, *Hydrothermal Synthesis of Zeolitic Coatings for Applications in Micro-structured Reactors,* Ordered Porous Solids: Recent Advances and Prospects, 2008.

13. Persson, A., B.J. Schoeman, J. Sterte, J.E. Otterstedt, *Synthesis of stable suspensions of discrete colloidal zeolite (Na, TPA) ZSM-5 crystals,* Zeolites, 1995. **15**(7): p. 611-619.

14. Mintova, S., V. Valtchev, and L. Konstantinov, *Adhesivity of molecular sieve films on metal substrates,* Zeolites, 1996. **17**(5): p. 462-465.

15. Robson, H., *Verified synthesis of zeolitic materials*. 2001:p.156-198: Elsevier Science.

16. Szostak, R., *Molecular sieves: principles of synthesis and identification,* 1997.

17. Feng, H., Y. Chen, C. Li, H. Shan, *In-situ synthesis of ZSM-5 on silica gel and studies on its catalytic activity,* Journal of Fuel Chemistry and Technology, 2008. **36**(2): p. 144-150.

18. Baerlocher, C., W.M. Meier, and D. Olson, *Atlas Of Zeolite Framework Types*, 2001: p. 79-150.

19. Van Bekkum, H., *Introduction to zeolite science and practice*, 2001: p.267-280.

20. Čejka, J. and H. Van Bekkum, *Zeolites and ordered mesoporous materials: progress and prospects: the 1st FEZA School on Zeolites, Prague, Czech Republic, August 20-21, 2005*. Vol. 157. 2005.

21. Hatay, M. and M.M. Oo, *Preparation of zeolite Y catalyst for petroleum cracking,* World Acad Sci Eng Technol, 2008. **48**: p. 114-120.

<div style="writing-mode: vertical">**Chapter 5**</div>

Development and Characterisation of Structured Catalysts

5.1 Introduction

Following the successful synthesis of Na–Y (Si/Al ratio = 2.72) and Na–ZSM-5 (Si/Al ratios = 11) on the FeCrAlloy wires oxidised at $1000^{o}C$ for 4 hours, modification was carried out to improve suitability for catalytic reaction. Post-synthesis treatments were ion exchange procedures and dealumination procedures. Prior to the modification of the zeolite from the Na–form to the H–form, a calcination process was performed to a remove any impurities and to ensure decomposition of the template in the case of the Na–ZSM-5. Dealumination of Na–Y was carried out using 70% concentration nitric acid to increase the Si/Al ratio. Following each treatment, the structure of the catalysts was assessed using XRD, SEM, EDAX, and NMR analysis.

5.2 Calcination and ion exchange

Zeolites are crystalline hydrated aluminosilicates, with large exchangeable valence cations and water molecules occupying the three-dimension structures. The ion exchange properties arise from a negative charge of trivalent aluminium in the structure, and a serious of decompositions, including removal of the template, and an ion exchange procedure have been used for post-synthesis modification throughout the preparation an acid catalyst utilized for industrial application in order to create the catalytically-active H-form of zeolite [1].

Prior to the ion–exchange procedure the powder and structured zeolite versions of Na–ZSM-5 and Na–Y zeolite were packed inside quartz tube reactors between glass wool plugs. The quartz reactors were heated in a furnace (Carbolite Corp) to $550^{o}C$ ($1^{o}C$ min^{-1}, 22 ml min^{-1} air flow) and held for 16 hours to remove any water and the template in the ZSM-5 case [2]. Once calcined the Na–ZSM-5 and Na–Y zeolite forms (1 g) of the powder and equivalent zeolite weight in structured catalyst were ion exchanged in order to obtain the NH_4–form. Ion exchange was accomplished using a 0.5 M ammonium nitrate solution (NH_4NO_3, with a purity > 98 % obtained from Sigma–Aldrich) at $80^{o}C$ under constant reflux condition with constant stirring (600 rpm) for 4 hours [3, 4]. The powdered exchanged Y-zeolite was filtered washed with one litre of de-ionised water, centrifuged for 10 minutes (3500 rpm), and then dried at 110°C overnight. Whereas, the structured zeolite was placed in an ultrasonic bath containing one litre of de-ionised water for 10 minutes. All NH_4-powder and NH_4 structured zeolite forms were calcined again at $500^{o}C$ to produce H-powder and H-structured zeolite form by removal of NH_3 (**Figure 5-1**). It should be noticed that ion exchanged and calcination can possibly result in a partial dealumination of the framework [5].
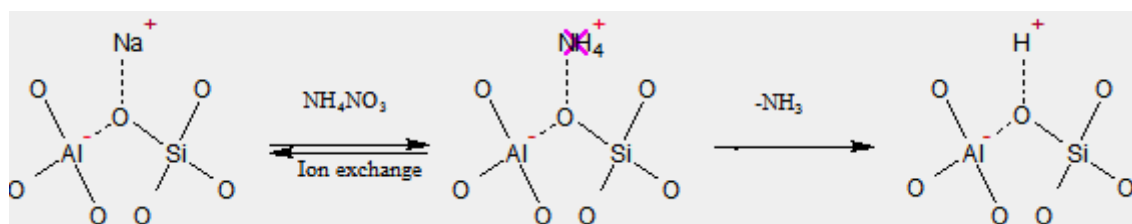
Figure 5-1: Ion-exchange of the Na-form of zeolite to the H-form.

Dealumination of the zeolite frameworks can create extra-framework aluminium species and their presence can be ascertained from the ^{27}Al MAS NMR spectra, where the octahedral and tetrahedrally coordinated aluminium species can be determined from the two peaks at ~0 and ~60 ppm, respectively. Dealumination can affect the zeolite frameworks structure, especially the Si/Al ratio the thermal stability, and the catalytic properties of the catalyst.

5.2.1 Characterisations of the calcined of powder and structured zeolite

The calcination of the powder and the structured Na-ZSM-5 and Na-Y zeolite was studied by monitoring the weight loss using TGA. Weight loses during heating occurs due to the loss of the volatile components, chemisorbed water and physisorbed water. In addition, in the case of the Na–ZSM-5, the removed template occurs. **Figure 5-2–Figure 5-5** show the typical weight loss curves versus time for the powder and structured Na-ZSM-5 and Na-Y zeolites.

The weight loss that occurred for all samples below typically 250°C resulted from desorption of water from powder and structured Na-ZSM-5 and Na-Y zeolites as shown in **Figure 5-2** and **Figure 5-4**. The structured Na-ZSM-5 zeolite has much lower water content (0.56%) compared to the powder form as there was much less zeolite present on the surface of the FeCrAlloy wire. Similarly, for powder and structured Na-Y zeolite losing was 19.36 and 1.46% respectively. The rate of weight loss shown in **Figure 5-3** and **Figure 5-5** are similar for both structured and powder zeolite.

In the powder and structured Na-ZSM-5 there was further weight loss due to the decomposition of the template (TPAOH) which occurred between 250 and 550°C. The DTG (derivative thermogravimetric) shown in **Figure 5-3** showed a maximum mass rate of weight loss around 420–425°C for both powder and structured Na-ZSM-5 zeolite observed at 425°C.
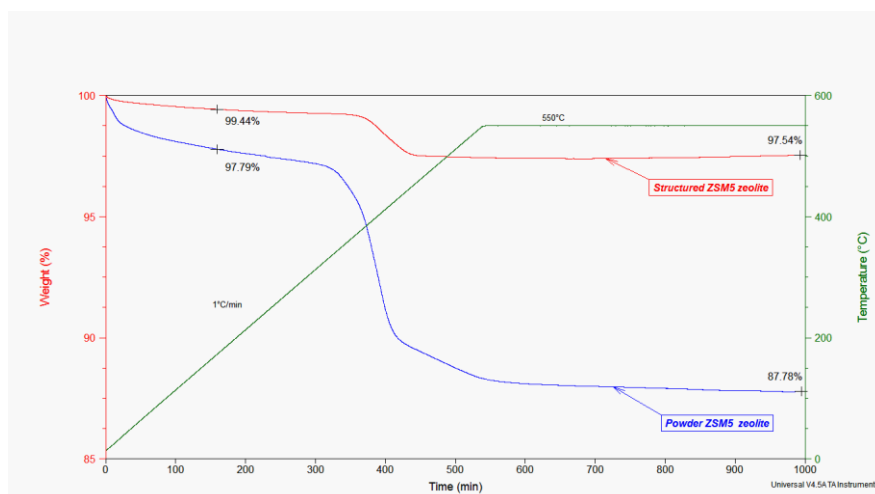
Figure 5-2: TGA analysis for the calcination of powder and structured Na-ZSM-5.
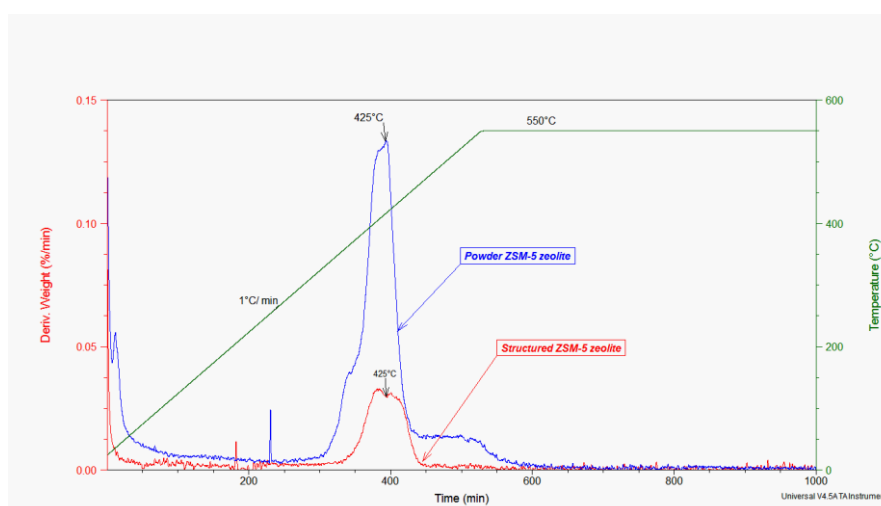
Figure 5-3: DTG analysis for the calcination of Powder and structured Na-ZSM-5.
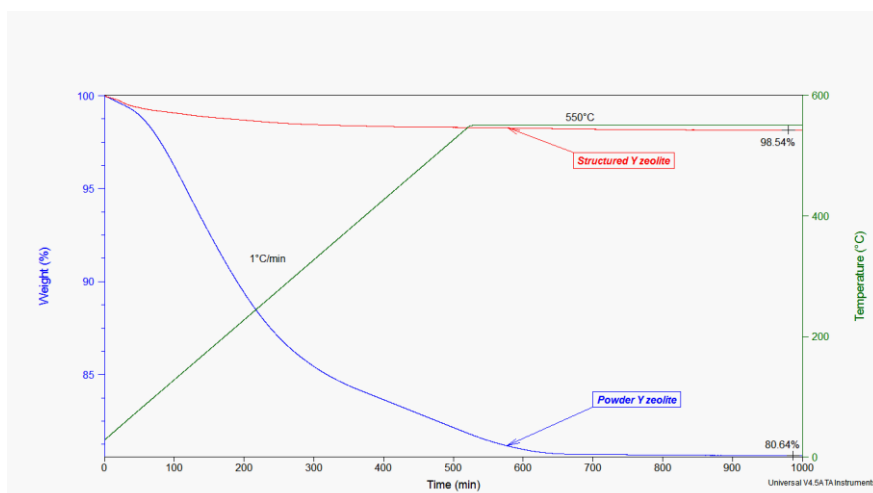
Figure 5-4: TGA analysis for the calcination of powder and structured Na-Y.
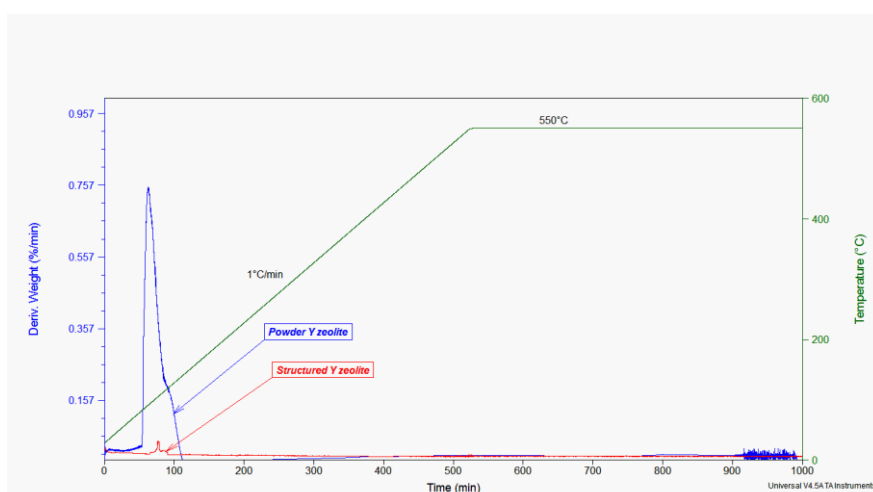
Figure 5-5: DTG analysis for the calcination of powder and structured Na-Y.

In summary, the overall weight loss observed for the Na-ZSM-5 and Na-Y zeolite powder framework was 12.22 and 19.36% respectively, while in the structured zeolite framework was 2.46 and 1.46%. An estimate of the zeolite weight grown on the FeCrAlloy sample was carried out using the TGA analysis and comparing it with the original weight of the analysis sample. The finding suggested the weight of the Na–ZSM-5 zeolite layer on the FeCrAlloy was approximately 40% of the total weight of the structured catalyst and for Na-Y zeolite layer on FeCrAlloy 8.1%.

A study of the morphology and the crystal size for both the powder and structured Na-ZSM-5 and Na-Y zeolite showed there was no noticeable change in the crystals size or shape after the calcination process for the powder and structured Na-ZSM-5 and Na-Y zeolite with this confirmed by the XRD results which showed no change in the structured of the zeolite (**Section 5.2.2**).

5.2.2 Characterisation of the ion-exchanged powder and structured zeolites

Scanning electron microscopy (SEM), energy dispersive and X-ray (EDAX) analysis were used to determine the sodium content of the powder and structured ZSM-5 and Y zeolite after the ion exchange treatments. Three points on the different crystals from each sample were randomly selected for EDAX analysis, the concentration of sodium ions within the powder Na-ZSM-5 and Na-Y zeolite framework found to be decreased. The sodium content for powder and structured ZSM-5 synthesis (the EDAX analysis for both were about the same ratios) decreased from 3.43 to 0.15%, during one ion exchange (**Figure 5-6**). For powder and structured zeolite Na-Y, the Na concentration dropped from 8.28 to 3% after one ion exchange treatment (**Figure 5-7**). The morphology and crystal size remained unchanged further to ion exchange treatment for all H-zeolites.

X-ray diffraction for structured and powder zeolites showed a small difference for Na–form and H–form (**Figure 5-8** and **Figure 5-9**). Overall, after the ion exchange, the crystallinity compared to the starting Na-zeolite form typically 92 and 89% for Na–ZSM-5 and Na–Y respectively. This work was in good agreement with Sato [5] and Fletcher [6]. They reported a drop in decreasing into zeolite crystallinity up to 25% after one ion exchange treatment which they attributed to the migration of the Na^+ in the Framework and NH_4^+ ions replacement in Y zeolite.
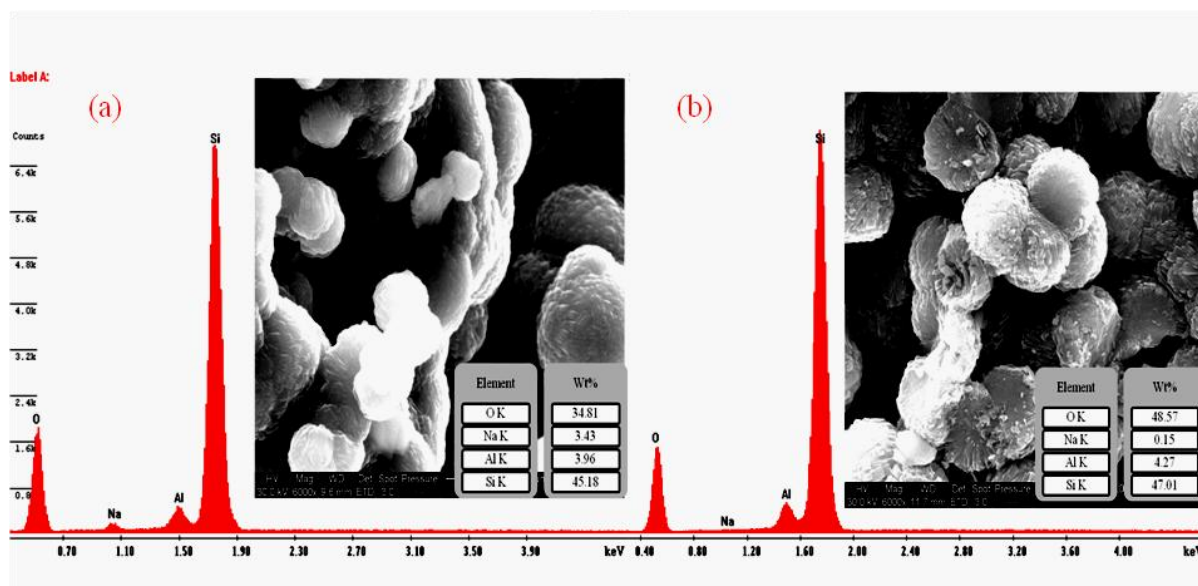
Figure 5-6: SEM and EDAX of (a) calcined structured Na-ZSM-5 and (b) structured H-ZSM-5 (0.15% Na).
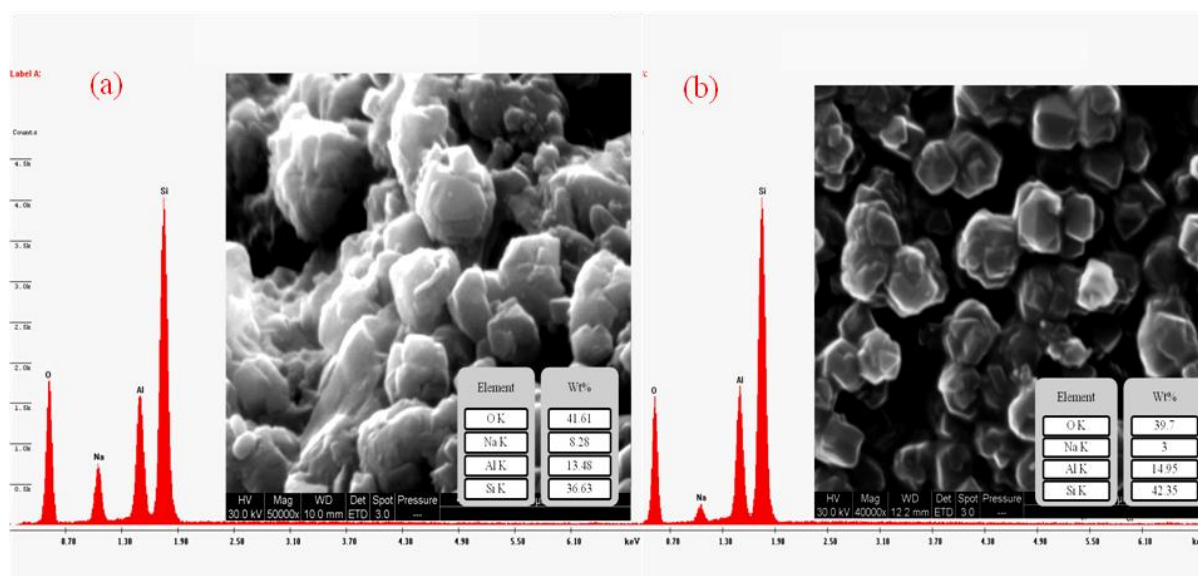
Figure 5-7: SEM and EDAX of (a) calcined structured Na-Y and (b) structured Na–HY (3%Na content).
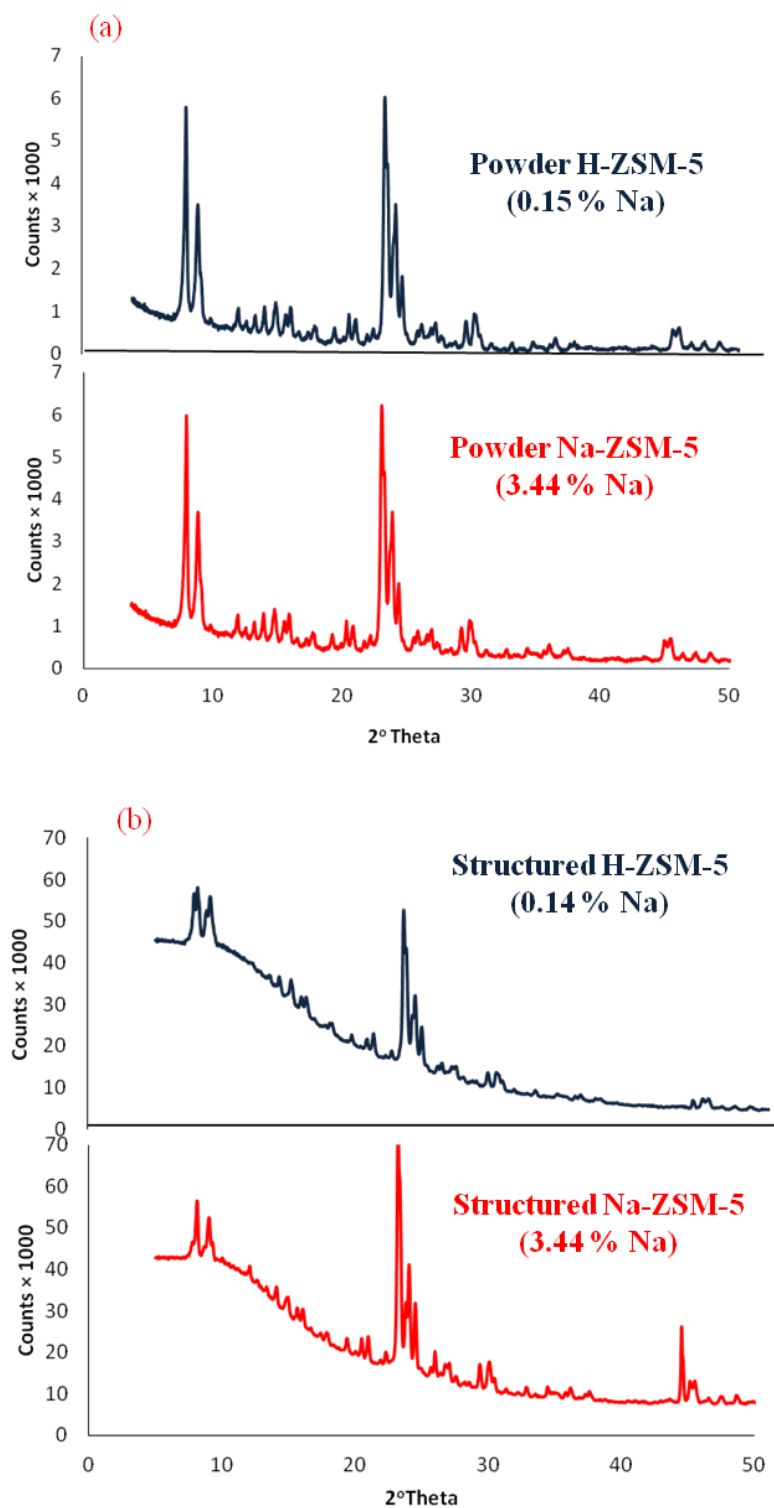
Figure 5-8: XRD comparison between calcined Na-ZSM5 and H-ZSM-5 for (a) structured and (b) powder.
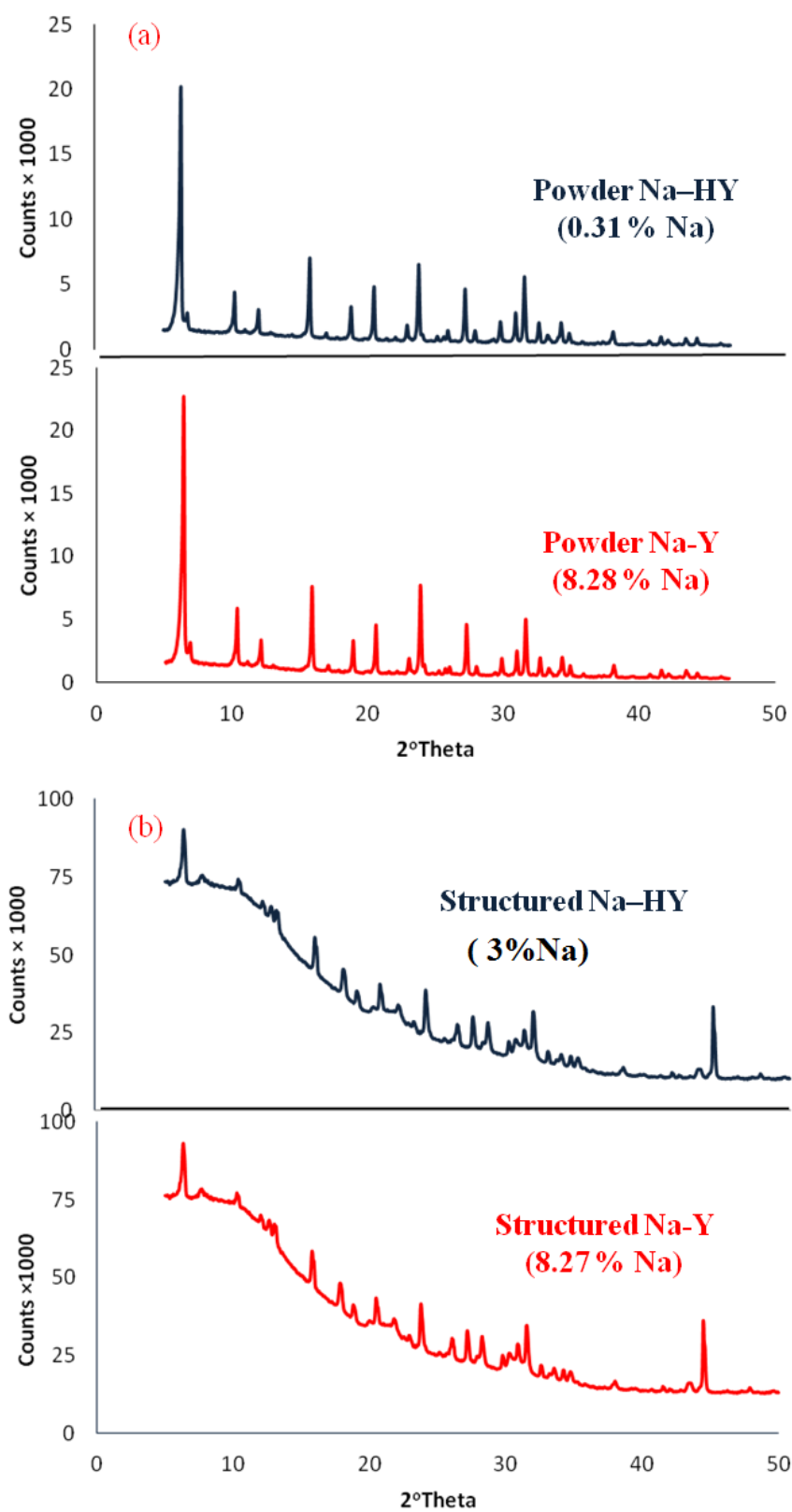
Figure 5-9: XRD comparison between calcined Na-Y and Na–HY for (a) structured and (b) powder.

The Si/Al ratios estimated by EDAX analysis for all of the zeolite samples before and after ion exchange were found to be similar for each structured and powder zeolite and typically H-ZSM-5 was 11 and Na–HY was 2.8. The Si/Al ratio for ZSM-5 and Y powder forms was calculated based on XRD and MAS–NMR with Si/Al ratios similar to the EDAX results. This suggested a uniform distribution of the Si/Al throughout each zeolite crystal and absence of the extra-framework species.

^{27}Al MAS-NMR spectra of the as-made Na-ZSM-5 and H-ZSM-5 are shown in **Figure 5-10** (a). There was one peak for both samples centered at 55.64 ppm which is attributed to the tetrahedrally coordinated aluminium species. The Na-Y and Na–HY exhibited a resonance peak at 60 ppm corresponding to tetrahedrally coordinated Al species (Al^{IV}) in the zeolite framework [7] as has been shown in **Figure 5-10**.

The BET isothermal surface area for all the zeolite powder samples was measured using a Micromeritics ASAP 2010. **Figure 5-11** showed the nitrogen adsorption–desorption isotherm comparison for Na-ZSM-5 with H-ZSM-5. The micropore volume for both sample were typically within 100 cm^3 g^{-1} and the hysteresis loop confirmed the present of the mesoporosity within the zeolite structure [8]. The BET surface area of Na–ZSM-5 was 256 m^2 g^{-1} and for the H–ZSM-5 was 284 m^2 g^{-1}. The hysteresis loop of the Na–Y and Na–HY in nitrogen adsorption–desorption isotherm appeared at high relative pressure (P/P$_o$= 0.9-1.0) due to the small crystals of the zeolite Y (**Figure 5-12**). The surface area was found to be 560 and 587 m^2 g^{-1} for Na–Y and Na–HY, respectively.

Since the catalytic reactions required high hydrothermal stability and suitable acidic and porous properties, zeolites with high Si/Al ratios and large mesopore surface areas have advantages in industrial process. In this research structured and powder zeolite H-ZSM-5 with 11 Si/Al was selected to perform n-heptane cracking without any further post-synthetic treatments. Whereas, structured and powder Na–HY were subjected to further treatments (dealumination), in order to increase catalyst stability.
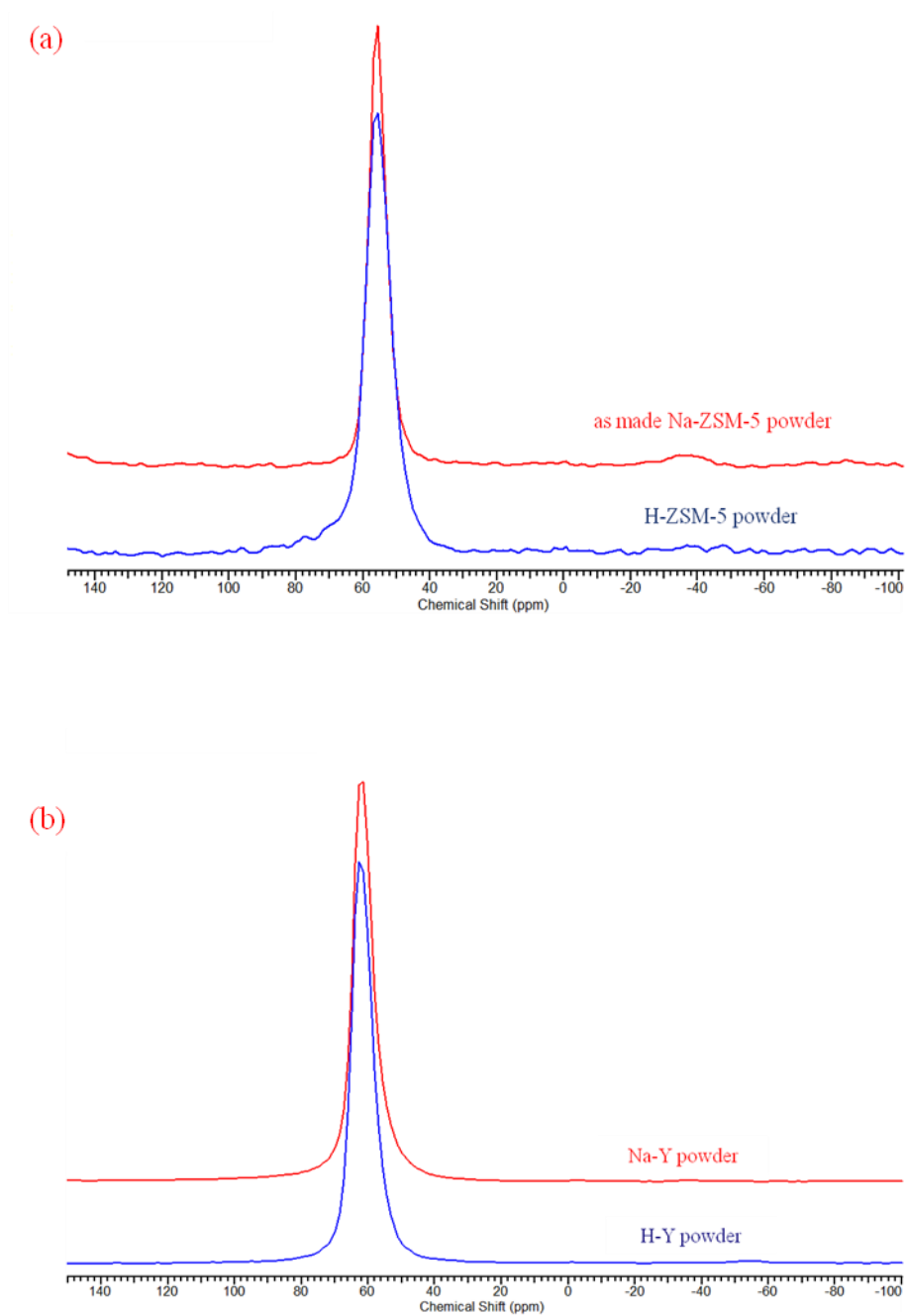
Figure 5-10: ^{27}Al MAS-NMR spectra for (a) Na- ZSM-5 and H-ZSM-5 powder (b) Na-Y and H-Y powder.
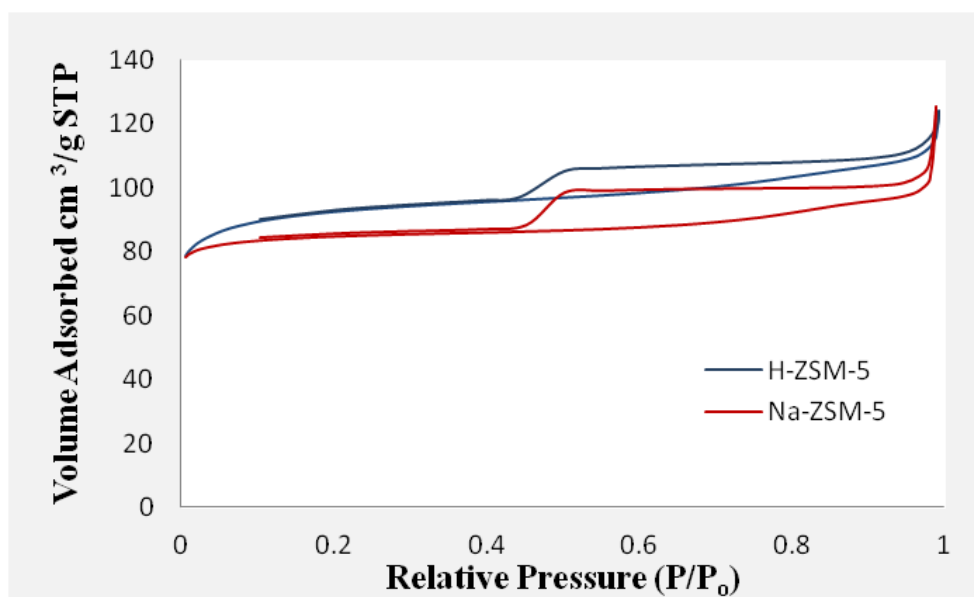
Figure 5-11: Nitrogen adsorption–desorption isotherms of Na-ZSM-5 and H-ZSM-5.
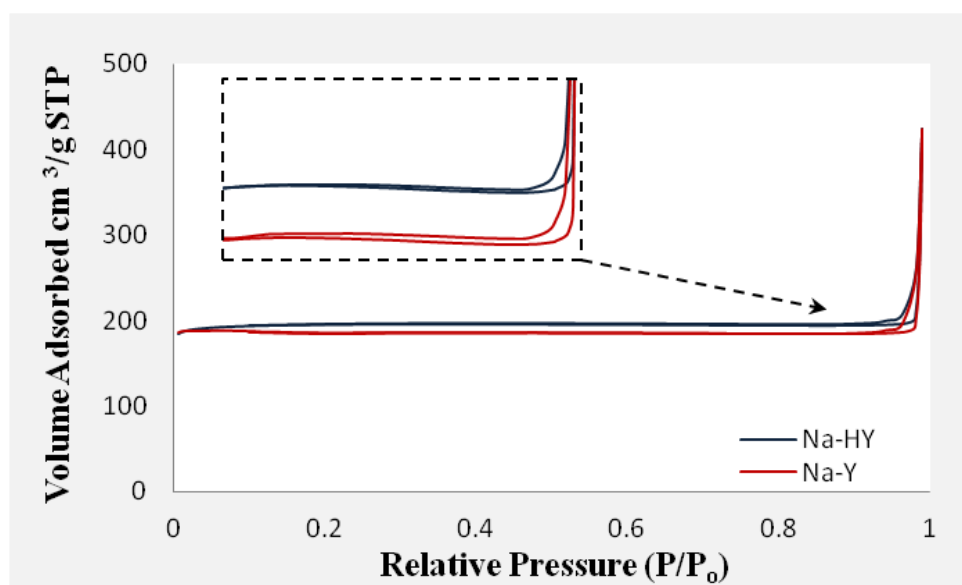
Figure 5-12: Nitrogen adsorption–desorption isotherms of Na-Y and Na–HY.

5.3 Dealumination of zeolite Y

Many catalytic processes, including cracking processes, use zeolites with high Si/Al ratios and suitable acidic properties. Zeolite Y synthesis yields directly a low Si/Al ratio structurally weak catalyst with high acidity related to the distribution of the aluminium in the zeolite framework [4, 9].

Modification of the zeolite by dealumination treatments was first reported by Barrer and Makki [10] in which they extracted aluminium species from clinoptilolite using hydrochloric acid. Later research showed that the use of ethylenediaminetetraacetic acid (EDTA) could increase the aluminium extraction efficiency [11]. To improve the thermal stability of the dealuminated zeolite Y, $SiCl_4$ has been used to refill the treatment vacancies by substitution of the extracted aluminium in the zeolite Y framework [12].

Dealumination process can also be achieved by hydrothermal treatments (known as steaming); the main problem with the steaming treatment is the formation of non-framework species left behind in the zeolite structure on dealumination framework. This leads to blockage and additional weak acid sit with a large difference in the Si/Al bulk versus Si/Al framework. These acid sites have been shown to be catalytically hydrocarbon transformation [13]. To help remove pecies and octahedral species, and leaching as stated has been commonly used to extract them [14]. In this research the structured and powder zeolite Na–Y and Na–HY were acid leached by using low pH ammonium ion exchange.

5.4 Dealumination using Low pH ion exchange

The catalytic properties of the zeolite can be controlled by controlling the Si/Al ratio of zeolite. This is a balance between the overall numbers of acid site and their acidity. Generally, the lower the framework aluminium species in the zeolite framework, the lowest number of acidic OH groups and the stronger the remaining acidity of the zeolite [15]. Zeolites with high–silica content (e.g. ZSM-5), can be produced without any dealumination treatment. However, the dealumination is

required to improve the properties of zeolite Y for purpose such as Fluid Catalytic Cracking (FCC). In this research, the goal was to dealuminate the structured and powder zeolite Y without seriously affecting the structure of the material and to establish a method to prepare structured and powder zeolite Y with favourable Si/Al ratios.

In order to study the effect of the level of cation present on the zeolite acid leaching treatment a Na–Y and 3wt% Na–HY zeolite powder was modified through acid dealumination with a mineral acid (nitric acid) to extract aluminium species (**Figure 5-13**). The pH of the dealumination process was varied in order to obtain USY zeolite, the optimum conditions were applied to modify the acidic properties.
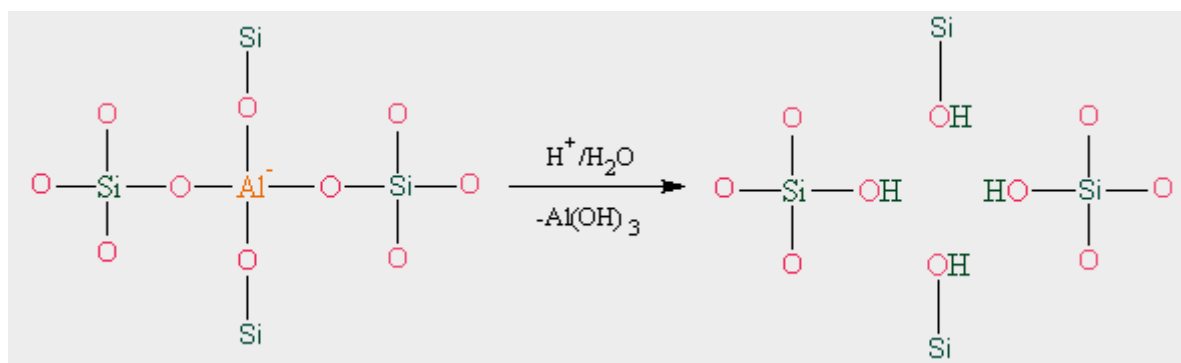
Figure 5-13: Schematic of the dealumination using mineral acid.

5.4.1 Dealumination of Na–Y powder zeolite

In order to limit the parameters influencing the dealumination treatment, in all experiments the same batch of as–synthesised powdered zeolite and the same molarities of ammonium nitrate salt were used. The pH of the mix slurry was lowered by adding specific quantities of mineral acid in three methods with three stages of acid leaching in each stage (**Table 5-1**). The amount of mineral acid (70% HNO_3) was adjusted at the beginning of each method by controlling the pH of the slurry and monitoring the dosage of the HNO_3 per gram of the starting Na–Y basis [16]. In all these experiments as–made zeolite (Na–Y) with 8.6%wt Na content was used.

Table 5-1: The amount of HNO$_3$ per grams of zeolite added and pH for the different methods.

	Method	1	2	3	Σ
I	zeolite name	^{a}YI$_1$	^{a}YI$_2$	^{a}YI$_3$	
	gHNO$_3$/g zeolite Na–Y	0.254	0.085	0.035	0.374
	pH	2.150	2.330	2.480	
II	zeolite name	^{a}YII$_1$	^{a}YII$_2$	^{a}YII$_3$	
	gHNO$_3$/g zeolite Na–Y	0.396	0.141	0.056	0.593
	pH	2.350	2.110	1.970	
III	zeolite name	^{a}YIII$_1$	^{a}YIII$_2$	^{a}YIII$_3$	
	gHNO$_3$/g zeolite Na–Y	0.685	0.236	0.068	0.989
	pH	1.500	1.500	1.500	

In the first stage of **I** method, 50 g of Na–Y zeolite, was dispersed in a 15%wt ammonium nitrate solution containing 50 g of NH$_4$NO$_3$. The pH of the slurry then lowered by adding 70 % HNO$_3$ solution; the mixed slurry was heated to 85°C for 60 min. Finally, the mixed slurry was then filtered in Büchner funnel on Whatman No52 filter paper and washed with de-ionised water until the washed water reached neutral pH. The filtered washed cake was dried at 100°C for 2 hours. The same procedure was repeated for the second and third stages expect the HNO$_3$ dosages for each stage [16].

The method **II** was the same general procedures as method **I** except the pH was adjusted from 2.35 to 1.97. Method **III** used a pH of 1.5. The zeolite samples were named as ^{a}Yn$_j$, where (a) is symbol for the parent zeolite, n represent the methods (**I**, **II**, and **III**) and j is the stages of treatment, as summarised in **Table 5-1**. The parent Na–Y samples was used as a standard reference to compare the degree of the crystallinity for the all acid leached samples using XRD.

5.4.2 Characterisation of the acid dealuminated Na–Y powder zeolite

The powder zeolite Y collected from the acid leaching treatment were characterised using the EDAX, XRD, and NMR. **Table 5-2** shows the EDAX analysis and Si/Al ratio of zeolites using surface analysis compared to the Na–Y analyses.

Although the ammonium nitrate concentration remained constant for each method (i.e. **I, II, and III**), the Na wt% in all samples was dramatically affected by the HNO_3 dosage removing large amounts of the associated sodium cations in the process of extracting the framework aluminium species. The amount of Na^+ removed increased with increasing amount of HNO_3 used. Similarly, the bulk Si/Al ratio for all methods and stages increased with the largest grams HNO_3/grams zeolite increase being method **III** with the highest HNO_3/ zeolite (0.989 g/g) [17].

Table 5-2: EDAX Elemental analysis using acid leached zeolite Na–Y.

	Si	Al	Na	Si/Al bulk
Na–Y	40.03	14.99	8.60	2.67
[a]**YI$_1$**	41.90	14.35	1.33	2.92
[a]**YI$_2$**	42.38	12.43	1.53	3.41
[a]**YI$_3$**	47.09	13.65	1.23	3.45
[a]**YII$_1$**	40.89	14.25	2.56	2.87
[a]**YII$_2$**	40.35	11.53	1.02	3.53
[a]**YII$_3$**	49.11	11.37	1.32	4.32
[a]**YIII$_1$**	47.09	13.65	1.23	3.45
[a]**YIII$_2$**	50.47	7.22	0.27	6.99
[a]**YIII$_3$**	55.96	5.69	0.05	9.89

The degree of the crystallinity was calculated from XRD patterns (**Figure 5-14**), where the total peak intensities of nine peaks for Na–Y zeolite were used as reference for the comparison using ASTM D3906 [18]. In addition, the unit cell and the framework Si/Al ratio were calculated using the d–spacing (**Equation 5-1**), the 2 ^{o}theta values, and the hkl values in **Equation 5-2** [19-21].

Finally, the ^{29}Si and ^{27}Al NMR–spectra for each zeolite sample are shown in **Figure 5-15** and **Figure 5-16**. In addition, the chemical Si/Al ratio was measured by ^{29}Si and ^{27}Al MAS–NMR spectrometer using **Equation 5-3**, and compared with bulk Si/Al obtained from EDAX and the framework Si/Al ratio measured using XRD, these results are summarised in **Table 5-3** and **Table 5-4**.

All techniques indicated the removal of the Al with the severity impacting on crystallinity. **Table 5-3** and **Figure 5-14** showed the shifting of the diffraction peaks to the higher 2θ values within the XRD patterns for the acid leached zeolite samples, which indicated by smaller d–spacing and the reduction of the unit cell parameters as had been confirmed by the result in **Table 5-4.**

The X–ray diffraction of method **I** and **II** zeolite samples were typical of zeolite Y and high framework intensity. In contrast, under more severe conditions (pH 1.5, method **III**) the peak intensities became much weaker and broader and indicated the collapse of the zeolite framework and the formation of an amorphous phase. These results were in good agreement with the works of Vassilakis [16].

Table 5-3: Shifting of 2°Theta values for XRD for dealumination treatment Na–Y with 8.6% Na content.

		Na–Y	^{a}YI$_1$	^{a}YI$_2$	^{a}YI$_3$	^{a}YII$_1$	^{a}YII$_2$	^{a}YII$_3$	^{a}YIII$_1$	^{a}YIII$_2$	^{a}YIII$_3$
2°Theta (θ)		6.202	6.264	6.288	6.341	6.255	6.289	6.339	6.289	6.254	
		10.136	10.206	10.220	10.276	10.193	10.223	10.274	10.223		
		11.893	11.953	11.979	12.032	11.951	11.982	12.030	11.982		
		15.649	15.719	15.737	15.793	15.711	15.740	15.791	15.740	15.720	
		18.674	18.751	18.770	18.825	18.741	18.770	18.823	18.770	18.739	Amorphous
		20.353	20.422	20.443	20.499	20.416	20.443	20.497	20.443		
		23.637	23.706	23.730	23.783	23.698	23.730	23.780	23.730	23.728	
		27.028	27.112	27.125	27.160	27.097	27.130	27.178	27.130	27.156	
		31.387	31.453	31.478	31.531	31.444	31.470	31.530	31.470	31.519	
		Na–Y	^{a}YI$_1$	^{a}YI$_2$	^{a}YI$_3$	^{a}YII$_1$	^{a}YII$_2$	^{a}YII$_3$	^{a}YIII$_1$	^{a}YIII$_2$	^{a}YIII$_3$
d–spacing		14.251	14.110	14.057	13.74	14.130	13.891	13.940	13.891	14.134	
		8.727	8.667	8.655	8.591	8.678	8.587	8.610	8.587		
		7.441	7.404	7.388	7.323	7.406	7.339	7.357	7.339		
		5.663	5.638	5.632	5.599	5.641	5.602	5.613	5.602	5.638	
		4.752	4.732	4.728	4.701	4.735	4.708	4.715	4.708	4.735	Amorphous
		4.363	4.349	4.344	4.320	4.350	4.327	4.333	4.327		
		3.764	3.753	3.750	3.735	3.755	3.738	3.742	3.738	4.735	
		3.299	3.289	3.288	3.275	3.291	3.278	3.281	3.278	3.284	
		2.850	2.844	2.842	2.832	2.845	2.835	2.838	2.835	2.838	
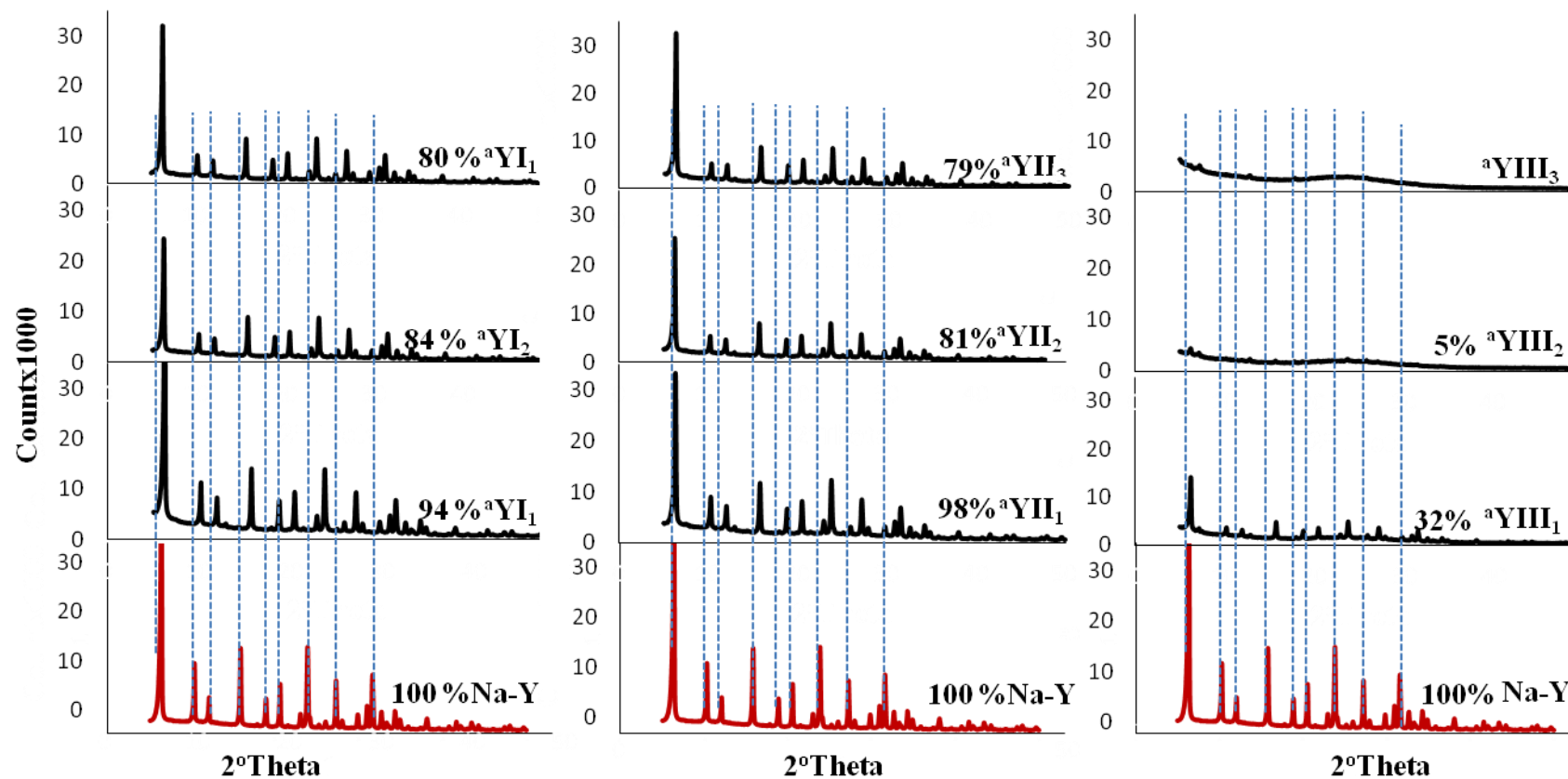
Figure 5-14: XRD patterns of acid leached zeolite Na–Y samples with 8.6% Na content for each dealumination method.

Table 5-4: Si/Al ratio for acid leached zeolite Na–Y with 8.6% Na content.

	Si/Al $_{Bulk}$	Si/Al $_{NMR}$	Si/Al $_{XRD}$	Si/Al	Crystallinity	a_o (Å)
Na–Y	2.7	2.7	2.7	2.7	100	24.684
^{a}**YI$_1$**	2.9	3.4	3.3	3.2 ± 0.5	94	24.570
^{a}**YI$_2$**	3.4	3.8	3.7	3.6 ± 0.5	84	24.536
^{a}**YI$_3$**	4.3	5.0	4.9	4.7 ± 0.5	80	24.450
^{a}**YII$_1$**	2.9	3.3	3.1	3.1 ± 0.5	98	24.585
^{a}**YII$_2$**	3.5	3.7	3.7	3.6 ± 0.5	81	24.533
^{a}**YII$_3$**	4.3	5.3	4.9	4.8 ± 0.5	79	24.442
^{a}**YIII$_1$**	3.5	4.0	4.0	3.8 ± 0.5	32	24.530
^{a}**YIII$_2$**	7	8.9	_	8.0 ± 0.5	5	_
^{a}**YIII$_3$**	9.9	11.5	_	10.7 ± 0.5	_	_

The Si/Al ratios were compared using different methodologies. There was an acceptable degree of correlation between the values. The bulk value comparing well with the MAS–NMR suggested that there was little non–framework Al present in the zeolite framework structure [5].

The NMR Si/Al ratio for the Na–Y was increased from 2.7 to 3.43, 3.81 and 5.02 for ^{a}**YI$_1$**, ^{a}**YI$_2$**, and ^{a}**YI$_3$**, respectively. This increased indicate that aluminium species had been extracted from the zeolite framework depended on the nitric acid dosage. The profile of the Si/Al ratio for the stage II was similar to that of stage I, the Si/Al ratio was increased to 5.30 from 2.7 for the Na–Y.

Figure 5-15 showed the ^{29}Si MAS–NMR spectra of acid dealuminated Na–Y zeolite. The Na–Y exhibited a resonance peak at 89, 95, 99, 101, and 105 ppm for Si (4Al), Si (3Al), Si (2Al), Si (1Al), and Si (0Al), respectively. As the nitric acid dosage increased, the characteristic bands developed on the right side of the NMR–spectra at 101 ppm and 105 ppm, and the left side hand of the NMR–spectra, assigned (4Al), Si (3Al), Si (2Al) reduced. Finally, the framework of the acid leached samples **^{a}YIII$_2$** and **^{a}YIII$_3$** were destroyed as confirmed by the XRD in **Figure 5-12**.

In addition, the ^{27}Al MAS–NMR spectra in **Figure 5-16** shows relatively constant intensity peak at 60 ppm, corresponding to the tetrahedrally coordinated aluminium species (Al^{IV}) in the zeolitic framework, during stage I, stage II and in **^{a}YIII$_1$** [22]. In contrast, a clear difference can be observed for **^{a}YIII$_1$** and **^{a}YIII$_1$** for the ^{27}Al MAS–NMR spectra in which the Al^{IV} shifted to 55 ppm and broadened. For **^{a}YI$_2$**, **^{a}YII$_1$,** and **^{a}YII$_2$** the Al^{IV} peak at 0 ppm was less evident than **YI$_3$**, **^{a}YII$_3$,** **^{a}YIII$_2$,** and **^{a}YIII$_3$** and the intensity of the peak at 0 ppm began to increase after each dealumination treatments with the peak at 60 ppm.

Figure 5-15: ^{29}Si–NMR spectra for acid dealuminated Na–Y samples with 8.6% Na content.
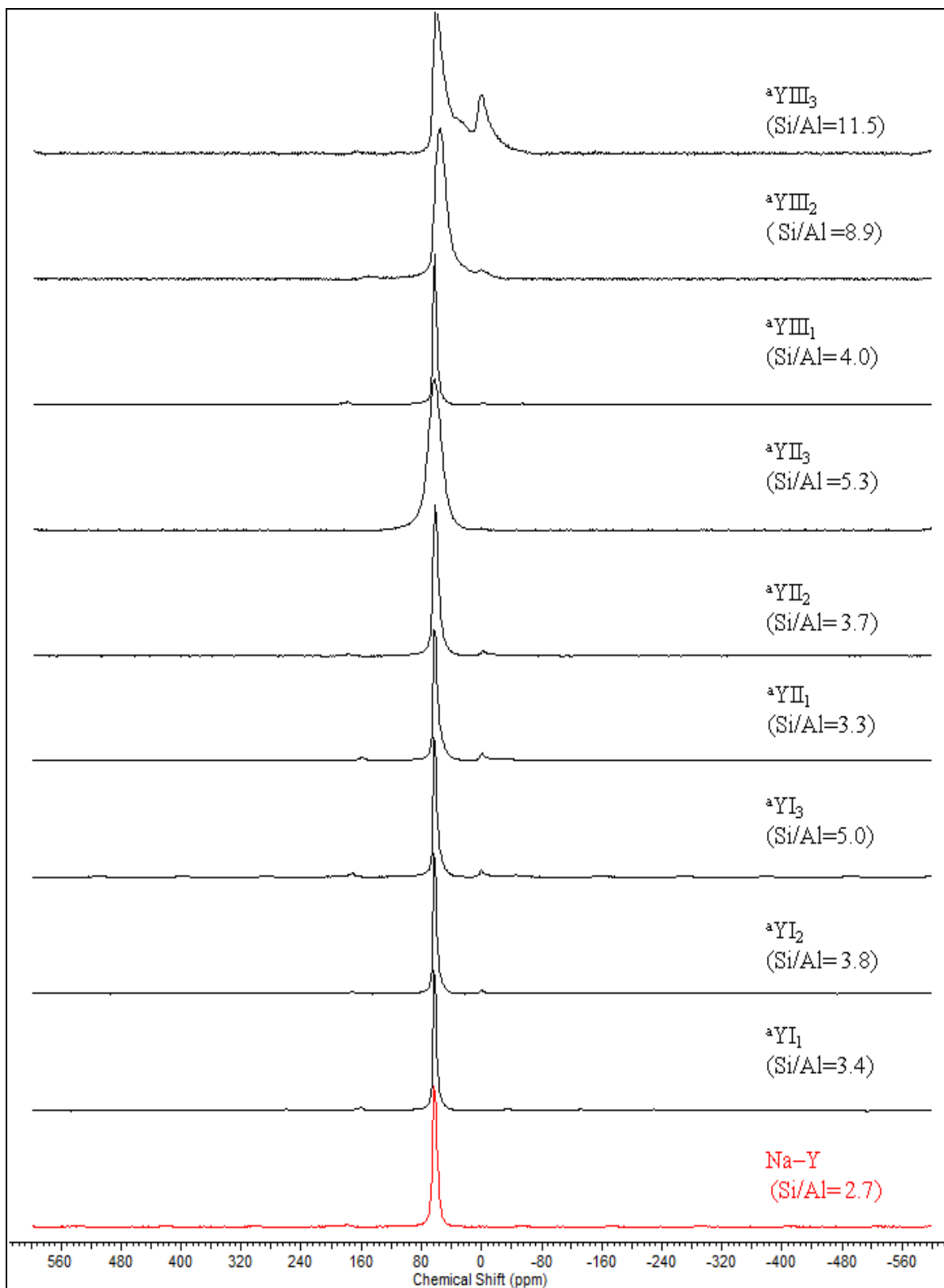
Figure 5-16:[27]**Al–NMR spectra for acid dealuminated Na–Y samples with 8.6% Na content.**

5.4.3 Dealumination of Na–HY powder zeolite (3% Na)

The same acid leaching techniques way used in **Section 5.4.1** except using a partially ion–exchanged NaY (3% wt Na). This was to assess the effect of the sodium might have on stabilising the zeolite Y framework. Using 50 g of Na–HY zeolite, the procedure of **Section 5.4.1** was repeated. Zeolite samples were named as $^{b}Y_{nj}$, where b is symbol for the parent Na–HY zeolite, n represented the methods used (**I**, **II**, and **III**) and j is stage of the treatment, as summarised in **Table 5-5**. Again the partially exchange Na–HY sample was taken as standard reference to compare the degree of the crystallinity.

Table 5-5: The amount of g HNO$_3$/g Na –HY and pH for different stages of each method.

Method		1	2	3	$\sum$
I	zeolite name	$^{b}YI_1$	$^{b}YI_2$	$^{b}YI_3$	
	gHNO$_3$/g zeolite Na–HY	0.254	0.085	0.035	0.374
	pH	2.150	2.330	2.480	
II	zeolite name	$^{b}YII_1$	$^{b}YII_2$	$^{b}YII_3$	
	gHNO$_3$/g zeolite Na–HY	0.396	0.141	0.056	0.593
	pH	2.350	2.110	1.970	
III	zeolite name	$^{b}YIII_1$	$^{b}YIII_2$	$^{b}YIII_3$	
	gHNO$_3$/g zeolite Na–HY	0.685	0.236	0.068	0.989
	pH	1.500	1.500	1.500	

5.4.4 Characterisation of the acid dealumination Na–HY powder zeolite

As listed in **Table 5-6**, the zeolites were dealumination using nitric acid and had Si/Al ratios ranging from 3.5 to 14.2. The achieved Si/Al ratio for the Na–HY acid leached samples was higher than that for the Na–Y samples. As observed previously, the bulk Si/Al ratio for all methods increased with each method and stage.

As previously observed, the sodium content in the Na–HY acid leached samples was significantly reduced with increasing the dosage of nitric acid in the each stage of treatments. In the most sever treatment (**III**) Na^+ was easily removed but less so in methods **I** and **II,** thus, the $^b YIII_2$ and $^b YIII_3$ the lowest Na concentration among the three stages after three cycle of acid leaching.

Table 5-6: EDAX analysis for acid leached zeolite Na–HY with 3% Na content.

	Si	Al	Na	Si/Al $_{bulk}$
Na–HY	42.4	15.0	3.0	2.8
$^b YI_1$	42.4	12.2	1.5	3.5
$^b YI_2$	49.1	10.4	0.9	4.7
$^b YI_3$	52.0	7.0	0.3	7.4
$^b YII_1$	50.3	13.7	1.3	3.7
$^b YII_2$	52.0	10.1	0.3	5.1
$^b YII_3$	64.0	7.9	0.2	8.1
$^b YIII_1$	38.3	6.5	0.7	5.9
$^b YIII_2$	41.9	3.9	0.0	10.9
$^b YIII_3$	52.0	3.7	0.0	14.2

Figure 5-17 showed the XRD patterns of the Na–HY acid leached samples. The powder XRD diffractograms illustrate the progressive breakdown of the crystalline structure of the zeolite and with the decreasing in the peak intensities of zeolite. High crystallinity was observed for zeolites using method **I** the XRD patterns of the **^{b}YI$_1$**, **^{b}YI$_2$** and **^{b}YI$_3$**. Under more severe conditions (pH < 2.11); the diffraction peaks disappear indicating a collapse of framework structure, with a broad band due to the amorphous phase dominating. It was reported [14, 23] that the structure of the zeolite Y collapse under severe acid leaching condition. Lee and Rees [24] showed that the aluminium can be extracted without considerable lattice destruction by controlling the amount of the mineral acid (HCl) applied so as not to not cause intense dealumination.

The unit cell and the framework Si/Al ratio were calculated using the XRD data listed in **Table 5-7**. As expected, as the aluminium reduced, the framework Si/Al ratios increased and the unit cell size of the zeolite decreased. The Si/Al a ratio was again calculated using different techniques (i.e. EDAX, XRD, and NMR) and good agreement shown (**Table 5-8**). This indicated uniformity in the distribution of the Si/Al atomic ratio in the zeolite framework structure after dealumination.

The Si/Al ratio measured using EDAX was generally lower than other analytical methods that there was non–framework Al present at increased Si/Al ratios. The NMR Si/Al for the Na–HY ratio during the stage **I** increased to 8.01 (**^{b}YI$_3$**) which was significantly higher than the Si/Al ratio observed for the Na–Y sample treated under same conditions (5.02 **^{a}YI$_3$**) with high crystallinity. The profile of Si/Al ratio of stage **II** and stage **III** was relatively similar to that of stage **I**; the ratio increased during each acid leaching cycle however, the zeolite peaks intensities were decreased with increasing of the amorphous background for **^{b}YII$_1$**, **^{b}YII$_2$** and **^{b}YIII$_1$** and completely destroying of the zeolite structure during **^{b}YII$_3$**, **^{b}YIII$_2$**, and **^{b}YIII$_3$**.

Sato [5] explain that the Na$^+$ ion in as–made zeolite (Na–Y) in located inside of the hexagonal prisms and during the ion exchange treatment and calcination process the Na species migrated to the outside of the hexagonal prisms. It is also

reported by Hensen [25] that the ion exchanged form of zeolite framework stability is lower than that of the as–made zeolite, hence, the distortion and deterioration of the framework preceded the dealumination and migration of Al.

Figure 5-18 details the ^{29}Si MAS–NMR spectra of Na–HY and acid dealuminated zeolite. The Na–HY showed the presence of five components, corresponding to Si (4 Al), Si (3 Al), Si (2 Al), Si (1 Al), and Si (0 Al). The effect of dealumination was clear as the Si (4 Al) disappeared, the Si (3 Al) and Si (2 Al) decreased significantly, and Si (1 Al) and Si (0 Al) showed increased. This fact showed that nitric acid can remove lattice aluminium from the zeolite framework. ^{29}Si MAS–NMR results were in accord with Al-Zaidi [3] who studied acid leaching of Y zeolite using HCl. For severely treated samples (^{b}YII$_3$, ^{b}YIII$_2$, and ^{b}YIII$_3$) the overlapping indicated a progressive and significant dealumination of the zeolite structure and XRD confirmed that as crystallinity was lost.

The ^{27}Al MAS–NMR spectra of Na–HY after various acid leaching treatments are shown in **Figure 5-19.** The analyses of the Na–HY detected a peak at 60 ppm corresponding to the tetrahedrally–coordinate aluminium species. The acid leached samples showed the presence of an octahedral aluminium peak at 0 ppm as a result of the treatment. Severely treated samples (^{b}YII$_3$, ^{b}YIII$_2$, and ^{b}YIII$_3$) the peak broadened at 60 ppm.

Table 5-7: Shifting of 2°Theta values for XRD with the dealumination treatment of Na–HY with 3% Na content.

	Na–HY	$^{b}YI_1$	$^{b}YI_2$	$^{b}YI_3$	$^{b}YII_1$	$^{b}YII_2$	$^{b}YII_3$	$^{b}YIII_1$	$^{b}YIII_2$	$^{b}YIII_3$
2°Theta (θ)	6.286	6.288	6.343	6.404	6.289	6.363		6.346		
	10.226	10.220	10.258	10.338	10.224	10.302		10.297		
	11.985	11.979	12.039	12.093	11.983	12.060		12.063		
	15.752	15.737	15.796	15.853	15.74	15.819	Amorphous	15.825	Amorphous	Amorphous
	18.788	18.770	18.832	18.885	18.771	18.850		18.860		
	20.470	20.443	20.508	20.565	20.443	20.526		20.537		
	23.760	23.730	23.792	23.844	23.73	23.807		23.837		
	27.166	27.125	27.199	27.245	27.13	27.206		27.235		
	31.521	31.478	31.538	31.593	31.471	31.554		31.631		
	Na–HY	$^{b}YI_1$	$^{b}YI_2$	$^{b}YI_3$	$^{b}YII_1$	$^{b}YII_2$	$^{b}YII_3$	$^{b}YIII_1$	$^{b}YIII_2$	$^{b}YIII_3$
d–spacing	14.211	14.057	13.935	13.803	13.901	13.891		13.927		
	8.705	8.655	8.624	8.557	8.591	8.587		8.592		
	7.390	7.388	7.351	7.319	7.341	7.339		7.337		
	5.654	5.632	5.610	5.591	5.602	5.602	Amorphous	5.600	Amorphous	Amorphous
	4.743	4.728	4.712	4.699	4.711	4.708		4.705		
	4.363	4.344	4.331	4.319	4.331	4.327		4.325		
	3.760	3.750	3.740	3.732	3.738	3.738		3.733		
	3.290	3.288	3.279	3.273	3.281	3.278		3.274		
	2.843	2.842	2.837	2.832	2.834	2.835		2.829		
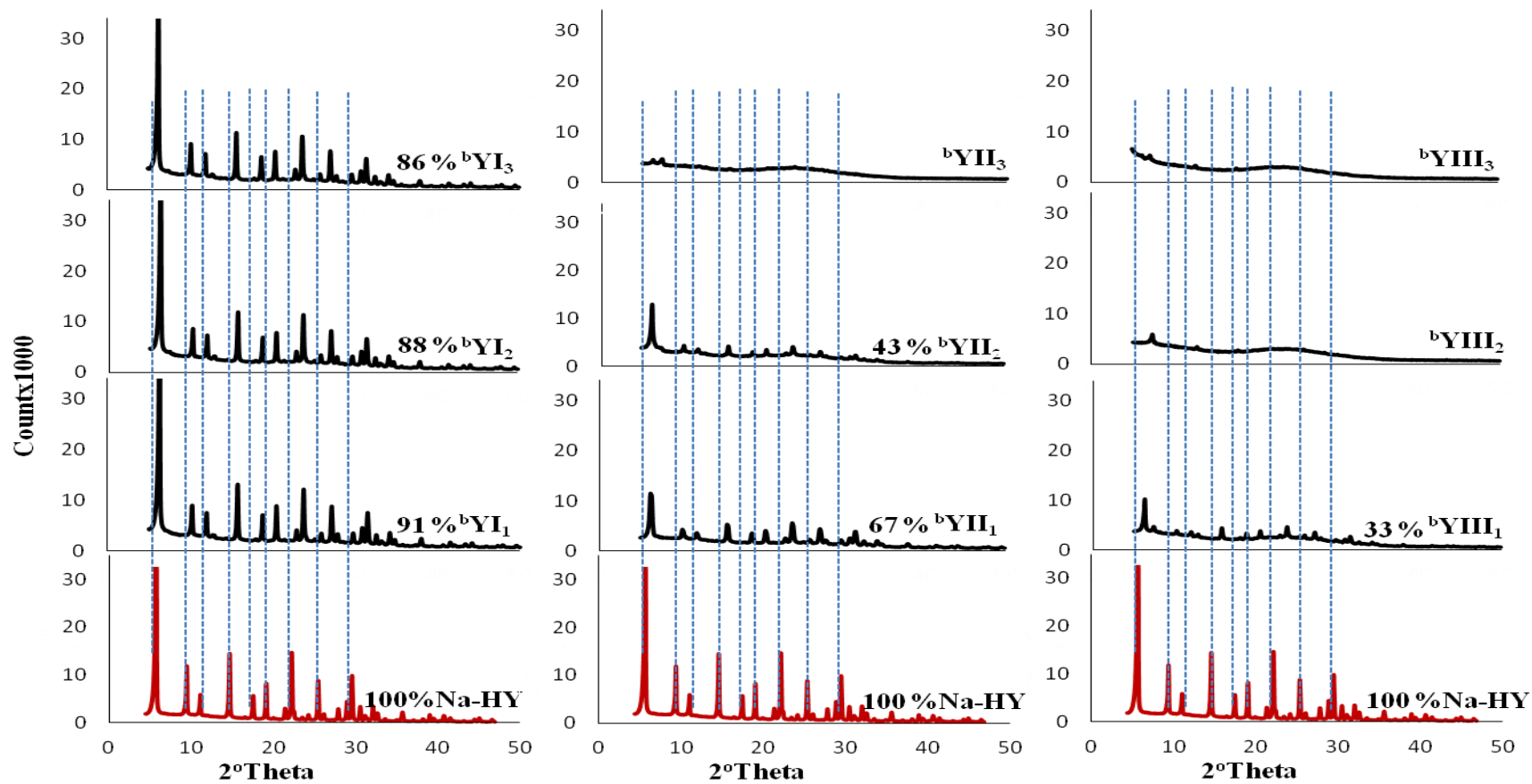
Figure 5-17: XRD patterns of acid leached zeolite Na–HY with 3% Na content.

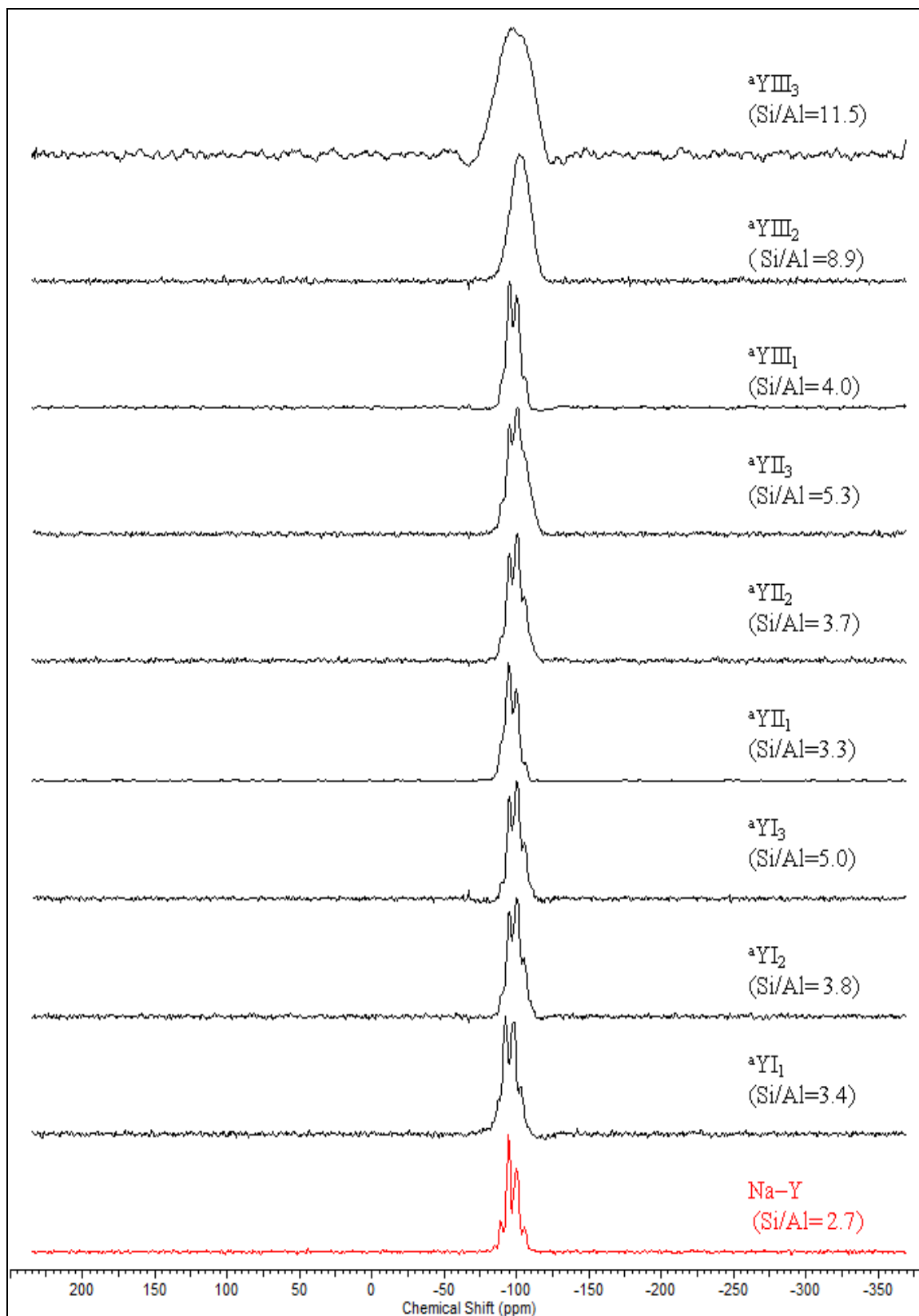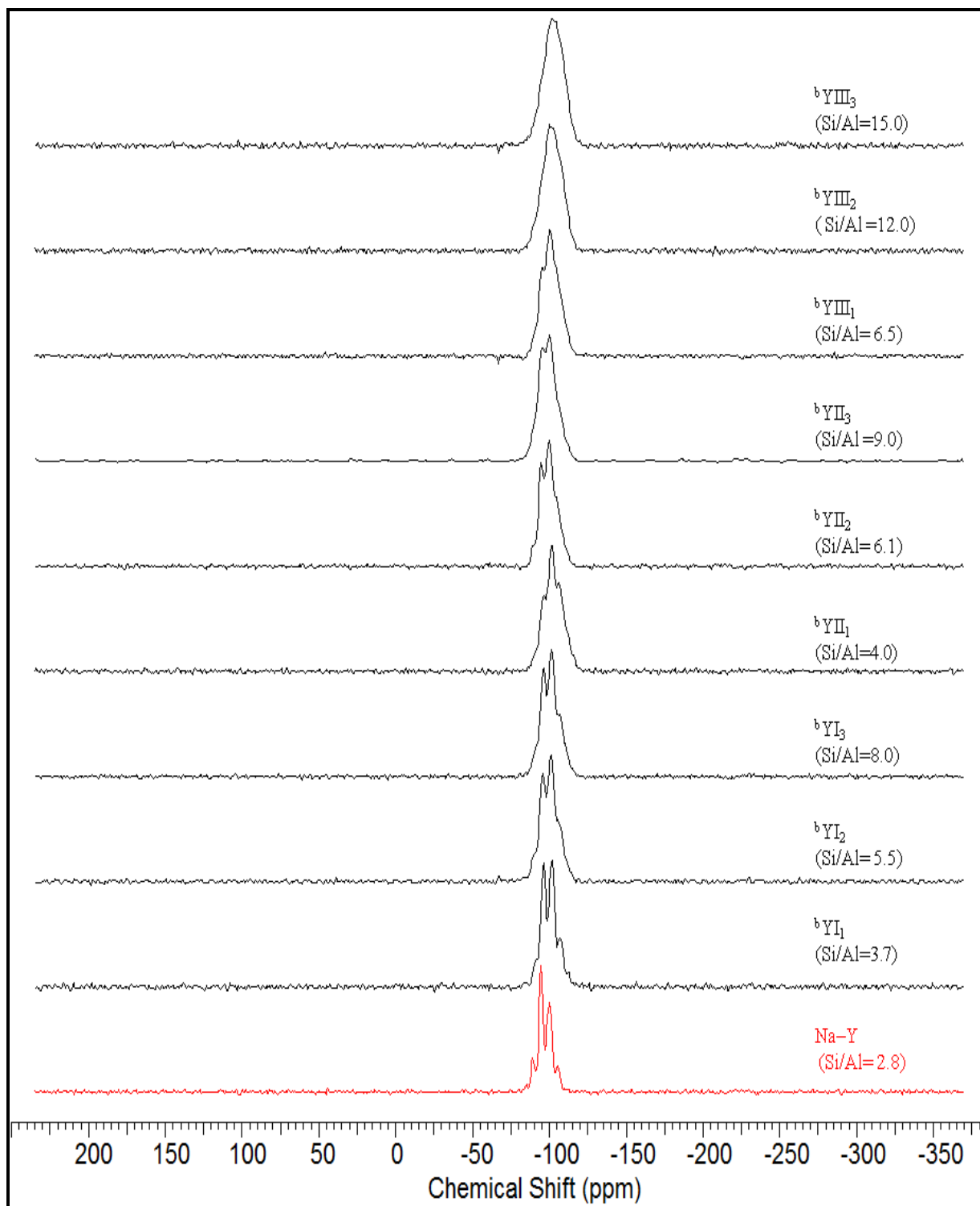**Figure 5-18: 29Si–NMR spectra for acid dealuminated Na–HY with 3% Na content.**
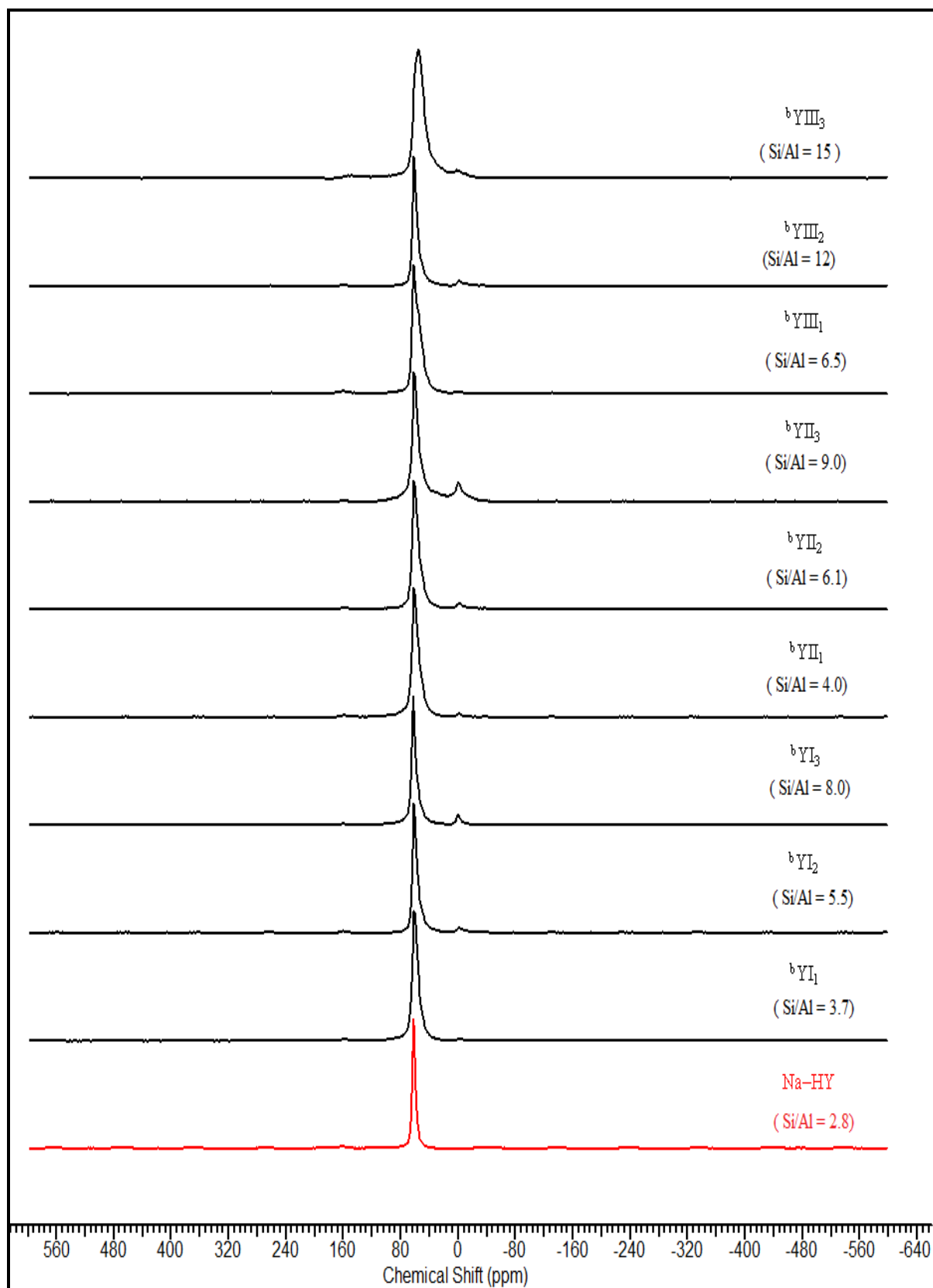
Figure 5-19: ^{27}Al–NMR spectra for acid dealuminated Na–HY with 3% Na content.

Table 5-8: Si/Al ratio for acid leached zeolite Na–HY with 3% Na content.

	Si/Al Bulk	Si/Al NMR	Si/Al XRD		Crystallinity	a_o (Å)
Na–HY	2.8	2.8	2.8	2.8 ± 0.0	100	24.624
[b]YI$_1$	3.5	3.7	3.7	3.6 ± 0.1	91	24.585
[b]YI$_2$	4.7	5.5	5.1	5.1 ± 0.4	88	24.442
[b]YI$_3$	7.4	8.0	7.8	7.8 ± 0.2	86	24.344
[b]YII$_1$	3.7	4.0	3.8	3.8 ± 0.2	67	24.530
[b]YII$_2$	5.1	6.1	6.0	5.7 ± 0.3	43	24.405
[b]YII$_3$	8.1	9.0	-	8.5 ± 0.5	-	-
[b]YIII$_1$	5.9	6.5	6.1	6.1 ± 0.4	33	24.396
[b]YIII$_2$	10.9	12.0	-	11.5 ± 0.5	-	-
[b]YIII$_3$	14.2	15.0	-	14.6± 0.4	-	-

Method **I** zeolites were further characterised using Micromeritics ASAP 2010 (**Figure 5-20).** The BET surface area of Na–HY (587 m^2 g^{-1}) decreased to 518, 427, 400 m^2 g^{-1} for **[b]YI$_1$**, **[b]YI$_2$**, and **[b]YI$_3$** respectively. This was expected due to the shrinking of the zeolite unit cell and extraction of the Al species from the zeolite framework.

In conclusion, the short study showed that the stability of the Na–Y zeolite with 8.6% Na content during the acid leaching with nitric acid was higher than the Na–HY zeolite 3% Na content under same conditions. These results agreed with the work of Koningsberger [26] who stated that the Al–O bond distance of 1.620 Å in Na–Y was shorter than that in H–Y with length of 1.700 Å and the electron density was lower in the H–Y than the Na–Y. Hence, the Al–O bond was weaker within crystal lattice structures H–Y type zeolite.

The data collected using different analytical method (EDAX, XRD, and NMR) for both Na–Y and Na–HY acid dealumination zeolite, indicated that Na$^+$ ion inside the zeolite structure can hinder the extraction of the aluminium species from

the zeolite lattice matrix in the acid dealumination process. The high Na content resulted in lower the Si/Al ratios and higher crystallinity on comparable treatments.

As a result of these finding method to produce $^{b}YI_3$ (called USY from now on) with a Si/Al ratio = 8, 0.3% sodium content and 86% crystallinity was chosen to treat the Na–HY structured zeolite, in the aim to tailor catalytic acidic properties.
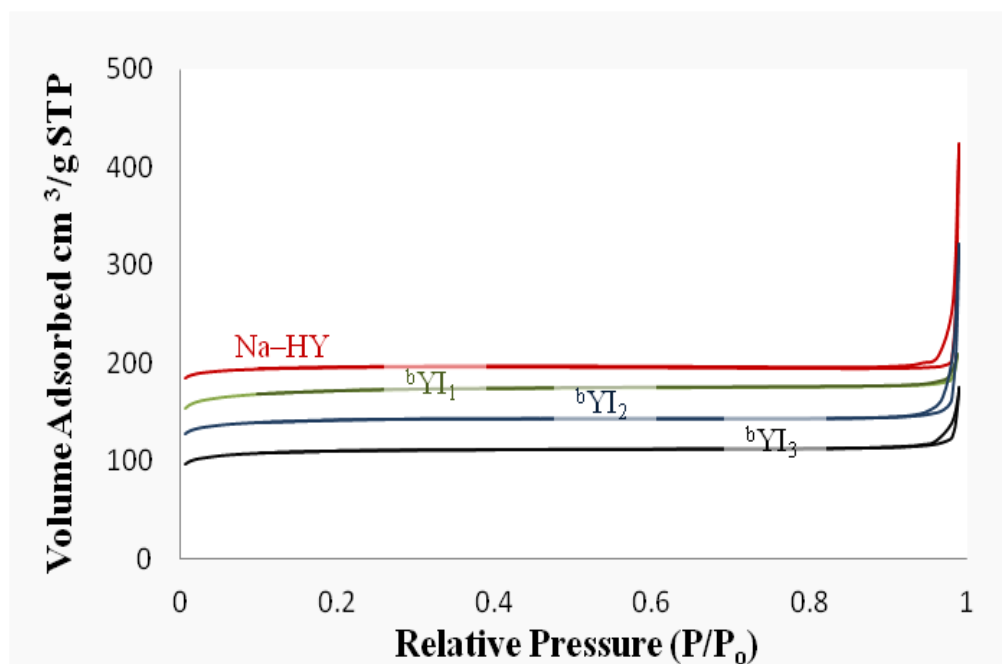
Figure 5-20: Nitrogen adsorption–desorption isotherm of Na–HY and acid leached YI zeolite.

5.4.5 Dealumination of Na–HY structured zeolite

The method to produced $^{b}YI_3$ was selected to produce USY structured zeolite. As it was difficult to obtain and an accurate measurement of the amount of zeolite grown on the pre–treated FeCrAlloy wires; thence the dosage of nitric acid (70% HNO_3) was altered at the beginning of each stage by controlling the pH of the solution [16].

Briefly, the Na–HY zeolite structured wires were subjected to a chemical treatment following the procedure described in method **I** (**Section 5.4.3**). Na–HY zeolite structured wires (50) were immersed in 15wt% ammonium nitrate solution. The pH of the solution was lowered to 2.15 by adding 70% HNO_3 solution; then the solution heated to $85^{o}C$ for 60 minutes with constant mixing. The wires were then

removed. Then, the wires were collected and thoroughly washed in ultrasonic bath with de-ionised water for 15 minutes and finally dried at 100°C for 2 hours.

The washed zeolite structured wires were immersed again in 15wt% ammonium nitrate solution. The pH solution was lowered to 2.11 by adding HNO_3 solution. Again the zeolite structured wires into solution were mixed at 85°C for a 60 min, washed using ultrasonic bath and de-ionised water and dried at 100 for 2 hours and the solution was analysed. The same procedure was followed for the third stage expects the pH was lowered this time to 1.97 [16].

5.4.6 Characterisation of the acid dealumination Na–HY powder zeolite

Identical profile on the Y zeolite framework of the acid leached Na–Y structured was confirmed from the data collected by the EDAX and the XRD techniques. The EDAX results revealed increasing Si/Al ratio during each acid leaching cycle with dropping in the Na content.

The Na–HY structure zeolite with 100% degree of crystallinity was used as the reference for the acid leached samples. **Table 5-9** showed that the nitric acid removed not only the aluminium species from the zeolite framework but it was also removed the associated Na^+ ion [27]. Also, the removed of aluminium species as observed by reducing the framework resulted in expected reduction in the lattice size. The crystallinity of the structured catalysts decreased from 100-85% as the acid ion–exchanged stages were repeated.

Figure 5-21 showed the influence of the extracting the aluminium species on the shrinking of the zeolite unit cell during each cycle, thence the increasing of Si/Al ratio in the bulk and slightly higher in the zeolite framework. This influence can be observed also in the shifting of the peaks diffraction to higher value of 2° theta and smaller d–spacing (**Figure 5-21**).

The value of the AlO_2 and framework Si/Al $_{XRD}$ ratio have been calculated using the data in **Table 5-10**. Successive treatment of **YI$_3$ structured** results in 21.31 aluminium specie residue in the zeolite framework. According to the extracted the aluminium species from the zeolite structure, the zeolite crystallinity was decreased to 84%.

Consequently, the all analytical method showed increase in the Si/Al ratios and decreasing with reduction in the size of the unit cell and reducing of the d–spacing of in the crystallinity degree. This indicated that extraction of the aluminium species was present inside the zeolite particles.

Accordingly, the characterisation showed the acid leaching procedure (**method I**) followed to altered catalytic acidic properties for both Y structured and powder zeolite was successful in generating powder and structured USY catalyst with 8 Si/Al ratio and crystallinity above 84.

Table 5-9: EDAX and XRD data for acid leached Na–HY structured zeolite with 3% Na content.

	EDAX data				XRD data			
	Si (wt %)	Al (wt %)	Na (wt %)	Si/Al	[Al O$_2$] unit $_{XRD}$	Si/Al	a° (Å)	Crystallinity
Na-HY structured	42.4	14.9	3.0	2.8	49.22	2.9	24.614	100
YI$_1$ structured	43.9	12.9	1.4	3.4	39.20	3.9	24.523	96.4
YI$_2$ structured	45.9	10.2	0.7	4.5	30.48	5.3	24.429	88.2
YI$_3$ structured	56.7	7.6	0.1	7.5	21.31	8.1	24.339	84.5

Table 5-10: Shifting of 2^oTheta values for XRD for dealumination treatment Na–HY structure zeolite with 3% Na content.

	Na–HY	YI$_1$	YI$_2$	YI$_3$		Na–HY	YI$_1$	YI$_2$	YI$_3$
	6.255	6.331	6.343	6.351		14.140	13.962	13.935	13.954
	10.193	10.258	10.388	10.343		8.691	8.5160	8.623	8.653
	11.951	12.007	12.039	12.093		7.434	7.371	7.351	7.362
	15.711	15.770	15.796	15.823		5.641	5.620	5.610	5.589
2^oTheta (θ)	18.741	18.791	18.832	18.875	d–spacing	4.746	4.722	4.712	4.691
	20.416	20.467	20.506	20.545		4.352	4.446	4.331	4.233
	23.698	23.750	23.792	23.812		3.754	3.746	3.739	3.713
	27.097	27.152	27.199	27.215		3.291	3.284	3.278	3.264
	31.444	31.511	31.538	31.583		2.850	2.839	2.836	2.833
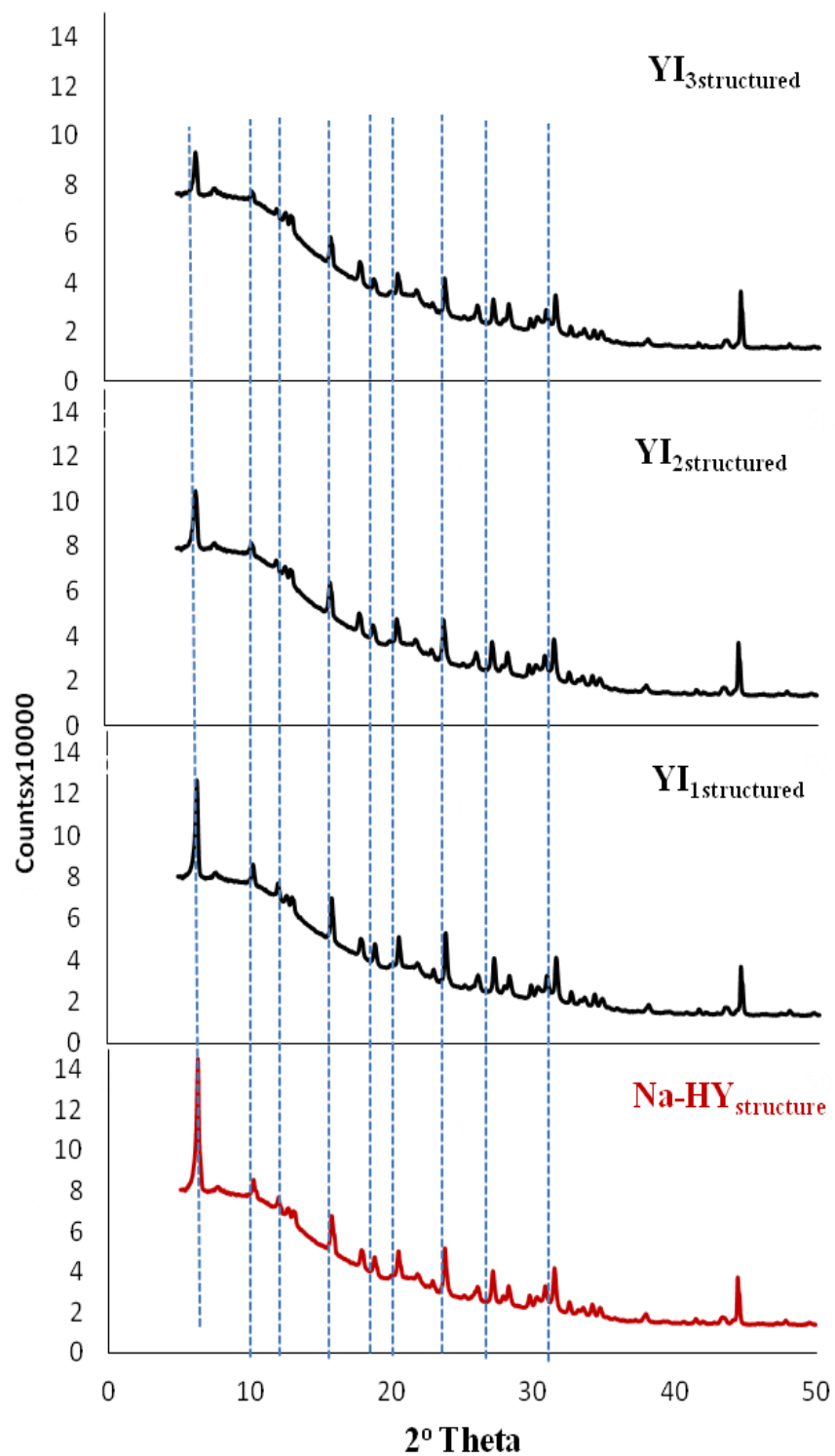
Figure 5-21: XRD patterns of acid leached zeolite Na–HY with 3% Na content.

Summary

This chapter detailed the successful development and full characterisation of an acidified ion exchange procedure to generate both powder and structured zeolite Y catalysts with a range of the Si/Al ratios suitable for n–heptane cracking.

Since the catalytic reactions required high hydrothermal stability and suitable acidic and porous properties, zeolites with high Si/Al ratios and large mesopore surface areas had been used in industrial process. In this research structured and powder zeolite HZSM-5 with 11 Si/Al was selected to perform n-heptane cracking without any furthermore post-synthesis treatments. Whereas, structured and powder Na–HY subjected to further treatments (dealumination), in order to increase the Si/Al ratio and catalytic properties.

In order to study the effect of the cation present on the zeolite acid leaching treatment the Na–Y 8.6% Na and Na–HY 3% wt Na zeolite powder were modified through acid dealumination with a mineral acid (nitric acid) to extract aluminium species. The pH of the dealumination process was varied in order to obtain acidic USY zeolite. Then, the optimum conditions were applied on zeolite Y structured catalyst to modify the acidic properties.

The Si/Al ratios were confirmed by three techniques; EDAX, XRD, and MAS–NMR. There was good agreement for all techniques and this suggested that the catalysts produced had little extra–framework Al trapped in the zeolite framework after dealumination.

Sodium cation inside the zeolite structure can hinder the extraction of the aluminium species from the zeolite lattice matrix in the acid dealumination process, therefore a partially ion exchanged Na–HY (3% Na content) was acid leached to produce the USY zeolite with Si/Al ratios = 6-8.

The method **I** chosen was based on the partially ion exchanged Na-HY zeolite with a Na content 3%. The range of catalyst produced was with 8 Si/Al ratios.

References

1.   Karge, H.G., J. Weitkamp, and P. Anderson, *Post-Synthesis Modification I*, 2002: p 1-8.

2.   Chou, Y.H., and Garforth, A.A., *Mesoporous ZSM-5 catalysts: Preparation, characterisation and catalytic properties. Part I: Comparison of different synthesis routes,* Microporous and Mesoporous Materials, 2006. **89**(1): p. 78-87.

3.   Al-zaidi, B.Y.S., *The Effect of Modification Techniques on the Performance of Zeolite-Y Catalysts in Hydrocarbon Cracking Reactions*, in *Chemical Engineering & Analytical Science*, 2011, University of Manchester: Manchester.

4.   Lutz, W., C. Rüscher, and D. Heidemann, *Determination of the framework and non-framework [SiO$_2$] and [AlO$_2$] species of steamed and leached faujasite type zeolites: calibration of IR, NMR, and XRD data by chemical methods,* Microporous and Mesoporous Materials, 2002. **55**(2): p. 193-202.

5.   Sato, K., Y. Nishimura, N. Matsubayashi, M. Imamura, H. Shimada, *Structural changes of Y zeolites during ion exchange treatment: effects of Si/Al ratio of the starting NaY,* Microporous and Mesoporous Materials, 2003. **59**(2–3): p. 133-146.

6.   Fletcher, P. and R.P. Townsend, *Exchange of ammonium and sodium ions in synthetic faujasites,* Journal of the Chemical Society, Faraday Trans. 1, 1982. **78**(6): p. 1741-1753.

7.   Thomas, J. and J. Klinowski, *The study of aluminosilicate and related catalysts by high-resolution solid-state NMR spectroscopy,* Advances in catalysis, 1985. **33**: p. 199-373.

8.   Cejka, J., H. Van Bekkum, A. Corma, and F. Schueth, *Introduction to Zeolite Molecular Sieves*, Vol. 168. 2007: Elsevier Science.

9.   Sohn, J.R., S.J. DeCanio, P.O. Fritz, and J.H. Lunsford, *Acid catalysis by dealuminated zeolite Y, 2. The roles of aluminum,* The Journal of Physical Chemistry, 1986. **90**(20): p. 4847-4851.

10.   Barrer, R.M. and M.B. Makki, *Molecular Sieve Sorbents from Clinoptilolite,* Canadian Journal of Chemistry, 1964. **42**(6): p. 1481-1487.

11. Kerr, G.T., *Chemistry of crystalline aluminosilicates. V. Preparation of aluminum-deficient faujasites,* The Journal of Physical Chemistry, 1968. **72**(7): p. 2594-2596.

12. Beyer, H.K., I. M. Belenykaja, F. Hange, M. Tielen, P. J. Grobet, and P. A. Jacobs, *Preparation of high-silica faujasites by treatment with silicon tetrachloride,* Journal of the Chemical Society, Faraday Transactions 1: Physical Chemistry in Condensed Phases, 1985. **81**(11): p. 2889-2901.

13. Lago, R., W.O. Haag, R.J. Mikovsky, D.H. Olson, S.D. Hellring, K.D. Schmitt, and G.T. Kerr, *The nature of the catalytic sites in HZSM-5-activity enhancement,* Studies in Surface Science and Catalysis, 1986. **28**: p. 677-684.

14. Yan, Z., D. Ma, J. Zhuang, X. Liu, X. Han, X. Bao, F. Chang, L. Xu, and Z. Liu, , *On the acid-dealumination of USY zeolite: a solid state NMR investigation,* Journal of Molecular Catalysis A: Chemical, 2003. **194**(1): p. 153-167.

15. Kooyman, P.J., P. van der Waal, and H. van Bekkum, *Acid dealumination of ZSM-5,* Zeolites, 1997. **18**(1): p. 50-53.

16. Vassilakis, J.G. and D.F. Best, *Novel zeolite compositions derived from zeolite Y*, 1991, US Patent 5,013,699.

17. Skeels, G.W., D.W. Breck, and D. in Olson, and A. Bisio, *Proceedings of the Sixth International Zeolite Conference, Reno, USA 10-15 July 1983.* Guildford, Surrey, UK: Butterworths.

18. Standards, A., *ASTM D3906-03.* 2008, Specification for Concrete Aggregates: West Conshohocken, PA.

19. Breck, D. and G. Skeels, *Zeolite Chemistry Π. The Role of Aluminum in the Hydrothermal Treatment of Ammonium-Exchanged Zeolite Y, Stabilization,* Molecular sieves II, 1977. **40**: p. 271.

20. Breck, D.W., *Zeolite molecular sieves, 1974.* New York, 1988: p. 379-392.

21. Fichtner-Schmittler, H., U. Lohse, G. Engelhardt, and V.Patzelová, *Unit cell constants of zeolites stabilized by dealumination determination of Al content from lattice parameters,* Crystal Research and Technology, 1984. **19**(1): p. K1-K3.

22. Thomas, J.M. and J. Klinowski, *The Study of Aluminosilicate and Related Catalysts by High-Resolution Solid-State NMR Spectroscopy*, in *Advances in catalysis*, H.P. D.D. Eley and B.W. Paul, Editors. 1985, Academic Press. p. 199-374.

23. Karge, H.G., *Post-synthesis modification of microporous materials by solid-state reactions,* Studies in Surface Science and Catalysis, 1997. **105**: p. 1901-1948.

24. Lee, E.F. and L.V. Rees, *Calcination of cerium (III) exchanged Y zeolite,* Zeolites, 1987. **7**(5): p. 446-450.

25. Hensen, E. and J. Van Veen, *Encapsulation of transition metal sulfides in faujasite zeolite for hydroprocessing applications,* Catalysis Today, 2003. **86**(1): p. 87-109.

26. Koningsberger, D.C. and J.T. Miller, *Local structure determination of aluminum in Y zeolite: application of low energy X-ray absorption fine structure spectroscopy,* Catalysis Letters, 1994. **29**(1-2): p. 77-90.

27. Wang, Q.L., G. Giannetto, and M. Guisnet, *Dealumination of zeolites III. Effect of extra-framework aluminum species on the activity, selectivity, and stability of Y zeolites in n-heptane cracking,* Journal of Catalysis, 1991. **130**(2): p. 471-482.

Chapter 6

n–Heptane Cracking Over Selected Powder and Structured Zeolite Catalysts

6.1 Introduction

Cracking refers to the breaking up of large hydrocarbons molecules into smaller and more useful molecules. This can be achieved either by applying high temperatures and pressure in thermal cracking processes, or by presence of a catalyst under lower temperatures and pressure in catalytic cracking processes [1]. Hence the thermal cracking of naphtha is a highly energy–consuming process (reaction temperature over 800°C) with light olefins (usually ethene, propene, and butenes) as the main product. Much research has been carried out on the hydrocarbon cracking to achieve a higher yield of light olefins through catalytic cracking [2-4]. Various catalysts (such as alumina, clay, and zeolites) have been studied to obtain light olefins under moderate conditions [5]. Despite the fact that ethene and propene were the main products in thermal cracking, the control of the

selectivity is problematic compared to the relative high selectivity in the catalytic cracking process [6].

Catalytic cracking has been known since 1915 when Speight [7] found that aluminium chloride could break long hydrocarbons molecules in heavy crude oil. Since then, catalytic cracking has become a vital reaction in the petroleum field. Catalytic cracking of the n–alkanes (i.e. n–pentane, n–hexane, n–heptane) has been used to study systematically the performance of catalysts and to elucidate reaction mechanisms [8-22].

Catalytic cracking involves the formation of carbenium and carbonium ions (carbocations) over the Brønsted and Lewis acid sites of zeolite by C-C bond rupturing. A series of reactions involved in the cracking of a hydrocarbon chain include isomerisation, ring formation, dehydrogenation and oligomerisation which result in very different product streams dependents on the zeolite catalyst used.

6.2 Alkanes cracking mechanism

Since 1973, it is generally accepted that the catalytic cracking of alkanes occurred predominantly on Brønsted acid sites by carbenium ion–type mechanism [14, 23]. Reducing the aluminium species in the framework enhanced of strong acid generation of the Brønsted sites, which influenced the catalytic cracking process activity [24, 25]. However, researchers have speculated that the strong Lewis acid sites also influence the catalyst cracking activity and deactivation [26]. More recently, it has been suggested that both the Brønsted acid sites and Lewis acid sites have enhanced the catalytic cracking activity and affect selectivity [27].

There are two proposed mechanisms a bimolecular or a monomolecular mechanism [14, 28]. Firstly, bimolecular mechanism [29] which is known as a classical chain process involving hydride transfer between two hydrocarbon molecules without direct interaction of the n–alkanes molecules as shown below:

$$RH + R_1^+ \rightarrow R^+ + R_1H$$
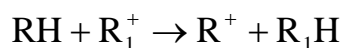
Where, the RH is n–alkanes (the reactant) and the R_1^+ is the carbenium ion (which is coordinated to the surface oxide ions) [30]. Following reaction short olefins produced by cleavage on the C–C bonds in β–scission reaction. In the β–scission reaction the C–C bonds tended to break in the middle of the hydrocarbons chain due to activation energies ($n-C_6H_{13}^+$ is shown below).
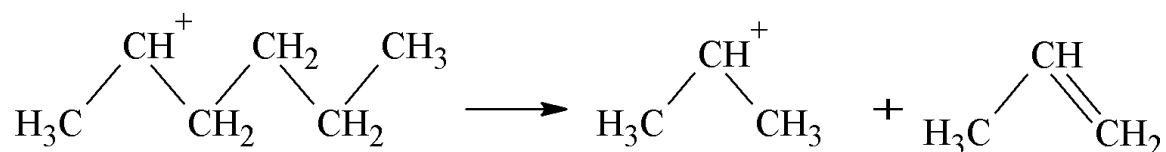
Hydride abstraction is a key intermolecular hydride transfer reaction. The hydride ion was abstracted from the RH (alkane molecules) to the start of the reaction by surface bound carbenium ion (R_1^+) followed by producing R_1H and smaller carbenium ion (a positive charge tricoordinated carbon atom, R_1^+). Then carbenium ion (R_1^+) is broken to produce the olefins and R_1^+. Since the carbenium is unstable, it can rearrange to generate a branched carbenium or can rearrange without increasing the branching of the chain through the shift of the hydride to form secondary and tertiary carbenium ion
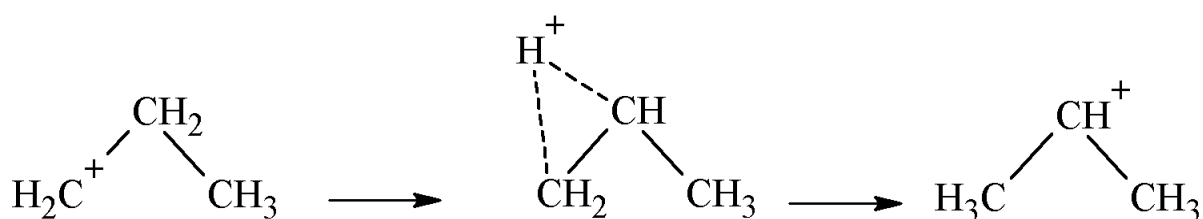
The formation of methane and ethane through β–scission reaction is very slow and not favoured due to the easier charge transfer from the secondary carbenium ion to the tertiary C–H bond [31]. Hence the activation energy for tertiary carbenium ions is 40 - 60 kJ mol^{-1}, while the formation of a secondary carbenium ion by H abstraction from the paraffin has activation energy of 70 - 105 kJ mol^{-1} [32, 33].

Nevertheless, the carbenium ion could be collapsed producing methane and ethane by the protonated alkanes [23, 32, 33]. The mainly product produce from the catalytic cracking reaction following this bimolecular mechanism is alkanes and olefins.

The rate determining step of the catalytic cracking mechanism is the hydride transfer step. Nevertheless, the impurity olefins in the feed or the thermal cracking reaction at high temperature might be generating the carbenium ion [31].

The second mechanism known as monomolecular cracking was established by Haag–Dessau in 1984 [34]. Monomolecular cracking mechanism involved the alkane protonation to form a carbonium ion (a positively charged pentacoordinaated, RH_2^+) with high–energy state.

$$RH + H^+ \rightarrow RH_2^+$$
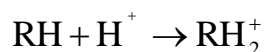
Three reactions were proposed for the carbonium ion which was adsorbed on the zeolite surface. The first and fastest reaction is hydrogen exchange by returning a proton to the zeolite surface. The second reaction is cracking the carbonium ion (RH_2^+) to produce alkane and a smaller carbenium ion by α–cracking reaction. If the carbenium ion released in α–cracking reaction desorbed from the zeolite surface with no further reaction, then the paraffin to olefins ratio should be unity. Finally, the carbonium ion (RH_2^+) donated a proton to catalyst and formed olefin and carbenium ion by dehydrogenation reaction with this reaction being the slowest reaction of three reactions.

$$RH_2^+ \rightarrow RH + H^+ \qquad \textit{(Dehydrogenation exchange)}$$

$$RH_2^+ \rightarrow R_1H + R_2^+ \qquad \textit{(α − cracking)}$$

$$RH_2^+ \rightarrow H_2 + R^+ \qquad \textit{(Dehydrogenation reaction)}$$
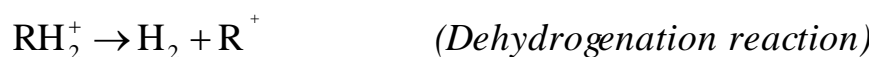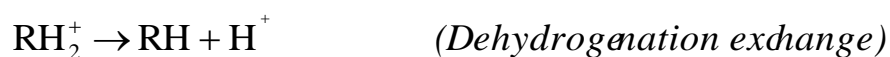
In general, the carbenium and carbonium (carbocations) are formed on Brønsted and Lewis acid sites of a zeolite by the cleavage of a C-C bond. The mechanism of carbenium formation involves three main steps as described by Bartholomew [35]. The first step is initiation step which started by protonation or H-abstraction on the Brønsted and Lewis acid sites of zeolite.

$$R_1 - CH = \underset{Olefins}{CH - R_2} + \underset{Br\o nsted\ site}{HZ} \xleftrightarrow{\text{Protonation}} R_1 - CH_2 - \underset{Carbenium\ ion}{CH^+ - R_2} + Z^-$$

$$R_1 - CH_2 - \underset{AlKane}{CH_2 - R_2} + \underset{Lewis\ site}{L} \xleftrightarrow{\text{H abstraction}} R_1 - CH_2 - \underset{Carbenium\ ion}{CH^+ - R_2} + HL$$
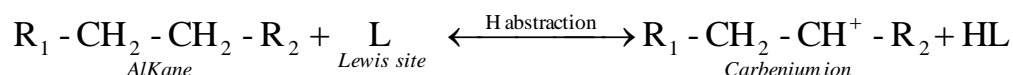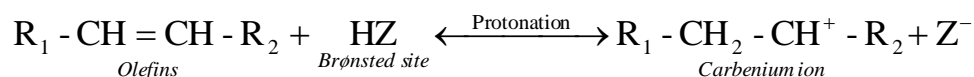
This is followed by β–scission by hydride transfer in the propagation step

Hydride transfer

$$R_1 - CH_2 - \underset{Carbenium\ ion}{CH^+ - R_2} + R_3 - CH_2 - \underset{Alkane}{CH_2 - R_4} \xleftrightarrow{\text{H transfer}} R_1 - CH_2 - \underset{Alkane}{CH_2 - R_2} + R_2 - CH_2 - \underset{Carbenium\ ion}{CH^+ - R_4}$$

β – scission

$$R_3 - CH_2 - \underset{Carbenium\ ion}{CH^+ - R_4} \xleftrightarrow{\text{H transfer}} \underset{Carbenium\ ion}{R_3^+} + \underset{Olefins}{CH_2 = CH - R_4}$$
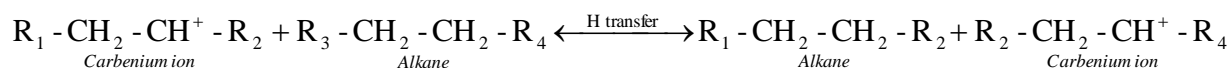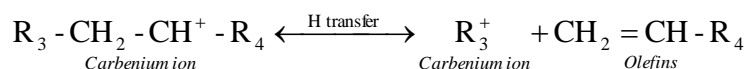
The termination step occurs by reaction of the carbenium ion either with a Brønsted base to form olefins reforming the Brønsted acid site or with a Lewis base to form an alkane and reforming Lewis acid site or by forming an alkane by a hydride ion extraction from coke.

Termination to an olefin

$$R_3^' - CH_2 - CH^+ - CH_3 \longleftrightarrow R_3^' - CH_2 = CH - CH_3 + H^+$$
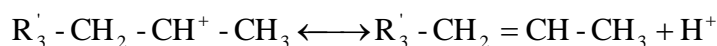
Side reaction such as; skeletal and/or cis–isomerisation, aromatics alkylation, dealkylation, branching, cyclisaion, and oligomerisation might occur beside the main reaction cracking mention before.

6.3 n–Heptane cracking reactions

In this thesis, the catalytic cracking of n–heptane has been studied on the structured and powdered form of both ZSM-5 and Y zeolite as a test reaction for naphtha cracking to evaluate the catalyst performance. Based on the previous section, the carbenium ion is the key to start cracking reaction and it can form by abstraction of a hydride ion from the alkane which has less reactivity to form a carbenium ion compared to olefin under the same operation conditions. Below is simplified reaction path for cracking n–heptane over zeolite.

Carbonium ion initiation

$$CH_3 - CH_2 - CH_2 - CH_2 - CH_2 - CH_2 - CH_3 \xrightarrow{\ H^+\ } CH_3 - CH_3^+ - CH_2 - CH_2 - CH_2 - CH_2 - CH_3$$
$$\text{n-heptane} \qquad\qquad\qquad\qquad \text{transition}$$

$$CH_3 - CH_3^+ - CH_2 - CH_2 - CH_2 - CH_2 - CH_3 \xrightarrow{\ -H_2\ } CH_3 - CH_2 - CH^+ - CH_2 - CH_2 - CH_2 - CH_3$$
$$\text{transition} \qquad\qquad\qquad\qquad \text{Carbenium ion}$$

β - scission

$$CH_3 - CH_2 - CH^+ - CH_2 - CH_2 - CH_2 - CH_3 \longrightarrow CH_3 - CH = CH_2 + CH_2^+ - CH_2 - CH_2 - CH_3$$
$$\text{Carbenium ion} \qquad\qquad\qquad\qquad \text{Olefin} \qquad\qquad \text{Carbenium ion}$$

Hydride transfer

$$CH_3 - CH = CH_2 + CH_2^+ - CH_2 - CH_2 - CH_3 \xrightarrow{\ -H\ } CH_3 - CH = CH^+ + CH_3 - CH_2 - CH_2 - CH_3$$
$$\text{Olefins} \qquad\qquad \text{Carbenium ion} \qquad\qquad\qquad\qquad \text{alkane}$$

$$CH_3 - CH = CH^+ \longrightarrow coke\ aromatics$$
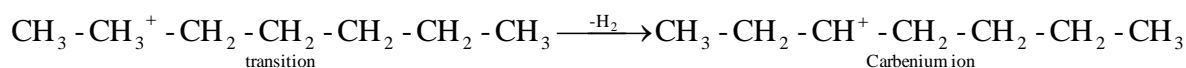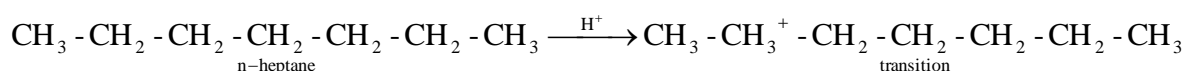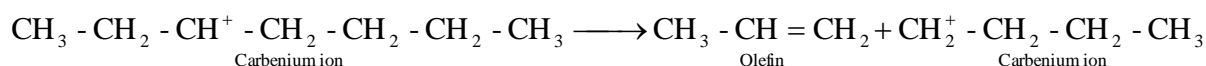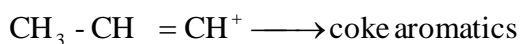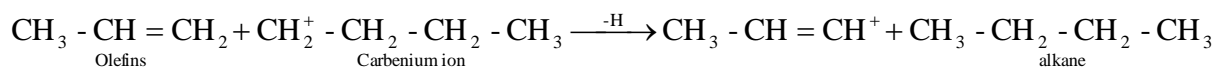
In hydride transfer, olefins convert to carbenium intermediate species on the acid catalysts at high conversion levels to form alkanes and hydrogen-deficient species [36], would be further convert to aromatic hydrocarbon and coke in dehydrogenation and cyclisation [37].

6.4 Kinetic modelling of alkane cracking (Pseudo–first order reaction)

A pseudo–first order kinetic equation has been accepted to describe the cracking [38-40].

$$R = k.C_A = -\frac{dC_A}{dt} \qquad \textbf{Equation 6-1}$$

Where, R = Rate of the reaction [mol cm^{-3} min^{-1}]

k = Rate constant [min^{-1}]

t = Reaction time [min]

C_A= Concentration of the reactant [mol cm^{-3}]

By integrating the **Equation 6-1** gives**:**

$$-\int_{C_{A^0}}^{C_A} \frac{dC_A}{C_A} = k\int_0^t dt$$

Where, at t = 0 the initial concentration of reactant A, So $C_A = C_A^o$ and t = t the $C_A = C_A$

$$\ln C_A = -kt + \ln C_{A^0} \qquad \textbf{Equation 6-2}$$

By rearrange the **Equation 6-2**

$$\ln \frac{C_A}{C_{A^o}} = -kt \qquad \textbf{Equation 6-3}$$

Therefore, $$C_A = C_{A^o}.e^{-kt} \qquad \textbf{Equation 6-4}$$

The concentration of reactant at any time through the cracking reaction can be described in term of fractional conversion of reaction (X_A), as following:

$$X_A = (C_{A^o} - C_A)/C_{A^o} \Rightarrow C_A/C_{A^o} = (1 - X_A) \qquad \textbf{Equation 6-5}$$

Rewrite **Equation 6-4** using **Equation 6-5:**

$$(1 - X_A) = e^{-kt}$$ **Equation 6-6**

By taking logarithm, **Equation 6-6** can be written also in the following form:

$$\ln (1 - X_A) = -k.t$$ **Equation 6-7**

Equation 6-7 can be rewritten substituting in for contact time.

$$-\ln (1 - X_A) = k'(W/F)$$ **Equation 6-8**

Where, W/F = Contact time of the reactant with catalyst [g h mol^{-1}]

$\quad$ F = Molar flow rate of reactant (n-heptanes) [mol h^{-1}]

$\quad$ W = Weight of the catalyst [g].

$\quad$ k' = Rate constant, calculated from the slope of plotting the contact time against($-\ln (1-X_A)$).

The apparent activation energy of the catalytic cracking reaction can be calculated using Arrhenius law (**Equation 6-9**), if the rate constant for different reaction temperature were determined [41, 42].

$$k = A.e^{-E_{app}/RT}$$ **Equation 6-9**

$$\ln k = -E_{app}/RT + \ln A$$ **Equation 6-10**

Where, k = Rate constant (reaction rate coefficient)

$\quad$ E_{app} = Apparent activation energy [kJ mol^{-1}]

$\quad$ T = Reaction temperature [K]

$\quad$ R = Molar gas constant [8.314 × 10^{-3} kJ mol^{-1} K^{-1}].

$\quad$ A = Frequency factor, which gives indication of the total number of collisions between reactants having the correct orientation to lead to products.

6.5 Determination of coke on used zeolite catalysts

Deactivation of the zeolite occurred due to coke deposited during the n–heptane cracking. Coke is a mixture of heavy side–products and can be produced either condensation or rearranging of carbonaceous matter in cracking reaction at low temperature ($>200^oC$) forming non–polyaromatic (light coke), or during hydrogen transfer steps on the zeolite acid sites at high temperature ($\square350^oC$) and plus the carbonaceous matter from the light coke formation [43, 44].

The amount of coke deposited on the structured and pelleted ZSM-5 and Y zeolite catalysts was calculated by monitoring the weight loss through coke burning using the thermogravimetric analysis (TGA).

The weight loss of coke of the selected coked catalyst (10 mg) were performed by rising the temperature at 10 ^oC min^{-1} to 600^oC under 50 ml min^{-1} nitrogen flow and held for 60 min to remove all the water and volatile components. Then temperature dropped by 10 ^oC min^{-1} to 200^oC and held for 30 min. Finally the gas was switched to air and temperature was raised again to 600^oC and maintained the isothermal condition at this temperature for 30 min to burn off the hard coke that covered the catalysts [43].

6.6 Catalyst packing

The selected structured and pelleted ZSM-5 and Y zeolite were packed into a 4 mm i.d. quartz micro-reactor and 10 mm i.d quartz micro-reactor. The bundles of 20 ZSM–5 or USY structured catalyst 25 mm length $\times$ 0.5 mm wires were loaded into the reactor with a zeolite equivalent weight for 0.05 g of ZSM–5 and 0.03 g Y zeolite for the 4 mm i.d. quartz micro-reactor and 0.1 g ZSM–5 and 0.05 g for 10 mm i.d quartz micro-reactor .

All zeolite powders were pelleted using a press and sieves of specific dimensions. The powders were pressed and held at 5 tons cm^{-2} for 30 second and then crushed using a mortar and pestle followed by sieving to obtain particles in the range 425 to 500 µm.

The powdered zeolite was pelleted and sieved (425–500 μm pellets). The same catalyst weight and bed height (by adding inert quartz glass beads) were used for the comparison. The catalysts under test were sandwiched between two layers of quartz wool and the micro-reactor was located in stable zone of the furnace (Carbolite MTF 12/12A). A thermocouple was placed with undirected contact at top of the catalyst bed and another was placed in the stable furnace zone to monitor the reaction temperature and set point temperature.

6.6.1 Gas Chromatography (GC)

The analyses have been performed on the products from the catalytic testing using an on–line a Varian 3400 FID gas chromatograph fitted with a PLOT Al_2O_3/KCl capillary column (50 m × 0.32 mm i.d.) is connected. 99.99% purity helium gas is the mobile phase with split ratio 100/1. The injector temperature and the detector temperature was set at 250°C hydrogen/air ratio is 1/10.

Gas chromatography (GC) analysis involves the separation of a mixture of volatile organic compounds. It can also be used in some cases to prepare pure compounds from a mixture [45].

In the GC, a carrier gas is used as a mobile gas, usually an inert gas (N_2, H_2, He, and Ar) to prevent any interaction between the carrier gas and analytes. The stationary phase is a microscopic layer of liquid and polymer support on an inert solid inside a glass tube. The sample is passed with the inert gas (mobile phase) through the column where the sample has differing degrees of interaction with the surface of the stationary phase and is transported through the column with different retention time from the solvent. Samples with low affinity to the stationary phase are eluted earlier than those with a strong adsorption on the stationary phase which is retained for a longer time. An amplifier is connected to the detector to magnify the signal collected at the detector at the end of the column and produce the chromatogram

There are different types of detectors. The most common types are the thermal conductivity detector (TCD) and the flame ionisation detector (FID), the latter of which is the one used for this research.

The FID is usually used with a capillary column and separated. Hydrocarbon sample are combusted in a hydrogen and air producing ions. The ions produced are accompanied with the released electrons. The free electrons are then collected by the detector producing a current which is proportional to the electrons. The amplified signal is then recorded. The GC–trace is represented by a series of peaks corresponding to the compound present and related to time.

6.7 Construction and commissioning of the reaction

The reaction system was constructed and commissioned to evaluate the catalysts performance (**Figure 6-1**). The gas flow rate was controlled by using mass flow controllers, MFC, (Brooks, 5850 TR) with the control unit and readout device (Brooks, 0154). In addition, the flow rates were determined with and without n–heptane. The flow rate of the gases were in entire system were calibrated using timer and bubbler flow meter.

The n–heptane (99.99 wt% Sigma-Aldrich) was added to the nitrogen feed by the use of a saturator consisted. This saturator consisted of three bubblers half filled with n–heptane and by flowing nitrogen through the bubblers connected in series, n–heptane was added to the feed. The bubblers were placed in ice bath.

The catalysts were activated prior to the cracking by heating from $25^{o}C$ to $550^{o}C$ in air (1 ^{o}C min^{-1}, 25 ml min^{-1}) and held isothermally at $550^{o}C$ for 16 hours. The behaviour of the structured and pelleted catalysts was studied using n–heptane cracking in a 4 mm i.d. quartz micro-reactor.
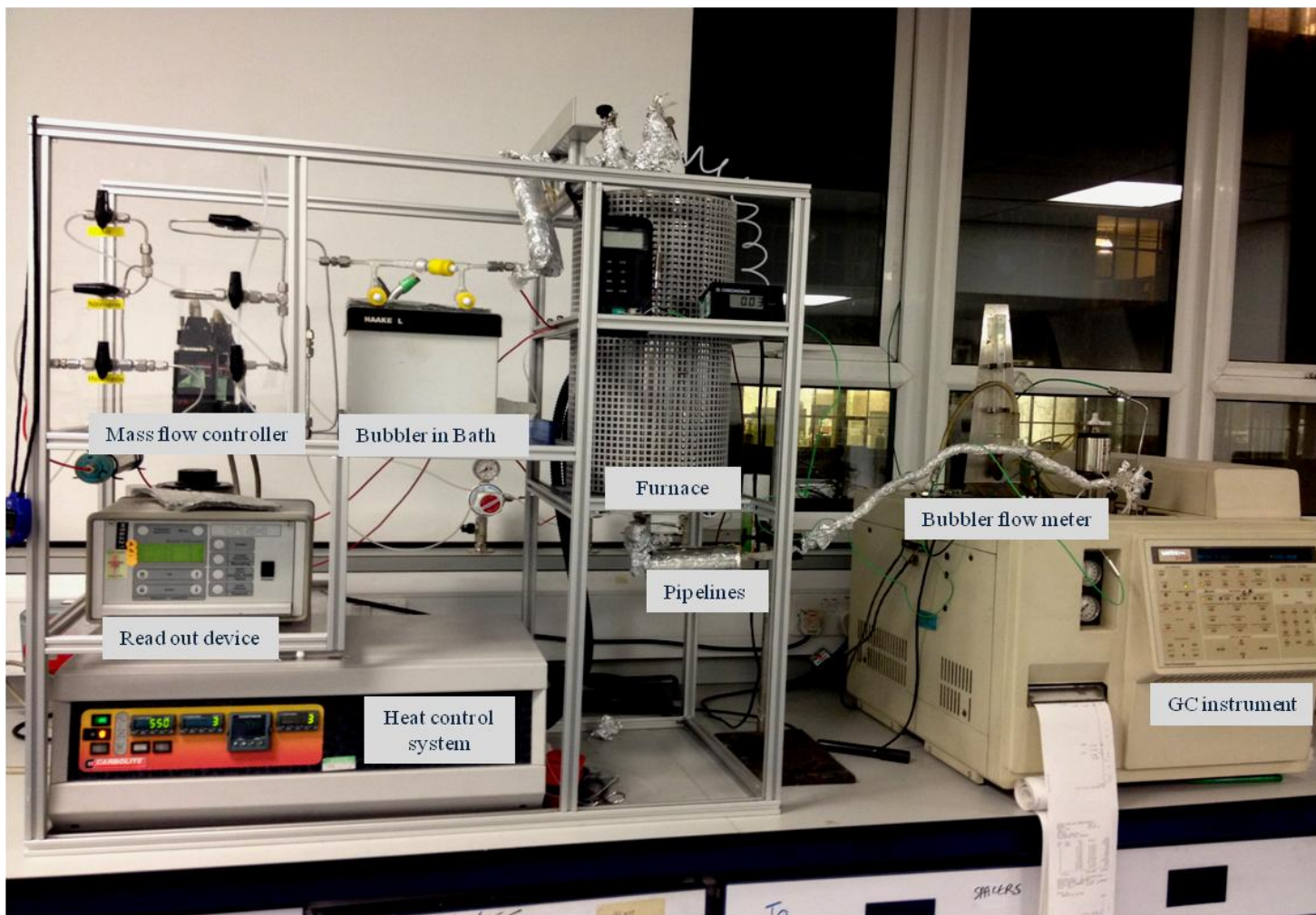
Figure 6-1: Catalytic fixed bed reactor system with online analysis.

All the stainless steel pipes connected between the reactor and the GC were lagged with heating wire (Electrothermal PLC, UK) and maintained at approximately 110°C to avoid any condensation of the reactant and products. The GC was connected to the reactor and samples analysed at regular intervals between 5 and 125 min. The GC was calibrated prior each test using 1% mole of methane, ethane, propane, iso-butane, iso-pentane, pentane in nitrogen (Linde Gas). In addition, liquid injections n-hexane, n-heptane, n-octane, toluene, and p-xylene were carried out and combined with the gas standard the response factor for FID of the GC were determined for hydrocarbons, as shown in **Appendix B**.

Following the catalysts activation, the catalysts were tested for stability or signs of deactivation by passing n-heptane vapour in nitrogen gas (3%, **Appendix C**) was pass into the catalyst bed at 450°C and W/F = 42 g h mol^{-1} (which is equivalent to 16.7 ml min^{-1} and 10 ml min^{-1} for the ZSM-5 and Y zeolite respectively). The product was sampled with time at 3, 25, 50, 75, 100, and 125 min (TOS).

Following the deactivation test, the reaction temperature was lowered to 325°C with only nitrogen flowing through the catalyst bed. When the system reached the steady state the n-heptane was carried into the reactor by nitrogen at W/F= 50 g h mol^{-1} and the products was then collect after 5 min (to stabilise the flow).

This procedure was then repeated for different W/F 42 and 24 g h mol^{-1} respectively (for W/F calculation see **Appendix C**). When the tests were completed, the n-heptane flow was turn off and temperature raise to 375°C and the previous steps were repeated. This was repeated at 450°C.

6.8 n–Heptane cracking over structured/pelleted ZSM-5 catalysts

6.8.1 n–Heptane cracking activity

The n–heptane cracking was first carried out on pelleted ZSM-5 zeolite in the 4 mm quartz micro-reactor at 450°C and 42 g h mol^{-1} and then the structured catalyst (ZSM-5 bundle) was tested under same condition for comparison. Further testing was achieved by scaling up the reactor to 10 mm i.d. quartz reactor. The n-heptane cracking conversion and product selectivity were calculated as follows:

$$Conversion(X\%) = \frac{nC_7^{feed} - nC_7^{unconverted}}{nC_7^{feed}} x100$$

Equation 6-11

$$Selectivity(S\%) = \frac{Product}{nC_7^{feed} - nC_7^{unconverted}} x100$$

Equation 6-12

The conversion of the n–heptane remained constant with time for both catalysts and in both 4 mm i.d and 10 mm i.d. quartz reactors. As expected ZSM-5 catalysts deactivated very little as shown in **Table 6-1** and **Figure 6-2**. The medium sized pores of the ZSM-5 inhibit coke forming by restricting secondary reactions that lead to intermediates products. Despite the increase in conversion with increasing catalyst amount from 0.05 g to 0.1 g, higher conversion was observed for pelleted catalyst compared to structured ZSM-5 catalysts. This is most likely explained by imperfect packing of narrower 4 mm quartz reactor with the bundle of 0.5 mm wires. Since the pelleted catalysts particles are typically (d/D) > (1/5-1/10); the layer wires and the difficulty in packing mean that (d/D) < (1/5-1/10) and hence channelling of n–heptane may occur, leading to lower the conversion. The layer wires showed a measurements of $>\times2$ for both catalysts; and reduced the conversion difference. However, the bindles of wires are still relatively loosely packed and hence lower conversion would be expected.

Figure 6-2 shows the data of catalysts stability for pelleted and structured in 4 mm reactor and in 10 mm reactor respectively with time, the selectivities of the different carbon fractions with time at 450°C remained constant over time (**Figure**

6-3–Figure 6-7). The C_3 fraction was the predominant fraction in all the catalysts followed by the C_4 and C_2 fractions respectively and no aromatics were observed (**Table 6-1**).

There were significant amounts of C_1 and C_2 when using the structured catalyst as well as iC_7 and nC_7, which suggests some additional catalyst sites available due to the metal support. The amount of C_1 and C_2 yield decreased when the better packed tube was used.

Comparison of the iC_4/nC_4 ratios an indication of primary and secondary reaction, **Table 6-1** shows that the structured 4 mm reactor has much less over reaction when using the smaller tube and the total olefins produced is the highest also.

The iC_4/nC_4 ratios are much closes in the 10 mm reactor and suggest a better comparison can be made and similarly the total olefins/alkanes ($\sum C_i^=/C_j$) are comparable.

Figure 6-3 shows that the product selectivities are very similar and those differences are probably accounted for by the poor packing in the case of the reactor containing the structured catalyst.

The selectivity to propene showed almost constant value just between 25 - 30% for all the tested catalysts and that agreed with result listed by Komatsu [8]. The limited pore diameter of ZSM-5 catalysts for n–heptane cracking where the C–H bond break to form n–heptene and hydrogen and that led to form olefins while in the protonation reaction light alkanes formed such as; methane and hexane, ethane and pentene and so forth [46]. The cracking rate of the product alkanes is lower than that of the n–heptane hence the bond energy of C–H decreased with increasing the carbon number of hydrocarbon, and the rate of protonation reaction increased with carbon number. Thus, it is most likely to form C_3–C_7 carbenium ion rather than C_2 carbenium ion in the protonation reaction. These olefins were converted β-scission cracking reaction, and secondary reaction (oligomerization and isomerisation) to form ethene, propene, and butenes.

Table 6-1: Catalytic performance for ZSM-5 structured and pelleted catalyst in 4 and 10 mm micro-reactor at 450°C and 42 g h mol^{-1} after 125 min of deactivation n–heptane cracking (moles/100 moles converted) .

	pelleted,10 mm	structured,10 mm	pelleted,4mm	structured,4 mm
C_1	1.0	1.4	1.0	2.5
C_2	5.6	7.0	4.0	9.2
$C_2^=$	7.8	7.4	6.8	7.3
C_3	15.0	16.9	24.5	11.7
$C_3^=$	30.3	25.4	29.3	25.0
iC_4	5.4	3.2	2.4	0.4
nC_4	10.6	9.0	10.2	8.7
$C_4^=$	15.9	17.4	14.7	19.6
iC_5	0.9	0.6	0.3	0.3
nC_5	1.7	2.1	0.8	1.7
$C_5^=$	5.6	6.6	5.8	6.5
iC_6	0.0	0.0	0.0	0.0
nC_6	0.0	0.0	0.0	0.0
$C_6^=$	0.0	0.0	0.0	0.0
iC_7	0.2	1.7	1.3	3.3
$C_7^=$	0.0	2.0	0.2	4.1
C_6H_6	0.0	0.0	0.0	0.0
Total	100.0	100.7	101.3	100.5
X%	74.0	43.6	35.0	19.4
iC_4/nC_4	0.51	0.36	0.24	0.05
$\sum C_i^=/C_j$	1.50	1.40	1.30	1.70
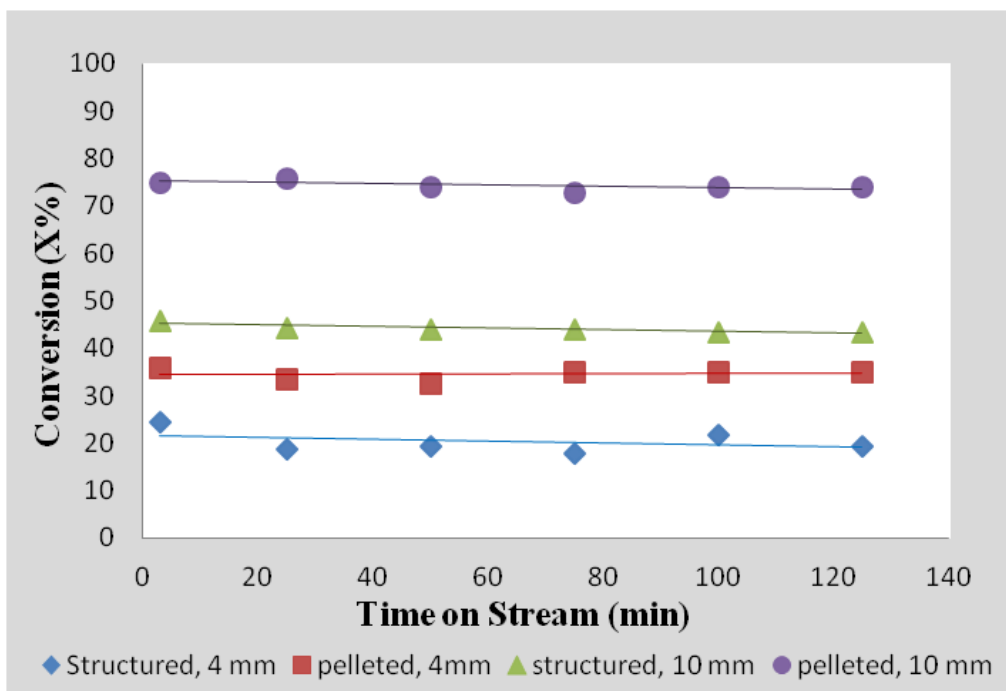
Figure 6-2: n-Heptane conversion with time for pelleted and structured ZSM-5 catalysts at 450°C and 42 g h mol^{-1} (in 4 and 10 mm micro-reactors).
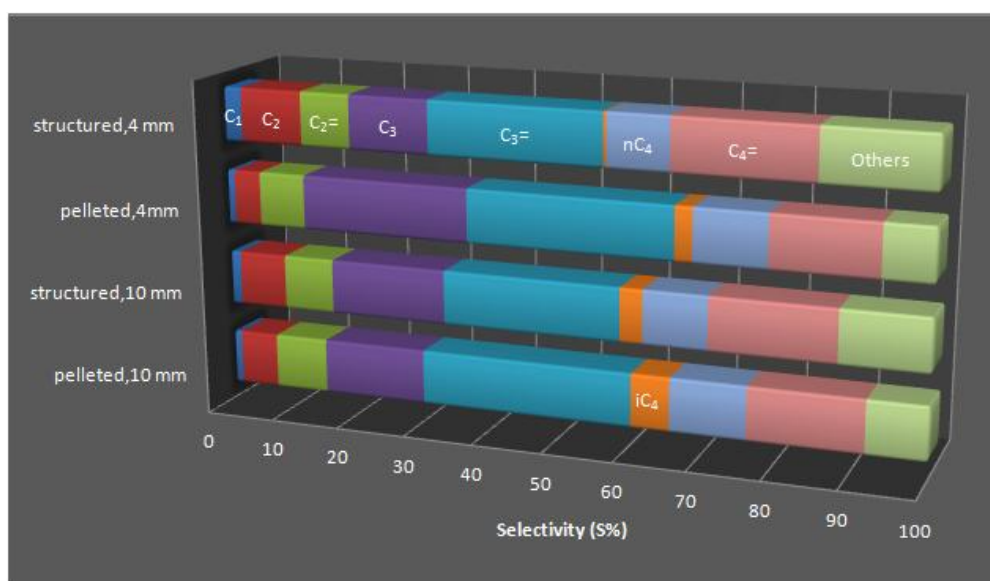
Figure 6-3: Product selectivity for ZSM-5 structured and pelleted catalyst in both 4 and 10 mm micro-reactor at 450°C and 42 g h mol^{-1}after 125 min on stream.
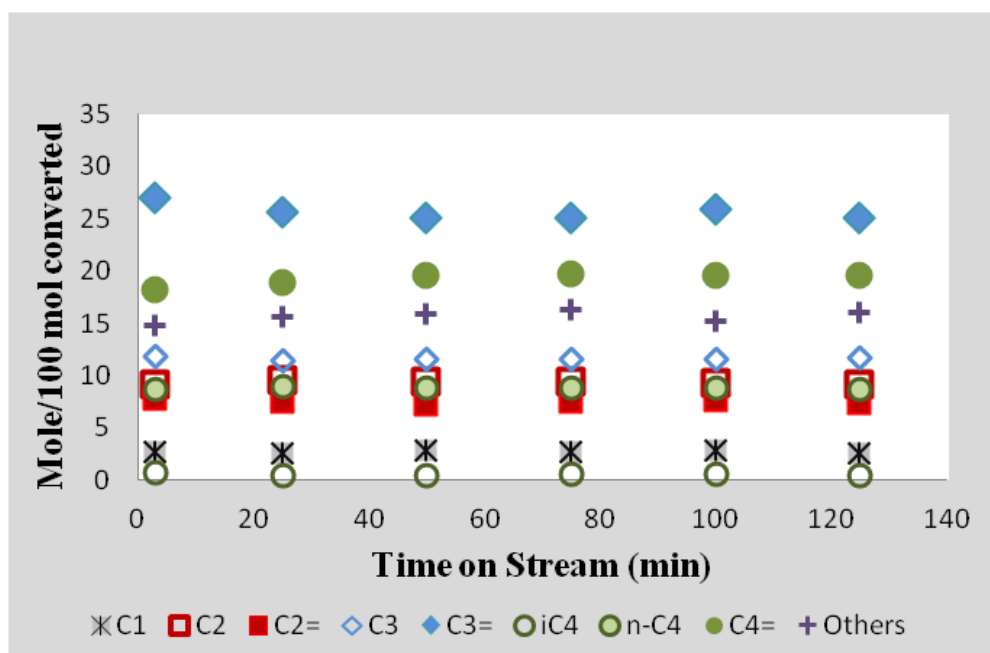
Figure 6-4: Light product selectivity for n-heptane cracking over structured ZSM-5 catalyst in 4 mm quartz micro-reactor at 450°C and 42 g h mol⁻¹versus time on stream.
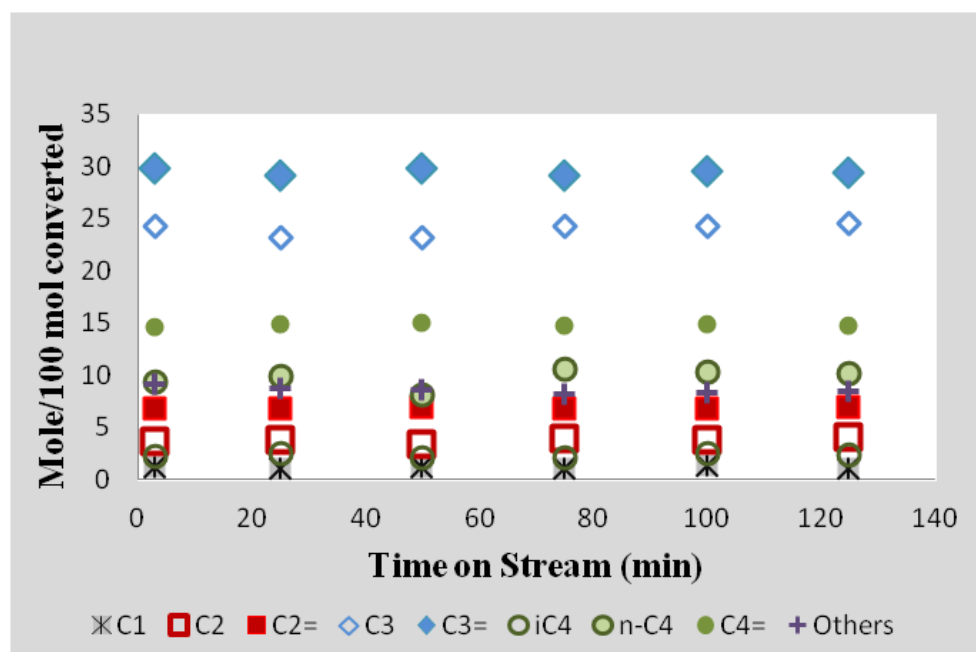
Figure 6-5: Light product selectivity for n-heptane cracking over pelleted ZSM-5 catalyst in 4 mm quartz micro-reactor at 450°C and 42 g h mol⁻¹versus time on stream.
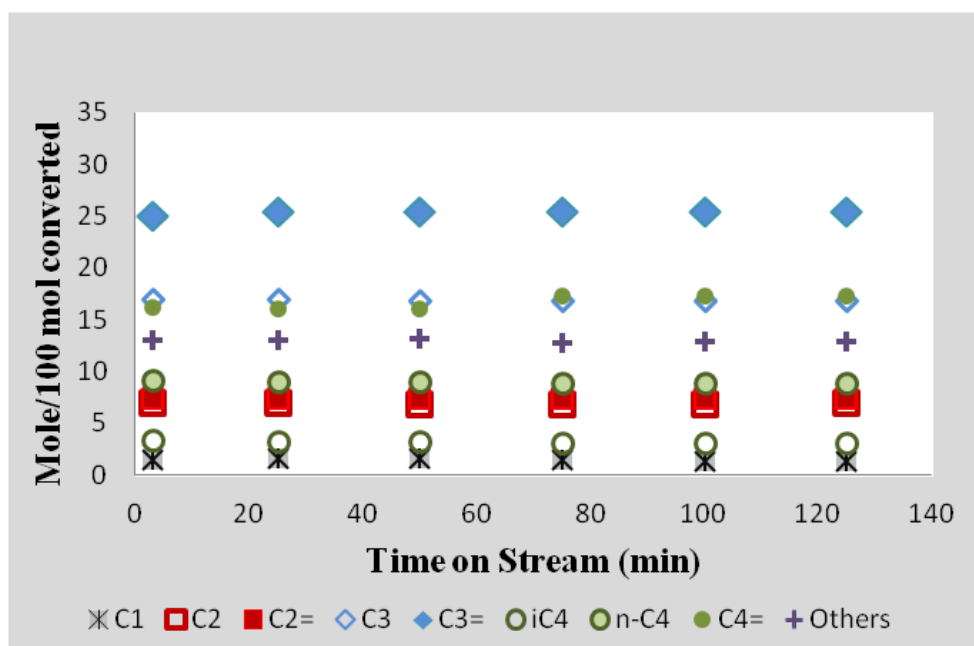
Figure 6-6: Light product selectivity for n-heptane cracking over structured ZSM-5 catalyst in 10 mm quartz micro-reactor at 450°C and 42 g h mol^{-1} versus time on stream.
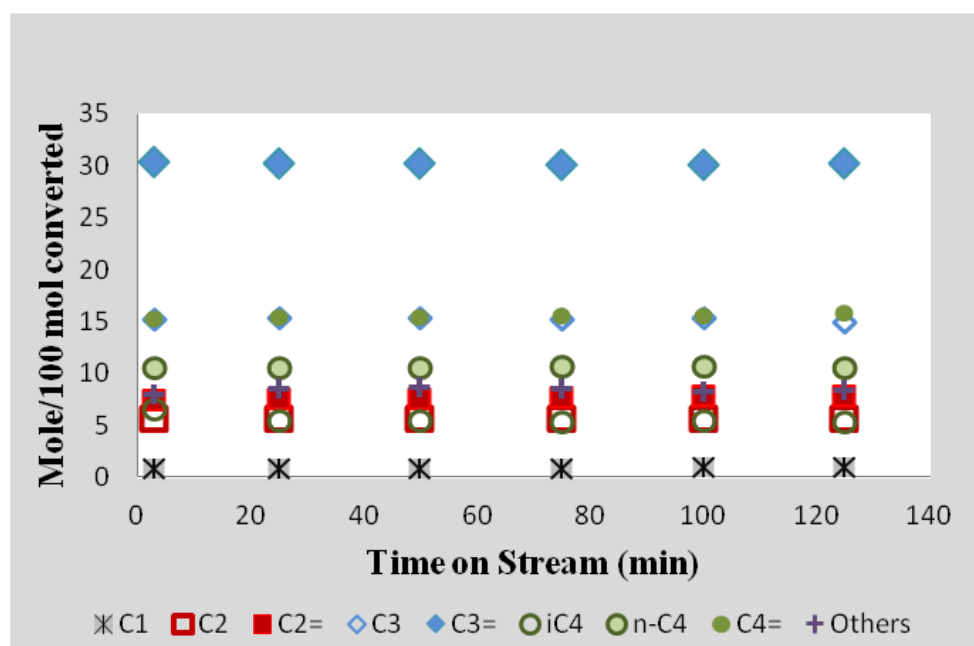
Figure 6-7: Light product selectivity for n-heptane cracking over pelleted ZSM-5 catalyst in 10 mm quartz micro-reactor at 450°C and 42 g h mol^{-1} versus time on stream.

6.8.2 Deactivation of structured/pelleted ZSM-5 zeolite

Figure 6-8 showed the TGA and DTG analysis of the structured and pelleted ZSM-5 in 4 mm and 10 mm quartz micro-reactor. There was two distinguished weight loss for all the selected catalysts during the experiment. First loss was observed through the heating under nitrogen flow which represented the H_2O and volatile materials, while the second represented the weight loss due to burning of remaining heavy deposited coke under air present.

The amount of the H_2O and volatile materials was calculated by the difference between the initial catalyst sample mass percent after heating under nitrogen to 600^oC and the sample mass percent before switching the flow to air. Whereas, the coke deposited was calculated by the difference of the sample mass percent after the heating with nitrogen and the mass percent at the end of the experiment. As expected the amount of coke formed increased with the n–heptane cracking conversion under same reaction temperature (**Table 6-2**).
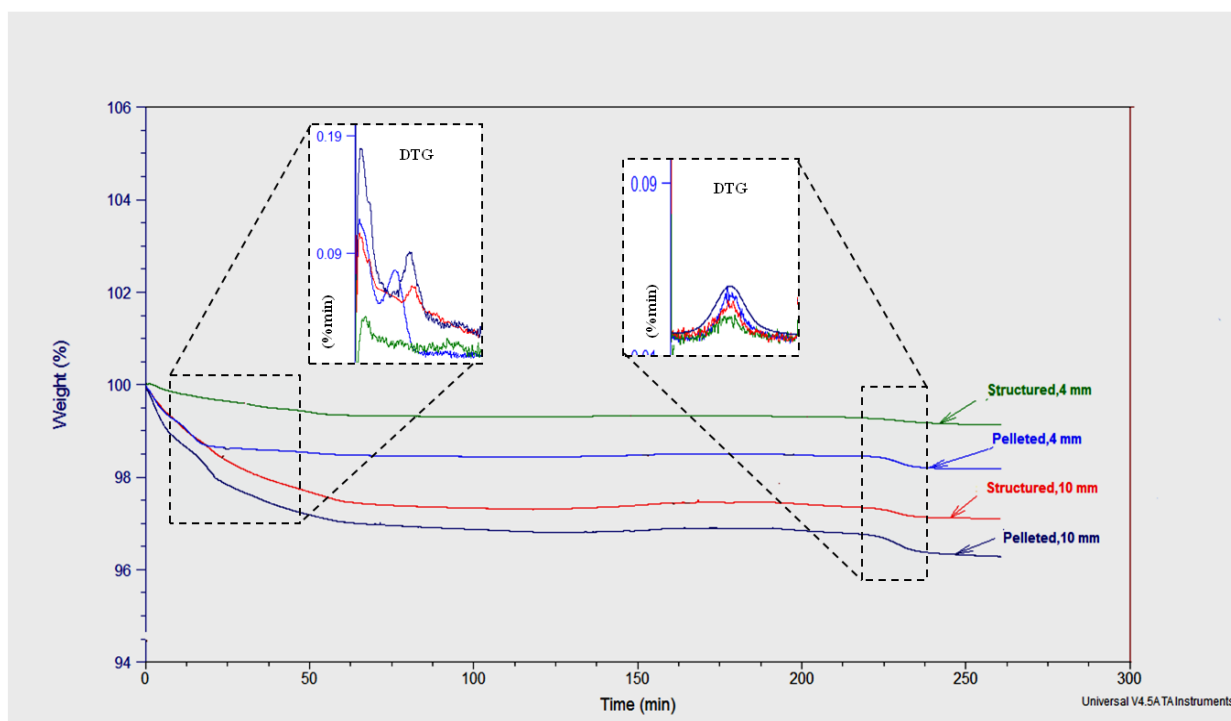
Figure 6-8: TGA analysis of the coke present on structured and pelleted ZSM-5 catalyst in 4 mm and 10 mm quartz micro-reactor.

Table 6-2: Coke formed on structured and pelleted ZSM-5 in both reactors (4 mm and 10 mm).

	pelleted,4 mm	structured, 4 mm	pelleted, 10 mm	structured, 10 mm
X (%)	35	19.4	74	43.6
Coke (%)	0.20	0.17	0.55	0.28

6.8.3 Determination of the kinetic parameters for n-heptane cracking over structured and pelleted ZSM-5 zeolite

After the initial deactivation studies, n–heptane cracking was carried out at different temperatures and flow rates to investigate the kinetic parameters. The results shown in **Figure 6-9** and **Figure 6-11** revealed that n–heptane cracking over both the structured and pelleted stabilised ZSM-5 catalysts in both the 4mm and 10 mm quartz micro-reactor followed the First order kinetic model (**Equation 6-8**).

Different contact times (24, 42, and 50 g h mol^{-1}) had been used by controlling the flow rates entering the fixed bed reactor (35, 20, and 16.7 ml min^{-1}, respectively). Three different temperatures (325, 375, and 450°C) were used with each contact time.

The rate constant for the all the selected catalysts increased with increasing temperature **Figure 6-12** and the pelleted catalysts had larger rate constants than the structured catalyst at each temperature attempted. Nevertheless, these results agreed with results obtained from the deactivation test at 450°C.

The apparent activation energies were estimated using the Arrhenius expression (**Equation 6-10)** as shown in **Figure 6-13** and are listed in **Table 6-3**. Overall, all catalyst showed E$_{app}$= 62.4 ± 2.0 kJ mol^{-1} which suggested surface reaction controlling mechanism and this in good agreement with the literature [47,48].
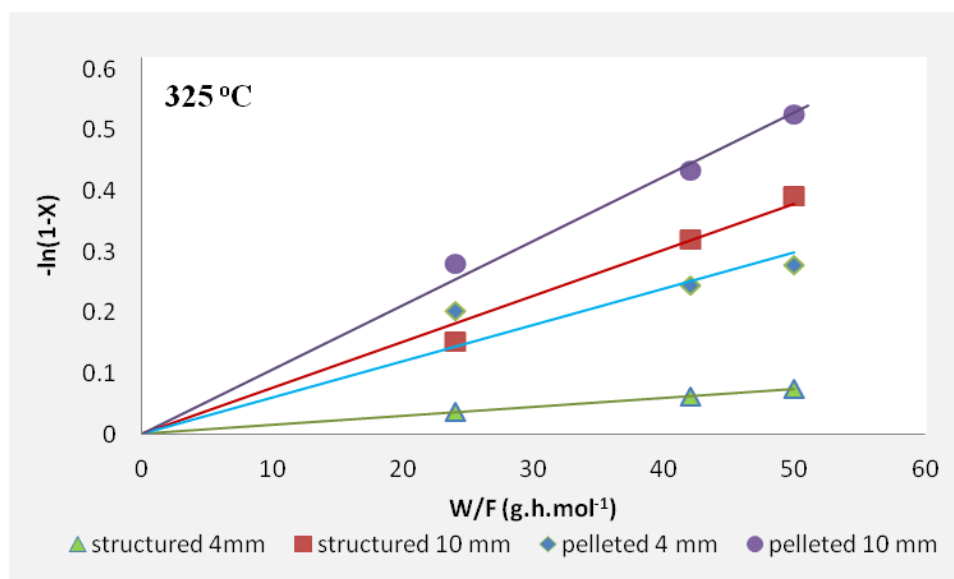
Figure 6-9: First order plot of n–heptane cracking over structured and pelleted ZSM-5 in 4 mm and 10 mm quartz micro-reactors at 325ºC.
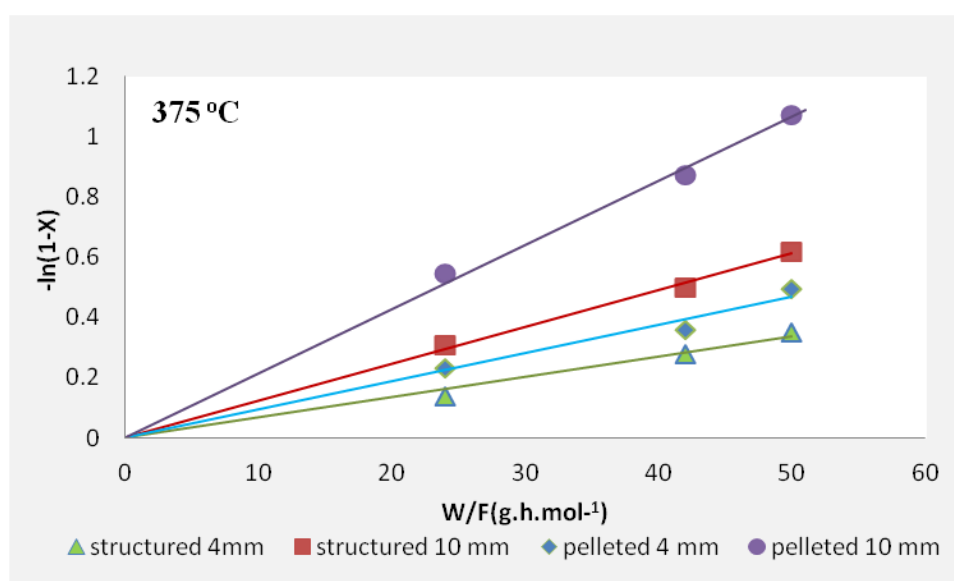
Figure 6-10: First order plot of n–heptane cracking over structured and pelleted ZSM-5 in 4 mm and 10 mm quartz micro-reactors at 375ºC.
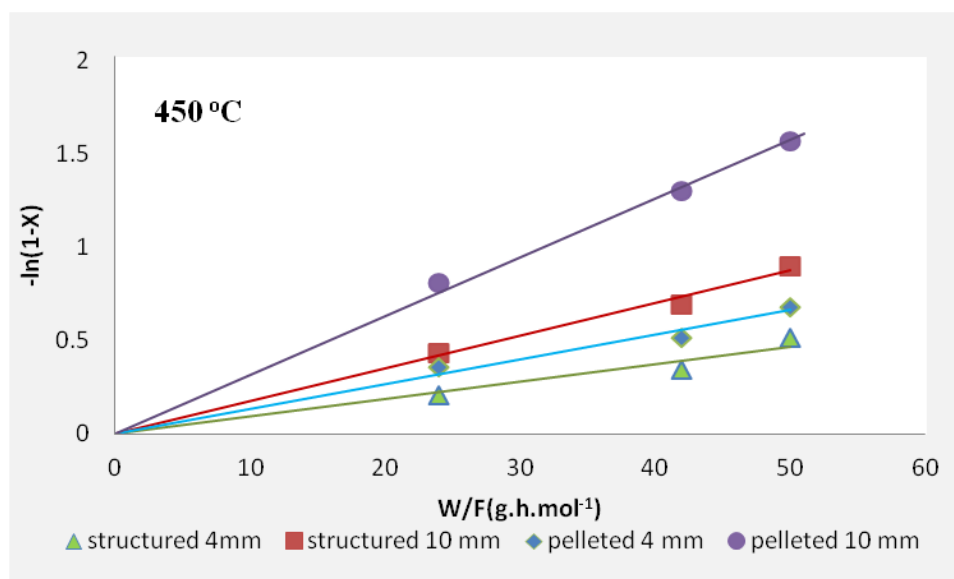
Figure 6-11: First order plot of n–heptane cracking over structured and pelleted ZSM-5 in 4 mm and 10 mm quartz micro-reactors at 450°C.
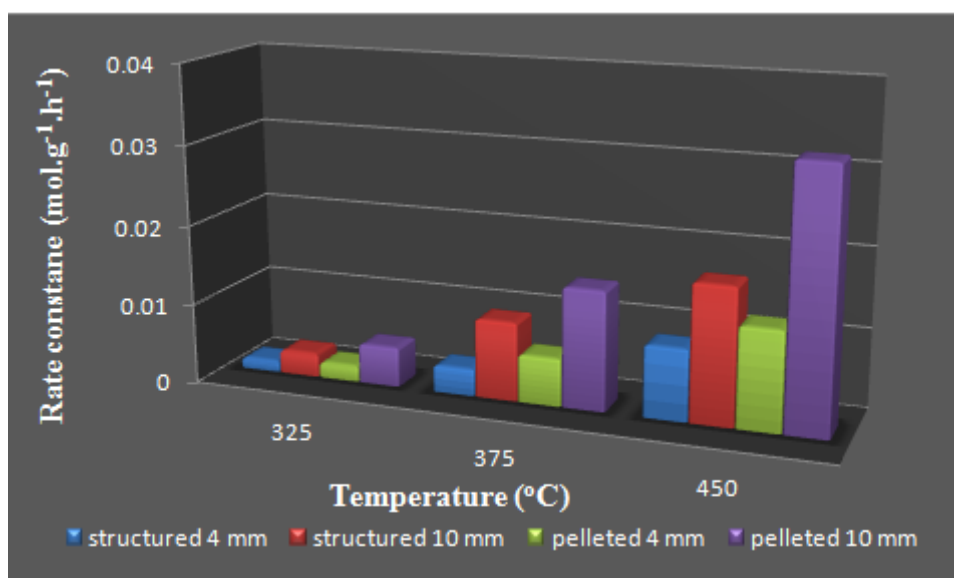
Figure 6-12: Rate constants for n–heptane cracking over structured and pelleted ZSM-5 in 4 mm and 10 mm quartz micro-reactors at different temperatures.
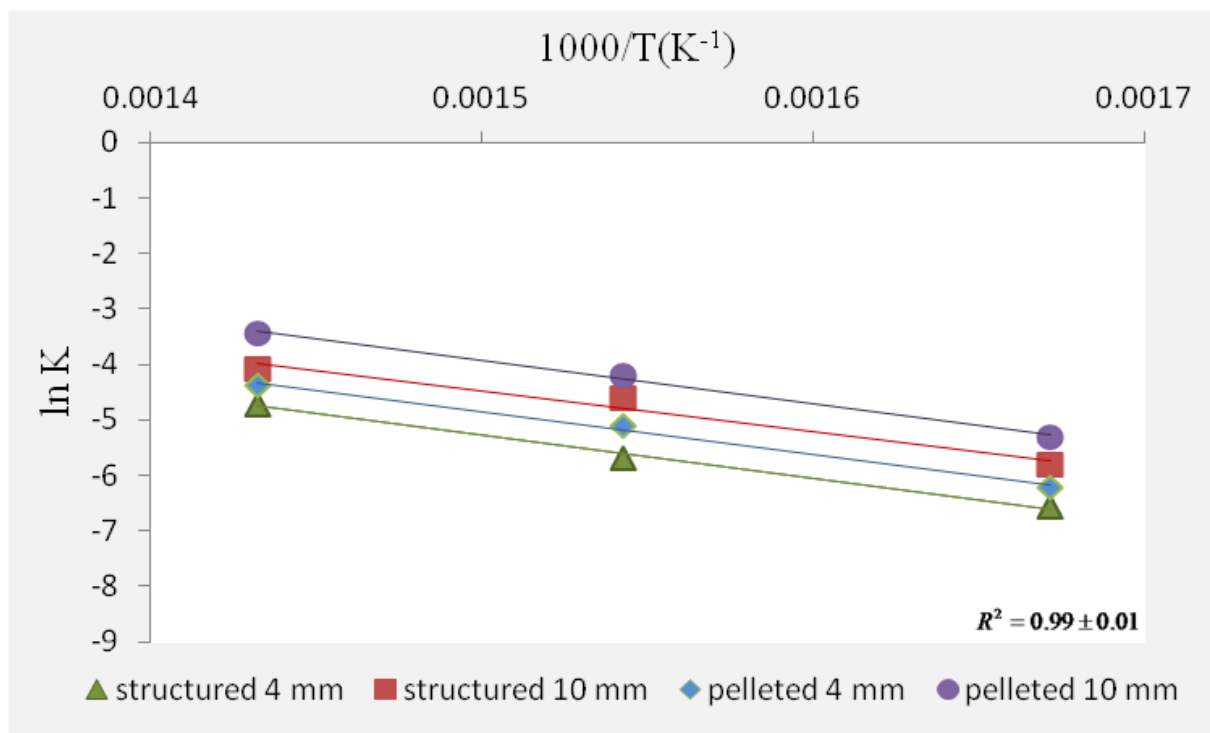
Figure 6-13: Arrhenius plot of n–heptane cracking over structured and pelleted ZSM-5 in 4 mm and 10 mm quartz micro-reactor at different temperatures.

Table 6-3: Summary of apparent activation energies for n–heptane cracking over structured and pelleted ZSM-5.

Selected catalysts	Structured 4 mm	structured 10 mm	pelleted 4 mm	Pelleted 10 mm
E_a(kJ mol^{-1})	60.5	61.0	63.6	64.3

6.9 n–Heptane cracking over structured/pelleted Y catalysts

6.9.1 n–Heptane cracking activity

The n–heptane was cracked over the pelleted Y zeolite in the 4 mm quartz micro-reactor at $450^{\circ}C$ and 42 g h mol^{-1} and then the structured catalyst (Y bundle) was test under same condition for comparison. Further testing was achieved by scaling up the reactor to 10 mm i.d. quartz reactor. The n-heptane cracking conversion and product selectivity were calculated using **Equation 6-11** and **Equation 6-12**.

A 0.03 gm of catalyst Y used for 4 mm i.d. reactor and 0.1 g for scale up reactor (10 mm i.d.). The n–heptane conversion data (X %) in relation to time on stream at different time were shown in **Figure 6-14**. Unlike the ZSM-5, zeolite Y deactivates rapidly. However, after 120 minutes there was only a small reduction in activity, and selectivity measurements were made. The major product was again $C_3^=$ but significantly more C_3 and iC_4 were also produce. There was also a very different product distribution when the large reactor was used. Almost twice the amount of olefins was produced (**Table 6-4 and Figure 6-15**) in the smaller reactor.

Overall, the pelleted catalysts exhibited higher initial activities and also after 125 minutes on stream (**Table 6-4**). The more open structure of zeolite Y with large α-cages allows for many secondary reactions to occur which are strictly hundred in the ZSM-5, hence the iC_4/nC_4 ratios is much higher. For examples comparison of the pelleted (10 mm i.d reactor) catalysts has iC_4/nC_4 ratios for zeolite Y = 4.6 and zeolite ZSM-5 = 0.51.

The dealuminated Y catalysts show higher total olefin yielded values than ZSM-5 and with surprisingly large amounts of heptanes as their activity is much reduced. **Figure 6-15** and **Table 6-4** shows how similar the product selectivities of the structured and pelleted catalysts were and confirm that the zeolite on FeCrAlloy behaved very similarly to that of the pelleted powdered catalyst.

Table 6-4: Catalytic performance for Y structured and pelleted catalyst in 4 and 10 mm micro-reactor at 450ºC and 42 g h mol^{-1} after 125 min after 125 min of deactivation n–heptanes cracking (moles/100 moles converted).

	pelleted,10 mm	structured,10 mm	pelleted,4mm	structured,4 mm
C_1	2.1	1.9	2.0	2.4
C_2	1.6	2.0	2.0	2.0
$C_2^=$	11.9	11.0	1.8	2.7
C_3	16.4	12.9	5.9	4.6
$C_3^=$	28.2	27.9	33.5	36.3
iC_4	11.9	12.7	8.1	8.5
nC_4	2.6	4.6	3.8	3.4
$C_4^=$	8.8	5.8	26.6	21.2
iC_5	0.8	1.8	0.8	1.3
nC_5	0.6	1.0	1.1	0.8
$C_5^=$	2.2	3.0	1.1	2.5
iC_6	0.0	0.0	0.0	0.0
nC_6	0.0	0.0	0.0	0.0
$C_6^=$	0.0	0.0	0.0	0.0
iC_7	1.9	2.0	2.1	1.8
$C_7^=$	11.2	12.9	11.1	13.2
C_6H_6	0.0	0.0	0.0	0.0
Total	100.1	99.8	100.0	100.8
$X\%_{at\ 125\ min}$	15.0	10.2	11.4	4.5
$X\%_{at\ 5\ min}$	69.5	48.5	59.5	49.0
iC_4/nC_4	*4.6*	*2.8*	*2.1*	*2.5*
$\sum C_i^=/C_j$	*1.65*	*1.54*	*2.9*	*3.1*
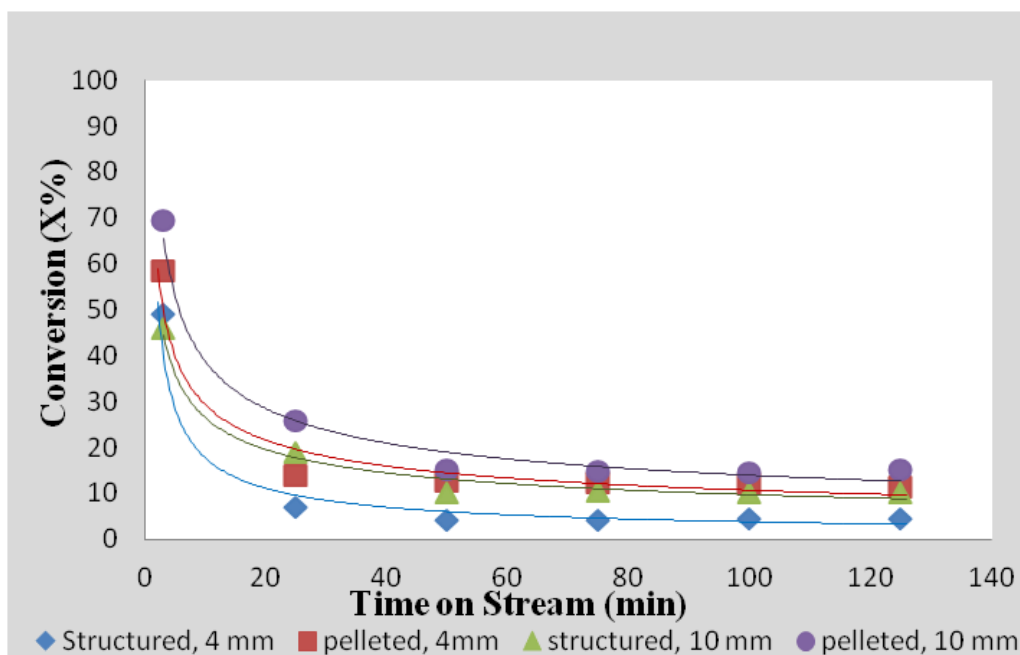
Figure 6-14: n-Heptane conversion with time for pelleted and structured Y catalysts at 450°C and 42 g h mol^{-1} after 125 min in both the 4 and 10 mm micro-reactor.
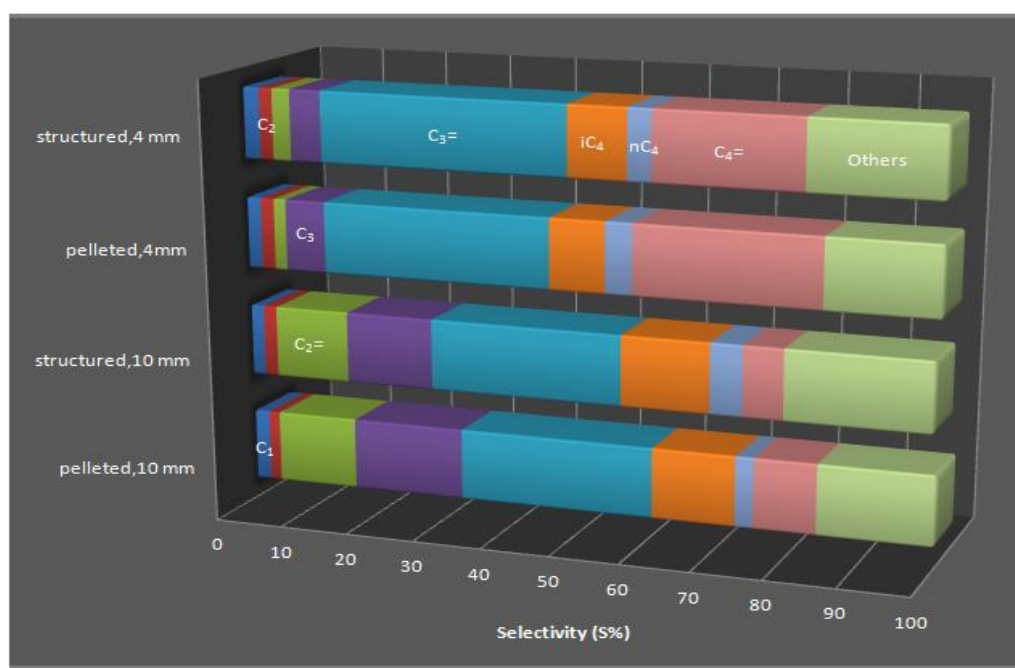
Figure 6-15: Product selectivity of the structured and pelleted Y catalyst in both the 4 and 10 mm micro-reactors at 450°C and 42 g h mol^{-1} after 125 min with significant deactivation.
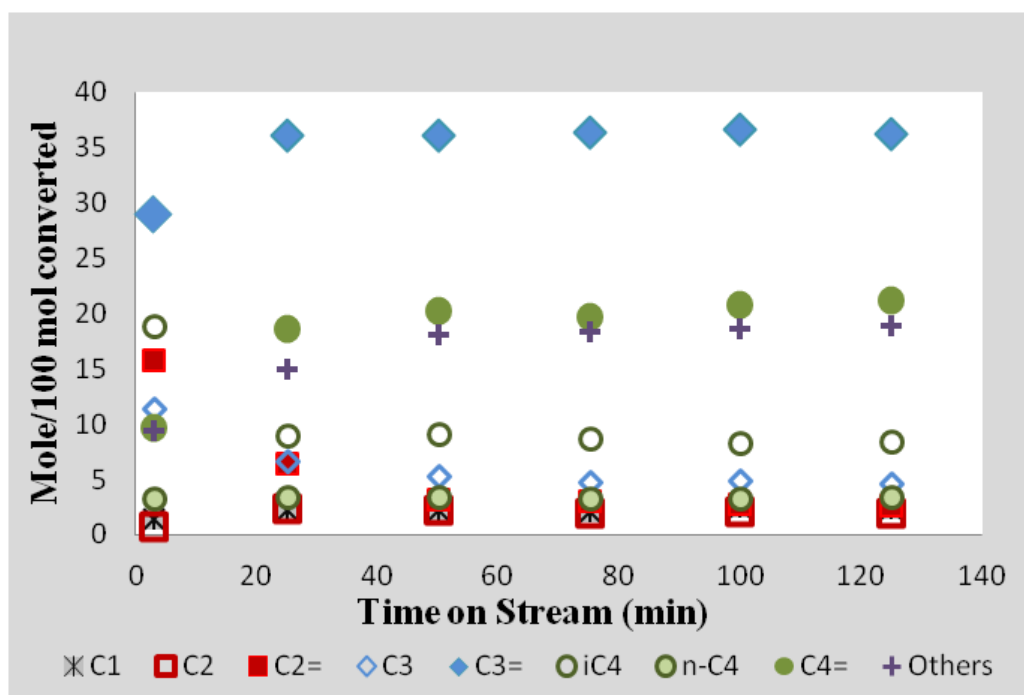
Figure 6-16: Light product selectivity in over structured Y zeolite in 4 mm quartz micro-reactor at 450ºC and 42 g h mol⁻¹ versus time on stream.
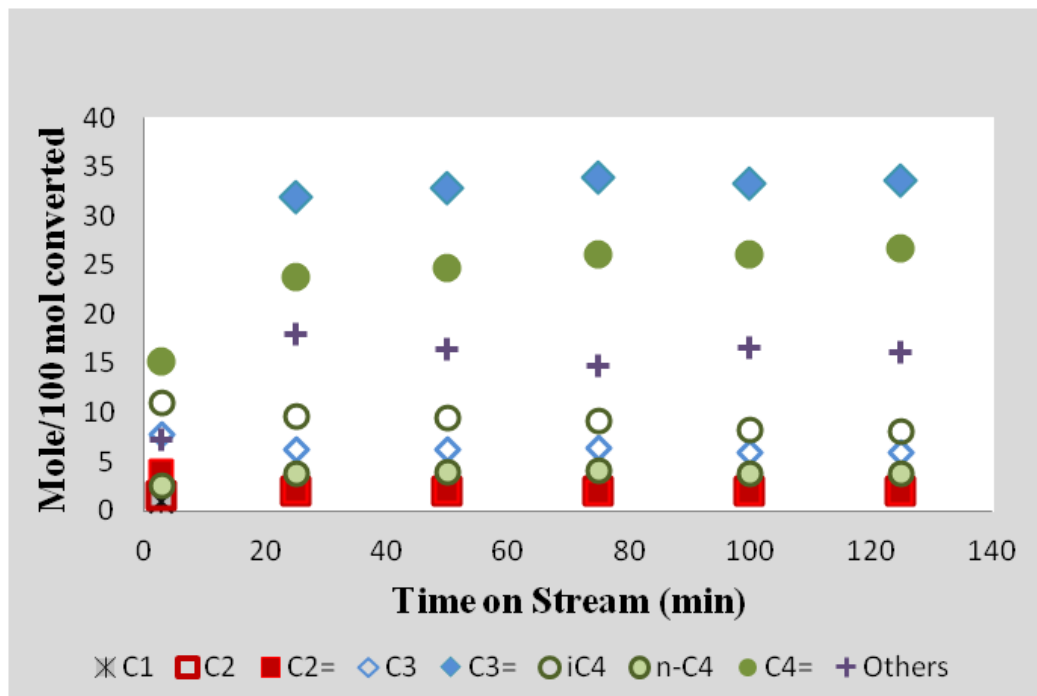
Figure 6-17: Light product selectivity over pelleted Y zeolite in 4 mm quartz micro-reactor at 450ºC and 42 g h mol⁻¹ versus time on stream.
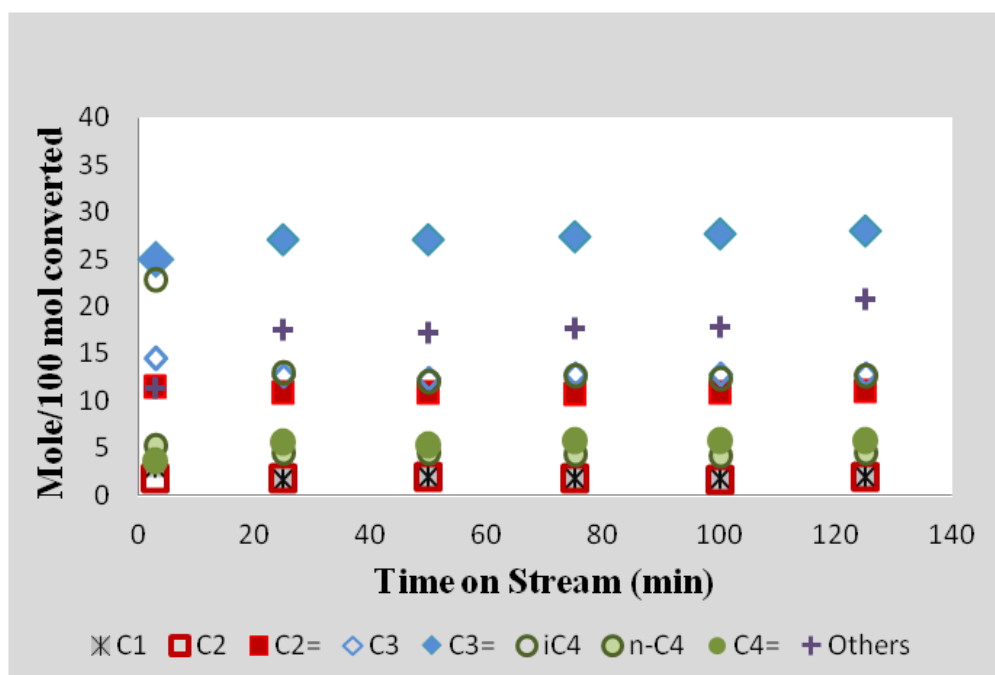
Figure 6-18: Light product selectivity over structured Y zeolite in 10 mm quartz micro-reactor at 450°C and 42 g h mol^{-1} versus time on stream.
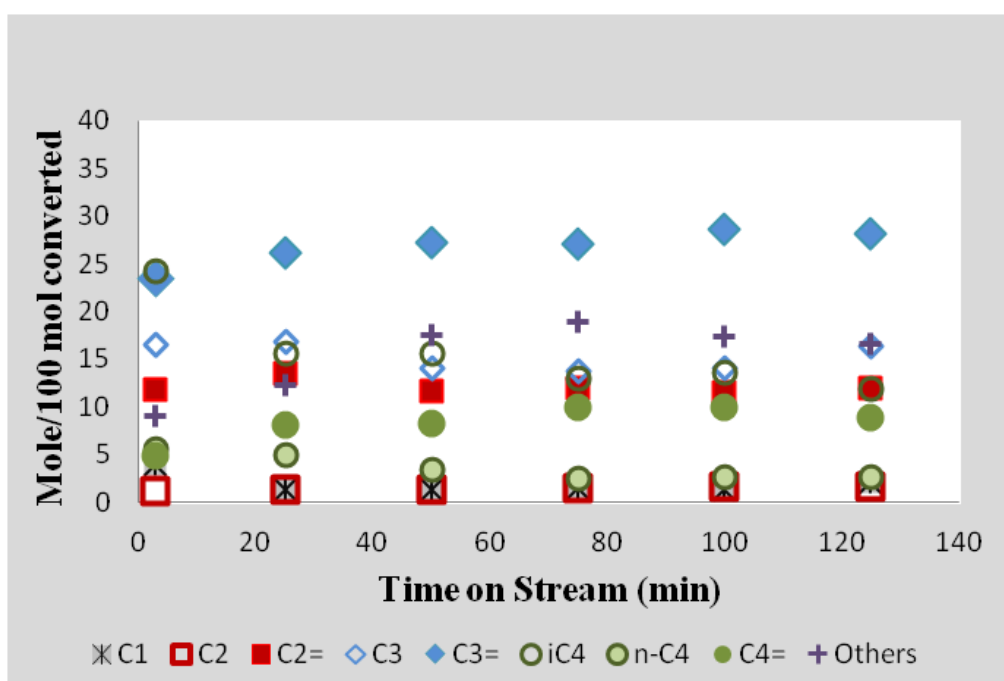
Figure 6-19: Light product selectivity over pelleted Y zeolite in 10 mm quartz micro-reactor at 450°C and 42 g h mol^{-1} versus time on stream.

The selectivity comparisons are shown in **Figure 6-16** – **Figure 6-19** as time on stream increased and as the conversion was decreasing rapidly. However, selectivities had stabilised quite quickly around 25 minutes and as stated earlier were similar for each catalyst tested in the small and large reactions. The catalysts placed in the 4 mm reactor showed much more primary olefinic products, compared to the 10 mm reactor.

6.9.2 Deactivation of structured/pelleted Y zeolite

The thermogravimetric analysis of the structured and pelleted Y in 4 mm and 10 mm quartz micro-reactor were revealed two distinguished weight loss for all the selected catalysts during the experiment (**Figure 6-20**). The H_2O and volatile materials was observed through the heating under nitrogen 0–100 minutes (DTG in **Figure 6-20**). While the second weight loss was due to the oxidation of heavies coke deposited (DTG in **Figure 6-20**).

The coke values are consisted with the smaller reactor packing of the wire supported catalyst being poor as the lower conversion and more olefinic products suggest the 10 mm reactor gave higher coke values and although the structured catalyst was lower, it was comparedable with the pelleted form.
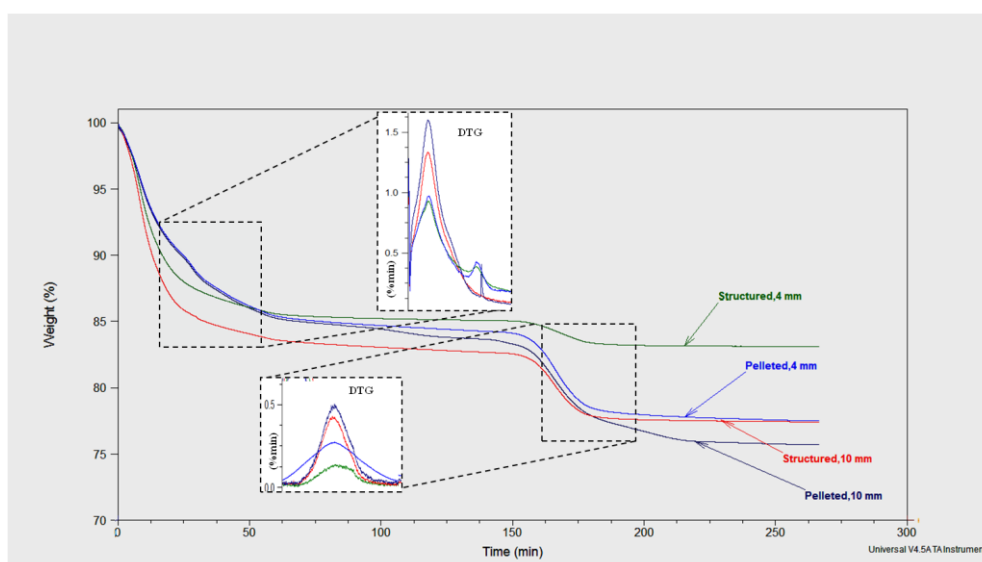
Figure 6-20: TGA analysis of the coke present on structured and pelleted Y catalyst in 4 mm and 10 mm quartz micro-reactor.

Table 6-5: Coke formed on structured and pelleted ZSM-5 in 4 mm and 10 mm quartz micro-reactor.

	pelleted, 4 mm	structured, 4 mm	pelleted, 10 mm	structured, 10 mm
X (%)	11.4	4.5	15.0	10.2
Coke (%)	7.1	2.0	8.0	5.6

6.9.3 Determination of the kinetic parameters for n-heptane cracking over structured and pelleted Y zeolite

Following the same procedure as outlined in **section 6.8.3** n–heptane cracking was carried out on structured and pelleted Y catalyst at different temperatures (325, 375, and 450°C) and W/F (24, 24, and 50 g h mol^{-1}) to investigate kinetic parameters. **Figure 6-21** and **Figure 6-23** confirmed that the n–heptane cracking over the both the structured and pelleted stabilised Y catalysts in both the 4 mm and 10 mm quartz micro-reactor gave reasonable agreements with a first order kinetic model (**Equation 6-8**).
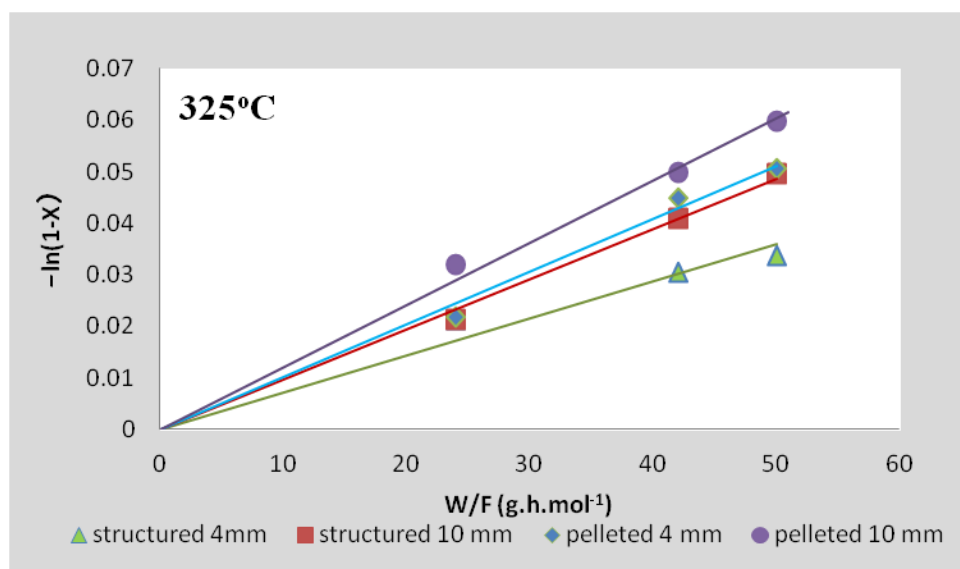
Figure 6-21: First order plot of n–heptane cracking over structured and pelleted Y catalysts in 4 mm and 10 mm quartz micro-reactors at 325°C.
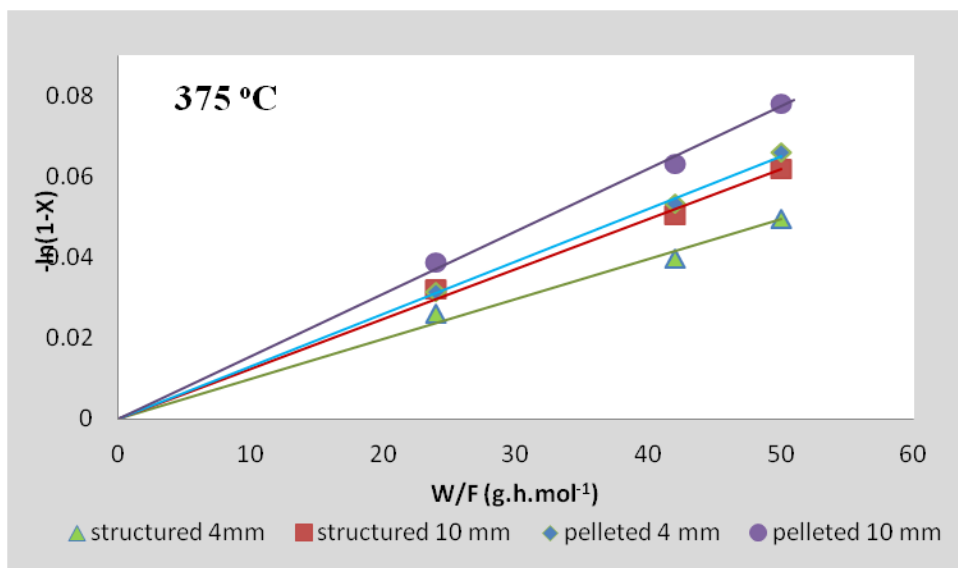
Figure 6-22: First order plot of n –heptane cracking over structured and pelleted Y catalysts in 4 mm and 10 mm quartz micro-reactors at 375°C.
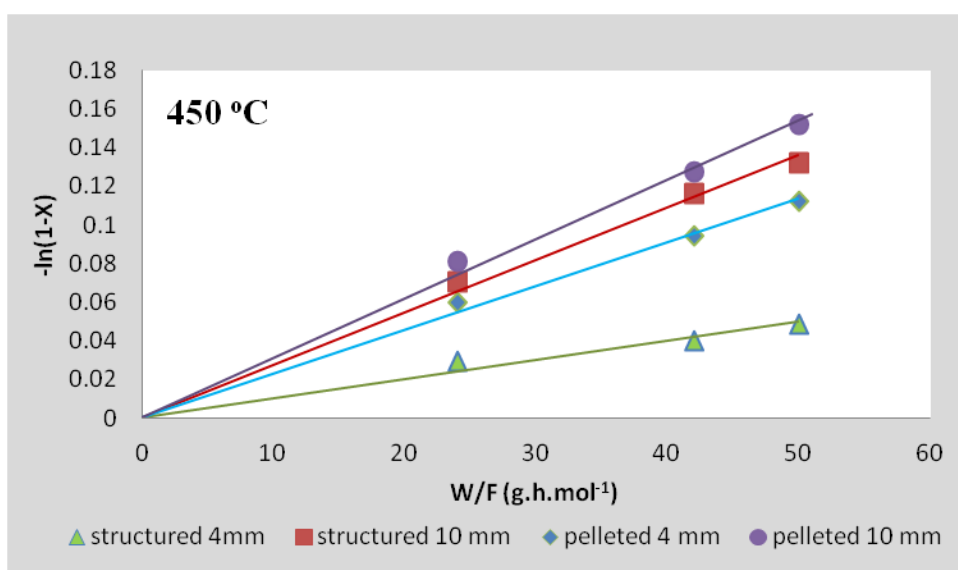
Figure 6-23: First order plot of n–heptane cracking over structured and pelleted Y catalysts in 4 mm and 10 mm quartz micro-reactors at 450°C.
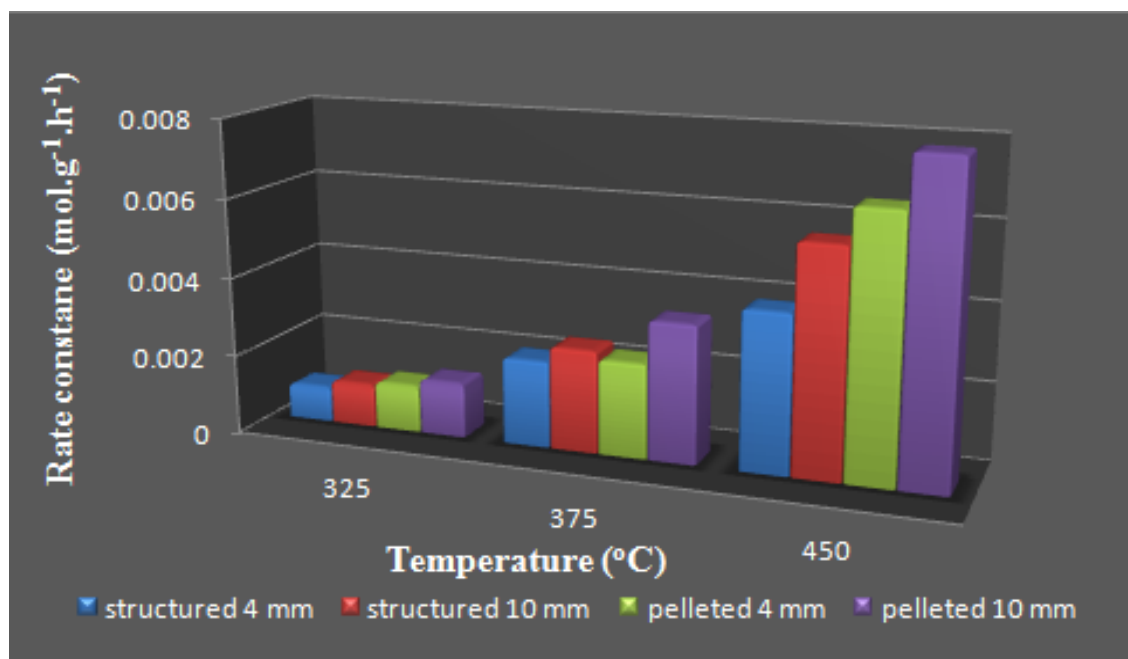
Figure 6-24: Rate constants for n–heptane cracking over structured and pelleted Y in 4 mm and 10 mm quartz micro-reactors at different temperatures.
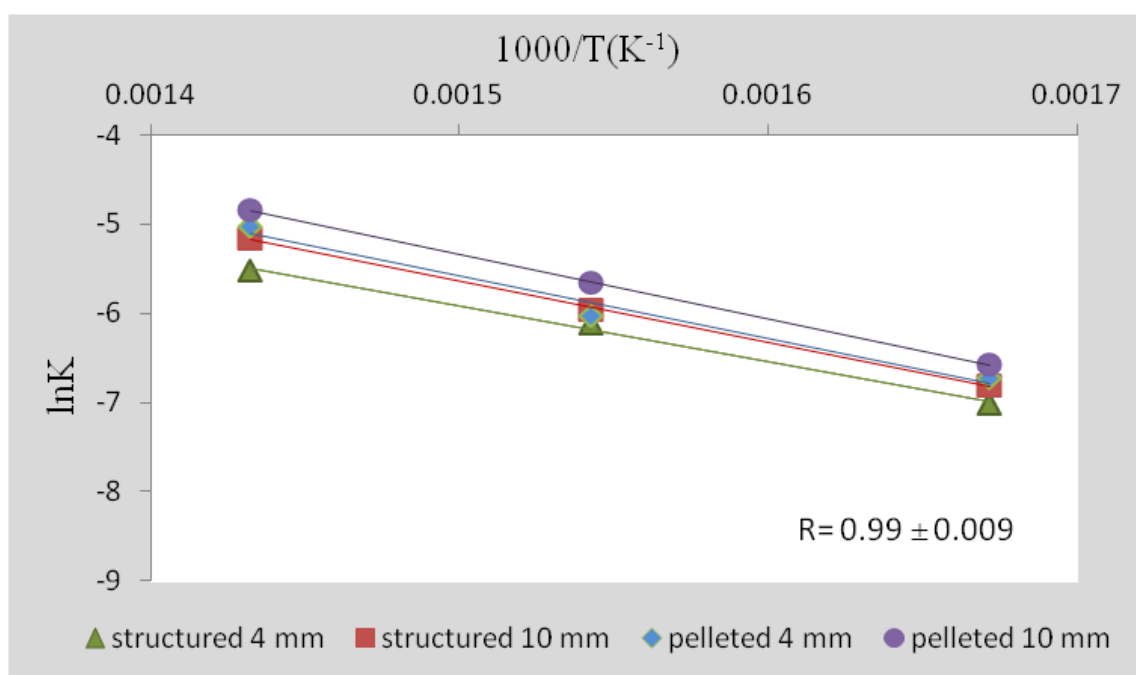
Figure 6-25: Arrhenius plot of n–heptane cracking over structured and pelleted Y in 4 mm and 10 mm quartz micro-reactor at different temperatures.

Table 6-6: Apparent activation energy of n–heptane cracking over structured and pelleted Y in 4 mm and 10 mm quartz micro-reactor at different temperatures.

Selected catalysts	Structured 4 mm	structured 10 mm	pelleted 4 mm	Pelleted 10 mm
E_a(kJ mol^{-1})	52.1	57.1	58.8	60.1

The rate constant for n–heptane cracking over structured and pelleted Y in 4 mm and 10 mm quartz micro-reactor increased with temperature as illustrated in **Figure 6-12.**

Typically the pelleted catalysts showed the higher rate constants compared to the structured equivalents. Again as might be expected based on the conversion, selectivity and coke data, the apparent activation energy was estimated (**Figure 6-25**) and found to be around 58 kJ mol^{-1} (**Table 6-6**).

Summary

The catalytic performance (activity, stability, and selectivity) of selected pelleted and structured ZSM-5 and Y zeolite catalysts was tested by n–heptane cracking.

Catalyst deactivation and selectivity was tested at 450°C at increasing time on stream. In addition, three temperatures (325, 375, and 450°C) and three contact times (24, 42, and 50 g h mol^{-1}) were carried out to determine kinetic parameters for the structured ZSM-5 and Y catalysts and compared with the pelleted ZSM-5 and Y catalysts under the same reaction conditions. It was confirmed that the structured ZSM-5 and Y catalysts have similar selectivity as the pelleted catalysts tested under the same reaction condition and despite the structured catalysts having lower conversion.

The differently in estimating the amount of catalyst on the FeCrAlloy wires and then in packing the wires into the 4 mm diameter reactor meant that channelling and less active catalyst bed to lower conversion. Better agreement was achieved again in the wider 10 mm reactor tube.

Despite these drawbacks, both ZSM–5 (Si/Al = 11) and the acid-leached zeolite Y (Si/Al = 8) structured catalysts showed similar product selectivities to their pelleted counterparts. Increased i–C_4 yields indicated more secondary reactions in the case of the pelleted catalysts supporting the lower activity observed for the structured catalysts. Zeolite Y showed the expected repaid deactivation with time on stream whereas, ZSM-5 showed stable activity throughout.

Apparent activation energies of approximately 60 kJ mol^{-1} for all catalysts suggested similar reaction mechanisms and that the surface reaction was controlling.

References

1. Htay, M.M. and O. Mya, *Preparation of zeolite Y catalyst for petroleum cracking,* World Academy of Science and Engineering and Technology, 2008. **48**: p. 114-120.

2. Yoshimura, Y., N. Kijima, T. Hayakawa, K. Murata, K. Suzuki, F. Mizukami, K. Matano, T. Konishi, T. Oikawa, and M. Saito, Catalytic cracking of naphtha to light olefins, Catalysis Surveys from Japan, 2001. 4(2): p. 157-167.

3. Taghipour, N., J. Towfighi, A. Mohamadalizadeh, L. Shirazi, and S. Sheibani, *The effect of key factors on thermal catalytic cracking of naphtha over Ce–La/SAPO-34 catalyst by statistical design of experiments,* Journal of Analytical and Applied Pyrolysis, 2013. **99**: p. 184-190.

4. Rahimi, N. and R. Karimzadeh, *Catalytic cracking of hydrocarbons over modified ZSM-5 zeolites to produce light olefins: A review,* Applied Catalysis A: General, 2011. **398**(1): p. 1-17.

5. Picciotti, M., *Novel ethylene technologies developing, but steam cracking remains king,* Oil and Gas Journal, 1997. **95**(25): p. 53-54, 57.

6. Wakui, K., K. Satoh, G. Sawada, K. Shiozawa, K. Matano, K. Suzuki, T. Hayakawa, Y. Yoshimura, K. Murata, and F. Mizukami, *Dehydrogenative cracking of n-butane using double-stage reaction,* Applied Catalysis A: General, 2002. **230**(1–2): p. 195-202.

7. Speight, J.G., *The chemistry and technology of petroleum*, Vol. 114. 2006:p. 10.

8. Komatsu, T. *Catalytic cracking of paraffins on zeolite catalysts for the production of light olefins*, in *20th Annual Saudi-Japan Symposium; Catalysts in Petroleum Refining and Petrochemicals, Dharan, Saudi-Arabia.* 2010.

9. Weitkamp, J. and L. Puppe, *Catalysis and zeolites: fundamentals and applications*, 1999:p. 22.

10. Le Van Mao, S. Melancon, C. Gauthier-Campbell, and P. Kletnieks, *Selective deep catalytic cracking process (SDCC) of petroleum feedstocks for the production of light olefins. I. The Catlever effect obtained with a two reaction-zones system on the conversion of n-hexane,* Catalysis letters, 2001. **73**(2): p. 181-186.

11. Chen, N., *Shape selective catalysis in industrial applications*. Vol. 65. 1996, p.282.

12. Buchanan, J., *The chemistry of olefins production by ZSM-5 addition to catalytic cracking units,* Catalysis T oday, 2000. **55**(3): p. 207-212.

13. Rajagopalan, K., A. Peters, and G. Edwards, *Influence of zeolite particle size on selectivity during fluid catalytic cracking,* Applied catalysis, 1986. **23**(1): p. 69-80.

14. Corma, A., J. Planelles, J. Sanchez-Marin, and F. Tomas, *The role of different types of acid site in the cracking of alkanes on zeolite catalysts,* Journal of catalysis, 1985. **93**(1): p. 30-37.

15. Miale, J., N.Y. Chen, and P. Weisz, *Catalysis by crystalline aluminosilicates: IV. Attainable catalytic cracking rate constants, and superactivity,* Journal of catalysis, 1966. **6**(2): p. 278-287.

16. Swift, H.E., J.J. Stanulonis, and E.H. Reynolds, *Process for increasing gasoline yield and quality during catalytic cracking of high metals content charge stocks using an alumina-aluminum phosphate-silica-zeolite catalyst*, 1979, US Patent 4,158,621.

17. Cardona, S.C. and A. Corma, *Tertiary recycling of polypropylene by catalytic cracking in a semibatch stirred reactor: use of spent equilibrium FCC commercial catalyst,* Applied Catalysis B: Environmental, 2000. **25**(2): p. 151-162.

18. Bolton, A. and R. Bujalski, *The role of the proton in the catalytic cracking of hexane using a zeolite catalyst,* Journal of Catalysis, 1971. **23**(3): p. 331-339.

19. Corma, A. and A. Orchilles, *Current views on the mechanism of catalytic cracking,* Microporous and Mesoporous Materials, 2000. **35**: p. 21-30.

20. Camblor, M., A. Corma, A. Martinez, F.A. Mocholi, and J.P. Pariente, *Catalytic cracking of gasoil: Benefits in activity and selectivity of small Y zeolite crystallites stabilized by a higher silicon-to-aluminium ratio by synthesis,* Applied catalysis, 1989. **55**(1): p. 65-74.

21. Ward, J.W., *Catalytic cracking process using ammonia-stable zeolite catalyst*, 1977, US Patent 4036739.

22. Arandes, J.M., *Effect of HZSM-5 zeolite addition to a fluid catalytic cracking catalyst. Study in a laboratory reactor operating under industrial conditions,* Industrial & Engineering Chemistry Research, 2000. **39**(6): p. 1917-1924.

23. Olah, G.A., J.R. DeMember, and J. Shen, *Electrophilic reactions at single bonds. X. Hydrogen transfer, alkylation, and alkylolysis of alkanes with methyl and ethyl fluoroantimonate,* Journal of the American Chemical Society, 1973. **95**(15): p. 4952-4956.

24. Shertukde, P.V., G. Marcelin, G. A. Sill, and W. K. Hall, *Study of the mechanism of the cracking of small alkane molecules on HY zeolites,* Journal of Catalysis, 1992. **136**(2): p. 446-462.

25. Kuehne, M., S.M. Babitz, H.H. Kung, and J.T. Miller, *Effect of framework Al content on HY acidity and cracking activity,* Applied Catalysis A: General, 1998. **166**(2): p. 293-299.

26. Ward, J.W., *The nature of active sites on zeolites: IV. The influence of water on the acidity of X and Y type zeolites,* Journal of catalysis, 1968. **11**(3): p. 238-250.

27. Hong, Y., V. Gruver, and J. Fripiat, *Role of Lewis Acidity in the Isomerization of n‑Pentane and o‑Xylene on Dealuminated H‑Mordenites,* ChemInform, 1995. **26**(21): p. 421–429.

28. Wielers, A., M. Vaarkamp, and M. Post, *Relation between properties and performance of zeolites in paraffin cracking,* Journal of Catalysis, 1991. **127**(1): p. 51-66.

29. Greensfelder, B., H. Voge, and G. Good, *Catalytic and thermal cracking of pure hydrocarbons: Mechanisms of Reaction,* Industrial & Engineering Chemistry, 1949. **41**(11): p. 2573-2584.

30. Babitz, S.M., B. A. Williams, J. T. Miller, R. Q. Snurr, W. O. Haag, and H. H. Kung, *Monomolecular cracking of n-hexane on Y, MOR, and ZSM-5 zeolites,* Applied Catalysis A: General, 1999. **179**(1–2): p. 71-86.

31. Kotrel, S., H. Knözinger, and B.C. Gates, *The Haag–Dessau mechanism of protolytic cracking of alkanes,* Microporous and Mesoporous Materials, 2000. **35–36**: p. 11-20.

32. Kissin, Y.V., *Chemical mechanisms of catalytic cracking over solid acidic catalysts: Alkanes and alkenes,* Catalysis Reviews, 2001. **43**(1-2): p. 85-146.

33. Jentoft, F.C. and B.C. Gates, *Solid-acid-catalyzed alkane cracking mechanisms: evidence from reactions of small probe molecules,* Topics in Catalysis, 1997. **4**(1): p. 1-13.

34.   Haag, W.O. and R.M. Dessau, *Duality of Mechanism for Acid-Catalyzed Paraffin Cracking* in *8th Int, Congress on Catalysis*. 1984: Berlin. p. 30.

35.   Bartholomew, C.H. and R.J. Farrauto, *Fundamentals of Industrial Catalytic Processes,* John Wiley & Sons, Inc.: New York, ISBN, 2006. **13**: p. 978-0.

36.   Gates, B.C., J.R. Katzer, and G.C. Schuit, *Chemistry of Catalytic Processes*, Vol. 311. 1979: McGraw-Hill New York.

37.   Komatsu, T., H. Ishihara, Y. Fukui, and T. Yashima, *Selective formation of alkenes through the cracking of n-heptane on Ca^{2+} exchanged ferrierite,* Applied Catalysis A: General, 2001. **214**(1): p. 103-109.

38.   Barthomeuf, D. and R. Beaumont, *X, Y, aluminum-deficient, and ultrastable faujasite-type zeolites: III. Catalytic activity,* Journal of Catalysis, 1973. **30**(2): p. 288-297.

39.   Scherzer, J. and A.J. Gruia, *Hydrocracking Science and Technology*, Vol. 66. 1996.

40.   Wang, L., B. Yang, and Z. Wang, *Lumps and kinetics for the secondary reactions in catalytically cracked gasoline,* Chemical Engineering Journal, 2005. **109**(1): p. 1-9.

41.   Boudart, M., *Two-step catalytic reactions,* AIChE Journal, 1972. **18**(3): p. 465-478.

42.   Hagelberg, P., I. Eilos, J. Hiltunen, K. Lipiäinen, V.M. Niemi, J. Aittamaa, and A.O.I. Krause, *Kinetics of catalytic cracking with short contact times,* Applied Catalysis A: General, 2002. **223**(1): p. 73-84.

43.   Chen, S. and G. Manos, *Study of coke and coke precursors during catalytic cracking of n-hexane and 1-hexene over ultrastable Y zeolite,* Catalysis Letters, 2004. **96**(3-4): p. 195-200.

44.   Froment, G., *Coke formation in catalytic processes: Kinetics and catalyst deactivation,* Studies in Surface Science and Catalysis, 1997. **111**: p. 53-68.

45.   Vardhani, P.A., *Chromatography and spectroscopy based approches in the study of functional plant constituents*, in *07241A2304*. 2010, Laila Impex, R & D center: vijayawada. p. 9-14.

46.   Rane, N., M. Kersbulck, R.A. Van Santen, and E.J.M. Hensen, *Cracking of n-heptane over Brønsted acid sites and Lewis acid Ga sites in ZSM-5 zeolite,* Microporous and Mesoporous Materials, 2008. **110**(2): p. 279-291.

47.   Jacobs, P.A. and J.A. Martens, *Introduction to Acid Catalysis with Zeolites in Hydrocarbon Reactions*, in *Studies in Surface Science and Catalysis*, H. van Bekkum, E.M. Flanigen, and J.C. Jansen, Editors. 199: p. 445-496.

48.   Corma, A., J. Monton, and A. Orchilles, *Cracking of n-heptane on a HZSM-5 zeolite. The influence of acidity and pore structure,* Applied Catalysis, 1985. **16**(1): p. 59-74.

Conclusions and Recommendations for Future Work

7.1 Introduction

This thesis has resulted in the development structured zeolite catalysts by growing of ZSM-5 and Y zeolites layers on the FeCrAlloy wires, which could now offer technical advantage for application in catalytic application. The catalytic properties of the structured zeolite catalysts have been explored using the n-heptane cracking.

This work covered:

- The pre-treatment method of the FeCrAlloy wires (substrate metal) and the effect of the oxidation time on the growth of aluminium oxide

on the metal surface and subsequent interaction with zeolite grown over the alumina layer.

- The growth of ZSM-5 and Y zeolite on FeCrAlloy wires and the influence of the synthesis parameters (substrate oxidation and crystallisation time) on the zeolite crystallisation process in the bulk phase (powder) and structured zeolite and on the properties of the structured zeolite catalyst was also studied.

- The post-synthesis treatment of powder and structured Na-ZSM-5 and Na-Y zeolite by calcination and ion exchange was also studied.

- Further post-synthesis modification to improve the catalytic properties was required in the zeolite Y case. This was achieved by acidified ammonium ion exchanged.

- The catalytic performance of optimised ZSM-5 and Y structured zeolite catalysts for n-heptane cracking and comparison of ZSM-5 and Y pellets in fixed-bed reactor was investigated.

The structured catalyst films generated as part of this investigation have been characterised using a range of techniques, including X-ray diffraction (XRD), Electron microscopy (SEM), Energy Dispersive X-ray analysis (EDAX) and Thermogravimetric Analysis (TGA), with the transition from oxide-on-alloy wires to hydrothermally synthesised uniformly zeolite coated surfaces being demonstrated using both SEM and XRD. The robustness of the coatings has been ascertained by subjecting these to thermal cycling (ambient to 550°C), with the results indicating that the synthesis time and gel compositions have a crucial effect on the quality of zeolite growth on the FeCrAlloy wires.

The cracking of n–heptane over the pellets and structured catalysts for both ZSM–5 and Y zeolite showed similar product selectivities, even when the reactor was packing was not optimum for similar amounts of catalyst with apparent activation energies of around 60 kJ mol^{-1}.

7.2 Synthesis of the structured zeolite catalyst

An in-situ crystallisation of the ZSM-5 and Y zeolite on the pre-treated FeCrAlloy surface support was successfully developed. The process consisted of pre-treating the FeCrAlloy wires by applying a physical pre-treatment method to the wires before they were oxidised at $1000^{o}C$. The optimum oxidation time was chosen to be 4 hours. Hence, the SEM and TGA analyses indicated that 4 hours oxidation of FeCrAlloy wires had the highest catalyst loading and excellent resistance to thermal cycling for both ZSM-5 and Y zeolites.

The effect of the crystallisation time on the growth of zeolite ZSM-5 and Y layers on the FeCrAlloy wires was studied. EDAX analyses of the Na–Y structured catalyst confirmed an increase in the zeolite weight gain, layer thickness and coverage surface was achieved when extending the crystallisation time, with zeolite loading on the wires for Na–ZSM-5 up to 35% wt (after 48 hours, at $180^{o}C$) and for Na–Y was 6.38 % wt (after 72 hours at $100^{o}C$).

Unlike the Na–ZSM-5, the zeolite Na–Y layer was thinner and only provided a layer of 23 μm thickness, after 72 hours, with Si/Al ratio equal to 2.72.

7.3 Development of the catalytic properties

The Na-form of structured and powder ZSM-5 and Y zeolites were modified (post synthesis). The Na–ZSM-5 form of structured and powder zeolite calcined and ion exchanged to remove template and obtain the H–form dropping the Na content from 3.43 % to 0.15 % with an overall Si/Al ratio equal 11.

Whereas, Na–Y structured and powder were subjected to further treatments (dealumination) in addition to the ion exchange and calcination, in order to increase the Si/Al ratio and the catalytic activity.

The dealumination process was applied to Na–Y (8.6% Na) and Na–HY (3wt% Na) zeolite to study the effect of the cation being present in the zeolite framework. The pH of the dealumination process was varied in order to obtain acidic USY zeolite.

Both the Na–Y and Na–HY dealuminated samples showed increased Si/Al ratios, measured using different analytical techniques; EDAX, XRD, and NMR, by increasing the dosage of the nitric acid in each stage for each method.

Finally, analysis showed that by following the ^{b}**YI$_3$** procedure a zeolite sample with a Si/Al ratio = 8, 0.3% sodium content had 86% crystallinity. The ^{b}**YI$_3$** procedure was chosen to treatment the Na–HY structured zeolite.

7.4 n–Heptane cracking over pelleted and structured zeolite

The n–C$_7$ cracking was carried out over both structured ZSM-5 and Y zeolites obtained by the in-situ hydrothermal synthesis method. The deactivation and selectivity tests were carried out to study the kinetics of the structured ZSM-5 and Y catalyst compared with the pelleted ZSM-5 and Y catalyst under the same reaction conditions. The development of the structured catalysts in particular zeolite Y could represent a promising route towards the realisation of novel microreactors.

n–C$_7$ cracking revealed lower cracking activities for both the structured catalysts with the most likely explanation being the imperfect packing of the fixed bed micro-reactor which allowed some degree of channelling of the reactant resulting in lower conversions. Despite the drawback, both ZSM–5 (Si/Al = 11) and the acid-leached zeolite Y (Si/Al = 8) structured catalysts showed similar product selectivities to their pelleted counterparts. Increased i–C$_4$ yields indicated more secondary reactions in the case of the pelleted catalysts supporting the lower activity observed for the structured catalysts. Apparent activation energies of approximately 60 kJ mol^{-1} for all catalysts suggested similar reaction mechanisms and that the surface reaction was controlling.

7.5 Future work recommendations

Structured catalysts formed from the growth of zeolites on substrates is an area of increasing interest due to the increased efficiency of the catalytic process, and the ability to provide superior heat transfer and thermal conductivity for both exothermic and endothermic processes [1]. However, the generation of structured catalysts represents a significant challenge when balancing the relationship variables between materials properties and catalytic performance, with the Na_2O, H_2O and Al_2O_3 gel composition playing a significant role in this dynamic, thereby affecting both the type and range of application [2]. Although not described in detail above, several trial syntheses were carried out using different zeolite gel composition (Na_2O, H_2O and Al_2O_3). However, additional work would be necessary to optimise the zeolite gel composition for the preparation of structured ZSM-5 and Y zeolite catalysts as well as other types of zeolite.

The study would extend to other zeolites and mesoporous catalysts and also to other form of FeCrAlloy, such as tubes. If successful then the tubes would be coated with different catalysts eternally and externally. It is the feasible to of exothermic and endothermic reactions being carried out simultaneous over the internal and external surfaces.

Further work specific to this thesis would be:

- The investigation of the zeolite layer thickness of on the catalytic performance of the structured catalysts.
- The loading a transition metal (e.g. platinum) on the structured catalyst and study the catalytic performance in hydrocaking reactions such as $n-C_7$.
- Investigation the effects of the pressure drop reducing and improve of heat transfer of the structured catalyst in large scale cracking system and compare the result with the pelleted form under same operation conditions.

References

1. Jansen, J., J.H. Koegler, H. Van Bekkum, H.P.A. Calis, C.M. Van Den Bleek, F.Kapteijn, J.A. Moulijn, E.R. Geus, and N.Van der Puil, *Zeolitic coatings and their potential use in catalysis.* Microporous and Mesoporous Materials, 1998. **21**(4): p. 213-226.

2. Al-Rubaye, R.T.A., B. Atilgan, R. J. Holmes, and A. A. Garforth, *Growing Zeolite Y on FeCrAlloy Metal.* World Academy of Science, Engineering and Technology, 2013(76): p. 889-893.

Appendix A

Muffle Furnace Calibration

The muffle furnace temperature was verified using a thermocouple and the heating and cooling monitored and plotted. Furthermore, 15 L min^{-1} air flow was used to accelerate cooling down the muffle furnace and cooling rate was also monitored and recorded.
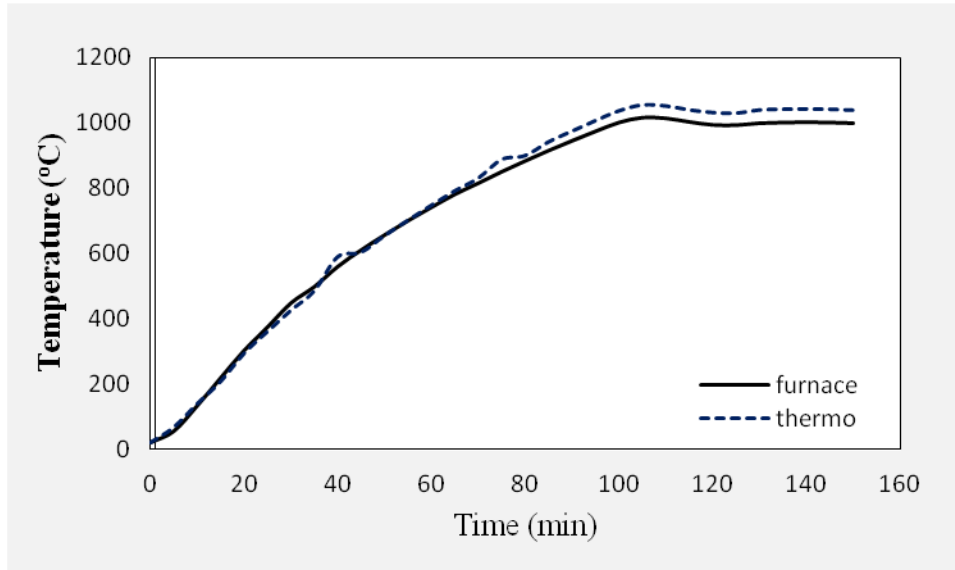
Figure A-1: Heating up rate for the set temperature 16.8^{o}C min^{-1} and 17.2^{o}C min^{-1} heating rate for the thermocouple temperature at the centre of the furnace.
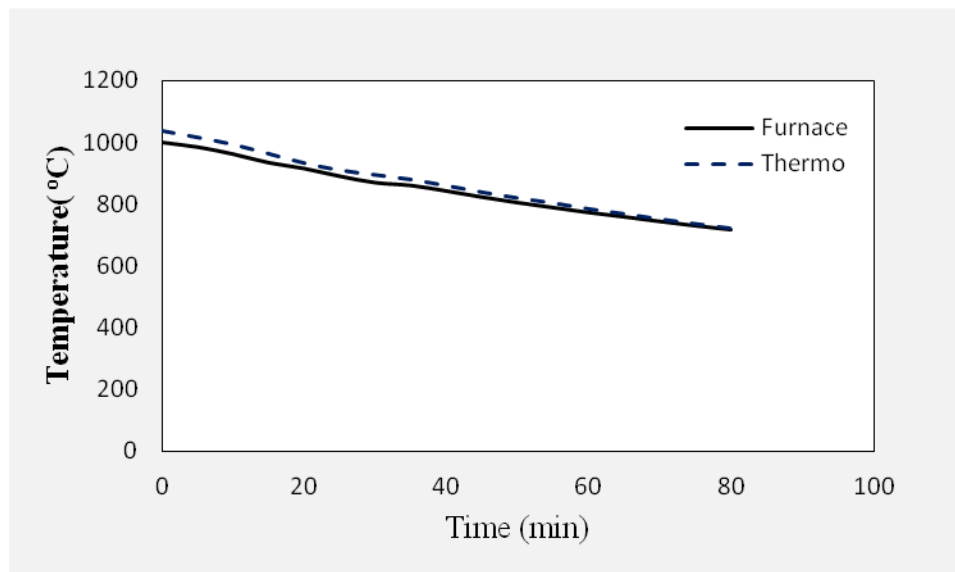
Figure A-2: Cooling down rate for the set temperature 3.8^{o}C min^{-1} and 6°C min^{-1} cooling rate for the thermocouple temperature at the centre of the furnace without air flow rate.
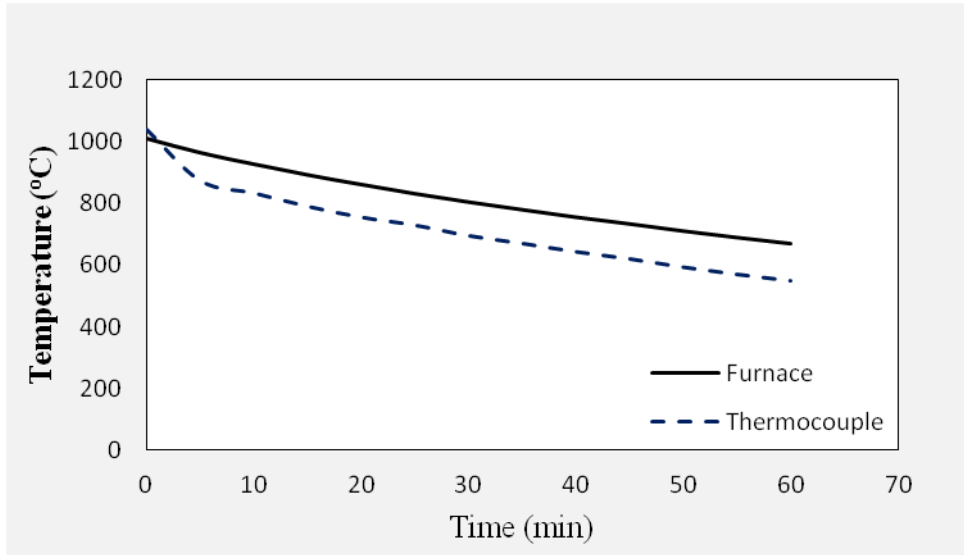
Figure A-3: Cooling down rate for the set temperature 6.2°C min^{-1} and 7°C min^{-1} cooling rate for the thermocouple temperature at the centre of the furnace.

<div style="writing-mode: vertical">**Appendix B**</div>

Gas Chromatography Calibration

A standard gas mixture (1 mol % of C_1, C_2, C_3, iC_4, nC_4, iC_5, and nC_5 in nitrogen gas, Linde Gas) was injected into a 250 µL sample loop fitted to a gas chromatograph (GC) prior to the cracking test in order to find the response factor (RF) for each component. The volume of each component in the sample loops (250 µL) was calculated from the molar concentration in the standard gas mixture then the number of moles of each component estimated (i.e. 1 mole gas = 22.4 L at 273 K) as shown in **Table B-1**. The standard gas was injected three times and an average measurement. The response factor was the ratio of the number of moles of the each component over the area count reading of the GC analysis for each component. The response factor (RF) for other components that might possible appear during n–heptane cracking and not present in the standard gas mixture (i.e.

$C_2^=$, $C_3^=$, $C_4^=$, and $C_5^=$) were estimated using a logarithmic relationship plotting the number of the carbon atoms C_n for each components in standard gas mixture versus the RF value (**Figure B-1**). For iC_6, nC_6, $C_6^=$, iC_7, nC_7, $C_7^=$, C_8, C_9 and C_{10} standard liquid samples were also injected to find the RF.

In summary, dependent on the regime used for GC analysis, **Figure B-2** and **Figure B-3** show the overall area under the peaks for each detected hydrocarbon in the product stream from USY and ZSM-5.

Table B-1: Calibration of GC and response factors for component in the standard gas mixture.

Name	Area count	mole%	Vol. Sample loop(μL)	Moles injected	$R_{F(moles/area)}$
C_1	181.6	1	2.5	1.116×10^{-7}	6.146×10^{-10}
C_2	348.8	1	2.5	1.116×10^{-7}	3.200×10^{-10}
C_3	497.4	1	2.5	1.116×10^{-7}	2.244×10^{-10}
iC_4	655.4	1	2.5	1.116×10^{-7}	1.703×10^{-10}
nC_4	576.2	1	2.5	1.116×10^{-7}	1.936×10^{-10}
iC_5	657.8	1	2.5	1.116×10^{-7}	1.697×10^{-10}
nC_5	505.4	1	2.5	1.116×10^{-7}	2.208×10^{-10}

The plot shows $y = -0.7446x - 9.2495$ and $R^2 = 0.99$, with x-axis labeled $Log(C_n)$ and y-axis labeled $Log(RF)$.
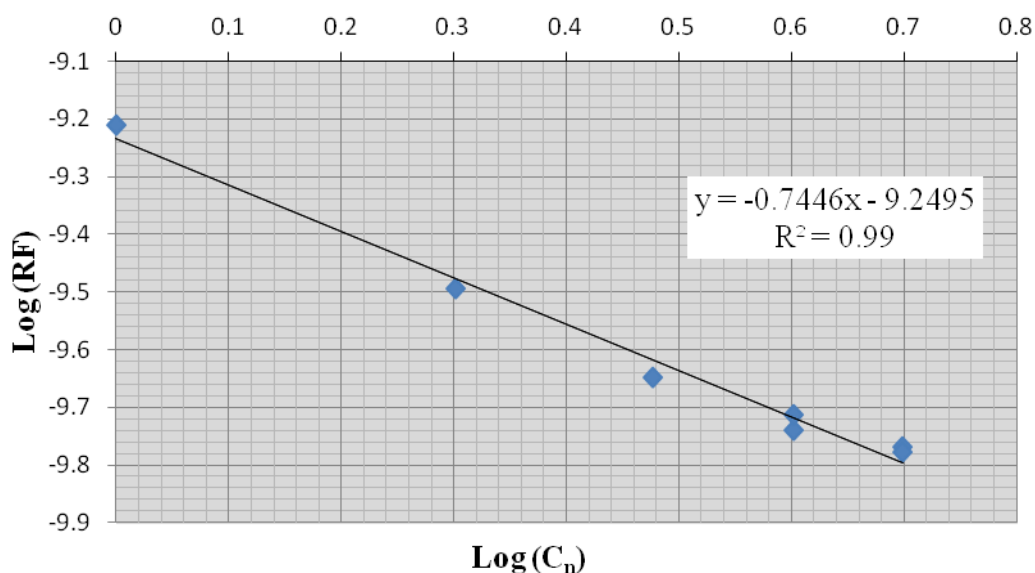
Figure B-1: logarithm correlation of RF with carbon number.
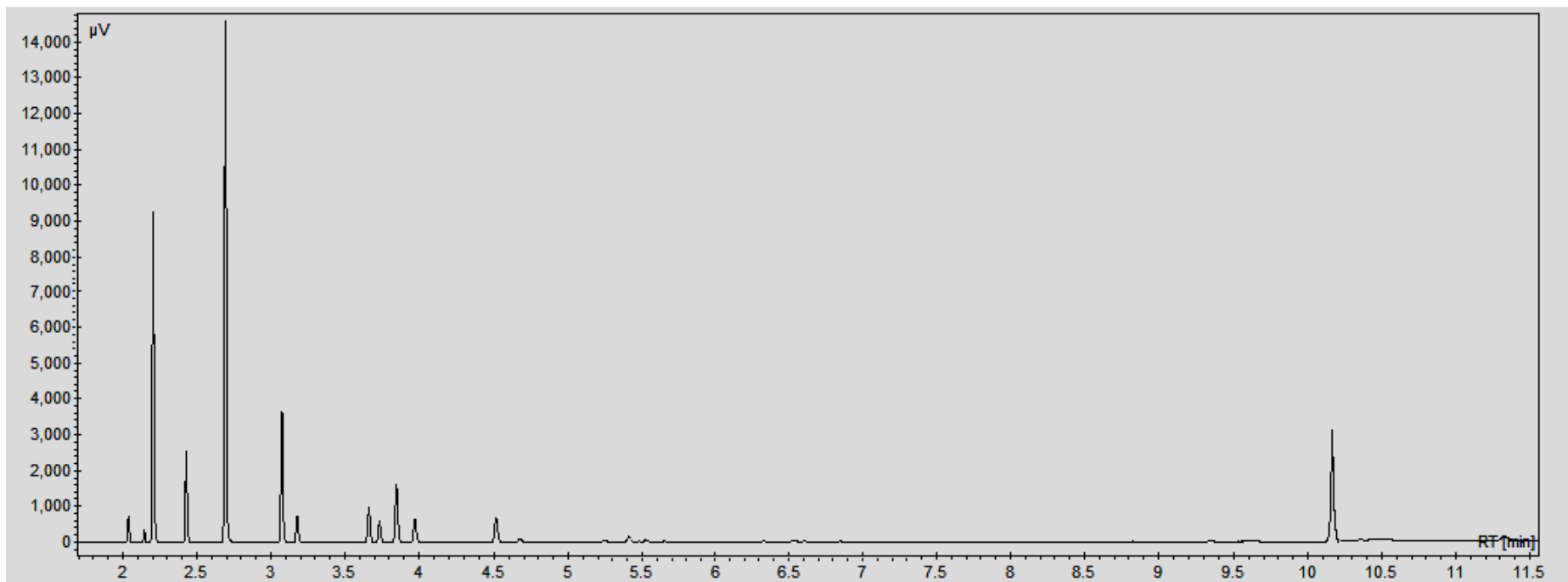
Figure B-2: Product trace of n-heptane cracking over ZSM-5 catalyst analysed by GC.
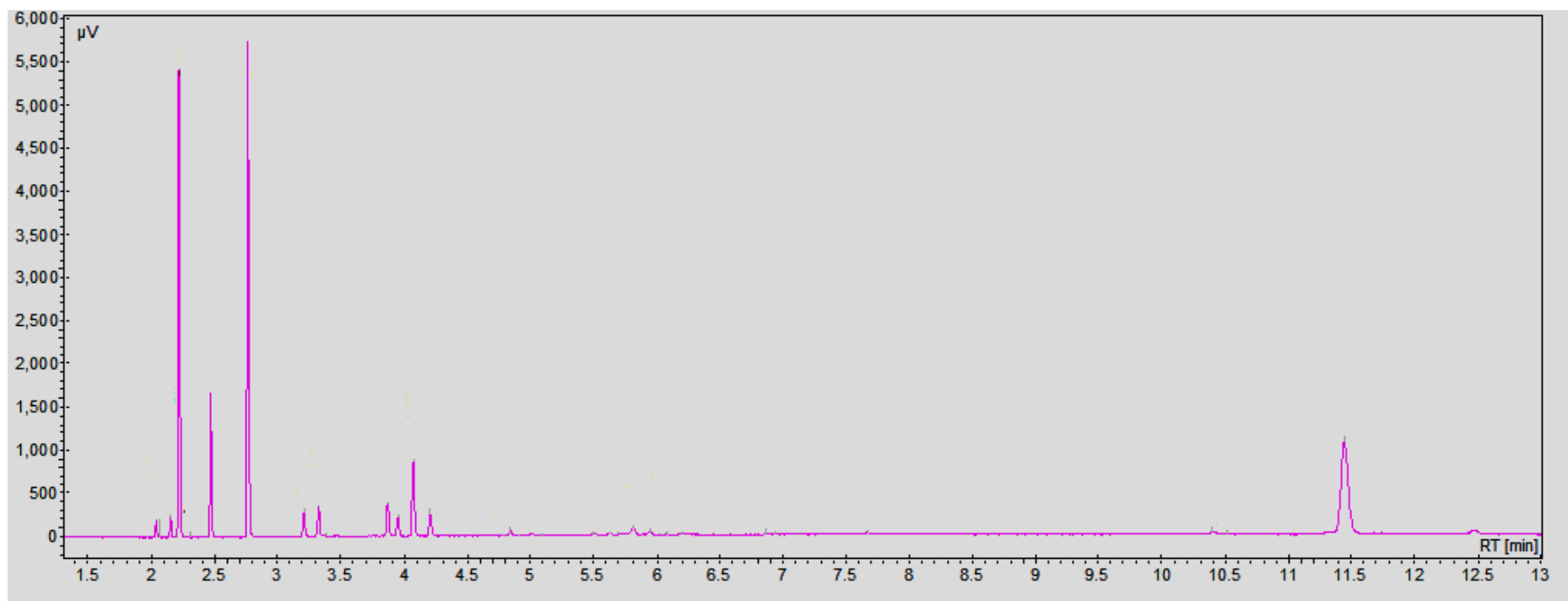
Figure B-3: Product trace of n-heptane cracking over USY.

Appendix C

Calculation of Contact Time of n-heptane in Fixed Bed Reactor

The molar percentage (mol%) of n–heptane was calculated by passing n-heptane through the quartz reactor under similar conditions used for the cracking testing, but without using any catalyst, using nitrogen gas as carrier at three different nitrogen flow rate (i.e 10, 35 and 100 ml min^{-1}). The experiment was carried out at 150°C to avoid any thermal cracking and the n–heptane (99.99wt% Sigma-Aldrich) was added to the nitrogen feed by the use of three bubblers half filled with n–heptane connected in series. The bubblers were maintained at an evaluated temperature by placing in an ice bath. The n–heptane molar percentage in the feed was found to be 3% as shown in **Table C-1.**

The contact times were calculated and the data was listed for both ZSM-5 and Y zeolite catalysts in **Table C-3** and **Table C-4**.

Table C-1: n-heptane molar percentage estimation using GC data.

N$_2$ flow (ml min^{-1})	n-C$_7$ area count	total area	n-C$_7$ feed (mol%)	mol/100 mol product	total flow (ml min^{-1})
10	1503.1	1512.9	3.06	99.352	10.184
35	1514.7	1524.8	3.08	99.338	35.650
100	1511.8	1521.0	2.98	99.353	101.728
Average ≈			3 %	99.3%	

Table C-2: Summary of contact time calculation for 0.05 g of ZSM-5 catalyst.

N$_2$ flow rate (ml min^{-1})	10	20	35	43	100
P (bar)	1.013	1.013	1.013	1.013	1.013
Pressure drop(bar)	0.040	0.04	0.04	0.04	0.04
Total pressure(bar)	1.053	1.053	1.053	1.053	1.053
Inlet temperature (K)	383.15	383.15	383.15	383.15	383.15
Flow (ml min^{-1})	16.700	20	35	43	75
R (cm^3 bar K^{-1} mol^{-1})	83.140	83.14	83.14	83.14	83.14
Total no moles (mol min^{-1})	0.00055	0.00066	0.0012	0.0014	0.0025
Flow rate of nC$_7$ (mol min^{-1})	1.660E-05	1.983E-05	3.471E-05	4.264E-05	7.438E-05
Catalyst weight (g)	0.050	0.05	0.05	0.05	0.05
W/F(g min mol^{-1})	3019.137	2520.979	1440.559	1172.548	672.261
W/F(g h mol^{-1})	50.319	42.016	24.009	19.542	11.2044

Table C-3: Summary of contact time calculation for 0.03 g of Y catalyst.

N_2 flow rate (ml min^{-1})	10	20	35	43	100
P (bar)	1.013	1.013	1.013	1.013	1.013
Pressure drop(bar)	0.04	0.04	0.04	0.04	0.04
Total pressure(K)	1.053	1.053	1.053	1.053	1.053
Inlet temperature (bar)	383.15	383.15	383.15	383.15	383.15
Flow (ml min^{-1})	10	12	21	43	75
R (cm^3 bar K^{-1} mol^{-1})	83.14	83.14	83.14	83.14	83.14
Total no moles (mol min^{-1})	0.00033	0.00040	0.00070	0.0014	0.0025
Flow rate of nC$_7$ (mol min^{-1})	9.917E-06	1.190E-05	2.082E-05	4.264E-05	7.438E-05
Catalyst weight (g)	0.03	0.03	0.03	0.03	0.03
W/F(g min mol^{-1})	3025.175	2520.979	1440.559	703.529	403.357
W/F(g h mol^{-1})	50.4196	42.016	24.009	11.725	6.723

Appendix D

Publications and presentations

List of publication

1. Alrubaye, R.T.A., B. Atilgan, R. J. Holmes, and A. A. Garforth, *Growing Zeolite Y on FeCrAlloy Metal.* World Academy of Science, Engineering and Technology, 2013(76): p. 889-893.

2. Alrubaye, R.T.A. and A. Garforth, *Generation of catalytic films of zeolite Y and ZSM-5 on FeCrAlloy metal.* Submit to Industrial & Engineering Chemistry Research 2013.

List of presentations

1. Al-Rubaye, R.T.A. and A. Garforth, *Generation of catalytic films of zeolite Y and ZSM-5 on FeCrAlloy metal*, in *36th British Zeolite Association conference*. April 8-10, 2013: Keele, England.

2. Al-Rubaye, R.T.A., B. Atilgan, R. J. Holmes, and A. A. Garforth, *Growing Zeolite Y on FeCrAlloy Metal*, in *International Conference on Biology, Environment and Chemistry*. April 14-15, 2013: Italy, Venice.

3. Al-Rubaye, R.T.A. and A. Garforth., *Zeolite Y and ZSM-5 Catalytic films on Fecralloy metal*, in *35th British Zeolite Association conference*. June, 2012: Chester, England.

4. Al-Rubaye, R.T.A. and A. Garforth. *Synthesis of thin zeolite and zeolite ZSM-5 films on Fecralloy*, in *Meeting of School of Molecular Sieves*. April 1-3, 2012. J. Heyrovský Institute of Physical Chemistry of ASCR, Academy of Sciences of the Czech Republic. Czech Republic.

5. Al-Rubaye, R.T.A. and A. Garforth, *ZSM-5 Zeolite Growth on Metal Alloy*, in *34th British Zeolite Association meeting*. April 11-13, 2011: Edinburgh, England.

6. Al-Rubaye, R.T.A. and A. Garforth. Synthesis *and Characterisation of Novel Alloy Supported Catalysts*, in *the Federation of European Zeolite Associations Conference*. July 3-7, 2011. Valencia, Spain.

Growing Zeolite Y on FeCrAlloy Metal

Abstract—Structured catalysts formed from the growth of zeolites on substrates is an area of increasing interest due to the increased efficiency of the catalytic process, and the ability to provide superior heat transfer and thermal conductivity for both exothermic and endothermic processes.

However, the generation of structured catalysts represents a significant challenge when balancing the relationship variables between materials properties and catalytic performance, with the Na_2O, H_2O and Al_2O_3 gel composition paying a significant role in this dynamic, thereby affecting the both the type and range of application.

The structured catalyst films generated as part of this investigation have been characterised using a range of techniques, including X-ray diffraction (XRD), Electron microscopy (SEM), Energy Dispersive X-ray analysis (EDX) and Thermogravimetric Analysis (TGA), with the transition from oxide-on-alloy wires to hydrothermally synthesised uniformly zeolite coated surfaces being demonstrated using both SEM and XRD. The robustness of the coatings has been ascertained by subjecting these to thermal cycling (ambient to 550^oC), with the results indicating that the synthesis time and gel compositions have a crucial effect on the quality of zeolite growth on the FeCrAlloy wires.

Finally, the activity of the structured catalyst was verified by a series of comparison experiments with standard zeolite Y catalysts in powdered pelleted forms.

Keywords—FeCrAlloy, Structured catalyst, and Zeolite Y.

I. INTRODUCTION

THIN layers of zeolite catalyst have previously been coated on a range of metal substrates, including stainless steel, carbon and α-Al_2O_3, with the choice of substrate influencing the performance of the catalyst [1], however metallic substrates such as FeCrAlloy offer high mechanical resistance, high thermal conductivity and the use of wires as the catalyst support presents a low pressure drop in relation to standard packed bed catalysts [2]. One of the major advantages of using a FeCrAlloy support is that the aluminium can be oxidised at high temperatures to form a thin film of aluminium oxide (Al_2O_3) on the surface [3, 4], and this oxide layer can then be used to anchor and subsequently grow an active zeolite phase [5]. The surface growth and development of a structured catalyst thus provids a significant enhancment on the surface area availabe for any catalysis reations, with the ability to vary the physical properties (residence time, dispersion, stability, heat and mass transfer and pressure drop across the bed) via growth conditions improving the range of processes and applications compatible with the system [6, 7].

The method of attachment of the Zeolite crystal onto the FeCrAlloy surface can be achieved through a number of routes. The first is the use of a dip coating method, which uses a binder to glue pre-synthesised zeolite crystals to the metal surface. An alternative method is the use of an in-situ growth of the zeolite crystals onto the substrate using the alumina formed on the metal surface as a partial source of Al required for the zeolite preparation [8]. In all cases, the pre-treatment step is crucial, as it requires the formation of uniformly thin aluminium oxide layer on the metal surface. This film then increases the wetting of the support by the synthesis gel mixture and/or promotes the nucleation of zeolite crystals[9-15].

As such, this paper presents a study of the effects of both the zeolite gel composition and in-situ zeolite gel crystallisation time for zeolite Y film formation, with an and evaluation of their catalytic performance for n-heptane cracking.

II. EXPERIMENTAL

A. SUPPORT PRE-TREATMENT

FeCrAlloy annealed wires (0.5 mm diameter) were supplied by GoodFellows with a pre-determined chemical composition by weight of Fe 72.8%, Cr 22%, Al 5%, Y 0.1%, and Zr 0.1 %.

The pre-treatment process was as follows; Oxide removeal using No.100 glass paper; immersion in 0.1M KOH at 25^oC for 10 minutes, followed by 0.1M HNO_3 solution at 80∘C for 5 min [13]. The wires were then rinsed with de-ionised water, placed in acetone and ultrasonicated for 10 minutes (Cam sonix C080T) and finally placed in de-ionised water and ultrasonicated for 10 minutes.

Thermal pre-treatment of the wires was conducted in a muffle furnace (Progen Scientific), ramped at a rate of 10^oC/min and held at 1000_oC 4h. The wire samples were suspended over a stainless steel support to ensure even oxidation of the surfaces and then removed from the furnace and rapidly cooled to ambient temperature.

B. PREPARING OF THE STRUCTURED CATALYST

The zeolite Y precursor gel was prepared from sodium aluminate (Fisher Scientific), colloidal silica (Ludox AS–40) and sodium hydroxide (Sigma–Aldrich), with the composition

Rana Th. A. Al-Rubaye is currently a PhD student at the School of Chemical Engineering and Analytical Science, University of Manchester, Oxford Road, Manchester, M13 9PL, UK and is also a Lecturer in the Chemical Engineering Department, College of Engineering, University of Bagdad, Baghdad, Iraq (Rana.Al-Rubaye@manchester.ac.uk).

Burcin Atilgan, is currently a PhD the School of Chemical Engineering and Analytical Science, University of Manchester, Oxford Road, Manchester, M13 9PL, UK.

Richard Holmes is a Lecturer in the School of Chemical Engineering and Analytical Science, University of Manchester, Oxford Road, Manchester, M13 9PL, UK (richard.holmes@manchester.ac.uk).

Arthur A. Garforth is a Senior Lecturer and the Head of Teaching in the School of Chemical Engineering and Analytical Science, University of Manchester, Oxford Road, Manchester, M13 9PL, UK (arthur.garforth@manchester.ac.uk).

range was carefully controlled within the range shown in the literature [16] with the starting gel composition being $3.3Na_2O:Al_2O:10SiO_2:120H_2O$. The pre–treated FeCrAlloy support wires were cut into lengths (2.5 cm) and inserted vertically into the gel mixture, with the synthesis performed under autogenous pressure at $100^{o}C$ for 4 days. The compositions were investigated and are summarised in Table I. By varying the amounts of the sodium aluminate (Fisher Scientific), Colloidal silica (Ludox AS–40 from Sigma–Aldrich) and sodium hydroxide (Sigma–Aldrich) use, it was possible to change the starting gel composition to be $xNa_2O:yAl_2O:10SiO_2:zH_2O$, where as the x= 2.3–4.3, y= 0.75–1.25, and z= 120–240 in molar ratios (Table I), and inorder to allow comparison with the literature, the gel compositions used in this work are highlighted in Fig1.

After the hydrothermal synthesis, both the zeolite gel precipitated in the autoclave and the coated wires were removed, rinsed and then ultrasonicated in de-ionised water for 10 min, where the as–made Na-Y zeolite powder (1 g) and all the structured zeolite were ion exchanged using a 0.5M ammonium nitrate solution (NH_4NO_3, purity > 98% Sigma–Aldrich) at $80^{o}C$ under constant reflux conditions with constant stirring (60–100 rpm) for 1 hour. These were then washed thoroughly with deionised water and dried at $100^{o}C$.

Post ion-exchange, the zeolite Y powder and structured zeolites were shown to have 3%Na content and were subjected to dealumination in order to produce an ultra-stable form of the zeolite Y. The dealumination process was performed using acidified ammonia nitrate, and the NH_4–Y powder or structured NH_4–Y zeolites were mixed with an ammonium nitrate solution (15% wt.) and the pH adjusted from 4.1 to 2.48 by the addition of HNO_3 (70%wt., Camlab Chemical, UK) [17].

TABLE I
DIFFERENT MOLAR COMPOSITIONS OF THE NAY GELS

| COMPOSITION	NaAlO$_2$ (g)	NaOH (g)	Ludox (g)	H$_2$O (g)
$2.3Na_2O:Al_2O_3:10SiO_2:120H_2O$	1	0.52	7.52	6.02
$2.7Na_2O:Al_2O_3:10SiO_2:120H_2O$	1	0.68	7.52	5.98
$3.0Na_2O:Al_2O_3:10SiO_2:120H_2O$	1	0.80	7.52	5.95
$3.3Na_2O:Al_2O_3:10SiO_2:120H_2O$	1	0.92	7.52	5.92
$4.3Na_2O:Al_2O_3:10SiO_2:120H_2O$	1	1.32	7.52	5.84
$3.3Na_2O:Al_2O_3:10SiO_2:180H_2O$	1	0.92	7.52	11.35
$3.3Na_2O:Al_2O_3:10SiO_2:240H_2O$	1	0.92	7.52	16.67
$3.3Na_2O:0.75Al_2O_3:10SiO_2:120H_2O$	1	1.35	10.04	7.93
$3.3Na_2O:1.25Al_2O_3:10SiO_2:120H_2O$	1	0.65	6.02	4.72
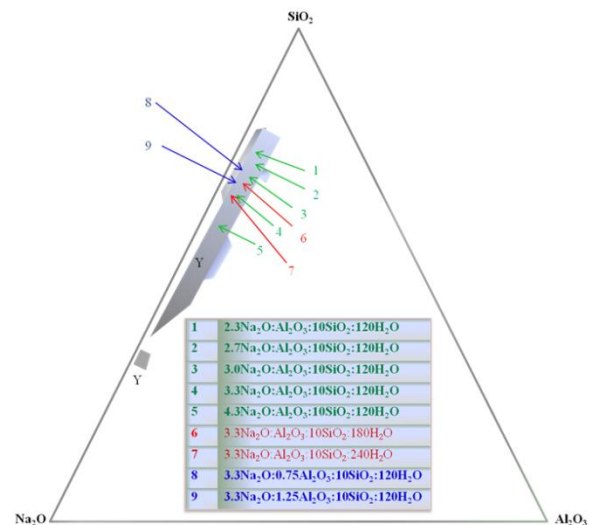
Fig. 1 Different molar compositions of the NaY gels

III. CHARACTERISATION

The crystal growth of the zeolite on the wire surface was compared with the crystal growth in the bulk phase using a Philips X' Pert PRO X–ray diffraction meter scanning $0.000832^{o}/min$ slit widths $1/8^{o}$ and $1/4^{o}$ over a 2θ range of 3°–50°. The powder zeolite samples were analysed similarly however a faster scanning rate of= $0.0289^{o}/min$ was used.

Calcination and adhesion of the zeolite layers for all samples was studied using thermogravimetric analyzer (Q5000-IR TA Instruments), and calcination was carried out by heating in air (25 ml/min) from ambient at a rate of 1 ^{o}C/min to 550 ^{o}C where the temperature was held for 480 min. The adhesion of the zeolite layers was tested by thermal cycling selected wires between ambient to 550 ^{o}C at 10 ^{o}C/min. The wires were held at both the high and low temperatures for 30 minutes and the process was repeated five times.

Surface morphology and chemical analysis were carried out on gold-coated powder and wires samples under high vacuum using the Quanta 200 FEI scanning electron microscopy and the Genesis software.

Energy Dispersive Spectrometry EDS spectroscopy was used to identify elements and count the impinging X-rays based upon their characteristic energy levels [18]. Since, a well polished surface is required for quantitative/qualitative analysis and concentration maps, two techniques were used. Firstly, the external surface of the wire was analysed directly using X–ray spot analysis on carbon or gold–coated samples. Secondly the analysis of the elements dispersed across different layers of the metal, oxide layer and coated zeolite was carried out. Wires samples were prepared by immersion vertically in a resin and then sectioned with diamond saw to obtain a clean surface. This surface was then ground with SiC sandpaper and polished with Al_2O_3 in order to obtain a smooth flat surface. The samples were then rinsed with alcohol to remove contamination and finally carbon or gold–coated.

IV. CATALYTIC CRACKING PERFORMANCE OF CATALYTIC FILMS

The behavior of the structured and pelleted catalysts was studied using a well characterised n–heptane cracking reaction in a 4 mm i.d. quartz reactor. Bundles of the USY structured catalyst wires were loaded into a reactor (2.5 cm length x 0.05 cm diameter) with a zeolite equivalent weight for Y of 0.03 gm. For comparison, the same bed length of pelleted USY zeolite catalyst of 1 gm (425–500μm pellets) were tested. The catalysts under test were sandwiched between two layers of quartz wool and the microreactor was located in the middle of the furnace (Carbolite MTF 12/12A). The catalysts were activated prior to the cracking by heating from $25^{o}C$ to $550^{o}C$ in air ($1^{o}C/min$, 25ml/min) and held isothermally at $550^{o}C$ for 16 hours. The n-heptane (99.99% Fluka) was supplied by flowing nitrogen through three bubblers connected in series and placed in an ice bath to maintain a constant temperature. All the stainless steel pipes connected between the reactor and the GC were lagged with heating wire (Electrothermal PLC, UK) and maintained at approximately $110^{o}C$ to avoid any condensation of the reactant and products. A Varian 3400 FID GC fitted with a PLOT Al_2O_3/KCl capillary column (50m×0.32 mm i.d.) was connected to the reactor and samples analysed at regular intervals between 5 and 125 min. All catalysts were studied at $450^{o}C$ with a W/F= 42 g.h/ mol and the activity and selectivity reported.

V. RESULTS

A. OPTIMUM THE GEL COMPOSITION OF ZEOLITE NA-Y GEL

Synthesis of zeolite Na–Y was performed using aluminosilicates gels of the general mole composition $xNa_2O:yAl_2O_3:10SiO_2:zH_2O$; where x=2.3–4.3, y=0.75–1.25, z=120–240 to study the properties of the zeolite growing on FeCrAlloy. For all the samples the crystallisation time was 4 days for the powder and structured zeolite.

The XRD data of the Na_2O molar ratio changed between 2.3 and 4.3 for powder samples confirmed the prsent of zeolite Na–Y. Phase–pure zeolite Na–Y was obtained from gel composed of $2.7Na_2O$, $3.0Na_2O$ and $3.3Na_2O$. However; the composition of the 4 day aged sample presented different XRD patterns because of the forming of different phases. The XRD patterns in Fig 2 illustrated the crystallisation of Faujasite (FAU), and Na–P1 (GIS) type zeolites together for the $4.3Na_2O$. Comparison of crystallinities in Table II Na_2O enhanced the crystal growth of the zeolite Na-Y however at higher Na_2O values the picture was more confusing. For the structured zeolite, the zeolite films were hard to characterise with the ratio being less than 4.3 Na_2O and at $4.3Na_2O$ ratio the major phase was the Na–P1 (GIS) type zeolites as shown in Fig 2.

ABLE II
DIFFERENT GEL COMPOSITIONS EFFECT ON THE CHARCTERISATION PROPERITES

COMPOSITION CHANGE OF THE GEL COMPOSITION

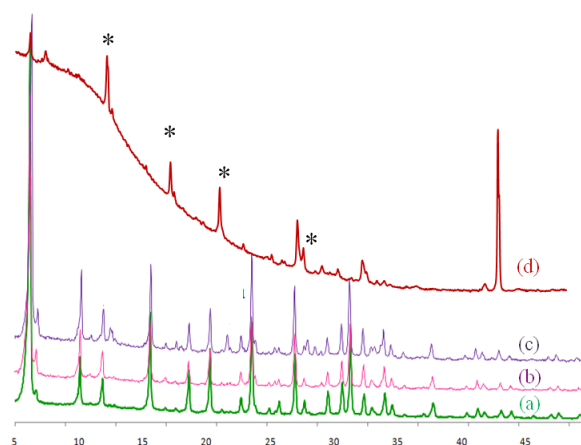|				
NaO_2 Ratio	2.3	2.7	3	3.3
H_2O Ratio	120	120	120	120
Al_2O_3 Ratio	1	1	1	1
Crystallinity %	34	47	67	100
Si/Al Ratio	2.97	2.86	2.76	2.47
Weight gain %	0.1	0.5	0.2	0.6
Cumulative coverage (g/m^2)	1.3	4.8	2.0	5.3
NaO_2 Ratio	2.3	2.7	3	3.3
H_2O Ratio	120	120	120	120

Fig. 2 XRD patterns the crystallisation of different phases for (a) $2.3Na_2O$, (b)$3.3Na_2O$, (c) $4.3Na_2O$ molar ratio for powder compared with (d) $4.3Na_2O$ structured catalyst. Impurities in the zeolite Y phase are highlighted (*)

It was shown that the crystalisation rate decreased zeolite Na–Y when there was an increase in the H_2O mole ratio using the formula; $3.3Na_2O:Al_2O_3:10SiO_2:zH_2O$ where the z=120, 180 and 240, and the effects of modifying the aluminium ratio for the synthesised zeolite Na–Y was monitored using the aluminium molar ratios of 0.75, 1 and 1.25. The samples were prepared following the same procedure as for the composition study in order to ensure that the properties of the each zeolite Na–Y sample remained constant for both the zeolite powder and the structured zeolite. The crystallisation time of 4 days was found to be suitable in order to produce a pure phase of the zeolite Na–Y, with the crystallinity of the zeolite Na–Y seeen to be decreased when there was an increae in the Al_2O_3 ratio in the gel compositon, The growth on the metal surface was determined using the XRD with the pure zeolite Na-Y phase detected at a typical low angle reflection of ($2\theta = 6.1 – 10.4^{o}$) for 0.75 Al_2O_3 (Fig 3).
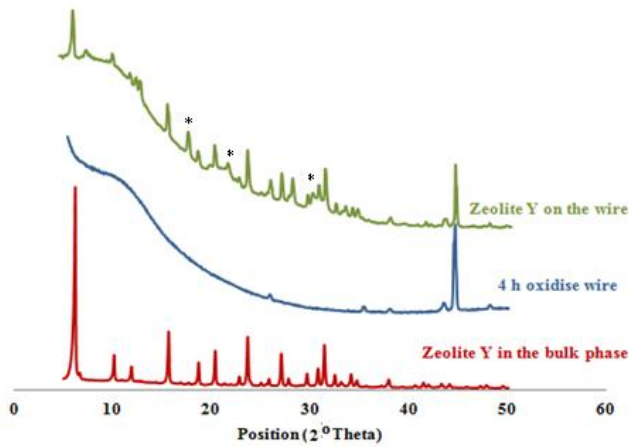
Fig. 3 XRD patterns of wire surface oxidised for 4 h, structured zeolite and zeolite Y in the bulk phase with 0.75 Al_2O_3 ratios for both. Impurities in the zeolite Y phase are highlighted (*)

SEM analyses of powder samples demonstrated that there was no significant change in the crystal size and morphology when increasing the Na_2O and H_2O. Whereas, in the Al_2O_3 ratio case, increasing Al_2O_3 ratio from 0.75 to 1.25, resulted in crystals forming with sharp edges and small sizes (Fig 4). The SEM images of the structured zeolite in Fig 5 illustrate that the zeolite crystals growth on FeCrAlloy has the same size and shape as the zeolites found in the bulk phase. However, the zeolite coverage (namely the increase in the mass of pure zeolite film grown on the FeCrAlloy and thus the surface area of the FeCrAlloy wires (g/m^2)) was different depending on the ratios of Na_2O and Al_2O_3 (Table II). Higher ratios of Na_2O led to thicker and eventually lumpier coatings with major formation of Na–P1 (GIS) type zeolites suggesting that a combination of coating and alumina dissolution was occuring.

The ESEM verified a scarce development of crystals was uniformly distrusted on the FeCrAlloy wire surface with the change of the coverage and layer thickness attributed to the deposition of new small crystals on top of the existing ones.
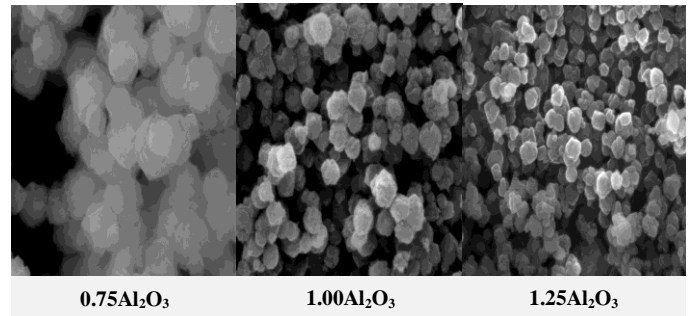

Fig. 4 SEM images of zeolite powder for different composition ($3.3Na_2O:yAl_2O_3:10SiO_2:120H_2O$; y=0.75 – 1.0 – 1.25)

The EDAX results for the different Na_2O mole ratio for both zeolite powder and structured zeolite samples demonstrated that by increasing the Na_2O and the Al_2O_3 ratios the Si/Al ratio is decreased from 2.97 to 2.07 and from 2.69 to 2.38, respectively, whilst the change in the H_2O ratio had no effect on the Si/Al ratio.

As was expected from the pure zeolite preparation, the amount of Na_2O had a significant effect on the crystallisation on the alloy support, with .higher Na_2O leading to thicker and eventually lumpier coatings with Na–P1 (GIS) type zeolites. Again water increase had little effect, but an increase in the molar ratio of Al_2O_3 in the composition affected the morphology and the structure of the zeolite coating surface and thus led to the formation of zeolite Y pure phase with trace impurities.
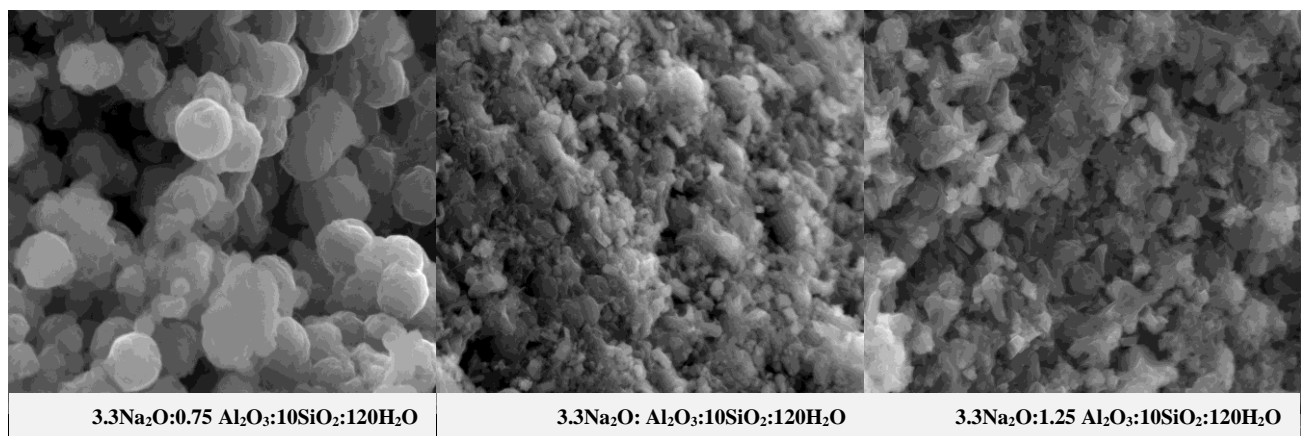

Fig. 5 SEM images of zeolite powder for different composition ($3.3Na_2O:yAl_2O_3:10SiO_2:120H_2O$; y=0.75 – 1.0 – 1.25)

B. CALCINATION OF ZEOLITE NA-Y

The calcination of the powder and structured Na–Y zeolite was studied by monitoring the weight lose using TGA, with the weight loses during heating is due to the loss of the volatile components, chemisorbed water and physisorbed water (Fig. 6 and Fig. 7).

The weight loss for all samples below $250^{o}C$ was due to desorption of moisture from both the powder and structured Na–Y zeolites as shown in Fig 6. For powder and structured Na–Y zeolite the major reduction was 19.36% and 1.46% due to loss water and volatile materials from zeolite framework structure. This was confirmed in the derivative thermogravimetric graphs (Fig. 7), which show small peaks below $250^{o}C$.

The weight loss from the Na–Y zeolite powder framework was 19.36%, while in the structured zeolite framework was 1.46%, where it was found that the weight of the Na–Y zeolite layer on the FeCrAlloy was approximately 8.1% of the total weight of the structured catalyst. Study of the morphology and the crystals size of the powder and structured Na–Y zeolite showed there was no noticeable change in the crystals size nor shape after the calcination process for the powder and structured Na–Y zeolite.
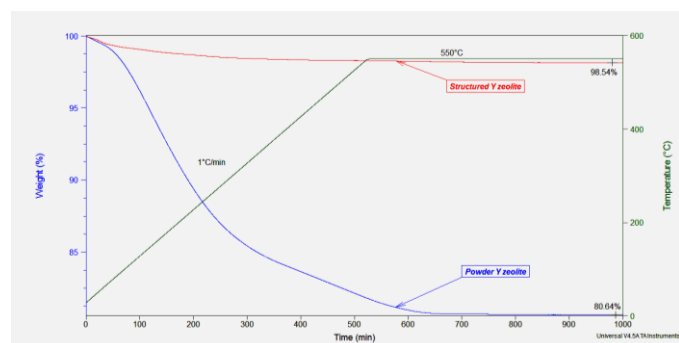

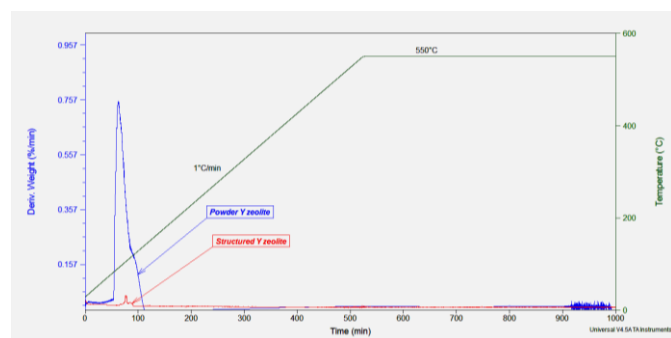Fig. 6 Thermal thermaogravimetric analysis for the calcination of powder and structured Na–Y

Fig. 7 Derivative thermaogravimetric analysis for the calcination of powder and structured Na–Y

C. CATALYST TEST FOR Y PELLETED AND STRUCTURED CATALYST

The Si/Al ratio for post synthetically modified powder and structured zeolite Y structured increased from 2.7 to approximately 8 (as determined by SEM/EDAX), with the catalytic activity of Y pellets (425–500µm) and bundles of structured Y catalyst grown on wires determined using n–heptane cracking in a fixed bed micro–reactor. The conversion of n–C_7 for an equivalent amount of catalyst at

$450^{o}C$ and W/F=42 g.h/mol for the two experiments and is presented in Fig. 8. As expected both catalysts deactivate rapidly with the pelleted Y catalyst showing the greater activity.
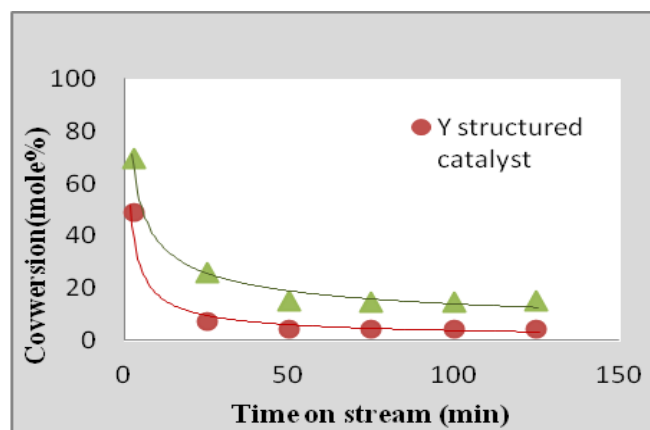

Fig. 8 Conversion of n-C_7 cracking for pelleted and structured USY at $450^{o}C$

Despite the higher conversion of the pelleted Y catalyst, the product selectivities of both catalysts at $450^{o}C$ were quite similar with $C_3^=$ and $C_4^=$ being the major products with neglible amounts of C_1 and C_5. The strongest sites deactivated first [19], and as such there was a rapid decrease in i–C_4 production accompanied by a rapid increase in $C_3^=$ and $C_4^=$ with time. Both catalysts behaved similarly and it was not too surprisingly apparent that the activation energy of 56 kJ mol^{-1} was determined for both.

VI. DISCUSSION AND CONCLUSIONS

Zeolite Y was successfully synthesised using a variety of gel compositions. After 4 days, when the Na_2O amount was increased, the XRD of the $4.3Na_2O:Al_2O_3:10SiO_2:120H_2O$ sample illustrated the crystallisation of Faujasite (FAU), and Na–P1 (GIS) type zeolites together. Altering the Al_2O_3 content in the gel also had an effect on the rate of crystallisation, the crystal size and the morphology, as the Al_2O_3 molar ratio in the composition increased, the crystal size decreased.

As was expected from the pure zeolite preparation, the amount of Na_2O has a significant effect on the crystallisation on the alloy support, with higher Na_2O concentrations leading to thicker and eventually lumpier coatings with Na–P1 (GIS) type zeolites. Again water increase had little effect butan increase in the molar ratio of Al_2O_3 in the composition affects the morphology and the structure of the zeolite coating surface and thus led to the formation of zeolite Y pure phase with trace of impurities. Finally n–C_7 cracking revealed lower cracking activities for the structured catalysts with the most likely explanation being that the imperfect packing of the fixed bed micro-reactor allowed some degree of channelling of the reactant resulting in lower conversions. However, the acid-leached zeolite Y (Si/Al = 8) structured catalysts showed similar product selectivities to their Pelleted counterparts. Increased i–C_4 yields indicated more secondary reactions in the case of the Pelleted catalysts supporting the lower activity observed for the structured catalysts. Apparent

activation energies of approximately 60 kJmol^{-1} for all catalysts suggested similar reaction mechanisms and that the surface reaction was controlling.

REFERENCES

[1] J. Jansen, et al., "Zeolitic coatings and their potential use in catalysis," Microporous and Mesoporous Materials, vol. 21, pp. 213-226, 1998.

[2] J. M. Zamaro, et al., "ZSM5 growth on a FeCrAl steel support. Coating characteristics upon the catalytic behavior in the NOx SCR," Microporous and Mesoporous Materials, vol. 115, pp. 113-122, 2008.

[3] C. Badini and F. Laurella, "Oxidation of FeCrAl alloy: influence of temperature and atmosphere on scale growth rate and mechanism," Surface and coatings technology, vol. 135, pp. 291-298, 2001.

[4] J. E. Samad, et al., "Structured catalysts via multiple stage thermal oxidation synthesis of FeCrAl alloy sintered microfibers," Chemical Engineering Journal, vol. 168, pp. 470-476, 2011.

[5] I. Yuranov, et al., "Zeolite/sintered metal fibers composites as effective structured catalysts," Applied Catalysis A: General, vol. 281, pp. 55-60, 2005.

[6] M. Tatlier, " Adsorption Heat Pumps Utilizing Zeolite Coatings Grown on Metal Surfaces. ," Master, Istanbul Technical University, Turkey, 2001.

[7] A. Dabrowski, Adsorption and its applications in industry and environmental protection vol. 120: Elsevier, 1999.

[8] V. Meille, "Review on methods to deposit catalysts on structured surfaces," Applied Catalysis A: General, vol. 315, pp. 1-17, 2006.

[9] R. Munoz, et al., "Zeolite Y coatings on Al-2024-T3 substrate by a three-step synthesis method," Microporous and Mesoporous Materials, vol. 86, pp. 243-248, 2005.

[10] Z. Wang, et al., "Synthesis of thin silicalite-1 films on steel supports using a seeding method," Microporous and Mesoporous Materials, vol. 52, pp. 191-197, 2002.

[11] S. Mintova, et al., "Adhesivity of molecular sieve films on metal substrates," Zeolites, vol. 17, pp. 462-465, 1996.

[12] X. Wu, et al., "Influence of an aluminized intermediate layer on the adhesion of a γ-Al$_2$O$_3$ washcoat on FeCrAl," Surface and coatings technology, vol. 190, pp. 434-439, 2005.

[13] M. Valentini, et al., "The deposition of γ-Al$_2$O$_3$ layers on ceramic and metallic supports for the preparation of structured catalysts," Catalysis today, vol. 69, pp. 307-314, 2001.

[14] M. Mies, et al., "Hydrothermal synthesis and characterization of ZSM-5 coatings on a molybdenum support and scale-up for application in micro reactors," Catalysis today, vol. 110, pp. 38-46, 2005.

[15] J. Čejka, Introduction to zeolite science and practice vol. 168: Elsevier Science, 2007.

[16] A. Kostinko John, "Factors Influencing the Synthesis of Zeolites A, X, and Y," in Intrazeolite Chemistry. vol. 218, ed: AMERICAN CHEMICAL SOCIETY, 1983, pp. 3-19.

[17] J. G. Vassilakis and D. F. Best, "Novel zeolite compositions derived from zeolite Y," ed: Google Patents, 1991.

[18] G. Danilatos, "Review and outline of environmental SEM at present," Journal of Microscopy, vol. 162, pp. 391-402, 2011.

[19] P. A. Jacobs and J. A. Martens, "Introduction to acid catalysis with zeolites in hydrocarbon reactions," Studies in Surface Science and Catalysis, vol. 58, pp. 445-496, 1991.

Curriculum vitae

Email: Rana.Al-rubaye@manchester.ac.uk
Alrubaye.Rana@gmail.com
LinkedIn: http://uk.linkedin.com/in/ranaalrubaye

Profile

PhD '' Catalytic films of zeolite Y and ZSM-5 on Fecralloy metal ''. University of Manchester,
I have over 7 year's lecturer assistance experiences in range of Iraq universities. I am enthusiastic about starting my career in a large international company that is recognised worldwide. I am excited about working with people from different backgrounds, and look forward to a job that will challenge my skills on a daily basis and will push me to the limit of my abilities, as I consider that to be the best way to develop oneself.

Education

2000 - 2004 **The University of Baghdad/Iraq**
MSc (Hons) Chemical Engineering (Obtained: 1st class)

During my MSc research at Baghdad University I have had the opportunity to work on a Synthesis of a Multi Purpose Grease to serve under sever conditions with Prof. A.H.A.K.Mohammed and got an honour degree on my research.

1996- 2000 **The University of Baghdad/Iraq**
BSc (Hons) Chemical Engineering (Obtained: 1st class)

During my time at university I have had the opportunity to work in teams with people from different backgrounds on a variety of projects. During a large Design project, I took the leadership of the team I was working with, while playing key roles as a team member and achieving results ahead of deadlines. I worked for 2 months internal ship program in Al-Dora Refinery Company in Iraq.

Work experience

A member of Iraqi Association of Engineers.
A member of Royal Society of Chemistry | Advancing the Chemical Sciences(AMRSC)

2002-2007 **University of Baghdad** A lecturer in the Chemical Engineering Department –College of Engineering; taught courses in engineering design, petroleum refining, lab. Unit operation, Lab of optimisation & numerical method and lab. of application of computer in Chem. Eng.(MATLAB). For the fourth year students. Also, Heat transfer courses and lab. of Optimization & numerical method for the 3rd year students. And analytical mathematics, eng. drawing for first year students.

2007-2009 **University of Al-Qadissiya** a lecturer in the Mechanical Engineering Department– College of Engineering; taught courses in Heat Transfer and design and building Heat transfer laboratory for the third year student. Also, I work as a Manager of IT unites in College of Engineering- University of Al-Qadissiya.

2009 – 2011 **The University of Manchester** (during term time)
Teaching assistant (for 1st, 2nd and 4th year Chemical Engineering students)
The teaching assistant position attracted me, as it provided the opportunity to improve my interpersonal and communication skills, whilst developing others. As a teaching assistant my responsibilities include:

- Planning, organising and delivering tutorial sessions to undergraduate and post graduate Chemical engineering students
- Developing detailed worked solutions for the tutorial questions to ensure that the best quality help is available to the students.
- Organising and monitoring activities, motivating group work and collaboration between students.
- Working with groups of 40 to 100 students
- A good grasp of a variety of concepts is required from me, as I have to be able to efficiently deliver the information to the students with different levels of understanding of the theory.

Honours and Awards

- Award by the Minister of Higher Education and Scientific Research on the 20th of June at the Iraqi Cultural Attaché London/UK.
- Award at the Annual Meeting of the British Zeolite Association. For presenting the work 'GENERATION OF CATALYTIC FILMS OF ZEOLITE Y AND ZSM-5 ON FECRALLOY METAL' at the XXXVI Annual Meeting of the British Zeolite Association held at Keel University on the 8-10th of April 2013.

Volunteer Experience

- Volunteer at Lab in a Lorry / the Institute of Physics (October 2012)
Lab in a Lorry aims to enthuse the next generation of scientists and engineers by giving young people (11-14 year olds) the opportunity to participate in experimental science in the way that it actually happens in the world of science: exploratory, often accidental, and informed by curiosity and intuition. The science experiments on board Lab in a Lorry are specifically designed for 11-14 year olds. The aim is to challenge their creativity, develop their teamwork skills and cultivate the inquisitive and resourceful approach needed to encourage more positive perceptions of the possibilities that science offers. Each lorry is a self-contained mobile physics laboratory that rolls up and is ready to go. The lorry is staffed by a full-time Operations Coordinator and usually at least volunteers.